

**MATERIALS FOR ADAPTIVE STRUCTURAL
ACOUSTIC CONTROL**

Period February 1, 1995 to January 31, 1996

Annual Report

VOLUME III

OFFICE OF NAVAL RESEARCH
Contract No.: N00014-92-J-1510

APPROVED FOR PUBLIC RELEASE — DISTRIBUTION UNLIMITED

Reproduction in whole or in part is permitted
for any purpose of the United States Government

L. Eric Cross

19960703 067

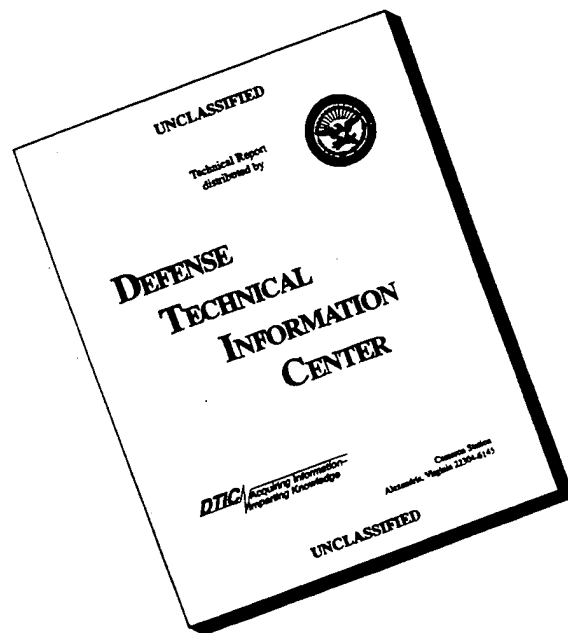
PENNSSTATE



THE MATERIALS RESEARCH LABORATORY
UNIVERSITY PARK, PA

DTIC QUALITY INSPECTED 1

DISCLAIMER NOTICE



THIS DOCUMENT IS BEST QUALITY AVAILABLE. THE COPY FURNISHED TO DTIC CONTAINED A SIGNIFICANT NUMBER OF PAGES WHICH DO NOT REPRODUCE LEGIBLY.

REPORT DOCUMENTATION PAGE

Form Approved
OMB No 0704-0188

Public reporting burden for this collection of information is estimated to average 1 hour per response, including the time for reviewing instructions, searching existing data sources, gathering and maintaining the data needed, and completing and reviewing the collection of information. Send comments regarding this burden estimate or any other aspect of this collection of information, including suggestions for reducing this burden, to Washington Headquarters Services, Directorate for Information Operations and Reports, 1215 Jefferson Davis Highway, Suite 1204, Arlington, VA 22202-4302, and to the Office of Management and Budget, Paperwork Reduction Project (0704-0188), Washington, DC 20503.

1. AGENCY USE ONLY (Leave blank)		2. REPORT DATE 3/13/96	3. REPORT TYPE AND DATES COVERED ANNUAL REPORT 02/01/95 TO 01/31/96	
4. TITLE AND SUBTITLE MATERIALS FOR ADAPTIVE STRUCTURAL ACOUSTIC CONTROL			5. FUNDING NUMBERS	
6. AUTHOR(S) L. ERIC CROSS				
7. PERFORMING ORGANIZATION NAME(S) AND ADDRESS(ES) MATERIALS RESEARCH LABORATORY THE PENNSYLVANIA STATE UNIVERSITY UNIVERSITY PARK, PA 16802			8. PERFORMING ORGANIZATION REPORT NUMBER	
9. SPONSORING/MONITORING AGENCY NAME(S) AND ADDRESS(ES) OFFICE OF NAVAL RESEARCH CODE 1513:NRJ 800 NORTH QUINCY STREET ARLINGTON, VA 22217-5660			10. SPONSORING/MONITORING AGENCY REPORT NUMBER GERALD T. SMITH OFFICE OF NAVAL RESEARCH RES. REP. 536 SOUTH CLARK STREET, RM 280 CHICAGO, ILLINOIS 60606-1588	
11. SUPPLEMENTARY NOTES				
12a. DISTRIBUTION/AVAILABILITY STATEMENT			12b. DISTRIBUTION CODE	
<div style="border: 1px solid black; padding: 5px; width: fit-content; margin: 0 auto;"> <p style="margin: 0;">DISTRIBUTION STATEMENT B</p> <p style="margin: 0;">Approved for public release</p> <p style="margin: 0;">Distribution Unlimited</p> </div>				
13. ABSTRACT (Maximum 200 words)				
SEE FOLLOWING THREE PAGES				
14. SUBJECT TERMS			15. NUMBER OF PAGES	
			16. PRICE CODE	
17. SECURITY CLASSIFICATION OF REPORT	18. SECURITY CLASSIFICATION OF THIS PAGE	19. SECURITY CLASSIFICATION OF ABSTRACT	20. LIMITATION OF ABSTRACT	

GENERAL INSTRUCTIONS FOR COMPLETING SF 298

The Report Documentation Page (RDP) is used in announcing and cataloging reports. It is important that this information be consistent with the rest of the report, particularly the cover and title page. Instructions for filling in each block of the form follow. It is important to *stay within the lines* to meet *optical scanning requirements*.

Block 1. Agency Use Only (Leave blank).

Block 2. Report Date. Full publication date including day, month, and year, if available (e.g. 1 Jan 88). Must cite at least the year.

Block 3. Type of Report and Dates Covered. State whether report is interim, final, etc. If applicable, enter inclusive report dates (e.g. 10 Jun 87 - 30 Jun 88).

Block 4. Title and Subtitle. A title is taken from the part of the report that provides the most meaningful and complete information. When a report is prepared in more than one volume, repeat the primary title, add volume number, and include subtitle for the specific volume. On classified documents enter the title classification in parentheses.

Block 5. Funding Numbers. To include contract and grant numbers; may include program element number(s), project number(s), task number(s), and work unit number(s). Use the following labels:

C - Contract	PR - Project
G - Grant	TA - Task
PE - Program Element	WU - Work Unit Accession No.

Block 6. Author(s). Name(s) of person(s) responsible for writing the report, performing the research, or credited with the content of the report. If editor or compiler, this should follow the name(s).

Block 7. Performing Organization Name(s) and Address(es). Self-explanatory.

Block 8. Performing Organization Report Number. Enter the unique alphanumeric report number(s) assigned by the organization performing the report.

Block 9. Sponsoring/Monitoring Agency Name(s) and Address(es). Self-explanatory.

Block 10. Sponsoring/Monitoring Agency Report Number. (If known)

Block 11. Supplementary Notes. Enter information not included elsewhere such as: Prepared in cooperation with...; Trans. of...; To be published in.... When a report is revised, include a statement whether the new report supersedes or supplements the older report.

Block 12a. Distribution/Availability Statement. Denotes public availability or limitations. Cite any availability to the public. Enter additional limitations or special markings in all capitals (e.g. NOFORN, REL, ITAR).

DOD - See DoDD 5230.24, "Distribution Statements on Technical Documents."

DOE - See authorities.

NASA - See Handbook NHB 2200.2.

NTIS - Leave blank.

Block 12b. Distribution Code.

DOD - Leave blank.

DOE - Enter DOE distribution categories from the Standard Distribution for Unclassified Scientific and Technical Reports.

NASA - Leave blank.

NTIS - Leave blank.

Block 13. Abstract. Include a brief (*Maximum 200 words*) factual summary of the most significant information contained in the report.

Block 14. Subject Terms. Keywords or phrases identifying major subjects in the report.

Block 15. Number of Pages. Enter the total number of pages.

Block 16. Price Code. Enter appropriate price code (*NTIS only*).

Blocks 17. - 19. Security Classifications. Self-explanatory. Enter U.S. Security Classification in accordance with U.S. Security Regulations (i.e., UNCLASSIFIED). If form contains classified information, stamp classification on the top and bottom of the page.

Block 20. Limitation of Abstract. This block must be completed to assign a limitation to the abstract. Enter either UL (unlimited) or SAR (same as report). An entry in this block is necessary if the abstract is to be limited. If blank, the abstract is assumed to be unlimited.

ABSTRACT

This report documents work carried forward over the fourth year of a five year ONR sponsored University Research Initiative (URI) entitled "Materials for Adaptive Structural Acoustic Control." The program has continued to underpin the development of new electro-ceramic, single crystal and composite materials combinations for both the sensing and actuation functions in adaptive structures.

For the lead based perovskite structure relaxor ferroelectric electrostrictors, new experimental and theoretical studies have underscored the critical role of nano-scale heterogeneity on either A or B sites of the ABO_3 in promoting dispersive dielectric response and the very strong opposing role of elastic stress and electrostrictive coupling in suppressing polarization fluctuations. Most important for practical application is the regimen where, under high electric field nano-polar regions begin to amalgamate into ferroelectric macro-domains with very mobile walls lead to unusually large extrinsic piezoelectric coefficients.

The program has explored a range of new relaxor:ferroelectric solid solutions which exhibit morphotropic phase boundaries between rhombohedral and tetragonal ferroelectric phases. Some of these compositions are much more tractable than PZT to grow in single crystal form. A major surprise is the very strong enhancement of the piezoelectric d_{33} and d_{31} in the crystal over that in the corresponding ceramic, and the massive anisotropy for different orientations and directions of poling. Optical studies suggest that the unusual effects reside largely in the extrinsic (domain controlled) response and we speculate about the mobility of walls in metastable phases, however further studies are required.

Antiferroelectric:ferroelectric phase switching studies in a wide range of compositions in the lead lanthanum zirconate stannate titanate system show that the first abrupt switchover to the rhombohedral ferroelectric phase only produces volume strain $\sim 0.2\%$ as checked both by dilatometry and by X-ray. There is a large enhancement under higher field to $\sim 0.6\%$ volume strain although the polarization does not change markedly. From thin film and single crystals studies there is mounting evidence of higher field ferroelectric:ferroelectric phase change, but again additional work is needed.

Size effect studies in perovskite ferroelectrics are continuing on this program and on the NSF/MRG in MRL. Scaling of the 90° stripe domains in thinned TEM samples of tetragonal composition begin to show departure from the accepted $1/2$ power law at sub micron sizes. The structure of domains under the three dimensional constraints of grains inside the ceramic is still however almost completely unknown. Computer modeling appear to show promise and codes are being explored which permit the mutual interactions to be varied and the corresponding two dimensional structures visualized.

In composite sensors, the focus has continued upon the flextensional configurations with the new inexpensive cymbal shaped amplifier proving superior in every respect to the original "moonie." The flat section on the cymbal end cap permits very easy stacking of elements and work is now in progress to develop large area panels for low frequency testing at the Penn State ARL.

Work has continued on the thin sheet 2:2 piezoceramic polymer composites, where the transverse poling and low density lead to a desirable combination of low electrical and low acoustic impedance. An alternative fabrication procedure using extruded PZT honeycomb appears most attractive.

Two problems of major importance in actuation have been topics for study. First what are the "intrinsic" material limitations for high strain electrically driven actuation in polarization controlled systems, and secondly what are the practical limitations in multilayer actuators as they are currently fabricated and how may they be alleviated. Work on the first topic is now largely completed, showing that strains $\sim 0.4\%$ could be switched more than 10^9 cycles in suitable PLZT compositions. Such reliability however requires near theoretical density, homogeneity, grain size control, critical attention to electrodes and electric field uniformity, none of which are adequately controlled in current actuator systems.

For practical actuators fabricated by inexpensive tape casting and co-firing techniques electrode termination is a major problem. In the simple MLC like designs, cracks initiate at field concentrations associated with the tip of the buried conductor layer. A new floating electrode design has been found to reduce this problem. For cracking near the end surfaces, poling of the termination layers reduces their stiffness and markedly improves performance. In the conventional structures it is also found that the floating electrode may be used directly as an acoustic emission pickup, giving early warning of cracking problems.

Under resonant driving conditions, the problems in actuators are markedly different. Heat build up and temperature run-away are significant problems traceable to dielectric loss, and new hard compositions and anti-resonant driving methods have been explored to reduce these problems.

In integration work on the high activity 0-3 composites in nearing completion. A new type of zig-zag actuator is being explored for the capability to combine both longitudinal and transverse actuation. Under a new ONR sponsored program with Virginia Polytechnic Institute and University new double amplifiers combining bimorph and flextensional concepts are being examined.

Processing studies permit the fabrication of the wide range of compositions and forms required in these material researches. Rate controlled sintering is proving to be highly advantageous, particularly for reducing delamination in integrated structures. Electrophoretic and

dielectrophoretic forming are showing promise in green assembly of thick film components where high green density is critical.

Thin film papers have been selected from the very broad range of work in MRL because of their relevance to transduction in piezoelectric and in phase switching systems.

**MATERIALS FOR ADAPTIVE STRUCTURAL
ACOUSTIC CONTROL**

Period February 1, 1995 to January 31, 1996

Annual Report

VOLUME III

OFFICE OF NAVAL RESEARCH
Contract No.: N00014-92-J-1510

APPROVED FOR PUBLIC RELEASE — DISTRIBUTION UNLIMITED

Reproduction in whole or in part is permitted
for any purpose of the United States Government

L. Eric Cross

PENNSSTATE



THE MATERIALS RESEARCH LABORATORY
UNIVERSITY PARK, PA

APPENDICES

VOLUME I

General Summary Papers

1. Cross, L.E., "Ferroelectric Materials for Electromechanical Transducer Applications," *Jpn. J. Appl. Phys.* **34**, 2525-2532 (1995).
2. Fernandez, J.F., A. Dogan, Q.M. Zhang, J.F. Tressler, and R.E. Newnham, "Hollow Piezoelectric Composites," submitted to *Sensors and Actuators: A. Physical* (1995).
3. Uchino, K., "Recent Developments in Ceramic Actuators—Comparison among USA, Japan and Europe," Workshop on Microsystem Technologies in the USA and Canada, Dusseldorf (1995).
4. Trolier-McKinstry, S., J. Chen, K. Vedam, and R.E. Newnham, "In Situ Annealing Studies of Sol-Gel Ferroelectric Thin Films by Spectroscopic Ellipsometry," *J. Am. Ceram. Soc.* **78** [7], 1907-1913 (1995).
5. Nair, N., A. Bhalla, and R. Roy, "Inorganic Lead Compounds in Electroceramics and Glasses," *Am. Cer. Soc. Bull.* **75** [1], 77-82 (1996).
6. Gentile, A. and F.W. Ainger, "Single Crystals," Chapter 9, Materials Science and Technology, A Comprehensive Treatment, **17A** Processing of Ceramics, Part 1 (R.J. Brook, editor), VCH Verlagsgesellschaft mbH, Weinheim, Fed. Repl. of Germany (1996).

Materials Studies

7. Choi, S.W., J.M. Jung, and A.S. Bhalla, "Dielectric, Pyroelectric and Piezoelectric Properties of Calcium-Modified Lead Magnesium Tantalate-Lead Titanate Ceramics."
8. Kim, Y.J., S.W. Choi, and A.S. Bhalla, "Dielectric, Pyroelectric Properties, and Morphotropic Phase Boundary in La-Doped $(1-x)\text{Pb}(\text{Mg}_{1/3}\text{Ta}_{2/3})-x\text{PbTiO}_3$ Solid Solution Ceramics", *Ferroelectrics* **173**, 87-96 (1995).
9. Alberta, E. and A.S. Bhalla, "A Processing and Electrical Property Investigation of the Solid Solution: $(x)\text{Pb}(\text{In}_{1/2}\text{Nb}_{1/2})\text{O}_3-(1-x)\text{Pb}(\text{Sc}_{1/2}\text{Ta}_{1/2})\text{O}_3$," submitted to *Ferroelectrics* (1995).
10. Zhang, Q.M., H. You, M.L. Mulvihill, and S.J. Jang, "An X-ray Diffraction Study of Superlattice Ordering in Lead Magnesium Niobate," *Solid State Comm.* **97** [8], 693-698 (1996).
11. Zhang, Q.M., J. Zhao, and L.E. Cross, "Aging of the Dielectric and Piezoelectric Properties of Relaxor Ferroelectric Lead Magnesium Niobate-Lead Titanate in the Electric Field Biased State," *J. Appl. Phys.* **79** (6), 1-7 (1996).

VOLUME II

Materials Studies (continued)

12. Zhang, Q.M., J. Zhao, T.R. Shrout, and L.E. Cross, "The Effect of Ferroelastic Coupling in Controlling the Abnormal Aging Behavior in Lead Magnesium Niobate-Lead Titanate Relaxor Ferroelectrics," submitted *J. Mat. Res.*
13. Mulvihill, M.L., L.E. Cross, and K. Uchino, "Low-Temperature Observation of Relaxor Ferroelectric Domains in Lead Zinc Niobate," *J. Am. Ceram Soc.* **78** (12) 3345-3351 (1995).
14. Mulvihill, M.L., L.E. Cross, and K. Uchino, "Dynamic Motion of the Domain Configuration in Relaxor Ferroelectric Single Crystals as a Function of Temperature and Electric Field," 8th Euro. Mtg. Ferroelectricity, Nijmegen (1995).
15. Mulvihill, M.L., K. Uchino, Z. Li, and Wenwu Cao, "In-Situ Observation of the Domain Configurations During the Phase Transitions in Barium Titanate," accepted *Phil. Mag. B* (1995).
16. Oh, K.Y., K. Uchino, and L.E. Cross, "Electric Properties and Domain Structures in Ba(Ti,Sn)O₃ Ceramics."
17. Cao, W., "Elastic and Electric Constraints in the Formation of Ferroelectric Domains," *Ferroelectrics*, **172**, 31-37 (1995).
18. Cao, W. and C.A. Randall, "The Grain Size and Domain Size Relations in Bulk Ceramic Ferroelectric Materials," accepted *J. Phys. Chem. Solids* (1995).
19. Cao, W., "Defect Stabilized Periodic Amplitude Modulations in Ferroelectrics," accepted *Phase Transitions* (1995).
20. Sopko, J., A. Bhalla, and L.E. Cross, "An Improved Quantitative Method for Determining Dynamic Current Response of Ppyroelectric Materials," *Ferroelectrics*, **173**, 139-152 (1995)

VOLUME III

Composite Sensors

21. Tressler, J.F., A. Dogan, J.F. Fernandez, J.T. Fielding, Jr., K. Uchino, and R.E. Newnham, "Capped Ceramic Hydrophones," submitted to Proc. IEEE Int'l Ultrasonics Symp., Seattle (1995).
22. Koc, B., A. Dogan, J.F. Fernandez, R.E. Newnham, and K. Uchino, "Accelerometer Application of the Modified Moonie (Cymbal) Transducer," submitted *Jpn. J. Appl. Phys.* (1995).
23. Zhao, J., Q.M. Zhang, and W. Cao, "Effects of Face Plates and Edge Strips on Hydrostatic Piezoelectric Response of 1-3 Composites," *Ferroelectrics* **173**, 243-256 (1995).
24. Wu, S.J., W. Qi, and W. Cao, "Numerical Study of Ultrasonic Beam Pattern of a 1-3 Piezocomposite Transducer," accepted *Proc. IEEE Trans. Ultrasonics, Ferroelectrics and Frequency Control*. (1995).

Composite Sensors (continued)—Volume III

25. Wang, H., Q.M. Zhang, and L.E. Cross, "Tailoring Material Properties by Structure Design--Radially Poled Piezoelectric Cylindrical Tube," *Ferroelectrics Lett.* (in press).
26. Zhang, Q.M. and X. Geng, "Electric Field Forced Vibration of a Periodic Piezocomposite Plate with Laminated Structure and Reflection and Transmission of a Plane Wave at the Fluid-Composite Interface," submitted to *IEEE Transactions on Ultrasonics, Ferroelectrics, and Frequency Control* (1995).
27. Geng, X., and Q.M. Zhang, "Dynamic Behavior of Periodic Piezoceramic-Polymer Composite Plates," *Appl. Phys. Lett.* **67** (21) (1995).
28. Zhang, Q.M., "Transverse Piezoelectric Mode Piezoceramic Polymer Composites with High Hydrostatic Piezoelectric Responses," *Proc. Int. Conf. on Electronic Components and Materials Sensors and Actuators*, Xi'an, China, 159-162 (1995)
29. Zhang, Q.M., H. Wang, J. Zhao, J.T. Fielding, Jr., R.E. Newnham, and L.E. Cross, "A High Sensitivity Hydrostatic Piezoelectric Transducer Based on Transverse Piezoelectric Mode Honeycomb Ceramic Composites," *IEEE Transactions on Ultrasonics, Ferroelectrics and Frequency Control* **43** (1), 26-42 (1996).
30. Zhang, Q.M., J. Chen, H. Wang, J. Zhao, L.E. Cross, and M.C. Trottier, "A New Transverse Piezoelectric Mode 2-2 Piezocomposite for Underwater Transducer Applications," *IEEE Transactions on Ultrasonics, Ferroelectrics, and Frequency Control* **42** (4), 774-780 (1995).
31. Cao, W., Q.M. Zhang, J.Z. Zhao, and L.E. Cross, "Effects of Face Plates on Surface Displacement Profile in 2-2 Piezoelectric Composites," *IEEE Transactions on Ultrasonics, Ferroelectrics, and Frequency Control* **42** (1), 37-41 (1995).
32. Cao, W. and W. Qi, "Plane Wave Propagation in Finite 2-2 Composites," *J. Appl. Phys.* **78** (7), 4627-4632 (1995).
33. Qi, W. and W. Cao, "Finite Element Analysis and Experimental Studies on the Thickness Resonance of Piezocomposite Transducers," accepted *Ultrasonic Imaging* (1995).
34. Cao, W. and W. Qi, "Multisource Excitations in a Stratified Biphase Structure," *J. Appl. Phys.* **78** (7), 4640-4646 (1995).

VOLUME IV

Actuator Studies

35. Uchino, K., "Materials Update: Advances in ceramic actuator materials," *Materials Lett.* **22**, 1-4 (1995).
36. Uchino, K., "Novel Ceramic Actuator Materials."
37. Aburatani, H., K. Uchino, and A.F. Yoshiaki, "Destruction Mechanism and Destruction Detection Technique for Multilayer Ceramic Actuators," *Proc. of the 9th Annual International Symposium on the Applications of Ferroelectrics*, 750-752 (1995).

Actuator Studies (continued)—Volume IV

38. Uchino, K. "Manufacturing Technology of Multilayered Transducers," *Proc. Amer. Ceram. Soc.*, Manufacture of Ceramic Components, 81-93 (1995).
39. Uchino, K. "Piezoelectric Actuators/Ultrasonic Motors--Their Development and Markets," *Proc. 9th ISAF*, 319-324 (1995).
40. Dogan, A., J.F. Fernandez, K. Uchino, and R.E. Newnham, "New Piezoelectric Composite Actuator Designs for Displacement Amplification," in press *Proc. Euroceram 95* (1995).
41. Onitsuka, O., A. Dogan, J.F. Tressler, Q.Su, S. Yoshikawa, and R.E. Newnham, "Metal-Ceramic Composite Transducer, The 'Moonie' ," *J. Intelligent Materials Systems and Structures* **6**, 447-455 (1995).
42. Fernandez, J.F., A. Dogan, J.T. Fielding, K. Uchino, and R.E. Newnham, "Tailoring High Displacement Performance of Ceramic-Metal Piezocomposite Actuators 'Cymbals' ," submitted to *IEEE Transactions on Ultrasonics, Ferroelectrics, and Frequency Control* (1995).
43. Hirose, S., S. Takahashi, K. Uchino, M. Aoyagi, and Y. Tomikawa, "Measuring Methods for High-Power Characteristics of Piezoelectric Materials," *Mat. Res. Soc. Symp. Proc.* **360**, 15-20 (1995).
44. Takahashi, S., S. Hirose, K. Uchino, and K.Y. Oh, "Electro-Mechanical Characteristics of Lead-Zirconate-Titanate Ceramics Under Vibration-Level Change," *Proc. 9th ISAF*, 377-382 (1995).
45. Takahashi, Sadayuki, Yasuhiro Sasaki, Seiji Hirose, and Kenji Uchino, "Electro-Mechanical Properties of $\text{PbZrO}_3\text{-PbTiO}_3\text{-Pb}(\text{Mn}_{1/3}\text{Sb}_{2/3})\text{O}_3$ Ceramics Under Vibration-Level Change," *Mat. Res. Soc. Symp. Proc.* **360**, 305-310 (1995).

VOLUME V

46. Zheng, Jiehui, Sadayuki Takahashi, Shoko Yoshikawa, Kenji Uchino, and J.W.C. de Vries, "Heat Generation in Multilayer Piezoelectric Actuators," submitted to *J. Am. Ceram. Soc.* (1995).
47. Uchino, Kenji, "Review: Photostriction and its Applications," in press *J. Innovations in Mater. Res.* (1995).
48. Chu, Sheng-Yuan, and Kenji Uchino, "Photo-Acoustic Devices Using $(\text{Pb,L a})(\text{Zr,Ti})\text{O}_3$ Ceramics," *Proc. 9th ISAF*, 743-745 (1995).

Integration Issues

49. Matsko, M.G., Q.C. Xu, and R.E. Newnham, "Zig-Zag Piezoelectric Actuators: Geometrical Control of Displacement and Resonance," *J. Intell. Mat. Syst. and Struct.* **6** (6), 783-786 (1995).
50. Xu, Baomin, Qiming Zhang, V.D. Kugel, and L.E. Cross, "Piezoelectric Air Transducer for Active Noise Control," submitted *Proc. SPIE* (1996).

Integration Issues (continued)—Volume V

51. Kumar, S., A.S. Bhalla, and L.E. Cross, "Underwater Acoustic Absorption by Collocated Smart Materials," accepted *Ferroelectric Letters* (1995).
52. Elissalde, Catherine and Leslie Eric Cross, "Dynamic Characteristics of Rainbow Ceramics," *J. Am. Ceram. Soc.* **78** [8], 2233-2236 (1995).

Processing Studies

53. Bowen, Christopher P., Thomas R. ShROUT, Robert E. Newnham, and Clive A. Randall, "Tunable Electric Field Processing of Composite Materials," *J. of Intelligent Material Systems and Structures* **6** (2), 159-168 (1995).
54. Zhang, Q.M., J. Zhao, T. ShROUT, N. Kim, and L.E. Cross, "Characteristics of the Electromechanical Response and Polarization of Electric Field Biased Ferroelectrics," *J. Appl. Phys.* **77** (5), 2549-2555 (1995).
55. Zhao, J., Q.M. Zhang, N. Kim, and T. ShROUT, "Electromechanical Properties of Relaxor Ferroelectric Lead Magnesium Niobate-Lead Titanate Ceramics," *Jpn. J. Appl. Phys.* **34**, 5658-5663 (1995).
56. Zipparo, M.J., K.K. Shung, and T.R. ShROUT, "Piezoelectric Properties of Fine Grain PZT Materials," *Proc. IEEE Int'l Ultrasonics Symposium* (1995).
57. Yoshikawa, Shoko, Ulagaraj Selvaraj, Paul Moses, John Witham, Richard Meyer, and Thomas ShROUT, "Pb(Zr,Ti)O₃[PZT] Fibers—Fabrication and Measurement Methods," *J. Intell. Mat. Syst. and Struct.* **6** (2), 152-158 (1995).
58. Hackenberger, W.S., T.R. ShROUT, A. Nakano, and R.F. Speyer, "Rate Controlled Sintering of Low Temperature Cofired Ceramic Multilayers Used for Electronic Packaging."
59. Randall, C.A., N. Kim, W. Cao, and T.R. ShROUT, "Domain-Grain Size Relation in Morphotropic Phase Boundary, Pb(Zr_{0.52}Ti_{0.48})O₃," 7th US:Japan Mtg. on Dielectric and Piezoelectric Ceramics, Tsukuba, 145-149 (1995).
60. Cann, David P., Clive A. Randall, and Thomas R. ShROUT, "Investigation of the Dielectric Properties of Bismuth Pyrochlores," accepted *Solid State Communication* (1995).

VOLUME VI

61. Mulvihill, Maureen L., Seung Eek Park, George Risch, Zhuang Li, Kenji Uchino, and Thomas R. ShROUT, "The Role of Processing Variables in the Flux Growth of PZN-PT Relaxor Ferroelectric Single Crystals."

Thin Films Ferroelectrics

62. Chen, H.D., K.R. Udayakumar, L.E. Cross, J.J. Bernstein, and L.C. Niles, "Dielectric, Ferroelectric, and Piezoelectric Properties of Lead Zirconate Titanate Thick Films on Silicon Substrates," *J. Appl. Phys.* **77** (7), 3349-3353 (1995).

Thin Films Ferroelectrics (continued)—Volume VI

63. Udayakumar, K.R., P.J. Schuele, J. Chen, S.B. Krupanidhi, and L.E. Cross, "Thickness-Dependent Electrical Characteristics of Lead Zirconate Titanate Thin Films," *J. Appl. Phys.* **77** (8), 3981-3986 (1995).
64. Chen, H.D., K.R. Udayakumar, C.J. Gaskey, and L.E. Cross, "Electrical Properties' Maxima in Thin Films of the Lead Zirconate-Lead Titanate Solid Solution System," *Appl. Phys. Lett.* **67** (23), 3411-3413 (1995).
65. Gaskey, C.J., K.R. Udayakumar, H.D. Chen, and L.E. Cross, "'Square' Hysteresis Loops in Phase-Switching Nb-Doped Lead Zirconate Stannate Titanate Thin Films," *J. Mater. Res.* **10** (11), 2764-2769 (1995).
66. Yamakawa, K., S. Trolrier-McKinstry, J.P. Dougherty, and S. Krupanidhi, "Reactive Magnetron Co-Sputtered Antiferroelectric Lead Zirconate Thin Films," *Appl. Phys. Lett.* **67** (14), 2014-2016 (1995).
67. Ravichandran, D., K. Yamakawa, A.S. Bhalla, and R. Roy, "Alkoxide Derived $\text{SrBi}_2\text{Ta}_2\text{O}_9$ Phase Pure Powder and Thin Films."
68. Thakoor, Sarita, A.P. Thakoor, and L. Eric Cross, "Optical Non-Invasive Evaluation of Ferroelectric Films/Memory Capacitors," *Mat. Res. Soc. Symp. Proc.* **360**, 157-167 (1995).

COMPOSITE SENSORS

APPENDIX 21

CAPPED CERAMIC HYDROPHONES

J.F. Tressler, A. Dogan, J.F. Fernandez, J.T. Fielding, Jr., K. Uchino,
and R.E. Newnham

International Center for Actuators and Transducers
Intercollege Materials Research Laboratory
Pennsylvania State University
University Park, PA 16802

ABSTRACT

Attaching specially shaped thin metal caps, each containing a shallow inner cavity, to the electroded surfaces of a piezoelectric ceramic will significantly enhance its hydrostatic sensitivity. The presence of the cavities allows the metal caps to convert a portion of the incident axial-direction stress into radial and tangential stresses of opposite sign, thus allowing the amplified d_{31} and d_{33} coefficients of the poled ceramic to now add together as opposed to subtracting from one another, thus magnifying the d_b . By capping a PZT-552 disk, the d_b can be amplified by a factor of nearly 100 and the g_b by a factor of almost 50. These particular hydrophones show the most promise for use in shallow water applications.

INTRODUCTION

When a poled piezoelectric ceramic, such as PZT, is subject to a hydrostatic pressure, a charge is developed in the poled direction. The magnitude of this charge is directly proportional to the material's hydrostatic charge coefficient, d_b , which is equal to its response from the thickness mode, d_{33} , plus its response from the planar mode, $d_{31}+d_{32}$. Unfortunately, the d_{31} ($=d_{32}$ due to symmetry) coefficient of PZT is opposite in sign and is approximately half the magnitude of its d_{33} coefficient; therefore, its d_b ($=d_{33}+2d_{31}$) is quite low. In addition, the hydrostatic voltage coefficient, g_b , is small due to the large permittivity of PZT. For instance, the composition PZT-552 used in this study has a d_b of only 50pC/N and a g_b of 2mV·m/N. As a result, bulk PZT exhibits a rather low receive sensitivity and is therefore a generally poor hydrophone if entirely submersed into water.

Over the course of the past 15 years, a number of PZT-polymer composite transducers with various connectivities have been developed

which magnify both the d_b and g_b coefficients and hence exhibit a greater hydrophone sensitivity [1-2]. The enhanced d_b arises mainly from the polymer phase attenuating much of the incident lateral stress, thus minimizing the d_{31} contribution to d_b . These polymer-ceramic composites also exhibit a lower density, which results in a better acoustical impedance match to water and an increased mechanical compliance. Disadvantages of these polymer-PZT composites include a low dielectric constant (i.e. capacitance), a greater pressure dependence on properties, and a high cost due to labor intensive fabrication techniques.

The moonie and cymbal-type transducers are based on the concept of the flextensional transducer and possess a 2-(0)-2 connectivity. These transducers consist of a poled piezoelectric or electrostrictive ceramic disk (fully electroded on each face) sandwiched between two shaped metal electrode endcaps, each containing a shallow air-filled cavity on their inner surface. In the case of the moonie transducer, the cavities are in the shape of a half moon, whereas the cymbal contains a truncated cone-shaped cavity (see Figure 1). The presence of these cavities allows the metal caps to serve as mechanical transformers for transforming a portion of the applied axial-direction stress into tangential and radial stresses of opposite sign. Thus, the d_{31} and d_{33} contributions of the PZT now add in the effective d_b of the device rather than subtract.

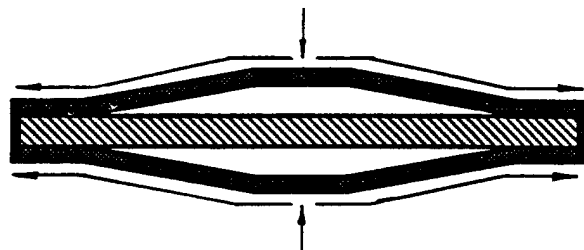


Figure 1: Cross-sectional view of the standard cymbal transducer. Arrows show direction of stress redistribution.

EXPERIMENTAL PROCEDURE

Cymbal Fabrication

Using metal foil between 120 μ m and 380 μ m thick, 12.7mm diameter caps were simultaneously cut and shaped. The cavity was 9.0mm in diameter and ranged in depth from 120 μ m to 500 μ m. These caps were then adhered to 1.00mm thick, 12.7mm diameter poled PZT-552 disks (Piezo Kinetics) using Emerson and Cuming insulating epoxy. To ensure proper alignment of the caps, the entire assembly was kept under pressure in a special die during the 24 hour curing step.

Cymbal Characterization

In order to characterize the quality of the metal-PZT bond, the admittance as a function of frequency was measured using an HP 4194A Impedance Analyzer. This technique was found to be very sensitive to both defects in the bonding layer as well as the presence of an unsymmetric bonding layer [3].

The capacitance, C , of the cymbal transducer was measured in air at both 100 Hz and 1 kHz using a Stanford Research Systems Model SR 715 LCR Meter. In addition, the capacitance was remeasured under hydrostatic pressure at 1 kHz using an HP 4192A LF Impedance Analyzer. The dielectric constant, K , was calculated from equation (1),

$$K = Ct/\epsilon_0 A \quad (1)$$

where A is the electrode area of the ceramic (12.7mm), t is the total thickness of the transducer, and ϵ_0 is the permittivity of free space.

d_h measurement

The effective d_h of the cymbal transducer as a function of hydrostatic pressure was measured using the system shown in Figure 2. The oil in the hydrostatic pressure chamber served as a sonic medium for the transmission of pressure (in this case at 30 Hz). The sample was exposed to this pressure equally in all directions and the charge in the poled direction was measured. At the same time a standard, Ca-doped lead titanate, with known d_h mounted next to the sample was measured in the same way while exposed to identical conditions. The d_h (short circuit current) was measured instead of g_h (open circuit voltage) since a single amplifying circuit

converted the current into a proportional voltage, thus reducing the problem of noise pickup and eliminating the problem of loading high impedance transducers. The relationship between the time-varying charge in the sample (dQ/dt) which produces current at the input of the op-amp, and the output voltage makes this circuit a current to voltage converter. Since the output voltage from the sample was compared to a standard, the exact value of the feedback resistor, R_f , became immaterial. The voltage at the input of the op-amp was equal to or nearly equal to zero volts (a virtual ground), thus making for a short-circuit measurement. In addition, all the voltages in the wiring connected to the samples were at ground, essentially eliminating the effect of stray capacitance between them and any other point in the system.

The effective hydrostatic voltage coefficient, g_h , for the hydrophone can be calculated from the measured d_h , as given in equation (2). The g_h coefficient is proportional to the hydrophone receive sensitivity, which is equal to the open circuit voltage measured at the terminals of a hydrophone per unit incident pressure.

$$g_h = d_h / K\epsilon_0 \quad (2)$$

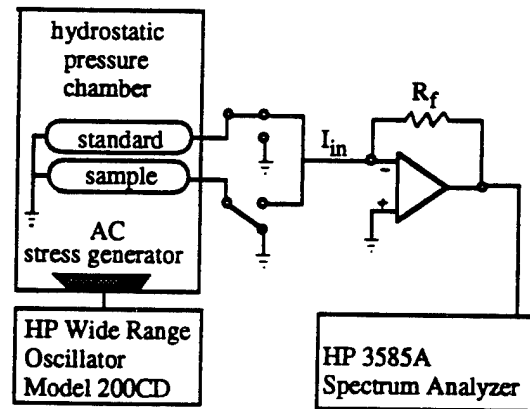


Figure 2: Experimental set-up used for performing d_h measurements.

EXPERIMENTAL RESULTS

The results presented in this paper will focus on the cymbal transducer, as the hydrostatic properties of the moonie transducer have been reported previously [4]. Figure 3 shows the admittance spectrum of a cymbal transducer with brass caps 250 μ m thick and a cavity depth

of 250 μ m. The first resonance, at 17kHz, is associated with the flexensional, or umbrella, mode of the endcaps, whereas the resonance at 175kHz is due to the radial mode of the ceramic. Sharp resonance peaks, combined with the absence of any spurious modes between the two primary resonances, are indicative of a high-quality metal to ceramic bond.

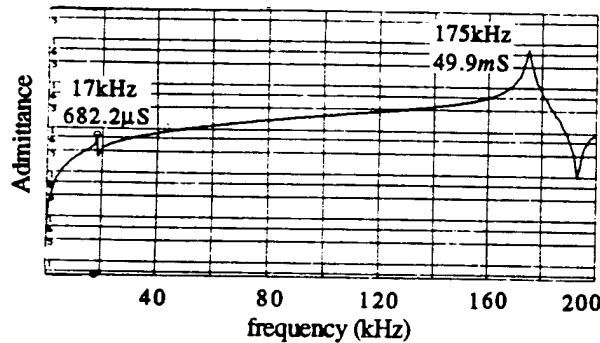


Figure 3: Admittance as a function of frequency for a cymbal transducer.

Figure 4 shows the dielectric constant and loss of a 2.0mm thick cymbal transducer (with brass endcaps) measured at 1kHz as a function of hydrostatic pressure. The capacitance of the cymbal was measured to be 3500pF, which is the same as when measured in air, and is about ten percent less than that of the bulk PZT-552 disk itself. The loss is also similar to that measured in air and is slightly larger than that of the bulk PZT due to the presence of the epoxy layer. The dielectric constant is independent of pressure within the working range of the hydrophone (1.4MPa).

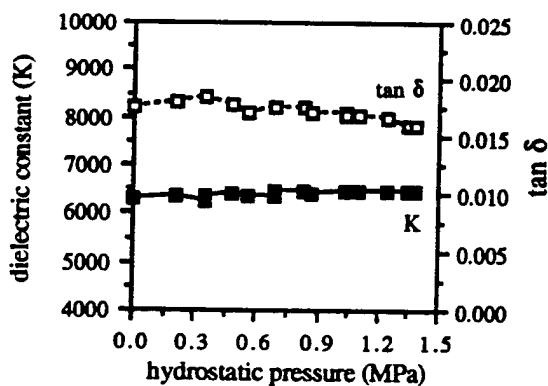


Figure 4: Dielectric constant and loss measured under pressure at 1kHz for a cymbal transducer with brass caps 250 μ m thick and a cavity depth of 250 μ m.

Figure 5 shows the pressure dependence of the effective d_h and g_h coefficients for various cymbal cap materials. The data show that as the cap material becomes stiffer, the pressure tolerance increases, but at a cost of reduced sensitivity. This is due to the stiffer metals being less able to radially transfer the incident axial stress to the ceramic. The more compliant metals, such as brass, can magnify the d_h of the PZT by a factor of 90 and the g_h by a factor of 45. Even very stiff metals like tungsten can amplify the d_h and g_h values of the PZT by factors of 30 and 15, respectively.

Both the d_h and g_h coefficients remain relatively constant within a certain working pressure range for each endcap material. For instance, kovar cymbals can be used repeatedly up to about 3MPa. However, once this range has been exceeded, the high sensitivity is not recoverable, presumably due to a buckling of the endcaps.

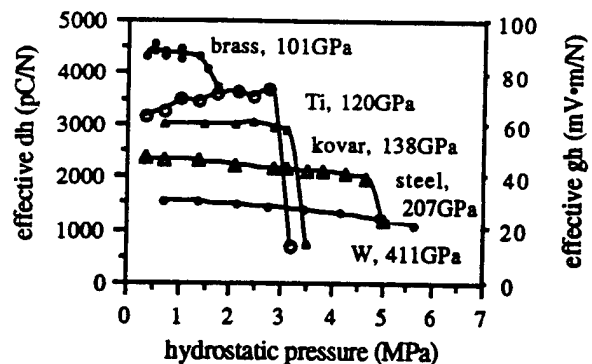


Figure 5: Effect of cap material (shown with its Young's Modulus) on the d_h and g_h of the cymbal transducers.

The first resonance frequency of the cymbal transducer with different cap materials is shown in Figure 6. This frequency appears to increase linearly as a function of the resonance frequency of a thin circular metal plate clamped around its circumference, and depends upon the metal's stiffness, density, and Poisson's ratio [5]. These results show that for a hydrophone with given dimensions, the resonance frequency can be varied simply by changing the cap material.

Figure 7 shows the influence of cap thickness on both the d_h and g_h coefficients. As cap thickness increases from 120 μ m to 380 μ m, pressure tolerance increases, but again at the cost of reduced sensitivity. For the transducer with 120 μ m thick caps, a $d_h \cdot g_h$ product exceeding $10^6 \times 10^{-15} \text{ m}^2/\text{N}$ is achieved, which is the highest ever reported for this size of hydrophone.

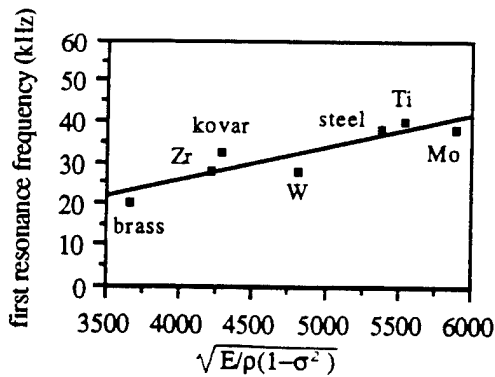


Figure 6: Effect of cap materials on the first resonance frequency of the transducer. In each case the caps were 250 μm thick and the cavity was 250 μm deep.

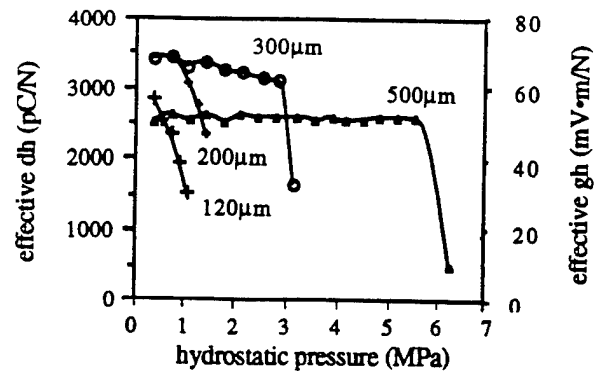


Figure 8: Effect of cavity depth on the d_b and g_b coefficients. The cap material was 250 μm thick kovar.

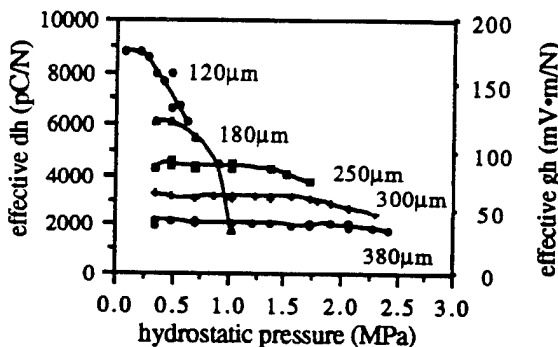


Figure 7: Influence of cap thickness on the d_b and g_b values. The cap material was brass with a 250 μm deep cavity.

Figure 8 shows how the cavity depth effects the d_b and g_b coefficients as a function of pressure. Very shallow cavities collapse at low pressures and do not permit the caps to transform axial stress into radial stresses very well, which accounts for the low sensitivity. As the cavity depth increases, both the pressure tolerance and the sensitivity are enhanced. At a cavity depth of 500 μm , though, the sensitivity decreases. This is due to the cavity shape now approaching that of a dome, which is very adept at withstanding very high pressures, as seen in the data, but is not as effective in transforming axial stress into radial stresses. Nevertheless, both the d_b and g_b coefficients are still quite high, 2500pC/N and 50mV·m/N, which are 50 and 25 times the value of the PZT, respectively.

CONCLUSIONS

The cymbal-type hydrophone is characterized by very large d_b and g_b coefficients while retaining the high dielectric constant (capacitance) and low losses of the piezoceramic. The pressure dependence of the sensitivity can be tailored simply by changing the cap material, cap thickness, or cavity shape. These transducers have the advantage of being thin, lightweight, and inexpensive to fabricate.

REFERENCES

- [1] R.Y. Ting, "Evaluation of New Piezoelectric Composite Materials for Hydrophone Applications," *Ferroelectrics*, vol. 67, pp. 143-157, 1986.
- [2] R.Y. Ting, "A Review on the Development of Piezoelectric Composites for Underwater Acoustic Transducer Applications," *IEEE Trans. on Inst. and Msmt.*, vol. 41, no. 1, pp. 64-67, Feb. 1992.
- [3] A. Dogan, S. Yoshikawa, K. Uchino, and R.E. Newnham, "The Effect of Geometry on the Characteristics of the Moonie Transducer and Reliability Issue," *Ultrasonics Symposium Proceedings*, 1994, pp. 935-939.
- [4] Q.C. Xu, S. Yoshikawa, J.R. Belsick, and R.E. Newnham, "Piezoelectric Composites with High Sensitivity and High Capacitance for Use at High Pressures," *IEEE Trans. on UFFC*, vol. 38, no. 6, pp. 634-639, Nov. 1991.
- [5] L.E. Kinsler, A.R. Frey, A.B. Coppens, and J.V. Sanders, *Fundamentals of Acoustics*, 3rd edn. New York: John Wiley & Sons, 1982, ch. 4, pp. 92-95.

APPENDIX 22

Accelerometer Application of the Modified Moonie (Cymbal) Transducer

Burhanettin KOC, Aydin DOGAN, Jose F. FERNANDEZ,

Robert E. NEWNHAM and Kenji UCHINO

International Center for Actuators and Transducers, Materials Research Laboratory,

The Pennsylvania State University, University Park, PA 16802, USA

(Received:)

The modified Moonie (Cymbal) transducer has been investigated for an accelerometer application. High effective piezoelectric charge coefficients (d_{33}) of the Cymbal transducer was observed around 15000 pC/N, which is much higher than that of the piezoelectric ceramic itself (~550 pC/N). With this feature the Cymbal trasducer is a good candidate for high sensitive accelerometer applications. The sensitivity of the Cymbal accelerometer was measured as a function of driving frequency and compared with the single plate ceramic disk which was used as driving component in the transducer. Besides, the geometry of the transducer such as endcap thickness, the effect of different PZT compositions and metal endcaps on sensitivity was investigated. The sensitivity 50 times better than the PZT disk was obtained.

KEYWORDS: accelerometer, piezoelectric effect, modified Moonie (Cymbal) transducer, sensitivity

1. Introduction

Accelerometers are used widely throughout engineering, both as research and development tools and as control-system components. However, the most popular application area is using of accelerometer for vehicle dynamics.¹⁾ Since the market especially for vehicle dynamics is very large, various types of accelerometer design have been reported.²⁻⁷⁾

One of the most popular techniques to measure acceleration is using the piezoelectric effect of materials. In the piezoelectric effect, no matter which mode is used, such as compression (longitudinal), bending or shear, the sensitivity of acceleration sensor depends on piezoelectric charge coefficients of the material. When a longitudinal mode is used, the sensitivity is directly proportional to d_{33} of the material. PZT-based ceramics exhibit a large d_{33} constant, but still it is not high enough to measure acceleration efficiently. Therefore, PZT-polymer composites have been used by Ohara and Miyayama and the sensitivity has been tripled in comparison with the single PZT plate.²⁾ The other way of improving sensitivity taken by Ohtsuki et al. was using multilayer piezoelectric ceramics,⁴⁾ with sacrificing the cost. Since piezoelectric sensors have various advantages such as fast response, which is very important for shock measurement, and simple detecting circuits, they are preferred for some applications such as safety and suspension systems in the automobile. A metal-piezoceramic composite structure with very high effective d_{33} constant may be a good alternative for acceleration sensors.

A metal-ceramic composite design, Moonie, was first used for hydrophones which sense weak pressure wave in fluid.⁸⁾ The metal endcaps of the Moonie were recently modified, and as an actuator higher displacements were obtained than multilayer actuators (See Fig. 1a).^{9,10)} The new transducer, "Cymbal", named after the endcap shape like cymbals, has also higher piezoelectric charge coefficients and an easy production method than the Moonie trasducer.

In this study, the cymbal transducer has been used to detect acceleration, with metal endcaps transferring a longitudinal stress into a radial stress. When the metal endcaps move radially due to the compressive stress, the bonded PZT disk is stretched. Therefore, the ineffective d_{31} of a single PZT

disk becomes effective, and that causes higher effective piezoelectric charge coefficient (d_{33}^{eff}) and thus much higher sensitivity.

Fig 1(a)
Fig 1(b)

2. Acceleration Sensitivity of the Cymbal

The force from a mass (m) due to acceleration ($F=ma$) is transferred through the two metal endcaps on to the PZT thin disk, and it causes a stress toward the circumference of the ceramic disk, most of which is in the radial direction and some part of which acts as a compressive stress in the thickness direction (Fig. 1 b)).

The polarization vector due to the stress acting on the polycrystalline piezoelectric disk is defined as:

$$\begin{bmatrix} P_x \\ P_y \\ P_z \end{bmatrix} = \begin{bmatrix} 0 & 0 & 0 & 0 & d_{15} & 0 \\ 0 & 0 & 0 & d_{15} & 0 & 0 \\ d_{13} & d_{13} & d_{33} & 0 & 0 & 0 \end{bmatrix} \begin{bmatrix} X_1 \\ X_2 \\ X_3 \\ X_4 \\ X_5 \\ X_6 \end{bmatrix}, \quad (1)$$

where, P_x , P_y and P_z are the polarization vectors in a cartesian coordinate, d_{13} , d_{33} and d_{15} are the piezoelectric charge coefficients of radial, longitudinal and shear mode and X_i 's ($i=1, \dots, 6$) are the stress components. In a cylindrical coordinate system, which is more suitable for the geometry of the piezoelectric thin disk, the stress components are;

$$X_1 = X_2 = -K_r F \quad (2)$$

$$X_3 = K_z F$$

and

$$X_4 = X_5 = X_6 = 0.$$

Then the polarization vector can be obtained as

$$P_z = (d_{33}K_z - 2d_{31}K_r)F. \quad (3)$$

Here, the proportional constants, K_r and K_z , depend on geometry of the metal endcaps and the piezoelectric ceramic disk such as thicknesses of the metal and ceramic disks, cavity angle of the metal endcap θ , Young's modulus of the metal endcaps and diameter of the piezoelectric disk. Note that the negative value of d_{13} acts positively because of the negative sign of the summation. Then, charge generation for the whole disk can be defined as:

$$Q = \pi r_2^2 (d_{33}K_z - 2 d_{31}K_r)m a \quad (4)$$

and finally the charge sensitivity of this transducer defined by the charge generation by unit acceleration becomes:

$$S_q = \pi r_2^2 (d_{33}K_z - 2 d_{31}K_r)m \quad [pC/(m/s^2)] \quad (5)$$

3. Experimental Procedure

The composite transducers were made of electroded ceramic disks (12.7 mm in diameter and 0.5, 1 or 2 mm in thickness) and metal endcaps (12.7 mm in diameter with thickness ranging from 0.18 to .30 mm). Piezoelectric properties of the PZT disks and elastic characteristics of the metal endcaps are given in Table I and Table II, respectively. Truncated-cone shape endcap was fabricated first by punching and then pressing the metal sheet up to 100 MPa to give 250 μ m cavity depth. The ceramic disk and metal endcaps were bonded together around the circumference with two component epoxy (Eccobond). The epoxy was distributed by taking care neither to fill the cavity nor to make open circuit between the endcaps and the electroded face of the PZT. After 24 hours epoxy curing process under a small pressure, the samples became ready for the measurements.

Table, 1
Table, 2

Figure 2 shows the experimental setup of the sensitivity measurement of the metal-ceramic composite transducer. The transducer was fixed with added mass(8.4 g) inside a housing unit. A commercialized accelerometer (PCB 302A02) was mounted on the top of the housing unit to produce a reference signal. A mini-shaker (Bruel & Kjaer 4810) was used to produce vibration. A charge amplifier circuitry has been used during the Cymbal and the single PZT disk measurement. The output signals (mV/G) of the purposed transducer and the commercial accelerometer were measured simultaneously with a digital oscilloscope (Tektronix TDS 310)

Fig 2

4. Result and Discussion

The metal endcaps of the Cymbal transducer transfer some part of the acceleration stress in the normal direction into the radial direction. Therefore, the sensitivity of the transducer depends not only on d_{33} but also on d_{31} of the piezo-ceramic. The Cymbal transducers with different piezoelectric

ceramics whose piezoelectric charge coefficients are different, are compared in Fig. 3. The ceramic with the larger d_{33} and d_{31} in magnitude provides the higher sensitivity. As shown in Table I, PZT-5H shows the highest d_{31} constant, and also shows the highest sensitivity to the acceleration. The identical zirconium endcaps were used for all transducers.

Fig 3

Figure 4 shows the sensitivity versus frequency of the PZT-5H single disk and of the Cymbal transducers with various metal endcaps. The output of the Cymbal transducer with Zirconium end caps was found to be about 50 times as large as that in PZT-5H itself. Considering the Young's modulus and the density of the PZT 5H ceramic ($E = 71 \text{ GPa}$, $\rho = 7.5 \text{ g/cm}^3$), it may be concluded that the elastic properties similar to the PZT are required to transfer the acceleration force effectively. It is also possible to compensate thermal dilatation effect on the piezoelectric material by choosing a suitable endcap metal. For example, when tungsten endcaps have been used temperature insensitive displacement actuators have been obtained.¹¹⁾

Fig. 4

The transferred stress from the metal endcaps, which act as springs, to the ceramic material depends also on the endcap geometry. Then, the sensitivity of the transducer is strongly affected by the thickness of the endcaps. When the endcaps are too thin, they deform without stretching the ceramic causing energy loss. On the contrary when they are too thick, they can not produce enough momentum in the radial direction, but the longitudinal stress on the edge of the ceramic disk. Figure 5 shows the endcap thickness dependence of the sensitivity. The thickness 0.18 mm provided the highest sensitivity for the brass endcaps.

Fig. 5

5. Conclusion

A metal-ceramic composite structure (Cymbal transducer) has been investigated for accelerometer applications. The Cymbal transducer has provided 50 times better sensitivity than the single PZT disk, which was used to make the Cymbal transducer.

The most significant result was that the sensitivity of the proposed acceleration transducer depended on the geometry and the structure such as the cavity dept, thickness, Young's modulus of the metal endcaps as well as piezoelectric properties.

References

- 1) G.A Macdonald: Sensors and Actuators **A21-23** (1990) 303.
- 2) Y. Ohara and M. Miyayama: Sensors and Actuators **A36** (1993) 121.
- 3) R.P. Sion, J.K. Atkinson and J.D. Turner: Sensors and Actuators **A37-38** (1993) 348.
- 4) Y. Ohtsuki, Y. Fuda and T. Yoshida: Jpn. J. Appl. Phys. Vol. **32** Part 1, No. 9B (1993) 4209.
- 5) K. Sato, K. Okamoto, Y. Fuda and T. Yoshida: Jpn. J. Appl. Phys. Vol. **33** Part 1, No. 9B (1994) 5378.
- 6) E. Abbaspour-Sani, R-H. Huang and C.Y. Kwok: Sensors and Actuators **A44** (1994) 103.
- 7) R., Hiratsuka, D.C. van Duyn, T. Otaredian and P. De Vries: Sensors and Actuators **A32** (1992) 380.
- 8) Q. C. Xu, S. Yoshikawa, J. R. Belsick and R. E. Newnham, IEEE UFFC Vol. **38** No. 6 (1991) 634.
- 9) A. Dogan: "Flextensional "Moonie & Cymbal" Actuators", Ph. D. Dissertation; (1994)
- 10) A. Dogan: "Flextensional Cymbal Transducer", USA Patent Application. PSU Invention Disclosure no. 94-1375, (1994)
- 11) J.F. Fernandez, A.Dogan, J.T.Fielding, , K. Uchino and R.E. Newnham, "Tailoring High Displacement Performance of Ceramic-Metal Composite Actuators "Cymbals"", IEEE UFFC, submitted.

Figure Captions

Figure 1. a) Structure of the modified Moonie (Cymbal).

b) Schematic compressive force transformation to the radial direction on a ideal metal endcap.

Figure 2. Experimental setup for the sensitivity measurement.

Figure 3. Dependence of the acceleration sensitivity on the PZT composition.

Figure 4. Sensitivity for various metal endcaps.

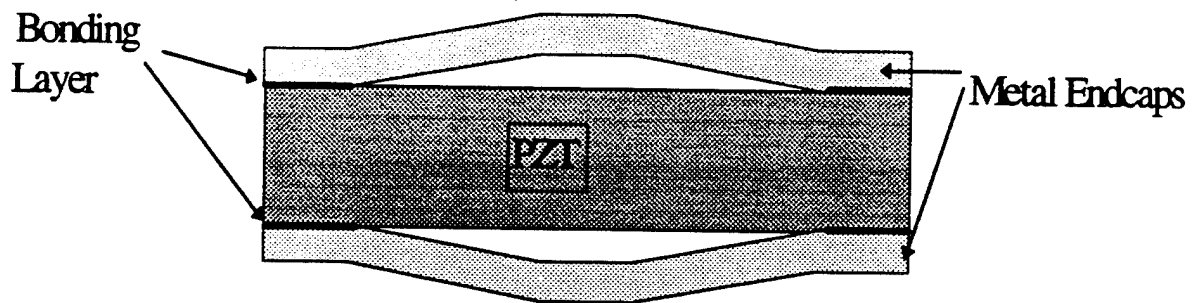
Figure 5. Dependence of the sensitivity on the endcap thickness.

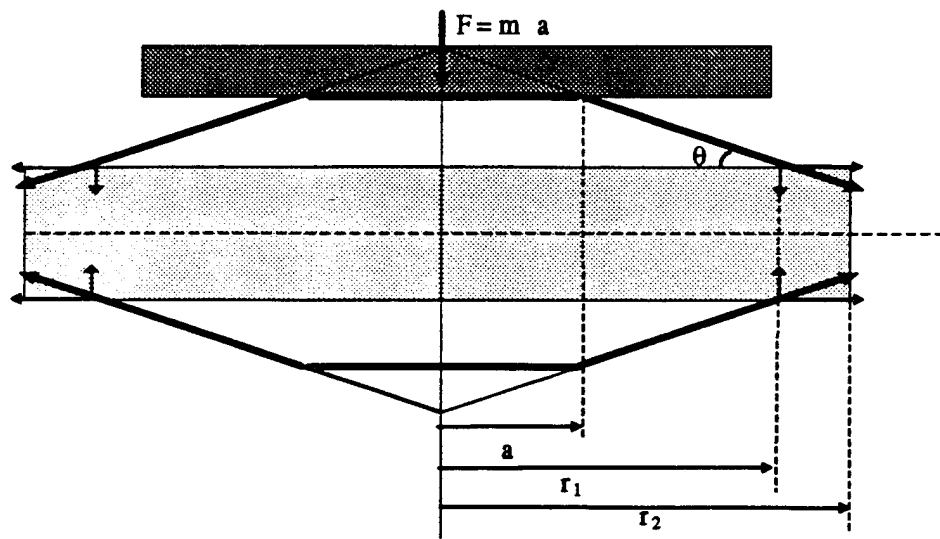
Table I. Piezoelectric properties of PZT disks used in the Cymbal transducer

CERAMIC	ϵ'	$\text{tg}\delta$	$d_{31}(\text{pC/N})$	$d_{33}(\text{pC/N})$
PZT 8D	1104	0.003	-107	289
PZT 5A	1802	0.016	-208	429
PZT 5H	3500	0.016	-285	581

Table II. Elastic characteristics of metal endcaps used in the Cymbal transducer

Metal Endcap	Density (g/cm ³)	Young's Modulus (E) (GPa)
Zirconium	6.49	77
Brass	8.53	110
Tungsten	19.30	405
PZT 5H	7.5	71





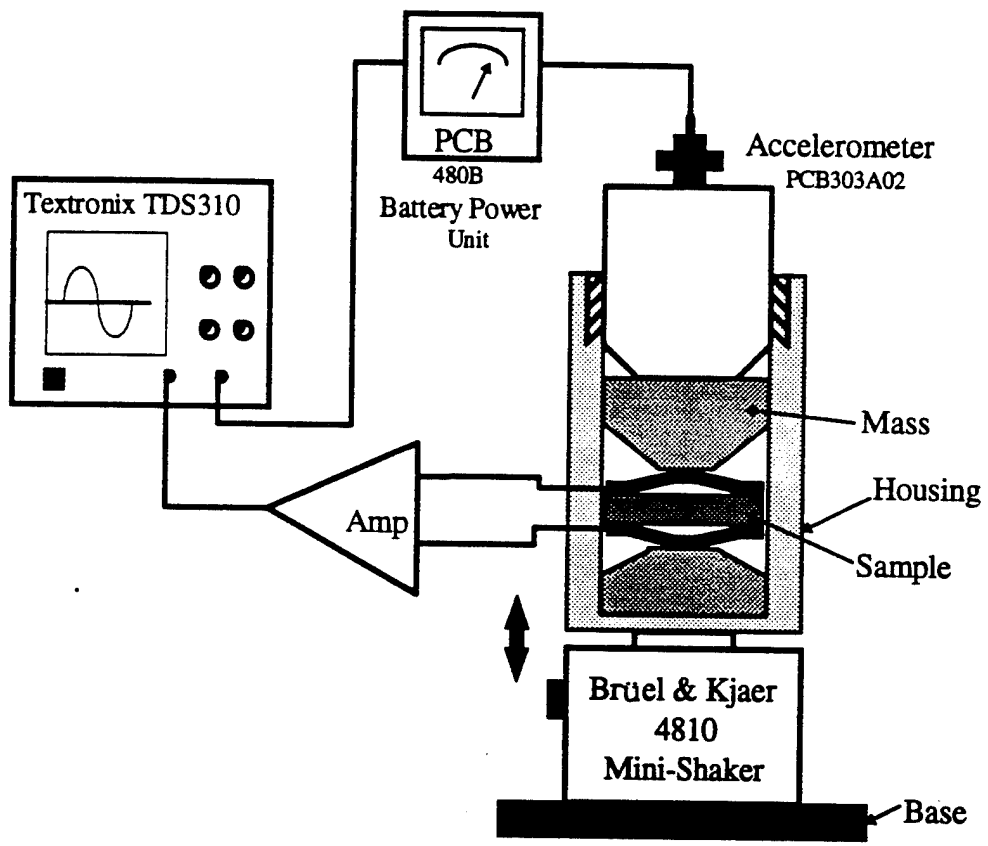


Figure 2, B. KOC, A. DOGAN, J. F. FERNANDEZ, R. E. NEWNHAM and K. UCHINO

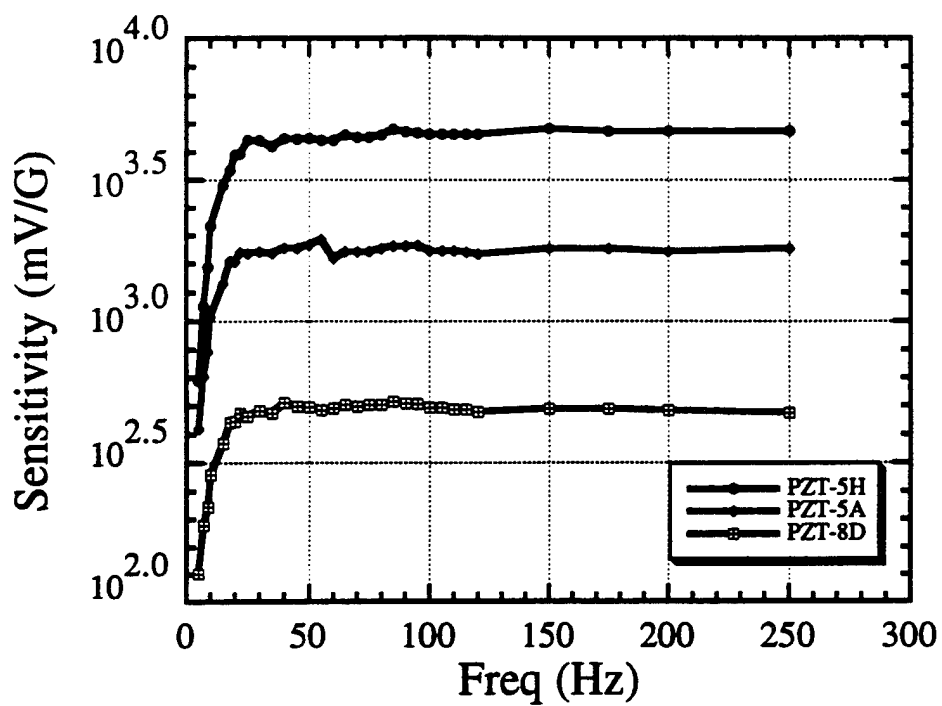


Figure 3. B. KOC, A. DOGAN, J. F. FERNANDEZ, R. E. NEWNHAM and K. UCHINO

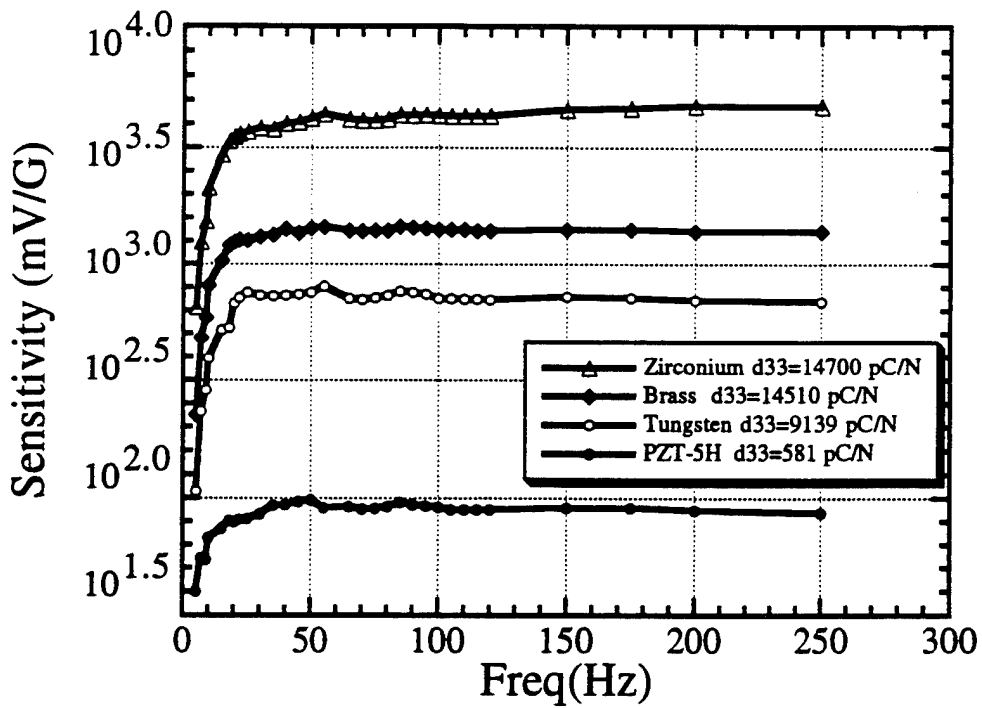


Figure 4, B. KOC, A. DOGAN, J. F. FERNANDEZ, R. E. NEWNHAM and K. UCHINO

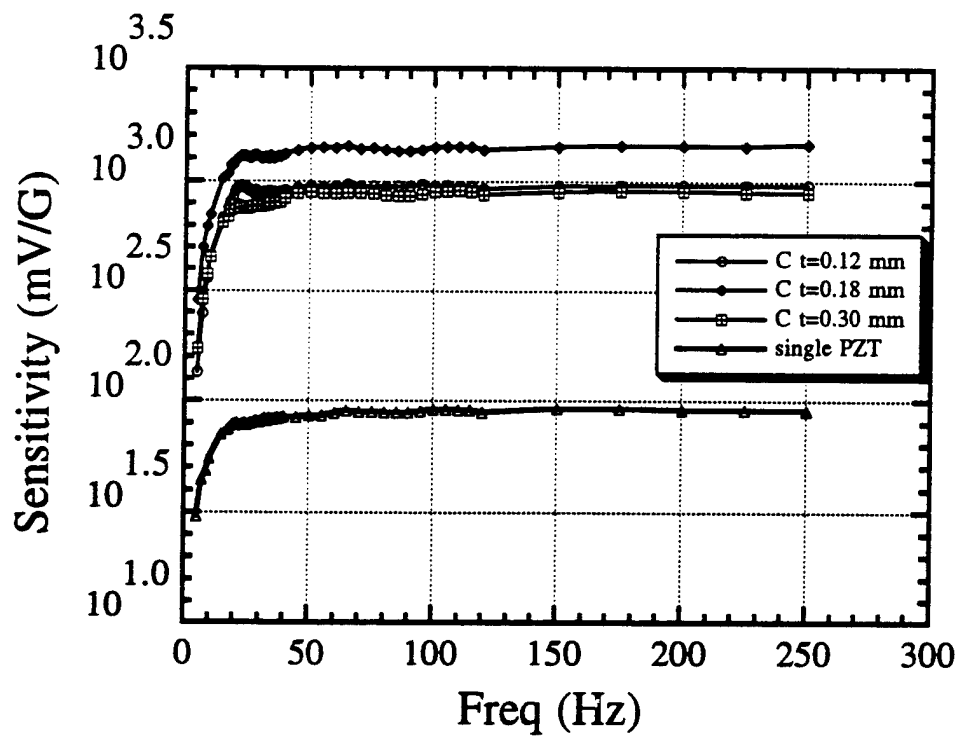


Figure 5. B. KOC, A. DOGAN, J. F. FERNANDEZ, R. E. NEWNHAM and K. UCHINO

APPENDIX 23

EFFECTS OF FACE PLATES AND EDGE STRIPS ON HYDROSTATIC PIEZOELECTRIC RESPONSE OF 1-3 COMPOSITES

J. ZHAO, Q. M. ZHANG† and WENWU CAO

*Intercollege Materials Research Laboratory, The Pennsylvania State University,
University Park, PA 16802, U.S.A.*

(Received May 2, 1995)

Piezoceramic-polymer composites with 1-3 connectivity provide higher hydrostatic figure of merit $d_h g_h$ and low density, which make them attractive for underwater applications. By incorporating rigid face plates on the composite electrode surfaces, the transverse piezoelectric response can be reduced effectively and d_h increased significantly. When edge strips are put on the lateral dimensions, the hydrostatic response of the composite may be further improved, depending on the ratio of the sample thickness to the sample lateral dimensions and the elastic properties of the edge strips. In this work the effects of the rigid face plates and the edge strips on the piezoelectric response of 1-3 composites with different lateral dimensions were investigated. All the experimental features can be well accounted for by using the shear-coupling model developed recently by us and the isostrain model. Based on these results the relationship between the d_h of the face plated 1-3 composite and the elastic properties of the polymer matrix as well as other design parameters is derived, which can serve as a guideline to optimize the material selection for 1-3 composites with larger hydrostatic response.

Keywords: Piezocomposite, hydrostatic piezoelectricity, mechanical properties.

I. INTRODUCTION

Piezoelectric ceramic-polymer composites with 1-3 connectivity possess many promising features which make them attractive for hydrostatic applications.^{1–5} As has been demonstrated, both theoretically and experimentally, with a small aspect ratio of the ceramic rods and a proper ceramic content, the piezoelectric hydrostatic figure of merit $d_h g_h$ (d_h and g_h are the piezoelectric hydrostatic charge and voltage coefficients respectively) of a composite can be substantially higher than the constituent ceramic phase.^{2,6} However, to fully utilize the potential of a 1-3 composite for hydrostatic applications, several issues have to be addressed. Small aspect ratio of ceramic rods will incur a high manufacturing cost and low reliability of the rods. The Poisson's ratio effect, which reduces the effect pressure on the polymer matrix in the ceramic rod poling direction by a factor of $(1 - 2\sigma)$ where σ is the Poisson's ratio of the polymer phase, drastically cuts down the effectiveness of the stress transfer from the polymer to the ceramic rods.⁷ In the past, a great deal of effort have been devoted to address these issues and some progress has been made. One of the effective ways to improve the hydrostatic response of a 1-3 composite is to glue rigid face plates on the two electrode surfaces, as schematically drawn in Figure 1(a). Throughout this paper, the following convention will be used: the 3-direction (or the z -direction) is along the ceramic rod axial (poling) direction, the 1 and 2-directions (or x and y -directions) are in the plane perpendicular to the poling directions.

†Author to whom all correspondence should be addressed.

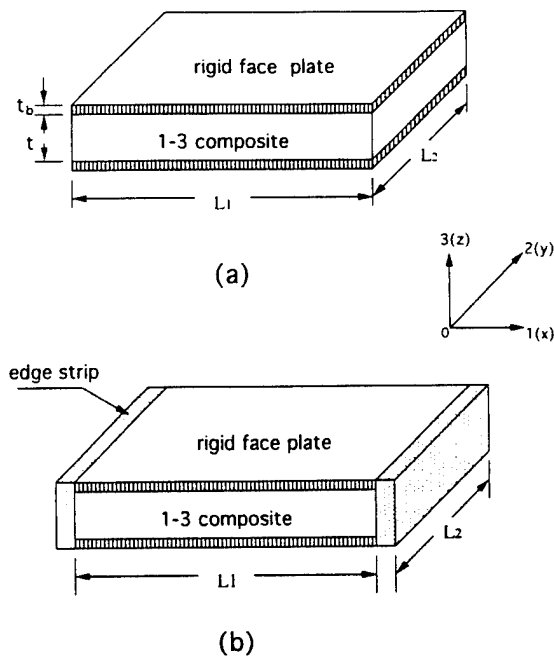


FIGURE 1 (a) Schematic drawing of a face plated 1-3 composite, (b) schematic drawing of a face plated 1-3 composite with edge strips at two end faces in the 1-direction.

The effect of rigid face plates on a 1-3 piezocomposite can be summarized as follows: (1) it improves the stress transfer between the ceramic rods and polymer matrix in the ceramic poling direction so that the composite approaches the isostrain situation; (2) it improves the bonding between the ceramic rods and polymer matrix; (3) it reduces Poisson's ratio effect and the d_{31} effect. The effect (1) has been investigated and the results have been reported in another publication.⁸ The reason for effect (2) is quite obvious. In this paper, the results of a recent investigation on effect (3) will be presented and in all the discussion, the stress transfer in the 3-direction is assumed to be that of isostrain results due to the face plates.

When rigid face plates are glued onto the two faces of a 1-3 composite, due to the fact that the elastic stiffness of the plates is much higher than that of the composite in the lateral dimensions, most of the pressure in these directions will be born by the face plates, which reduces the effective d_{31} and d_{32} coefficients of the whole sample and increases d_h since $d_h = d_{33} + d_{31} + d_{32}$. In addition to that, the much reduced lateral pressure on the polymer matrix greatly reduces the Poisson's ratio effect.

Based on an earlier work by Wang *et al.*⁹ to treat the clamping effect of the face plates on 1-3 composites and the isostrain model^{2,3,5} to calculate the effective material properties of the composite, a theoretical treatment will be presented in this paper, which quantitatively analyzes how various parameters affect these two effects and provides a general guideline to the design of a face plated 1-3 composite.

For a face plated 1-3 composite, as shown schematically in Figure 1(a), the clamping effect of the face plates in the lateral dimensions is through shear force, a situ-

ation quite similar to a 2-2 composite. As has been demonstrated earlier,^{2,10} the effectiveness of this clamping effect will depend on the sample dimension, especially, the ratio of the 1-3 composite thickness t to its lateral dimension L . To evaluate this dimensional effect, experiments were carried out systematically on 1-3 composites with different ratio of t/L . The results are in excellent agreement with the theoretical calculation based on the shear coupling model.¹⁰

To improve the stress transfer in the lateral directions between the face plates and 1-3 composite, one can put edge strips on the end faces of the face plated 1-3 composite, as schematically drawn in Figure 1(b). The effect of the edge strips on the hydrostatic response of 1-3 composite with different dimensions was also investigated and will be reported in the paper.

II. EXPERIMENTS

Two 1-3 composites with 15% volume content ceramic rods and different polymer matrix were made and tested. The polymer matrix for the first composite (labeled as composite I) is Spurr's epoxy and the second one (labeled as composite II) is polyurethane mixed with 50% volume of microballon of about 20 μm size. As listed in Table I, the two have quite different elastic properties.¹¹ The ceramic rods of lead zirconate titanate (PZT) used for the two composites were manufactured by CPSS Co. (MA). The composition of the rods is similar to that of PZT-5H and the diameter of the rods is 1.10 mm. The piezoelectric and dielectric properties of the PZT rods used for the two composites are also listed in Table I. Both composites were poled at a poling voltage of 25 kV/cm at room temperature for three minutes.

The initial dimensions of the composite with Spurr's epoxy matrix are: $t = 5.62$ mm, $L_2 = 27$ mm, and $L_1 = 38.5$ mm. Brass plates with thickness $t = 0.79$ mm were used as the face plates and J-B weld cement of J-B weld Co. was used to glue the brass plates to the composite. Glass reinforced polymer (GRP) plate ($t = 1.6$ mm) and alumina plate ($t = 3.5$ mm) were tested for edge strip materials. The bonding between the edge strip and face plated 1-3 composite was provided by a 5 minute epoxy of Devcon Corporation.

The initial dimensions of the composite with polyurethane mixed with 50% microballon matrix are: $t = 5.54$ mm, $L_2 = 35$ mm, and $L_1 = 52.5$ mm. Since the elastic stiffness of the polymer matrix here is much lower than that of Spurr's epoxy, a GRP plate ($t = 1.6$ mm) was used for the face plates. Silver epoxy (Insulating Materials Inc.) was used to glue the face plates and 1-3 composite together. For this structure, only alumina plates ($t = 3.5$ mm) were used as edge strips. The elastic properties of the face plate materials as well as the plates thickness are summarized in Table II.¹²

The effective dielectric constant ϵ , the piezoelectric hydrostatic charge coefficient

TABLE I
Some properties of the polymer matrix and PZT rods for the two composites

	s'_{11} (m^2/N)	σ^p	d_{33} (pC/N)	d_{31} (pC/N)	ϵ
Composite I	$2 \cdot 10^{-10}$	0.36	450	-208	2333
Composite II	$5 \cdot 10^{-8}$	0.36	481	-222	2533

TABLE II
Properties of face plates

	t (mm)	s_{11} (m^2/N)	s_{12}
GRP	1.6	2.63×10^{-11}	-0.789×10^{-11}
Brass	0.79	0.97×10^{-11}	-0.32×10^{-11}

d_h , piezoelectric d_{33} coefficients were evaluated for these composites. Surface profile scans using a double beam laser dilatometer were also made to characterize the nonuniform strain distribution in the face plated 1-3 composites.¹³ The dielectric constant was measured using a HP multi-frequency RLC meter (HP 4192A). The d_h was measured by a comparison method where the test sample and a standard sample with known d_h value are subjected to the same quasi-static pressure (50 Hz) and the charge outputs from the two samples were compared. d_{33} coefficient of the samples was measured using both a Berlincourt d_{33} meter and a laser dilatometer. The effective d_{31} coefficient of the composites was evaluated using a laser dilatometer and will be discussed in detail later in the text. The dimensional effect of face plated 1-3 composites was investigated by reducing the sample length L_1 while keeping L_2 constant. All the relevant material parameters were evaluated for samples with different L_1 .

To distinguish the hydrostatic charge coefficient d_h measured for a 1-3 composite without face plates and with face plates, d_h and d_h^f are used corresponding to the two situations. The same convention will also be used for the other parameters when needed.

III. EXPERIMENTAL RESULTS FOR COMPOSITE I

Shown in Figure 2 is d_h^f of face plated 1-3 composite with Spurr's epoxy matrix measured at different L_1 . For comparison, d_h of the composite without face plates was also measured and it is 43 pC/N. Clearly, without face plates, d_h of the composite is not any better than the ceramic rods even though its $d_h g_h$ value is improved owing to the smaller effective dielectric constant of the composite. Face plates significantly increase the hydrostatic piezoelectric response of a composite. Figure 2 also shows that d_h^f decreases drastically with decreasing L_1 , which is caused by the incomplete clamping of the face plates on the 1-3 composite for samples with large t/L ratio.

If the composite is effectively clamped in the lateral dimensions by the face plates, it is expected that the whole sample will exhibit very small d_{31} and d_{32} coefficients. Figure 3(a) shows the lateral strain profiles, measured by the double beam laser dilatometer, in the 1-direction of face plated composite for different L_1 while L_2 was kept constant and the samples were driven with an electric field of 1 V/m. These surface profiles are quite similar to those of 2-2 composites measured earlier, which is consistent with the fact that a 1-3 composite with face plates can be viewed as

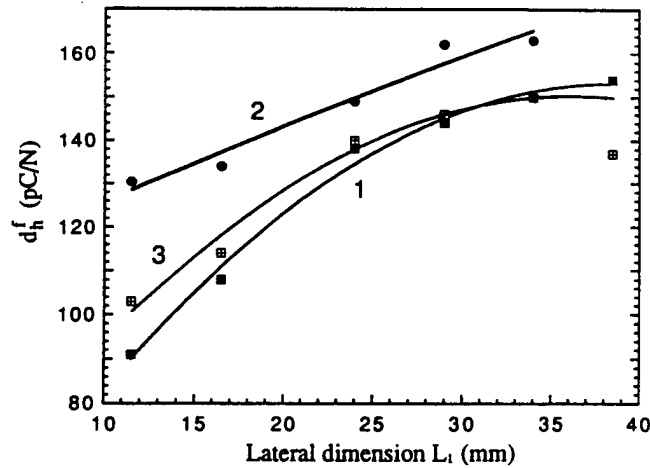


FIGURE 2 The hydrostatic charge coefficient of composite 1 (Spurs epoxy matrix) as a function of the sample lateral dimension L_1 . Curve 1 is for the composite without edge strips, curve 2 is for the composite with alumina edge strips, and curve 3 is for the composite with GRP edge strips. Solid lines are drawn to guide eyes.

one repeating unit of a large 2-2 composite. Because of the non-uniform strain profile in the lateral directions, d_{31}^f should be calculated using the relation $d_{31}^f = \bar{\epsilon}_1/E_3$ where $\bar{\epsilon}_1$ is the averaged strain in the 1-direction and E_3 is the applied electric field in the 3-direction. The results are plotted in Figure 3(b). For the composite without face plates, $d_{31} = -128$ pC/V. Evidently, the value of d_{31} is greatly reduced by the face plates especially when t/L_1 is small. As L_1 decreases, the clamping effect of face plates becomes less effective which leads to the rapid increases of d_{31}^f .

In practice, a face plated 1-3 composite may not reach the limit $t/L \rightarrow 0$ for which d_h^f reaches maximum. Therefore, it is useful to know how much d_h^f of a face plated 1-3 composite is off from its limiting value. From our earlier work on 2-2 composites,¹⁰ it can be shown that both d_h and d_{31} follow approximately a linear relationship with t/L . Indeed, the data here, when plotted against t/L_1 , fall on a straight line, as shown in Figure 4. Hence, the limiting value of d_h^f and d_{31}^f can be extrapolated from the figure. For this composite structure, in the $t/L_1 \rightarrow 0$ limit, d_h^f should reach 180 pC/N and $d_{31}^f = 15.5$ pC/N. Since this d_h^f value is for the sample with $L_2 = 27$ mm, in the limit of both t/L_1 and $t/L_2 \rightarrow 0$, d_h^f should be above 200 pC/N. For the sample investigated, at $L_1 = 38.5$ mm and $L_2 = 27$ mm d_h^f value is 160 pC/N, which is already about 80% of the limiting value.

To improve the clamping effect of the face plates on 1-3 composites, edge strips were added on this face plated composite. Shown in Figure 5 are the comparison of strain profiles of the sample of $t/L_1 = 0.196$ with and without edge strips. Two different edge strips were used here, one is GRP plate (thickness = 1.6 mm) and the other is alumina plate (thickness = 3.5 mm). It is evident that the edge strips improve the uniformity of the strain profiles. For the alumina plates, the measured d_{31} value is -18.5 pC/N, which is very close to the limiting value of d_{31}^f at $t/L_1 \rightarrow 0$. However, the effect of GRP plates is much smaller due to its relatively lower elastic stiffness and small thickness.

The comparison of the hydrostatic charge coefficient d_h between the three config-

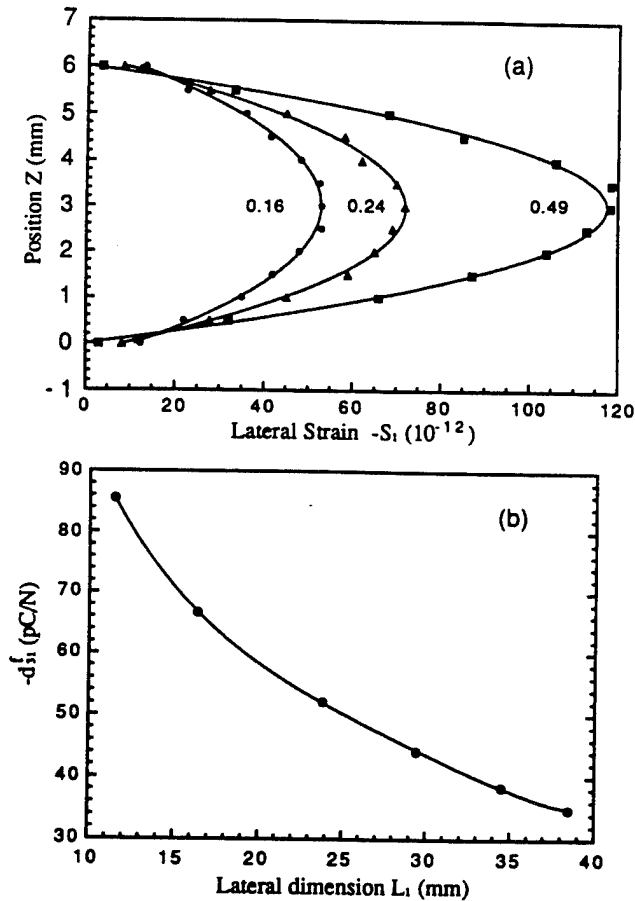


FIGURE 3 (a) The lateral strain S_1 profile of the composite I under 1 V/m driving electric field for different t/L_1 ratio. The label for each curve is the ratio t/L_1 . The incomplete clamping of the face plates on 1-3 composite is reflected by the non-uniform strain profile of S_1 , (b) the dependence of d'_{31} on the sample lateral dimension L_1 .

urations (without edge strips, with GRP edge strips, and with alumina edge strips) is shown in Figure 2. The effect of GRP edge strips is not significant. When an edge strip is used in face plated composite structure, it will influence the composite response in two opposite ways. On one hand, it reduces d_{31} for samples with finite t/L , hence enhances d_h . On the other hand, it will clamp the composite in the 3-direction in the region near it, which leads to the reductions of d_{33} and d_h . This latter effect is illustrated in Figure 6 where the surface profiles in the ceramic poling direction (the 3-direction) for face plated composite with and without edge strips are compared. The interface between the edge strip and the face plated composite is located at $x = 0$. Due to the cancellation of the two competing effects, the GRP edge strips do not change d_h very much as has been shown in Figure 2. In the limit of $t/L \rightarrow 0$, the three configurations should yield the same d_h . That is, as far as the hydrostatic response is concerned, the edge strips do not make much difference when t/L is very small. However, the edge strips do have the effect of reducing shear stress

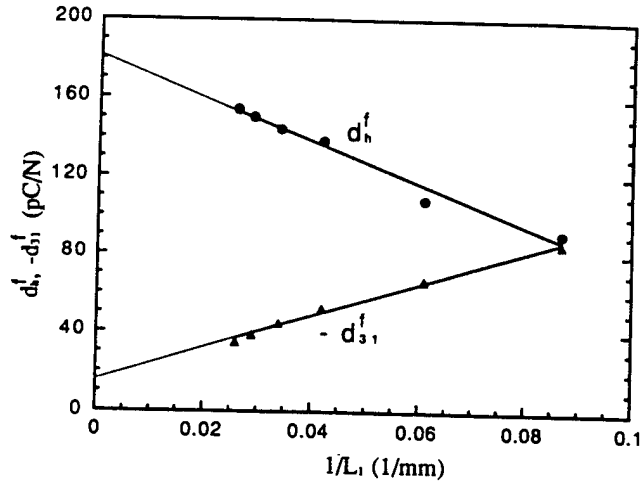


FIGURE 4 The linear relationship between d_n^f , d_{31}^f and $1/L_1$.

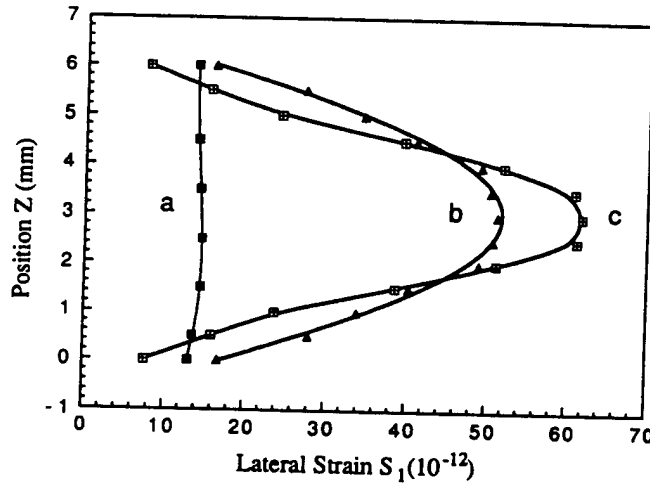


FIGURE 5 The comparison of the strain profile S_1 for the face plated composite I at $t/L_1 = 0.196$. Curve *a* is for the composite with alumina edge strips, curve *b* is for the composite with GRP edge strips, and curve *c* is the one without edge strips. The composites were driven under 1 V/m electric field.

concentration at the side boundaries of the face plate-1-3 composite interface, which improve the mechanical integrity of the composite structure.

IV. EXPERIMENTAL RESULTS FOR COMPOSITE II.

The polymer matrix of polyurethane mixed with microballon has much smaller Young's modulus and Poisson's ratio compared with Spurr's epoxy as listed in Table I. Without face plates, the composite II has a d_n of 45 pC/N and a d_{31} of -130 pC/N. Although softer polymer matrix reduces the polymer self-loading, the much re-

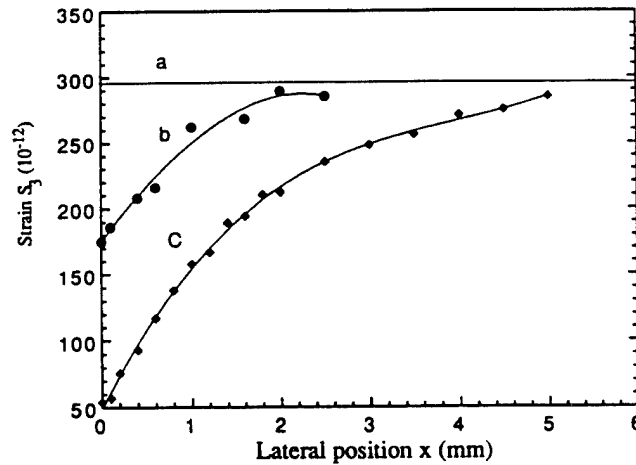


FIGURE 6 The effect of edge strips on the longitudinal strain S_3 . For the comparison, S_3 for the composite without edge strips is shown in curve *a*. Curve *b* is for the composite with GRP edge strips and curve *c* is for the alumina edge strips. The interface between the face plated composite and edge strip is at $x = 0$.

duced shear modulus of the polymer matrix also reduces the stress transfer between the polymer matrix and ceramic rods resulting in a small d_h . With GRP face plates, d_h value is increased significantly as shown in Figure 7(a). Similar to the composite I, d'_h also exhibits a strong t/L_1 dependence. The dimensional dependence of d'_{31} was also measured and is plotted in Figure 7(b). Though d'_{31} value here is comparable to those of composite I, d'_h is clearly much higher for the composite with a soft polymer matrix. As will be shown later in the paper, this increase is due to the reduction in the polymer matrix self-loading which produces a higher effective stress level in the ceramic rods.

The influence of 3.5 mm thick alumina edge strips on the hydrostatic response of this face plated composite is also shown in Figure 7(a). The improvement of the edge strips on this face plated composite is only about 10% at most. This is the result of edge strip clamping on d_{33} response of the composite since with a soft polymer matrix, the elastic stiffness in the 3-direction is much smaller than that of the edge strips and the effect of clamping in the 3-direction will be more severe in composite II.

For composite II, the plots of d'_h and d'_{31} as a function of t/L_1 did not fall on a straight line. It was also found that the dielectric constant and piezoelectric constant d'_{33} of the sample decreased as the sample dimension L_1 decreases. All these are quite different from the results of composite I. Careful inspection on composite II reveals that some PZT rods in the composite were broken when the sample was recycled during the hydrostatic measurement and during the cutting process to reduce L_1 . To correct this, the dielectric constant ϵ of individual PZT rods was measured and the data is used to calculate the percentage α of the broken rods in the samples by assuming the sample dielectric constant do not depend on the sample lateral dimensions if no ceramic rod is broken in the sample. Using this method, the measured d'_{33} , d'_h and d'_{31} were corrected by dividing them by the factor of $(1 - \alpha)$ at the corresponding L_1 value. After this correction, d'_{33} becomes almost independent

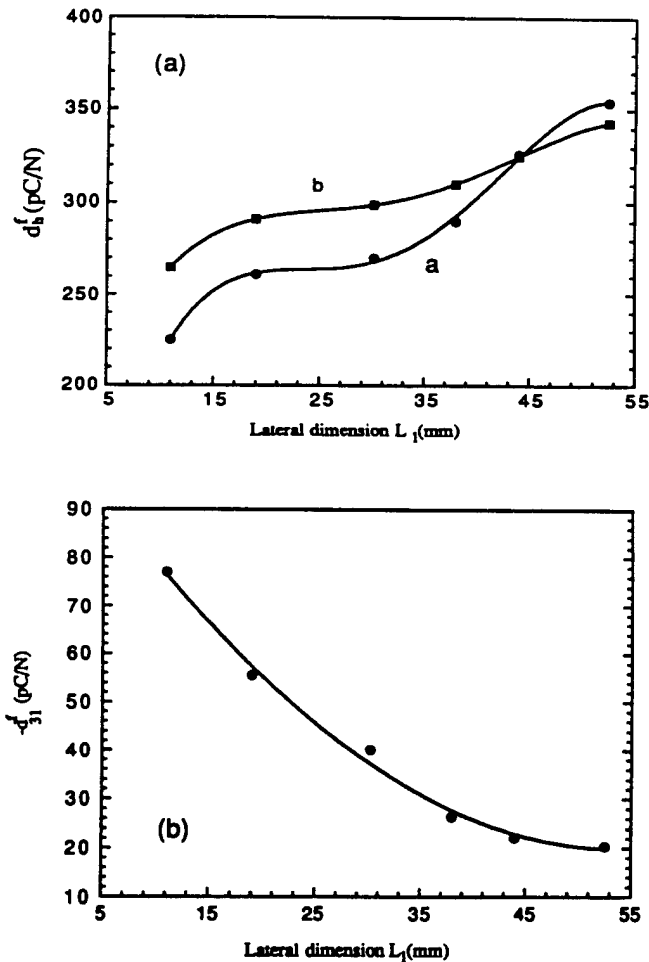


FIGURE 7 (a) The dependence of d'_h on the sample lateral dimension L_1 for the composite II. Curve *a* is for the composite without edge strips and curve *b* is that with alumina edge strips. (b) The dependence of d'_{31} on the sample lateral dimension L_1 for the composite II.

of the sample lateral dimension as we have expected. The results after the correction for d'_h and d'_{31} are plotted in Figure 8 and indeed, the data follow a linear relationship with $1/L_1$. From the linear extrapolation, the limiting values of d'_h and d'_{31} at $1/L \rightarrow 0$ are obtained and they are 440 pC/N and -6.6 pC/N respectively. Therefore, the hydrostatic figure of merit for this configuration can be as high as $50,600 \cdot 10^{-15} \text{ m}^2/\text{N}$.

In Table III, the values of d_h , d_{31} , d'_h , d'_{31} , measured at smallest t/L_1 ratio, and the values of d'_h , d'_h at $t/L_1 \rightarrow 0$, as well as the hydrostatic figure of merit for the two composites are listed. Needless to say, the exceptionally high $d_h g_h$, high d_h , light weight, and relative easiness of manufacturing face plated 1-3 composites make them superior compared with currently available hydrophone designs.

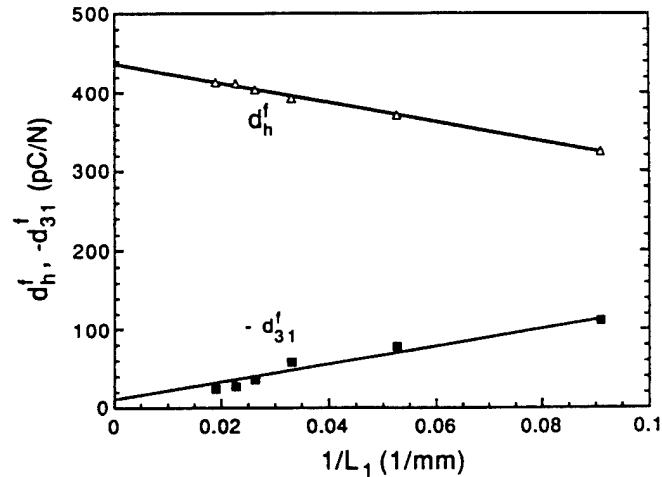


FIGURE 8 The modified d_h^f and d_{31}^f (corrected for the broken rods in the composite) as a function of $1/L_1$.

TABLE III
Summary of the properties of the two composites

	d_{31} (pC/N)	d_h	d_{31}^f	d_h^f	d_{31}^f (limit)	d_h^f (limit)	$d_h^f g_h^f$ (limit) (m^2/N)
Composite I	-128	43	-34.8	154	-17	181	7378 (10^{-15})
Composite II	-130	45	-23.9	414	-6.6	438	50,600 (10^{-15})

* d_{31} and d_h are for 1-3 composite without face plates, d_{31}^f and d_h^f are for 1-3 composites with face plates at their initial dimension, d_{31}^f (limit) and d_h^f (limit) are taken from figures 4 and 8.

V. THEORETICAL TREATMENT OF CLAMPING EFFECT OF FACE PLATES ON 1-3 COMPOSITES

From the experimental results in the sections III and IV, it is clear that in order to have a high hydrostatic response of a face plated 1-3 composite, a polymer matrix with a low Young's modulus is preferred. On the other hand, a 1-3 composite made of soft polymer matrix such as foamed polyurethane used here has the problem of low mechanical integrity, which may result in failure of a device. In practice, one has to balance these two effects. In this section, we will present a theoretical treatment which relates various design parameters to the hydrostatic response of a face plated 1-3 composite.

Clamping effect of stiff face plates on a soft piezoelectric material has been analyzed by Wang *et al.*

$$d'_{31} = d'_{32} = \frac{\bar{d}_{31}}{1 + \frac{2(\bar{s}_{11} + \bar{s}_{12})}{\gamma(s_{11}^b + s_{12}^b)}} \quad (1)$$

$$d'_{33} = \bar{d}_{33} + \frac{\bar{s}_{13}(d'_{31} + d'_{32} - 2\bar{d}_{31})}{\bar{s}_{11} + \bar{s}_{12}} \quad (2)$$

$$d'_h = \bar{d}_{33} + \bar{d}_{31} \frac{2\gamma(s_{11}^b + s_{12}^b) - 4\bar{s}_{31}}{\gamma(s_{11}^b + s_{12}^b) + 2(\bar{s}_{11} + \bar{s}_{12})} \quad (3)$$

where the quantities on the left hand side of the equations are those for the face plated samples. The quantities with a bar on the top (such as \bar{d}_{31}) on the right hand side of the equations are those for the soft piezoelectric material and the superscript b refers to the face plate. $\gamma = t/t^b$ is the thickness ratio of the piezoelectric material to the face plate. Equations (1), (2), and (3) are derived under the condition that the lateral strains in the face plate and the soft piezoelectric material are equal, a situation corresponds to $t/L \rightarrow 0$ limit here.

To use these equations for the face plated 1-3 composite, the effective material properties have to be evaluated. Though the behavior of composites without face plates can be quite different from that calculated based on the isostrain model, it is shown that the difference of the strain profile between the polymer and ceramic rods in the 3-direction becomes very small for composites with thick face plates, and the composite can be treated using the isostrain model.⁸

The basic assumption for the isostrain model used here is that the strains in both the polymer and ceramic rods in the 3-direction are equal while the stresses in the 1- and 2-directions in the two constituents are the same. Based on these assumptions, it can be derived

$$\bar{d}_{33} = \frac{\bar{D}}{T_3} = \frac{V^c s_{33}^p d_{33}^c}{V^c s_{33}^p + (1 - V^c) s_{33}^c} \quad (4)$$

$$\bar{s}_{33} = \frac{\bar{S}_3}{T_3} = \frac{s_{33}^p s_{33}^c}{V^c s_{33}^p + (1 - V^c) s_{33}^c} \quad (5)$$

where the superscripts p and c refer to the polymer and ceramic, respectively.

Assuming the sample is subjected to a stress T_1 in 1 or 2 direction, from the constitutive relations and isostress assumption, one can get

$$S_3^c = s_{33}^c T_3^c + s_{13}^c T_1 \quad (6)$$

$$S_1^c = s_{11}^c T_1 + s_{13}^c T_3^c \quad (7)$$

$$S_2^c = s_{12}^c T_1 + s_{23}^c T_3^c \quad (8)$$

For the polymer phase, similar equations can be obtained by simply replacing superscript c by p . Furthermore,

$$V^c T_3^c + (1 - V^c) T_3^p = 0 \quad (9)$$

$$\bar{D}_3 = d_{33}^c T_3^c V^c + d_{31}^c T_1 V^c \quad (10)$$

$$\bar{S}_2 = V^c S_2^c + (1 - V^c) S_2^p \quad (11)$$

$$\bar{S}_1 = V^c S_1^c + (1 - V^c) S_1^p \quad (12)$$

Solving these equations yields:

$$\frac{\bar{S}_3}{T_1} = \frac{\bar{S}_3}{T_1} = \frac{s_{33}^c s_{13}^p (1 - V^c) + V^c s_{11}^p s_{13}^c}{V^c s_{33}^p + s_{33}^c (1 - V^c)} \quad (13)$$

$$\bar{s}_{11} = (1 - V^c)[s_{12}^p + s_{13}^p (s_{13}^p - s_{13}^c) V^c c_a] + V^c [s_{12}^c - s_{13}^c (s_{13}^p - s_{13}^c) (1 - V^c) c_a] \quad (14)$$

$$\bar{s}_{12} = (1 - V^c)[s_{12}^p + s_{13}^p (s_{13}^p - s_{13}^c) V^c c_a] + V^c [s_{12}^c - s_{13}^c (s_{13}^p - s_{13}^c) (1 - V^c) c_a] \quad (15)$$

$$\bar{d}_{31} = d_{33} V^c c_a [s_{13}^c (s_{13}^p - s_{13}^c) (1 - V^c)] + d_{31} V^c \quad (16)$$

where $c_a = 1/((1 - V^c)s_{33}^c + s_{11}^p V^c)$. From these relations, d_h^l and d_{31}^l are calculated for the two composite structures investigated. Some of the material parameters used for the calculations have been listed in Tables I and II and the elastic compliance data for PZT-5H are used for the ceramic rods.¹⁴ ($\gamma = 7.1$ for spurrs epoxy composite and $\gamma = 3.46$ for polyurethane composite). The calculated results for the composite with Spurrs epoxy matrix (composite I) are, $d_h^l = 171$ pC/N and $d_{31}^l = -17.6$ pC/N; and for the composite with foamed polymer matrix (composite II), $d_h^l = 480$ PC/N and $d_{31}^l = -0.2$ PC/N. These values are in very good agreement with the experimental data when extrapolated to t/L_1 and $t/L_2 \rightarrow 0$ limit. It indicates that the theoretical results here provide quite accurate prediction on the hydrostatic response of a face plated 1-3 composite.

From the above equations, the relationship between the hydrostatic response of a face plated 1-3 composite and s_{11}^p and σ of the polymer can be derived:

$$d_h^l = d_{33} s_{11}^p V^c c_a + [V^c d_{31} - V^c (1 - V^c) d_{33} c_a (s_{13}^c + \sigma s_{11}^c)] \quad (17)$$

$$\left\{ \frac{2\gamma(s_{11}^c + s_{12}^c) - 4c_a [V^c s_{11}^p s_{13}^c - s_{33}^c \sigma s_{11}^c (1 - V^c)]}{\gamma(s_{11}^c + s_{12}^c) + 2[V^c (s_{11}^c + s_{12}^c) + (1 - V^c) s_{11}^c (1 - \sigma) - 2V^c c_a (1 - V^c) (s_{13}^c + \sigma s_{11}^c)^2]} \right\}$$

Figure 9(a) shows the dependence of d_h^l on s_{11}^p for three different Poisson's ratio of the polymer matrix: $\sigma = 0.15, 0.3$, and 0.4 . GRP is used here as face plates. The ceramic used in the calculation is PZT-5H.¹⁴ The ceramic rods content of 15% and a γ of 3.5 are used in the calculation. From Figure 9(a), it is clear that the effect of the Poisson's ratio of the polymer phase on d_h^l depends critically on the elastic compliance of the polymer. When the elastic compliance of the polymer matrix is below, for example, 5×10^{-8} , there is little change in d_h^l when the Poisson's ratio is increased from 0.15 to 0.4. However, a drastic decrease of d_h^l with σ occurs for polymers with smaller elastic compliance. Furthermore, there is not much decrease in d_h^l when s_{11}^p is reduced from 5×10^{-8} (close to the value of the foamed polyurethane used for the composite II) to 5×10^{-9} , a polymer ten times harder than the polymer matrix used for the composite II. With an elastically stiffer polymer matrix, the mechanical integrity of the device is improved significantly while there is not much loss in the hydrostatic response. This illustrates that for a composite with a polymer matrix ten times stiffer than the polymer matrix for the composite II, there is little reduction in the hydrostatic figure of merit while there is a substantial increase in its mechanical integrity. Apparently, Spurrs epoxy is not a suitable choice either for the polymer matrix for the face plated 1-3 composite discussed here.

Figure 9(b) shows the dependence of d_h^l on s_{11}^p with different ratio γ (thickness ratio of 1-3 composite to the face plate) with $\sigma = 0.3$ for the polymer matrix, which should

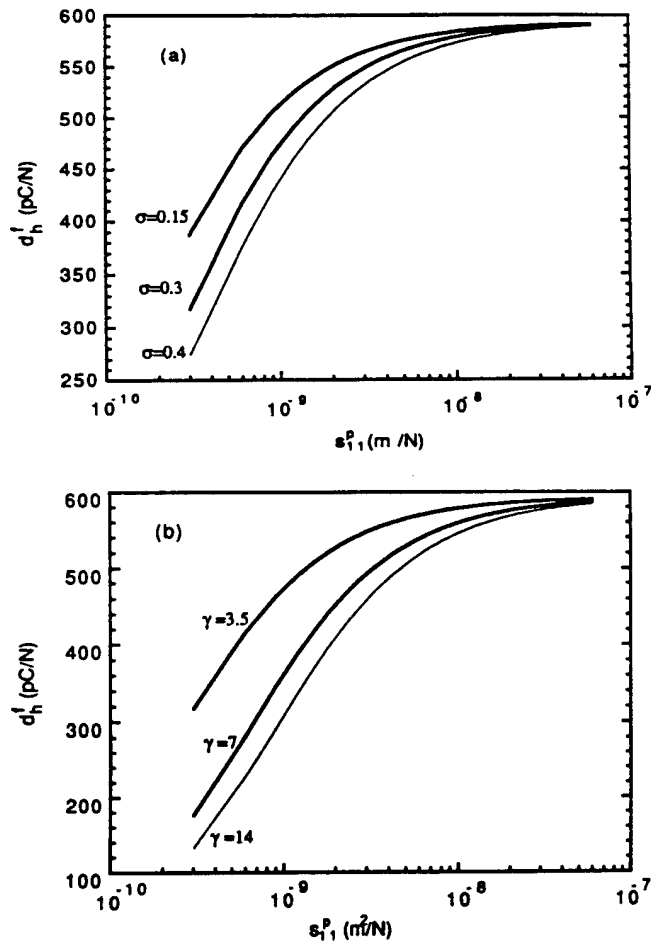


FIGURE 9 (a) The dependence of d_h' of a face plated 1-3 composite, which has 15% PZT 5H rod content and GRP face plates with $\gamma = 3.5$, on the compliance s_{11} of the polymer matrix. Three Poisson's ratios are used: $\sigma = 0.15, 0.3$, and 0.4 as labeled on the figure. The curves are calculated using Equation (17). (b) The dependence of d_h' of a face plated 1-3 composite, which has 15% PZT 5H rod content and GRP face plates, on the compliance s_{11} of the polymer matrix for different γ (the thickness ratio of the face plate t_f and the 1-3 composite t).

provide valuable information on the selection of face plate thickness in reference with the thickness of 1-3 composite.

VI. SUMMARY

The hydrostatic response of a 1-3 composite can be significantly increased by using face plates to (1) improve the stress transfer in the 3-direction; (2) reduce the Poisson's ratio effect and d_{31} effect; (3) improve the mechanical integrity of the composite structure. In this paper, we show that for a face plated 1-3 composite with a soft

polymer matrix and 15% ceramic rod content, its hydrostatic figure of merit $d_h g_h$ can reach more than $50,000 \times 10^{-15}$ (m^2/N). However, due to the nature of the shear coupling between the face plates and 1-3 composite, the hydrostatic response of a face plated 1-3 composite will depend on the sample lateral dimensions. The hydrostatic response will increase as the ratio of the thickness to the lateral dimension (t/L) becomes small, for a large t/L ratio, improvement of the hydrostatic response due to the face plates is not significant. One possible method to increase d_h for samples with a large t/L ratio is to use edge strips. However, the study here shows that the effect is not significant due to the two opposite roles an edge strip plays on a face plated 1-3 composite. Therefore, the key to increase hydrostatic response is to use small t/L ratio for a face plated 1-3 composite.

To balance the requirement of high hydrostatic sensitivity and mechanical integrity, a proper polymer matrix with the right elastic properties should be used. In the paper, we showed that the two face plated composites tested represent the two extreme cases with the Spurr's epoxy matrix on the hard side and the polyurethane with 50% microballon on the soft side of the polymer matrix spectrum. A polymer matrix with its elastic properties in between the two would be a good choice to balance the two requirements as mentioned previously. In general, the theoretical results presented here can provide a useful guideline for the optimum design of face plated 1-3 composites.

ACKNOWLEDGMENTS

The authors wish to thank Fiber Materials, Inc. for providing the 1-3 composite with polyurethane matrix (the composite II). The authors also wish to thank Dr. W. Smith and Dr. W. Reader for many stimulating discussions. This work was supported by the Office of Naval Research.

REFERENCES

1. R. E. Newnham, D. P. Skinner and L. E. Cross, *Mat. Res. Bull.*, **13**, 525 (1978).
2. K. A. Klicker, Ph.D. Thesis, The Pennsylvania State University, 1980.
3. T. R. Gururaja, Ph.D. Thesis, The Pennsylvania State University, 1984.
4. W. A. Smith and B. A. Auld, *IEEE Trans. UFFC*, **38**, 40 (1991).
5. M. J. Haun and R. E. Newnham, *Ferroelectrics*, **68**, 123 (1986).
6. Wenwu Cao, Q. M. Zhang and L. E. Cross, *J. Appl. Phys.*, **72**, 5814 (1992).
7. Q. M. Zhang, Wenwu Cao, H. Wang and L. E. Cross, Proc. IEEE ISAF8 252, 1992.
8. Wenwu Cao, Q. M. Zhang, J. Zhao and L. E. Cross, preprint and to be published.
9. H. Wang, Q. M. Zhang, L. E. Cross and A. O. Sykes, submitted to *Ferroelectrics* (1993).
10. Q. M. Zhang, Wenwu Cao, J. Zhao and L. E. Cross, submitted to *IEEE Trans. UFFC* (1993).
11. C. G. Oakley, Ph.D. Thesis, The Pennsylvania State University, 1991.
12. CRC Handbook of Chemistry and Physics, CRC Press, Inc., 1980-1981.
13. Q. M. Zhang, S. J. Jang and L. E. Cross, *J. Appl. Phys.*, **65**, 2808 (1989).
14. PZT-5H is the trade mark of Morgan Matric Inc., Vernitron Div. for its La doped PZT. From the data sheet, $d_{33} = 593$ (pC/N), $d_{31} = -275$, $s_{11} = 1.65 \times 10^{-11}$ (m^2/N), $s_{12} = -0.478 \times 10^{-11}$, $s_{33} = 2.08 \times 10^{-11}$, $s_{13} = -0.845 \times 10^{-11}$.

APPENDIX 24

NUMERICAL STUDY OF ULTRASONIC BEAM PATTERN OF A 1-3
PIEZOCOMPOSITE TRANSDUCER

Shih-jeh Wu[†], Wenkang Qi^{††} and Wenwu Cao^{*}

[†] Department of Mechanical Engineering

^{††} Bioengineering Program

^{*} Department of Mathematics and

Intercollege Materials Research Laboratory

The Pennsylvania State University, University Park, Pennsylvania 16802

ABSTRACT

A comprehensive numerical study of the radiation beam pattern from a 1-3 ceramic polymer composite ultrasonic transducer has been carried out. The goals are to establish a simulation procedure and to evaluate how the nonuniform vibration profile of the composite affects the radiation pattern compared to a uniformly vibrating transducer. With the imposed absorbing boundary condition at the outer fluid boundary, the nonuniform surface vibration profile and the velocity distribution of the composite transducer under a pulse and a continuous wave driven situations are calculated using finite element method. The radiation pattern from the transducer is then calculated from the velocity distribution at the transducer surface by solving the Helmholtz integral equation using boundary element method.

INTRODUCTION

Piezocomposite with 1-3 type connectivity [1,2] has gained wide popularity as transducer material, especially in medical diagnostic ultrasound and under water acoustics. The main reason is due to the high electromechanical coupling coefficients and the low acoustic impedance [3]. Different transducer configurations (i.e., changing the geometric of the ceramic pillars, ceramic-polymer ratio etc.) have been designed to fit particular needs, such as beam width, focal length and efficiency [4]. However, due to the complexity of the composite structure, the true performance of the design can not be modeled by the widely used KLM model [5]. Besides, current transducer designs require large amount of experimental testing which is both costly and time consuming [6,7]. With the increasing demand on better transducer, there is a need for a computational scheme to simulate the performance of composite transducer designs, i.e., to study the details of the electromechanical vibrations and to calculate the acoustic beam characteristics at the design stage.

The fast development of the computer technology makes it possible now to solve large scale problems using finite element method [8]. In this paper we report a comprehensive simulation of a 1-3 composite transducer operation using finite element method (FEM) and boundary element method (BEM). Both the vibration characteristics of the transducer under water loading and the acoustic beam profiles under CW and pulse driven situations were analyzed. The objective of this study is to provide a general simulated design and testing procedure and to study the influence of nonuniform transducer surface vibration on the acoustic beam characteristics.

The vibrational and electromechanical characteristics of a 1-3 composite transducer has been intensively investigated using finite element method [7, 8] with or without water loading. Mode coupling and shear wave propagation are the most concerned problems in a composite transducer design. The results from the analysis of the vibration modes are quite different for the cases of with and without water loading condition [8]. Traditionally, the major problem for solving the elasticity problem under water loading had been the coupling of piezoelectric ceramic and polymer to the medium. The calculation involves fluid acoustic field far away from the transducer,

Appendix A:

In Eq.8 two integrals are to be evaluated, i.e.,

$$\iint_{s_n} \frac{\partial}{\partial n_s} \frac{e^{-ikr(x,\sigma)}}{r(x,\sigma)} ds(\sigma) \text{ and } \iint_{s_n} \frac{e^{-ikr(x,\sigma)}}{r(x,\sigma)} ds(\sigma) \quad (\text{A1})$$

When the distance of the point of interest is much large than the transducer dimension, the variable r can be approximated as follows,

$$r^2 = |\mathbf{r} \cdot \mathbf{r}| = R^2 + \delta^2 - 2 \mathbf{R} \cdot \delta \approx R^2 \left(1 - \frac{2 \mathbf{R} \cdot \delta}{R^2} \right) (\because R \gg \delta \text{ in far field}) \quad (\text{A2})$$

where δ measures the distance of a point on the transducer surface from the center of the transducer. Therefore,

$$r \approx R \sqrt{1 - \frac{2 \mathbf{R} \cdot \delta}{R^2}} = R \hat{\mathbf{R}} \cdot \delta, \left(\hat{\mathbf{R}} = \frac{\mathbf{R}}{R} \right) \quad (\text{A3})$$

Thus we have the simple form for the integrands:

$$\frac{\partial}{\partial n_\sigma} \frac{e^{-ikr(x,\sigma)}}{r(x,\sigma)} \approx ik \frac{e^{-ikR}}{R} \hat{\mathbf{R}} \cdot \mathbf{n} e^{ik\hat{\mathbf{R}} \cdot \delta} \quad (\text{A4})$$

$$\frac{e^{-ikr(x,\sigma)}}{r(x,\sigma)} \approx \frac{e^{ikR}}{R} e^{ik\hat{\mathbf{R}} \cdot \delta} \quad (\text{A5})$$

Eq. (A1) can be easily integrated with this simplification.

5814-5821, 1992.

13. W. Cao and W. K. Qi, "Plane Wave Propagation in Finite 2-2 Composites" J. Appl. Phys., vol. 78, pp. 4627-4632, 1995.

14. W. Cao and W. Qi, "Multi-Source Excitations in a Stratified Biphase Structure", J. Appl. Phys., vol. 78, pp. 4640-4646, 1995.

which greatly increases the complexity and the computation time. The new finite element technology utilizes absorbing boundary condition (impedance at the boundary matched to the fluid media) at the interface to represent the radiation condition. This method can greatly reduce the computation time without sacrificing the accuracy of the solutions.

The calculation of the sound field radiated from a baffled piston has been studied two decades ago [9,10] for both tone burst and pulse response cases either by numerical integration or by applying Huygen's principle. However, the assumption of uniform vibration, infinite baffle, infinite boundary, and the lack of closed-form solution for elements not in circular shape render the calculations deviate from true situation [12]. The radiation acoustic field from vibrating piston can be calculated by solving the Helmholtz integral equation [11] as long as the vibration velocity distribution on the surface is known. This involves discretizing the piston surface, similar to the boundary element method. The advantages are much fewer elements being involved in the calculation than solving the whole acoustic field in entire space using FEM. Considering the merits of both methods we have carried out an analysis using the two software packages: ANSYS® (FEM) and CHIEF (BEM) to analyze the transducer vibration profile and the acoustic radiation field.

THEORETICAL ANALYSIS

There are three different aspects in the theoretical analysis. They are briefly described below:

(1) Piezoelectric coupling

The constitutive equations governing the stress $\{T\}$, strain $\{S\}$, electric field $\{E\}$, and electric flux $\{D\}$ can be expressed as:

$$\begin{aligned}\{T\} &= [c] \{S\} - [e]^T \{E\} \\ \{D\} &= [e] \{S\} + [\epsilon] \{E\}\end{aligned}\tag{1}$$

where $[c]$ is the elastic stiffness matrix, $[e]$ and $[e]^T$ are respectively the piezoelectric coupling and the permittivity matrices. The equations of motion are given by:

$$\begin{aligned}
[m] \{\ddot{U}\} + [K_{uu}] \{U\} + [K_{u\phi}] \{\phi\} &= \{F\} \\
[K_{\phi u}] \{U\} + [K_{\phi\phi}] \{\phi\} &= \{Q\}
\end{aligned} \tag{2}$$

where $[m]$ is the mass matrix, $\{U\}$ is the displacement vector, $[K_{uu}]$ is the elastic stiffness matrix, $[K_{u\phi}]$ and $[K_{\phi u}]$ are the piezoelectric coupling matrices, $[K_{\phi\phi}]$ is the dielectric matrix, $\{F\}$ is the force vector, $\{\phi\}$ is the potential vector and $\{Q\}$ is the charge vector, respectively. Equations for the polymer phase are simpler because the electromechanical coupling is vanished.

(2) Fluid structure interaction:

The governing equation of acoustic field in fluid is the Helmholtz equation. The degree of freedom (DOF) of finite element formulation for the fluid is the pressure at each node. In matrix formulation, the governing equations for the acoustic field in fluid is quite similar to that of the polymer phase,

$$\begin{aligned}
[M_f] \{\ddot{P}\} + [K_f] \{P\} &= \{F_f\} \\
[M_s] \{\ddot{U}\} + [K_s] \{U\} &= \{F_s\}
\end{aligned} \tag{3}$$

where $[K_f]$ is the fluid equivalent "stiffness" matrix, $[M_f]$ is the fluid equivalent "mass" matrix, $\{P\}$ is the unknown nodal pressure, $\{F_f\}$ is the fluid load applied at the fluid structure interface, $[K_s]$ is the structure "stiffness" matrix, $[M_s]$ is the structure mass matrix, and $\{F_s\}$ is the load applied at the structure interface.

By matching the loads at the fluid structure interface we have the augmented matrix equation of fluid structure interaction with the coupling matrix $[R]$ as follows:

$$\begin{aligned}
[M_s] \{\ddot{U}\} + [K_s] \{U\} &= \{F_s\} + [R] \{P\} \\
[M_f] \{\ddot{P}\} + [K_f] \{P\} &= \{F_f\} - \rho_0 [R]^T \{\ddot{U}\}
\end{aligned} \tag{4}$$

Because the solid and the fluid region have different degree of freedom, a particular solid-fluid interface element containing both pressure and displacement DOFs is used which is designed to solve Eq.(4).

(3) Helmholtz integral equation:

If S is a closed surface in space, the acoustic field on or exterior to the surface

S can be formulated according to the integral Helmholtz equation [11]:

$$\int_S \left\{ p(\sigma) \frac{\partial G(x, \sigma)}{\partial n \sigma} + i \omega \rho v(\sigma) G(x, \sigma) \right\} ds(\sigma) = \begin{cases} p(x) & \text{for } x \text{ ext. } S \\ \frac{1}{2} p(x) & \text{for } x \text{ on } S \end{cases} \quad (5)$$

where σ is the coordinate of the point on S and $G(x, x')$ is the Green's function at x with respect to x' ,

$$G(x, x') = \frac{1}{4 \pi} \frac{e^{-ik|x-x'|}}{|x-x'|}, \quad k = \frac{\omega}{c} \quad (6)$$

In Eq.(5) the $p(\sigma)$ and $v(\sigma)$ are respectively the pressure and the velocity on surface S . If we discretize the surface S the relation between the surface pressure and the surface velocity can be expressed in the following matrix form

$$[A] \{P\} = [B] \{V\} \quad (7)$$

where $\{P\}$ represents the pressure at each subdivision on the surface S and $\{V\}$ is the velocity matrix at the same location on S . The coefficient matrices $[A]$ and $[B]$ are as follows,

$$\begin{aligned} A_{mn} &= \frac{1}{2} \delta_{mn} - \int_{S_n} \frac{\partial}{\partial n \sigma} G(\zeta_m, \sigma) ds(\sigma) \\ B_{mn} &= i \omega \rho \int_{S_n} G(\zeta_m, \sigma) ds(\sigma) \end{aligned} \quad (8)$$

where S_n is a subdivision of S , ζ_m is the coordinate of the center at subdivision S_m . The pressure field can be obtained from Eq. (7) once the velocity distribution is known. In order to provide the CHIEF program a set of input surface velocity distribution, we have used the simple relation at the solid fluid interface, i.e.,

$$V = \frac{P_0}{Z_{water}} \quad (9)$$

where Z_{water} is the acoustic impedance of water and P_0 is the acoustic pressure in the fluid adjacent to the solid surface. The velocity at each element is taken from the average value of 4 adjacent nodes with rectangular mesh since the FEM calculates nodal values whereas CHIEF takes only the averaged value on an element.

When only the far field pressure is of interest, the calculations of $[A]$ and $[B]$ matrices can be greatly simplified (see Appendix A).

RESULTS AND DISCUSSIONS

The material properties of the transducer under study are listed in Table I. Because of symmetry, only 1/8 of the 1-3 composite transducer has been analyzed using FEM, the model analyzed is shown in Fig.1, where the faces near the reader and at the bottom are symmetry planes. This model represents a full size composite of a $8 \times 8 = 64$ ceramic pillars embedded in the polymer. The center frequency of this composite transducer is 2.53 MHz. We have performed calculations in both CW and pulse mode.

(a) CW mode

The steady state surface vibration pressure at resonant frequency calculated from ANSYS® is shown in Fig.2 (a)-(c). Fig 2(a) is the direct view of the composite transducer surface, Fig, 2(b) and 2(c) are the vibration amplitude and the phase distribution in gray scale. We can see a strong nonuniformity from Fig. 2 both in terms of the amplitude and the phase. There is also an obvious amplitude difference between the pillars at the center of the composite and those at the edge. Two possible reasons may account for this phenomenon: one is the edge effect which reflects the fact that the edge pillars have relatively lighter loading, and the other is the coupling of lateral modes to the thickness mode.[13,14] In order to understand the effect of inhomogeneous surface vibration, we have calculated both the beam pattern generated by the composite transducer and by a uniform vibrating piston. The results are shown in Figs. 3, 4, and 5. Fig. 3(a) is the illustration of the pressure distribution on the transducer surface and Fig. 3(b) is the 2-D (x-z plane) near field pressure. Fig.4 plots the near field axial pressure variation and Fig. 5 is the far field pattern on the x-z plane (z axis is the direction normal to the transducer surface).

Surprisingly, the difference between the beam patterns generated by the uniform and the nonuniform vibrations is not significant, especially in the far field. This result contradicts the common belief that the beam pattern will be seriously distorted due to the nonuniformity of transducer surface vibration. One possible explanation for this result is that the polymer phase does not emit significant energy. We are currently trying some experimental works to verify this result.

(b) Pulse mode

In imaging applications, the transducer is operated in a pulse mode. It is therefore necessary to calculate the propagation of the pressure pulse in the medium. Such calculation is accomplished in a process depicted in the flow diagram of Fig. 6. The duration of the simulated driving triangular pulse is 10^{-8} second. In order to illustrate the method, moderate damping was applied to allow some ringing. A total of 128 velocity maps were calculated for a duration of 1.05×10^{-5} seconds using the transient function of ANSYS. The transient vibration response at each subelement of the transducer surface is decomposed into 128 frequency components via Fast Fourier Transform (FFT). Each of the frequency components is then fed into the CHIEF program and the corresponding pressure components of the acoustic field were calculated. Finally, the transient acoustic pulse at each location is reconstructed via Inverse Fast Fourier Transform (IFFT) from these frequency components of the pressure pulse.

Fig. 7 is sequence of snapshots of the pressure distribution resulting from a single pulse drive. We can clearly see the ringdown along the axial direction and the off axial direction pressure distribution. Sidelobe structures are also visible on the snapshot. The width of the pulse becomes wider as it propagates and the peak pressure value gradually decreases.

In order to see the spreading of the effective beam width we have calculated the root mean square(RMS) pressure of the pulse at each location for the near field as show in Fig. 8. The effective beam pattern is similar to a single frequency CW beam pattern except slight wider beam width. Fig. 9 is the RMS along the axial direction. Compared with Fig. 4, we can see that the near field shows deviation from the CW beam pattern, but the far field pressure distribution is very similar to the CW case except the beam becomes slightly wider.

SUMMARY AND CONCLUSIONS

We have successfully performed a combined FEM and BEM analysis on a 1-3 type piezocomposite transducer. The combination of the two numerical techniques enables us to analyze the acoustic beam pattern generated by the nonuniformly vibrating transducer. To our surprise, the difference of the generated pressure field distribution caused by the nonuniformity is not significant

except near the transducer surface. In the far field, the beam pattern is quite similar to that of a uniformly vibrating piston.

An important advancement from this work is the development of a computational scheme for the propagation of a finite length pulse in the medium. This allows us to study the pulse shape deformation as it propagates. Some degree of broadening of the pulse is found but the RMS pressure distribution appears to be very similar to a single frequency CW pressure distribution.

ACKNOWLEDGMENT

This research is sponsored by the Office of Naval Research under contract No. N00014-93-1-0340 and the Whitaker Foundation under special opportunity grant.

REFERENCES:

1. R. E. Newnham, Skinner D. E. and Cross L. E., "Connectivity and Piezoelectric- pyroelectric composites," *Mater. Res. Bull.*, vol. 13, pp. 525-536, 1978.
2. R. E. Newnham, Bowen L. J., Klicker K. A., and Cross L. E., "Composite Piezoelectric Transducer," *Materials in Engineering*, vol. 2, pp. 93-106, 1980.
3. W. A. Smith, "The Role of Piezocomposites in Ultrasonic Transducers," *Proc. 1989 IEEE Ultrason. Symp.*, pp. 755-766, 1989.
4. W. A. Smith and Bertram A. Auld, "Modeling 1-3 Composite Piezoelectrics: Thickness Mode Oscillations," *IEEE Trans. on Ultrason., Ferroelec. and Freq. Contr.*, vol. 38, pp. 40-47, 1991.
5. R. Krimholtz, Leedom D., and Matthaei G., "New Equivalent Circuits for Elementary Piezoelectric Transducers," *Electronics Lett.*, vol. 6, pp. 398-399, 1970.
6. W. A. Smith, "Modeling 1-3 Composite Piezoelectrics: Hydrostatic Response," *IEEE Trans. on Ultrason., Ferroelec., and Freq. Contr.*, vol. 40, pp. 41-49, 1993.
7. J. A. Hossack and Heyward G., "Finite Element Analysis of 1-3 Composite Transducers," *IEEE Trans. on Ultrason., Ferroelec., and Freq. Contr.*, vol 40, pp. 618-629, 1991.
8. J. H. Jeng, Bao X. Q., Varadan V. V., and Varadan V. K., "A Complete Finite Element Eigenmode Analysis for a 1-3 Type of Piezoelectric Composite Transducer Including the Effect of Water Loading and Internal Losses," *Proceedings of the 1988 IEEE ultrasonic symposium*, pp. 685-688, 1988.
9. J. C. Lockwood and Willette J. G., "High-speed Method for Computing the Exact Solution for the Pressure Variations in the Nearfield of a Baffled Piston," *J. Acoustic Soc. of Am.*, vol. 53 (3), pp. 735-741, 1973.
10. A. Weyns, "Radiation Field Calculations of Pulsed Ultrasonic Transducer: Part 1 -Planar Circular, Square and Annular Transducers," *Ultrasonics*, vol. 18 (4), pp. 183-188, 1980.
11. G. W. Benthien, Barach D. and Dillete D., *CHIEF User's Manual*, Sept. 1988.
12. W. Cao, Zhang Q. and Cross L. E., "Theoretical Study on the Static Performance of Piezoelectric Ceramicpolymer Composites with 1-3 Connectivity," *J. Appl. Phys.*, vol. 72, pp.

LIST OF FIGURE CAPTIONS:

Fig.1 1/8 of the 1-3 piezocomposite transducer studied using ANSYS.

Fig.2 (a) Surface of the actual positions of the ceramic pillars; (b) Distribution of the amplitude of pressure on the transducer surface under 1.0 Volt (peak to peak) 2.53 MHz CW operation; (c) distribution of the phase angle of the vibration pressure on the transducer surface.

Fig.3 Acoustic near-field radiation beam pattern on the central plane $y = 0$. ($x > 0$, $z > 0$), under 2.53 MHz CW operation.

Fig.4 Axial (z-axis) acoustic pressure distribution under 2.53 MHz CW operation.

Fig.5 Angular distribution of the far-field (x-z plane) acoustic radiation under 2.53 MHz CW operation.

Fig.6 Calculation process for the acoustic radiation beam pattern under 10^{-8} second triangular electric pulse excitation.

Fig.7 Snapshots of a propagating acoustic pulse in the far-field.

Fig.8 Distribution of the RMS pressure in the near-field under pulse excitation.

Fig.9 Axial (z-axis) distribution of RMS pressure under pulse excitation.

Table 1 Elastic Stiffness Matrix C (10^{10} N/m²), piezoelectric constants e (10^{-12} C/N), dielectric constant ϵ (ϵ_0), coupling constants k and density ρ (kg/m³)

	C_{11}	C_{12}	C_{13}	C_{33}	C_{44}	C_{66}
Polymer	0.349			0.349	0.13	0.13
PZT	13.0483	8.34907	8.82772	12.1148	2.29885	2.3462

	e_{15}	e_{31}	e_{33}	ϵ_{11}	ϵ_{33}	k_{15}	k_{31}	k_{33}	k_t	ρ
PZT	741	-274	593	1700	1470	.675	0.39	0.75	0.50	7800
polymer				4	4					1097

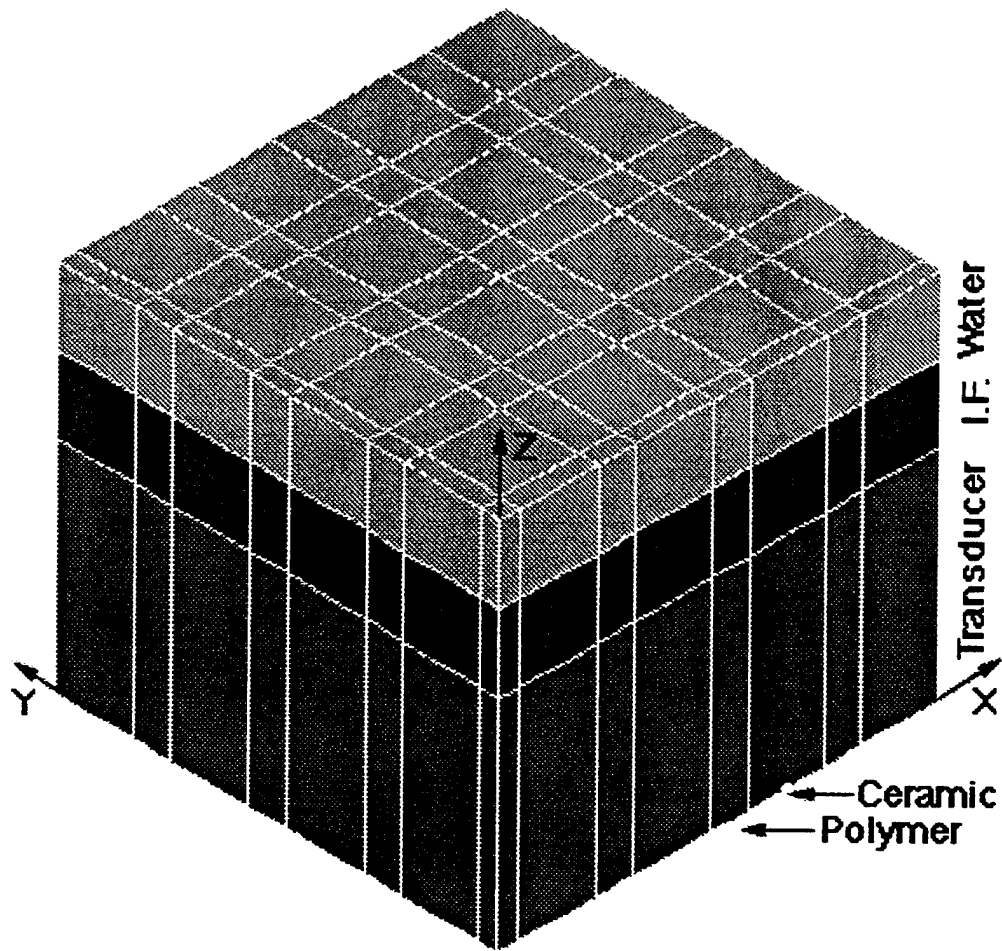


Fig. 1

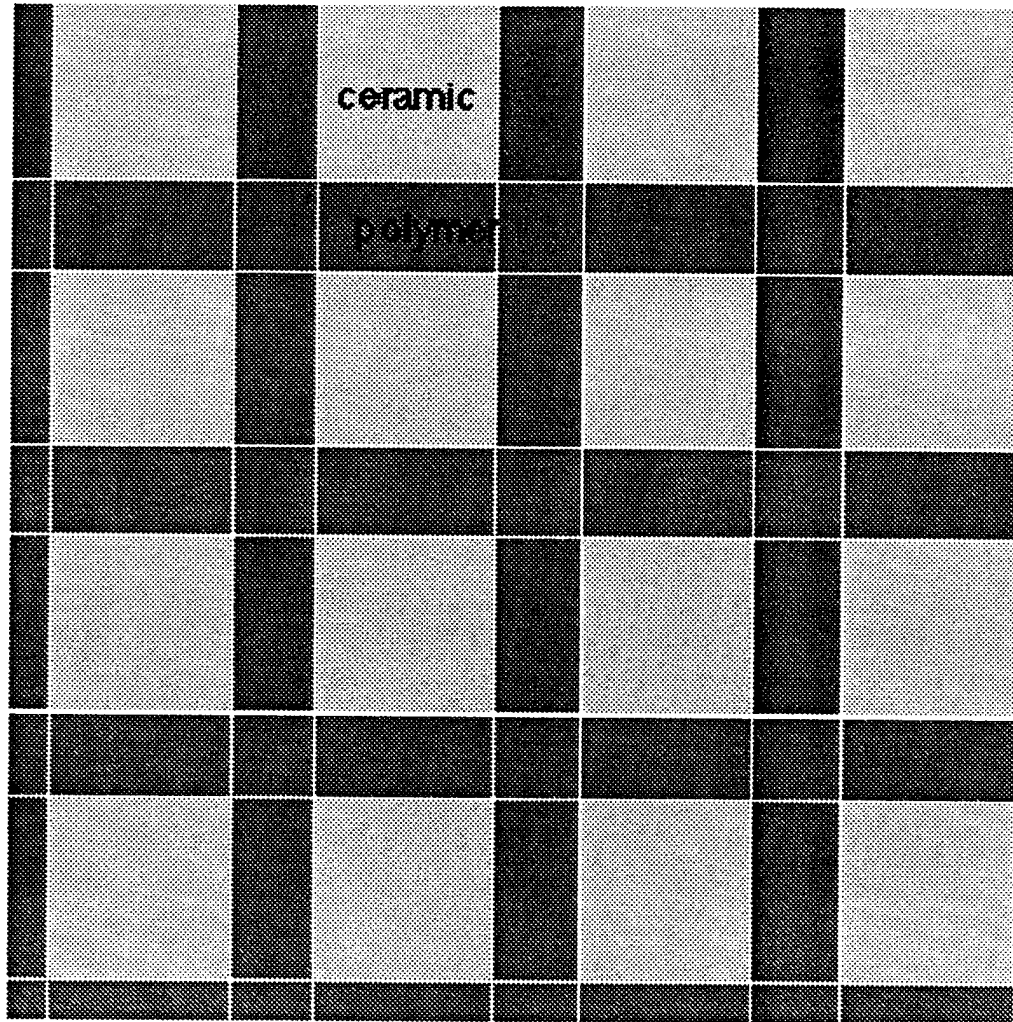


Fig. 2 (a)

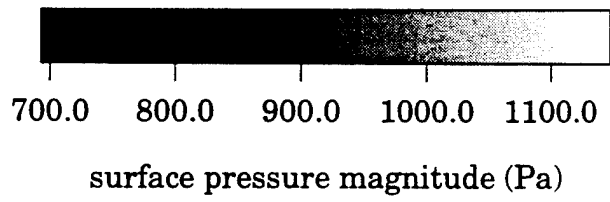
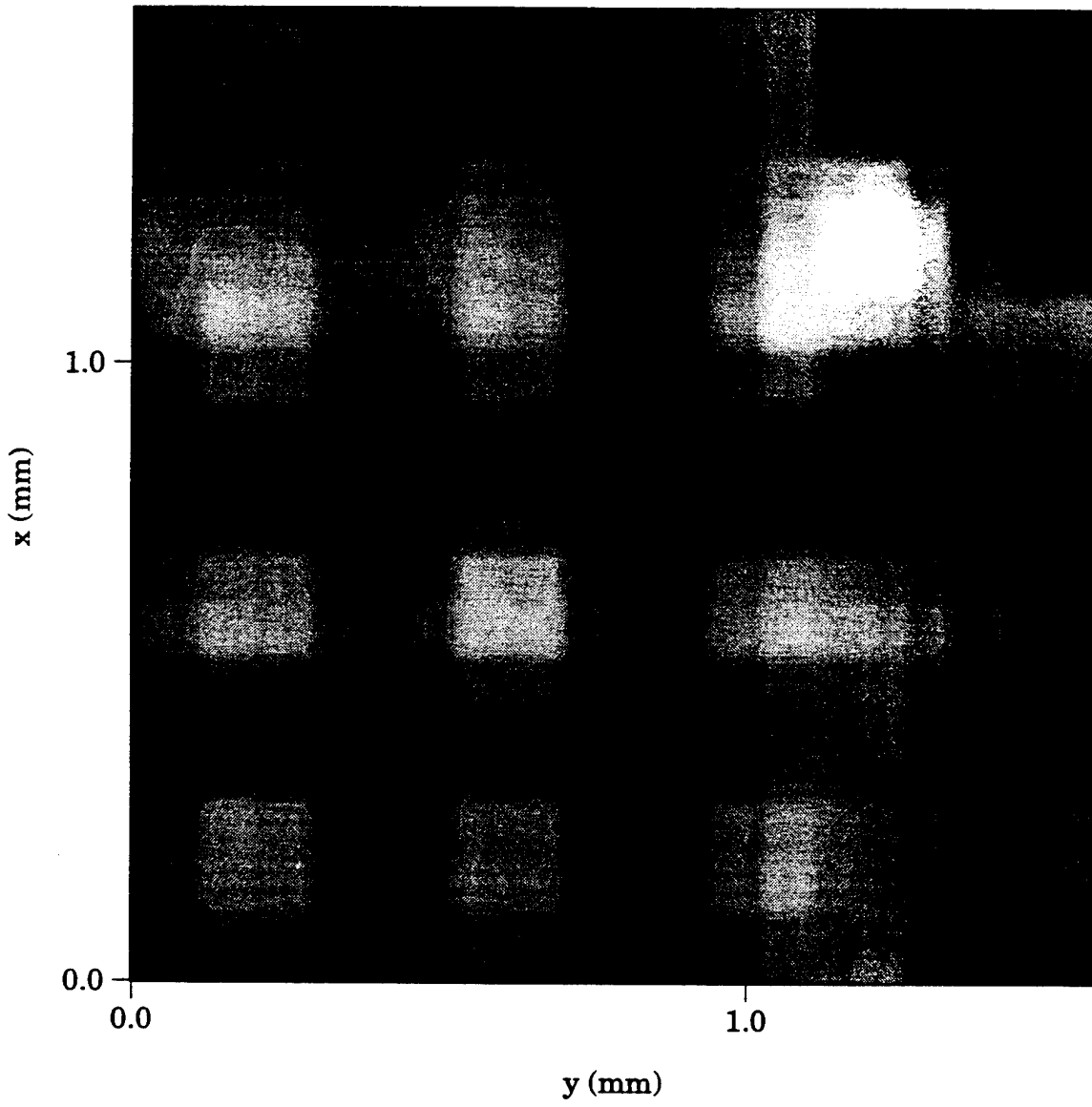
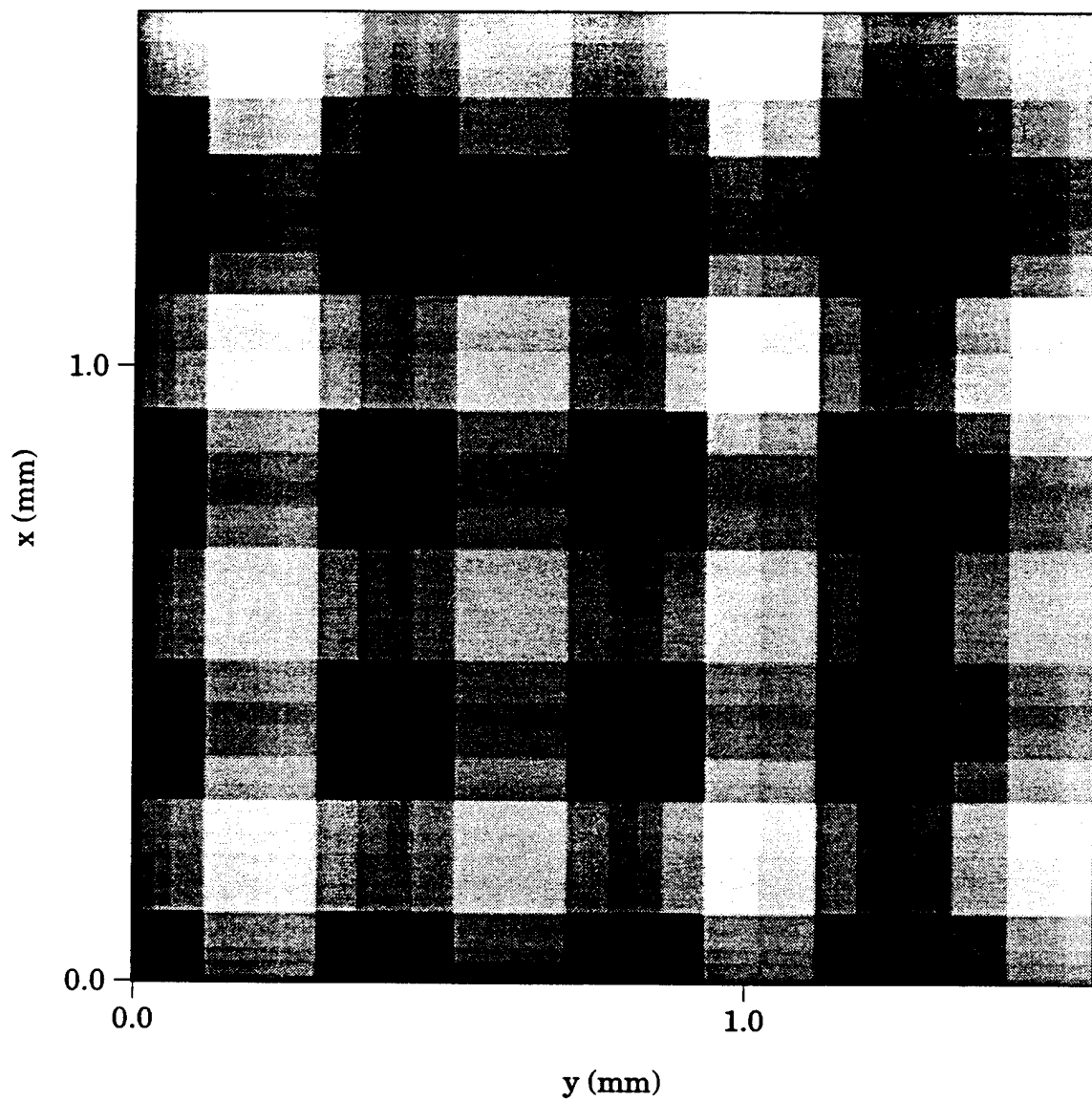


Fig. 2 (b)



-0.40 -0.20 -0.00 0.20
surface pressure phase angle (Rad)

Fig. 2 (c)

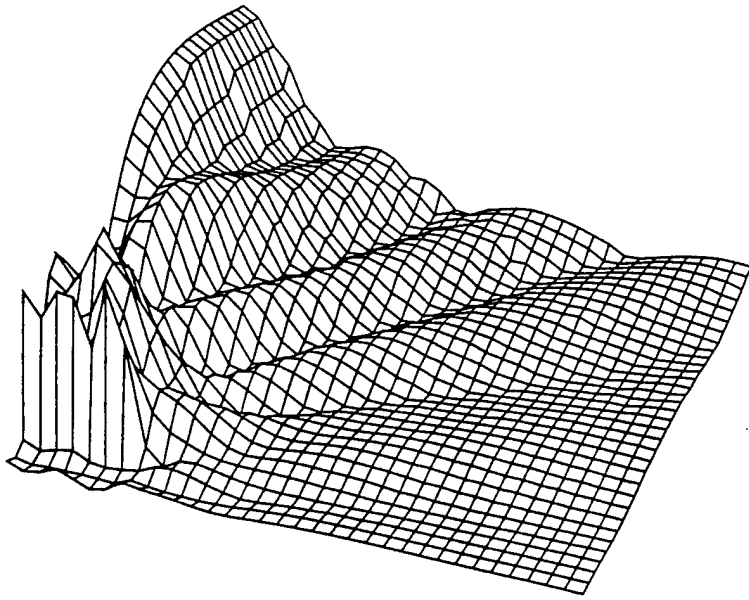


Fig. 3

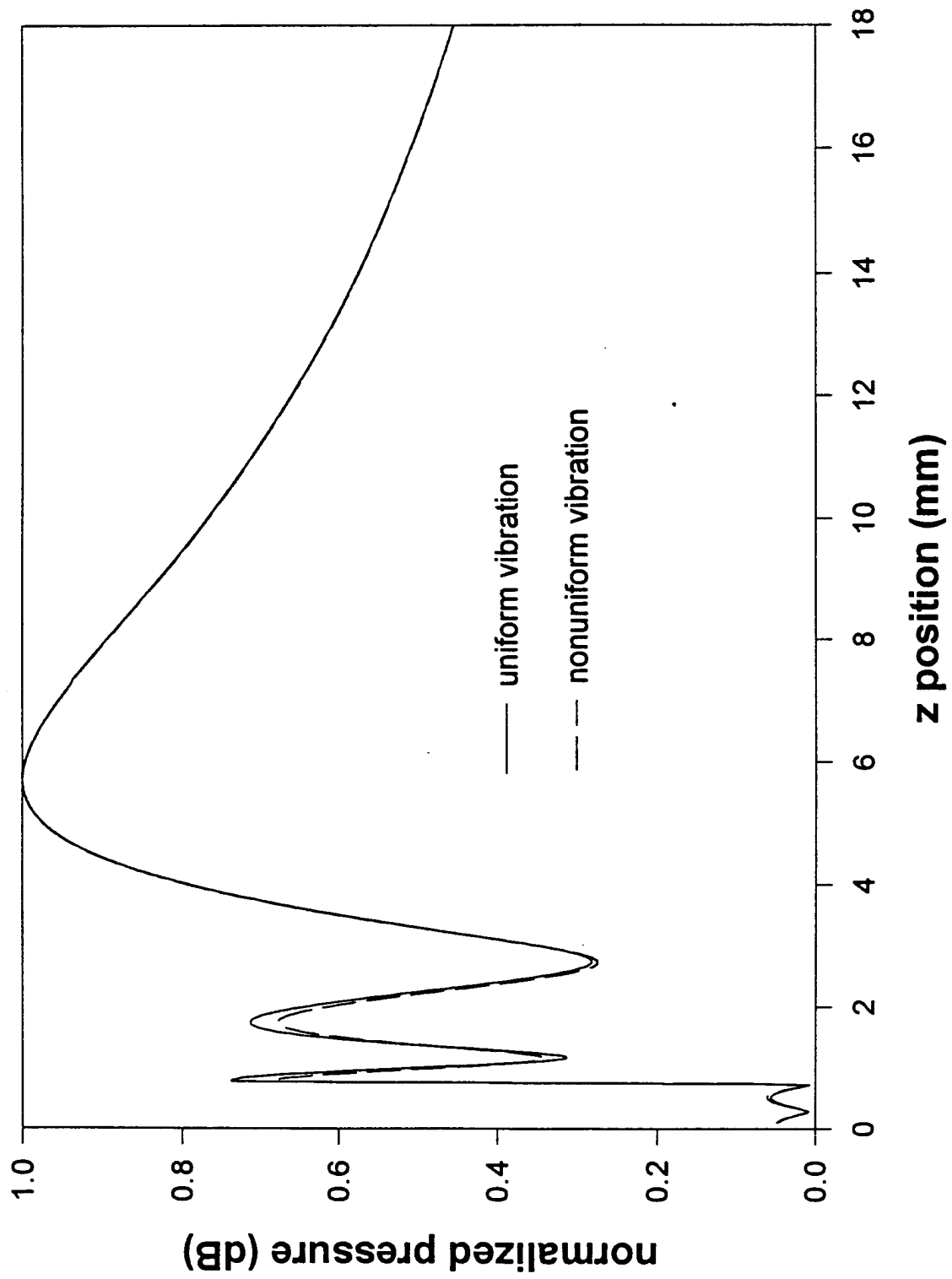


Fig. 4

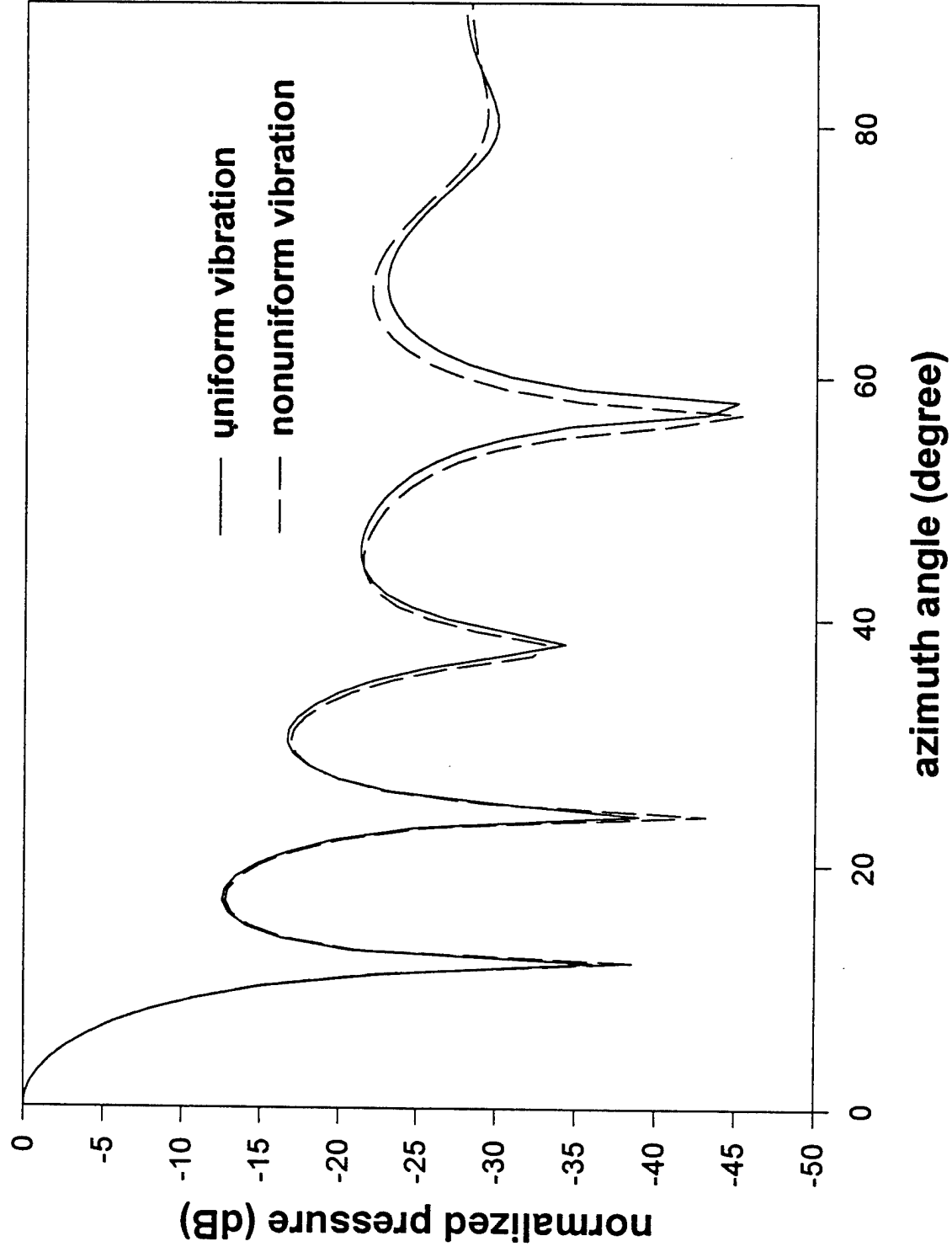


Fig. 5

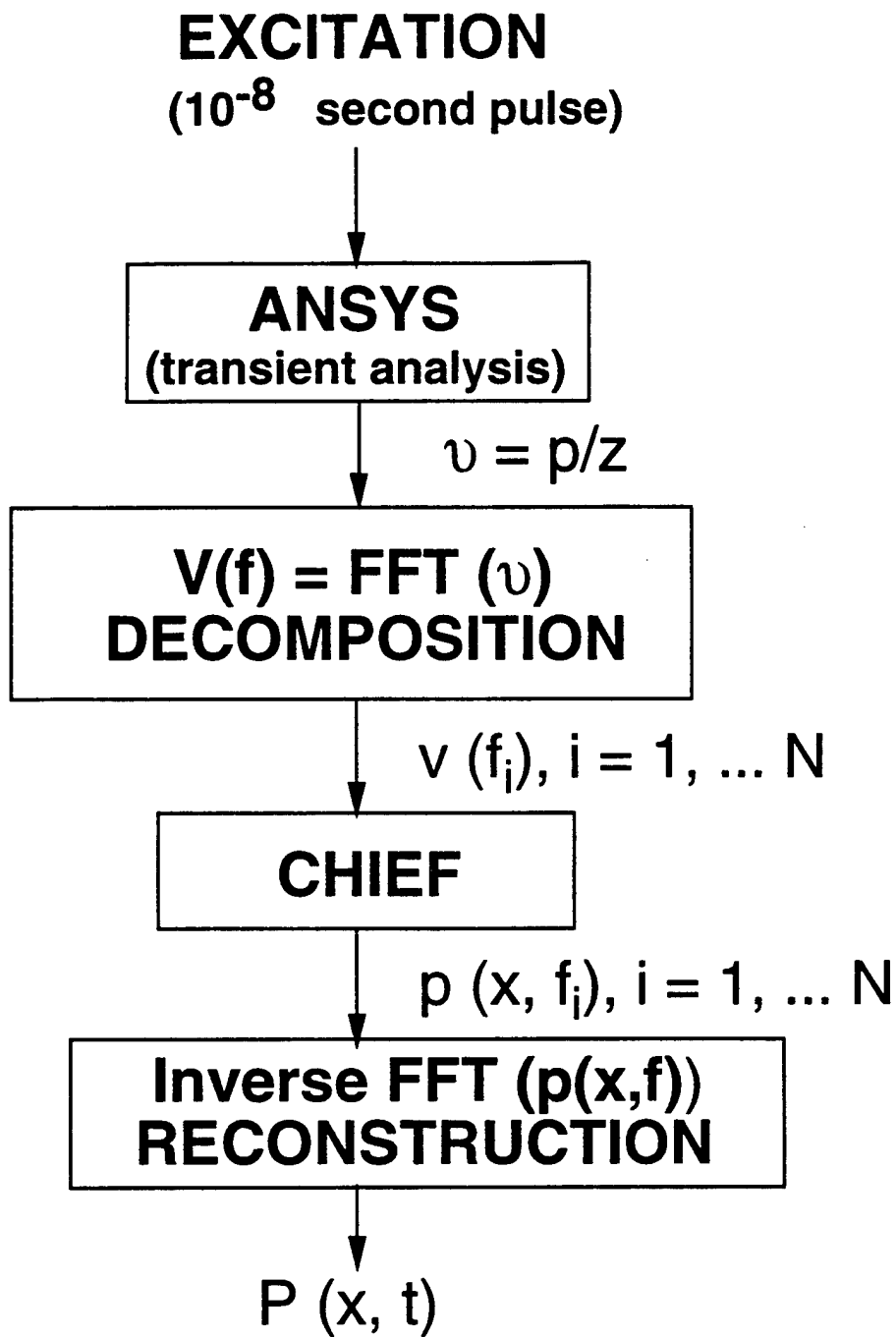


Figure 6

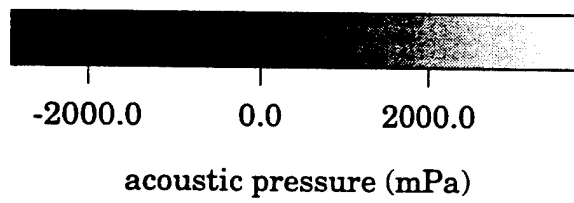
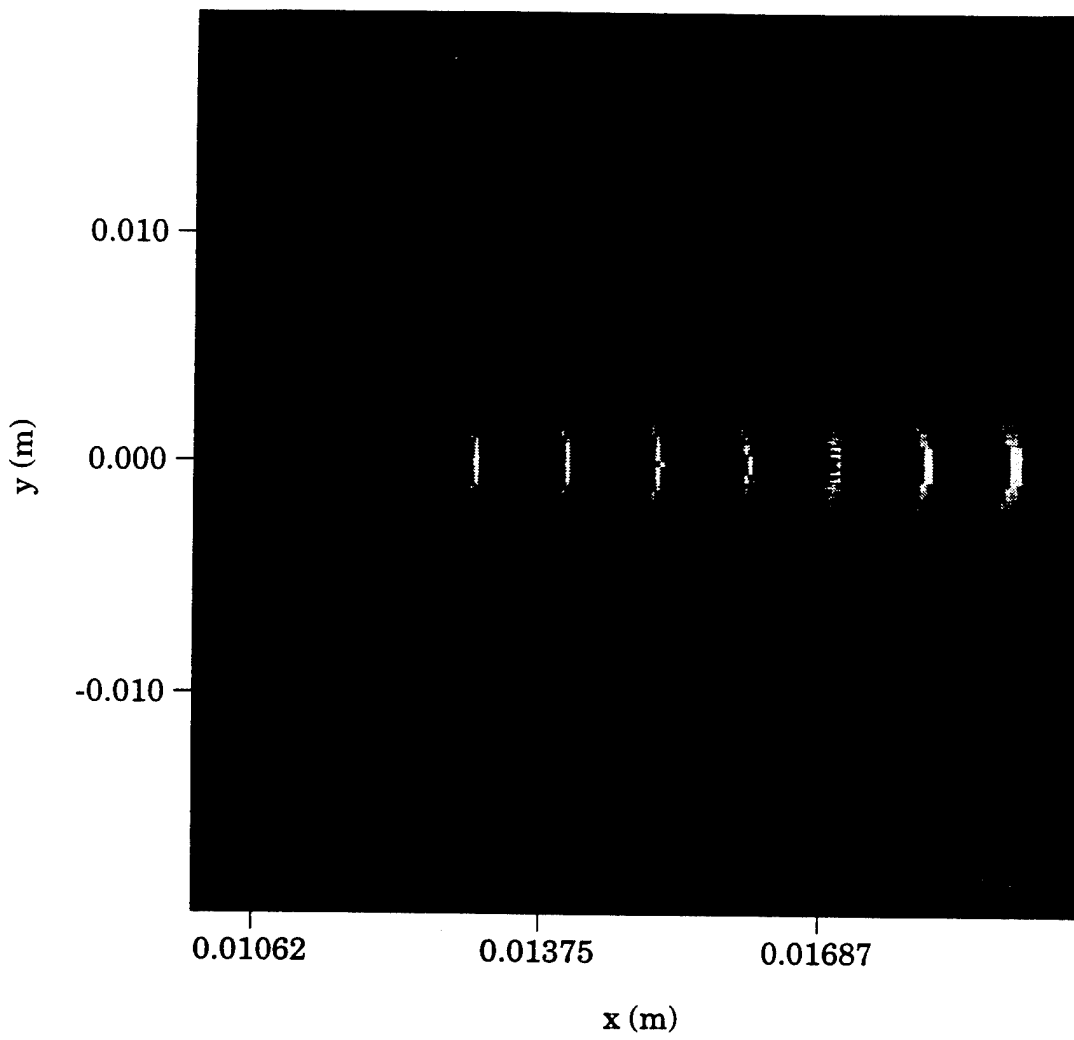


Fig. 7

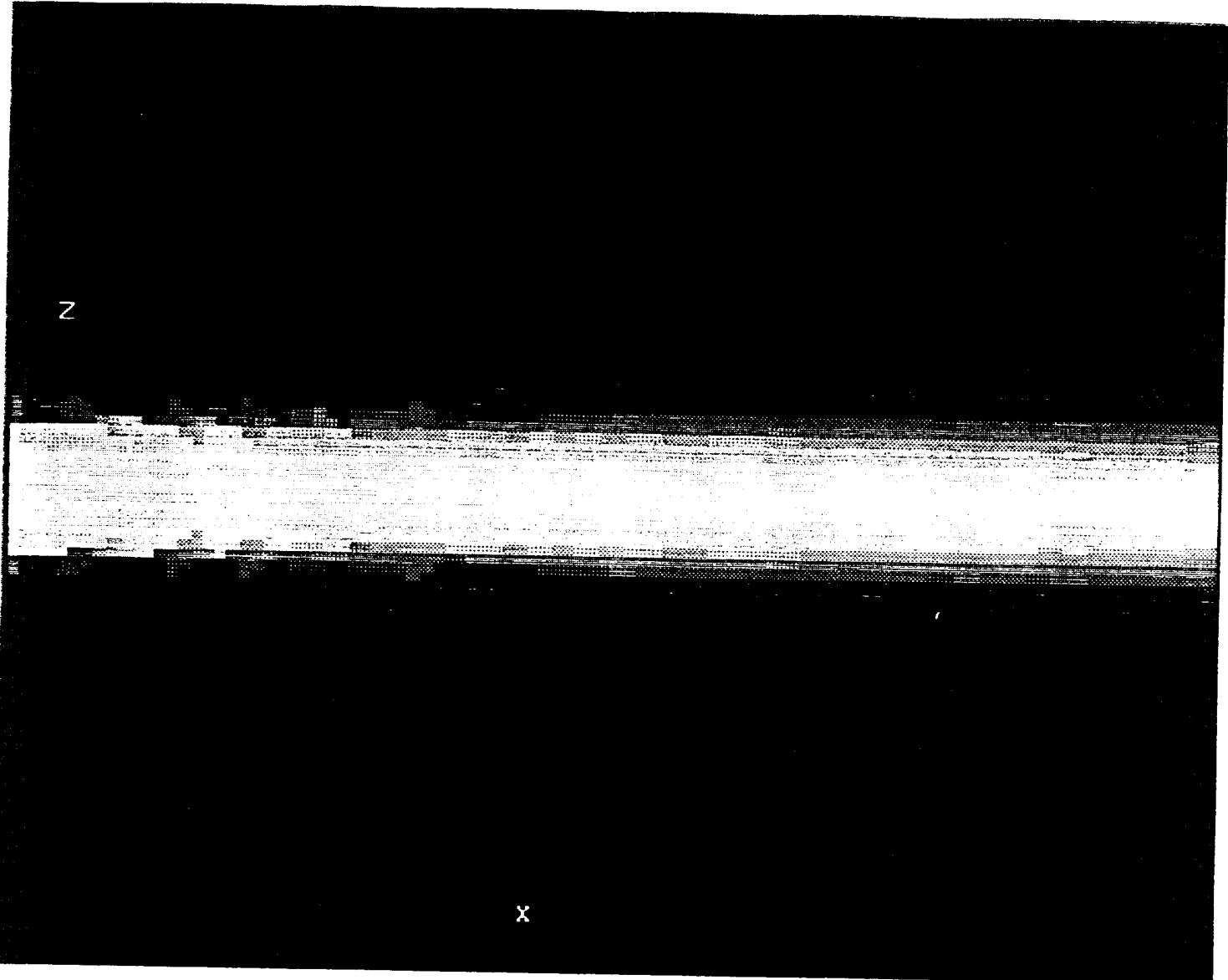


Fig. 8
(

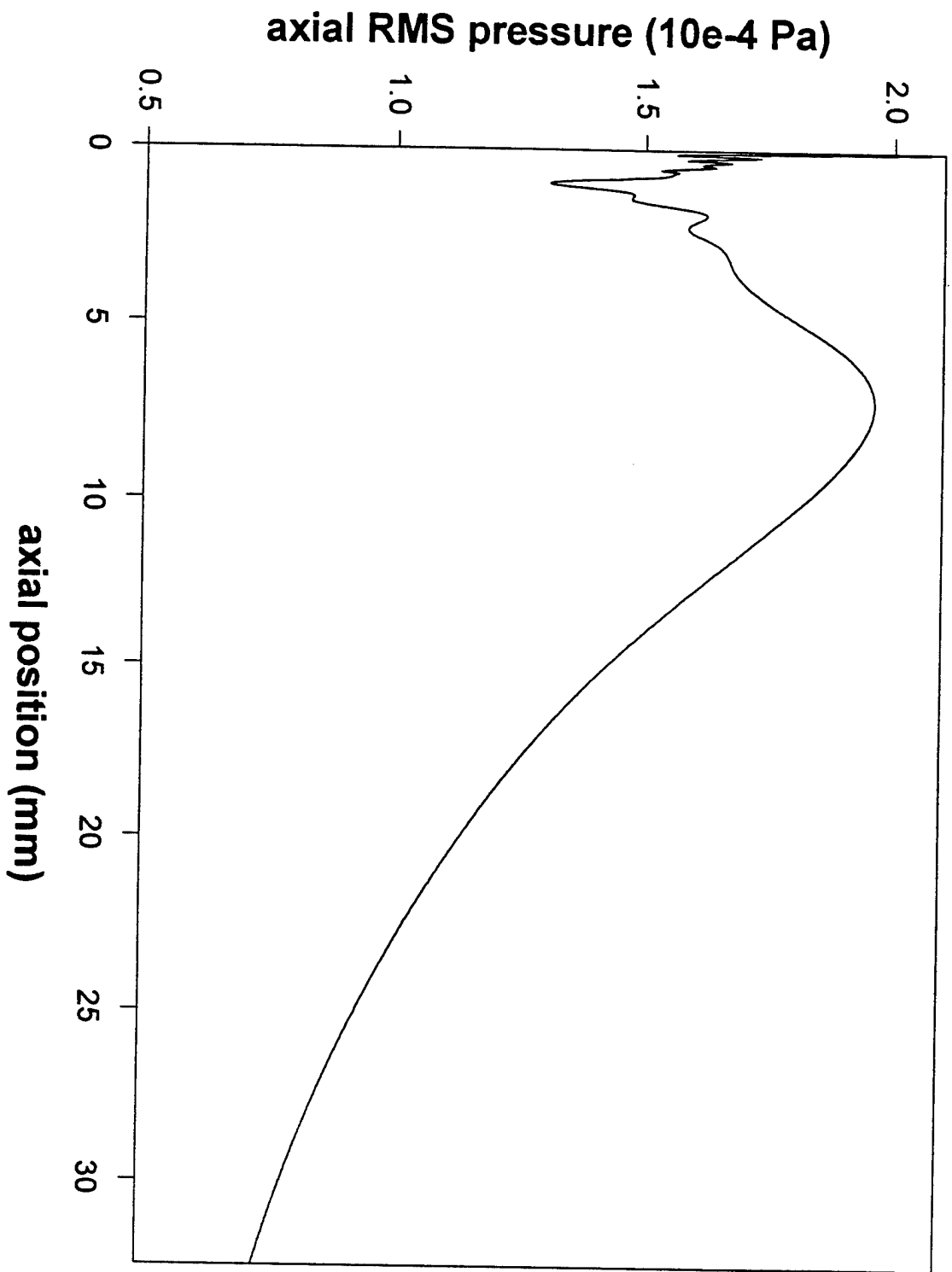


Fig. 9

APPENDIX 25

TAILORING MATERIAL PROPERTIES BY STRUCTURE DESIGN--- RADIALLY POLED PIEZOELECTRIC CYLINDRICAL TUBE

H. WANG, Q. M. ZHANG and L. E. CROSS
Materials Research Laboratory
The Pennsylvania State University
University Park, PA 16802

C. M. TROTTIER
Fiber Materials Inc.
Biddeford, ME 04005

Abstract: In many applications such as hydrophone and ultrasonic transducers, materials with large piezoelectric anisotropy are preferred in order to suppress the interfering signals from lateral modes. It has been shown that piezoelectric anisotropy can be significantly improved by structure design. For instance, for a radially poled cylindrical tube, the effective transverse piezoelectric response can be tuned to zero. In this work, the effective piezoelectric responses of lead zirconate titanate (PZT) and lead magnesium niobate-lead titanate (PMN-PT) ceramic cylindrical tubes were studied. Large piezoelectric anisotropy with a high effective uniaxial coefficient has been obtained for both materials. It has been shown that near zero effective d_{31} can be achieved for a PZT tube with a proper dimension ratio of r_o/R_o , where r_o and R_o are inner and outer radii of the tube, respectively. While for a PMN-PT tube, the effective piezoelectric responses can be tuned by the ratio of r_o/R_o as well as the bias field because the induced piezoelectric coefficients d_{33} and d_{31} and their ratio $|d_{33}/d_{31}|$ are all functions of the bias field.

INTRODUCTION

Conventional piezoelectric lead zirconate titanate (PZT) ceramics are widely used in many transducer applications. The materials have high electromechanical coupling coefficients and large piezoelectric strain constants d_{33} and d_{31} . However, the piezoelectric anisotropy, which is measured by d constant ratio $|d_{33}/d_{31}|$ or coupling constant ratio $k_t k_p$, where k_t and k_p are thickness and planar coupling coefficients, respectively, of the materials is quite small. In the applications where large piezoelectric anisotropy is required PZT ceramics are not favorable candidates. For example, in underwater hydrophone applications, an important material parameter is hydrostatic coefficient $d_h (=d_{33} + 2d_{31})$. In order to achieve a large d_h constant it is desirable to use materials with a large ratio of $|d_{33}/d_{31}|$ since d_{33} and d_{31} have opposite signs. Similarly, for ultrasonic transducers, materials with high piezoelectric anisotropy can transmit

ultrasonic wave in the poling direction with minimal interference from lateral modes. Previous efforts to improve piezoelectric anisotropy of a device were mainly focused on the selection of materials with large ratio of $|d_{33}/d_{31}|$, including single phase ceramics and ceramic/polymer composites. For example, lead titanate (PT) ceramic possesses large lattice anisotropy. Under certain processing conditions modified PT ceramics showed unusually large ratio of the thickness to the planar coupling coefficients and, consequently, a large ratio of $|d_{33}/d_{31}|$.^{1,2} Piezoelectric ceramic/polymer composites can also be engineered to exhibit high piezoelectric anisotropy.³

Another approach to increase piezoelectric anisotropy is by material structure design. Even for the materials with small piezoelectric anisotropy as PZT ceramics, by proper design of material structure it is possible to enhance the effective longitudinal coefficient d_{33} meanwhile to suppress the effective transverse coefficient d_{31} . Piezoelectric ceramic cylindrical tubes are commonly employed as stress sensors. Recently it has been shown that when poled in the radial direction, the effective d_{33} constant of a ceramic tube with a large ratio of length to wall thickness can reach an exceptionally large value.⁴ In addition, analysis has indicated that the effective d_{31} constant can be tuned from positive to zero, and to negative by varying the ratio r_o/R_o of the tube, where r_o and R_o are inner and outer radii, respectively, and/or by changing the ratio $|d_{33}/d_{31}|$ of the ceramic. Besides providing large piezoelectric anisotropy, the structure is also very attractive in the applications where large surface displacement is required since the effective d_{33} constant is proportional to the ratio of the length to the wall thickness and can be much higher than those of PZT and PT based ceramics.

In this paper, the results of recent investigations of the effective piezoelectric responses of lead magnesium niobate-lead titanate (PMN-PT) and PZT ceramic cylindrical tubes are reported. High piezoelectric anisotropy and large uniaxial coefficients have been obtained. The effects of non-uniformity of electric field and bias-field dependence of induced piezoelectric coefficients on the effective piezoelectric responses of PMN-PT tubes are discussed.

PIEZOELECTRIC RESPONSES OF A CYLINDRICAL TUBE

Piezoelectricity can be described by the constitutive equations. When mechanical stress (T) and electric field (E) are chosen as independent variables, the mechanical strain (S) and electric displacement (D) responses are described by:

PIEZOELECTRIC CYLINDRICAL TUBE

$$S_i = s_{ij}T_j + d_{in}E_n \quad (1a)$$

$$D_m = d_{mj}T_j + \epsilon_0 K_{mn}E_n \quad (1b)$$

where s_{ij} are elastic compliances, K_{mn} are dielectric constants, ϵ_0 is free space permittivity and d_{mj} are piezoelectric strain coefficients. Eq. (1b) describes the direct effect, where electric charges are induced by a stress while Eq.(1a) describes the converse effect, where strains are induced by an electric field.

Shown in Fig. 1 is a schematic drawing of a piezoelectric cylindrical tube and its coordinate system. Electrodes are on the inner and outer wall surfaces and the polarization of the material is along the radial direction. The piezoelectric responses from the direct and the converse effects of such system were analyzed by several authors.⁵⁻¹⁰ In their works, the voltage developed in the system by pressure or transmitting responses induced by an electric field were obtained. Recently, the analytical results of the effective piezoelectric strain constants d_{33} and d_{31} of a radially poled ceramic tube have been reported.⁴ It has also been shown that for such a system, the effective piezoelectric d constants determined from the converse effect are equal to those from the direct effect. For the cylindrical tube structure, the effective d constants are defined as:

$$\frac{\Delta L}{L} = d_{33}^{\text{eff}} \frac{V}{L} \quad (2a)$$

$$\frac{\Delta D}{2R_0} = d_{31}^{\text{eff}} \frac{V}{L} \quad (2b)$$

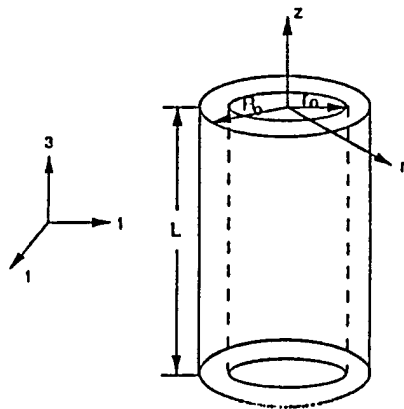


FIGURE 1 Schematic drawing of a cylindrical tube

where ΔL and ΔD are the displacements in the axial and radial directions under an applied voltage V , respectively, and L is the length of the tube. The effective piezoelectric d constants have the expressions:

$$d_{33}^{\text{eff}} = d_{31} \frac{2L}{(R_o + r_o) \ln(R_o/r_o)} \quad (3a)$$

$$d_{31}^{\text{eff}} = \frac{L}{(R_o + r_o) \ln(R_o/r_o)} \left[\left(1 + \frac{r_o}{R_o}\right) d_{31} + \left(1 - \frac{r_o}{R_o}\right) d_{33} \right] \quad (3b)$$

Two assumptions were used in the derivations of above equations. First, it was assumed that the material is elastically isotropic and the material parameters d_{33} and d_{31} are constant throughout the sample. Secondly, the strain responses in axial and radial directions are independent. Therefore, the requirements for the sample geometry are thin-wall ($R_o \gg (R_o - r_o)$) or long tube ($L \gg (R_o - r_o)$).

It can be seen from Eqs. (3a) and 3(b) that the effective longitudinal response of a tube depends only on the piezoelectric d_{31} constant of the material while the effective transverse response of a tube is a competition between the piezoelectric d_{33} and d_{31} modes through the tube dimensions. For piezoelectric ceramics such as PZT and PT, material parameters d_{33} and d_{31} are fixed after the poling. Therefore, the only way to tune the transverse response of a piezoelectric ceramic tube is to change the ratio of r_o/R_o . In Fig. 2, the calculated effective d_{33} and d_{31} constants of a PZT-500¹¹ ceramic tube are depicted as functions of the ratio of r_o/R_o . The outer radius and the length of the tube are 5.08 mm and 12.70 mm, respectively. As can be seen, when ratio r_o/R_o is near 0.38, the effective d_{31} of the tube is almost zero and the effective d_{33} constant is around -1200 pC/N resulting in large piezoelectric anisotropy.

As illustrated by Eq. (3b), the transverse piezoelectric response of a radially poled cylindrical tube depends not only on the ratio of r_o/R_o of the tube, but also on the ratio of $|d_{33}/d_{31}|$ of the material. For relaxor ferroelectrics, of which piezoelectric d_{33} and d_{31} coefficients can be induced by a DC bias field, the ratio of $|d_{33}/d_{31}|$ changes with the bias field. Therefore, the effective d_{31} constant of a cylindrical tube made of relaxor ferroelectric ceramic can be tuned by the bias field.

EXPERIMENTAL DETAILS

The major aims of this work were to experimentally investigate the piezoelectric

PIEZOELECTRIC CYLINDRICAL TUBE

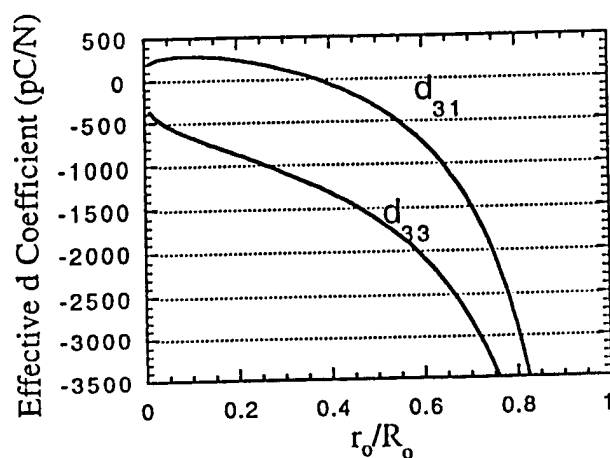


FIGURE 2 Calculated effective d constants of a PZT ceramic tube as functions of the dimension ratio

responses of a radially poled ceramic cylindrical tube and to increase the piezoelectric anisotropy by structure design. For most PZT ceramics, the d constant ratio $|d_{33}/d_{31}|$ is around 2.2. Therefore, when the dimension ratio r_0/R_0 of a PZT ceramic tube is close to 0.38, near zero transverse response can be obtained as seen from Fig. 2. In this work, normal piezoelectric ceramic PZT-500 and relaxor ferroelectric ceramic PMN-PT (90/10) were used. To achieve high piezoelectric anisotropy, the tube dimensions were designed based on Eqs. (3a) and (3b). The sample dimensions are listed in Table 1. PMN-PT tubes were purchased from TRS Ceramic Inc. and poled PZT-500 tubes were purchased from Piezo Kinetic Inc.. Gold sputtering and silver paste were used for the electrodes of PMN-PT samples. Low frequency dielectric constant and polarization of PMN-PT ceramics as functions of temperature were measured by a LCR meter (HP4274A) and a pA meter (HP4140B), respectively, with a computer controlled temperature regulation system. Material parameters d_{33} and d_{31} and the effective piezoelectric responses of the tube samples were measured by a double-beam laser interferometer.

RESULTS AND DISCUSSIONMaterial Properties

The induced d_{33} and d_{31} of an electrostrictive material are both functions of the electric bias field and are proportional to the dielectric constant (ϵ/ϵ_0) and polarization (P) of the material. In order to obtain high induced piezoelectricity, materials with high dielectric constants and large polarization are preferred. For relaxor ferroelectrics, in the temperatures above T_d and near T_m , where T_m is the temperature of maximum dielectric constant and T_d is the depolarization temperature, large reversible polarization and high dielectric constant are achievable. Consequently, large material parameters d_{33} and d_{31} can be obtained.

TABLE I Sample dimension of cylindrical ceramic tubes

Sample	R_o (mm)	r_o (mm)	L (mm)
PZT-500	2.56	1.01	12.70
PMN-PT-1	2.54	1.27	12.70
PMN-PT-2	2.54	1.02	12.70

PMN Ceramics are relaxor-type ferroelectrics with a broad and frequency-dispersive dielectric constant peak. Near the diffuse transition region, its dielectric constant can be over 30,000. Modification of the composition by normal ferroelectrics $PbTiO_3$ can shift the transition temperature from $T_m \sim -10^\circ C$ to that near room temperature, which is desirable for most applications. In this work, cylindrical tubes made of 0.9PMN-0.1PT ceramic were used. Plotted in Fig. 3 are the dielectric constant and the polarization of the material as functions of temperature measured at frequency of 1 kHz. As can be seen from the diagram, the depolarization temperature T_d and the temperature of maximum dielectric constant of the material T_m are around $10^\circ C$ and $50^\circ C$, respectively. The dielectric constant is about 15,000 in room temperature.

PIEZOELECTRIC CYLINDRICAL TUBE

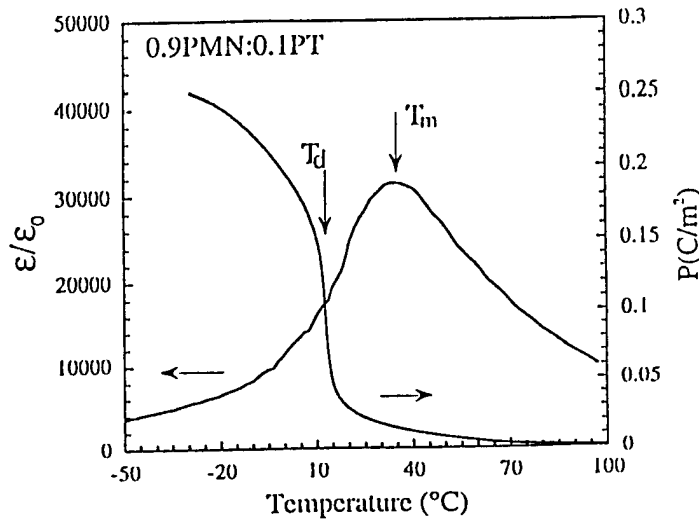


FIGURE 3 Dielectric constant and polarization of PMN-PT (90/10) ceramic as functions of temperature

At temperatures above T_d , piezoelectricity can be induced by a DC bias field. Shown in Figs. 4 (a) and (b) are the induced transverse and longitudinal piezoelectric constants of 0.9PMN-0.1PT ceramic as functions of bias field, respectively, measured at frequency of 500 Hz. Clearly, induced d_{33} and d_{31} coefficients increase linearly with bias field until they reach a peak. Depicted in Fig. 5 is the change of the ratio $|d_{33}/d_{31}|$ with the bias field. The overall ratio of the material is higher than those of most PZT ceramics, which are around the value of 2.2. In addition, in the field range of 1 - 4 kV/cm, this ratio increases with the bias field. Therefore, even for fixed dimensions (r_o/R_o) the effective d_{31} constant of a PMN-PT tube can be adjusted by the bias field.

Effective Piezoelectric Response of a Radially Poled Tube

The material parameters d_{33} and d_{31} of PZT ceramics are fixed after the ceramics are poled. Therefore, the transverse piezoelectric response of a radially poled PZT cylindrical tube only depends on its dimensions. As indicated in Fig. 2, when the ratio of r_o/R_o is 0.372, the calculated effective d_{31} constant of a PZT-500 tube is zero. For the PZT-500 samples used in this study, the ratio of r_o/R_o was 0.395. Shown in Fig. 6 are effective d_{33} and d_{31} coefficients of a PZT-500 tube measured at low frequencies. The effective d_{33} constant is about -1300 pC/N and the effective d_{31} constant is about -50 pC/N. Obviously, compared with the material parameters ($d_{33} = 3/4$ pC/N and $d_{31} = -171$ pC/N), piezoelectric anisotropy is greatly enhanced in this structure. For PMN-PT ceramic tubes the effective responses also depend on the DC bias field because the induced

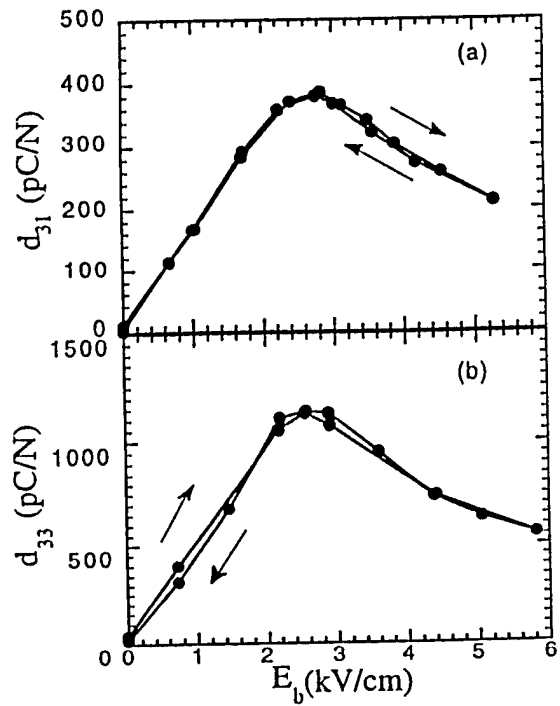


FIGURE 4 Induced piezoelectric d_{31} (a) and d_{33} (b) coefficients of PMN-PT (90/10) ceramic

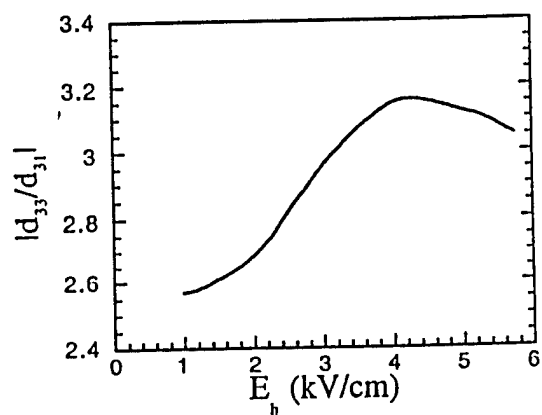


FIGURE 5 The d constant ratio as a function of bias field

PIEZOELECTRIC CYLINDRICAL TUBE

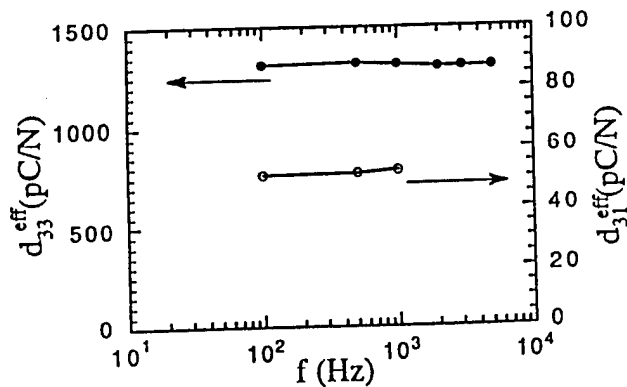


FIGURE 6 Effective d constants of the PZT-500 tube as a function of frequency

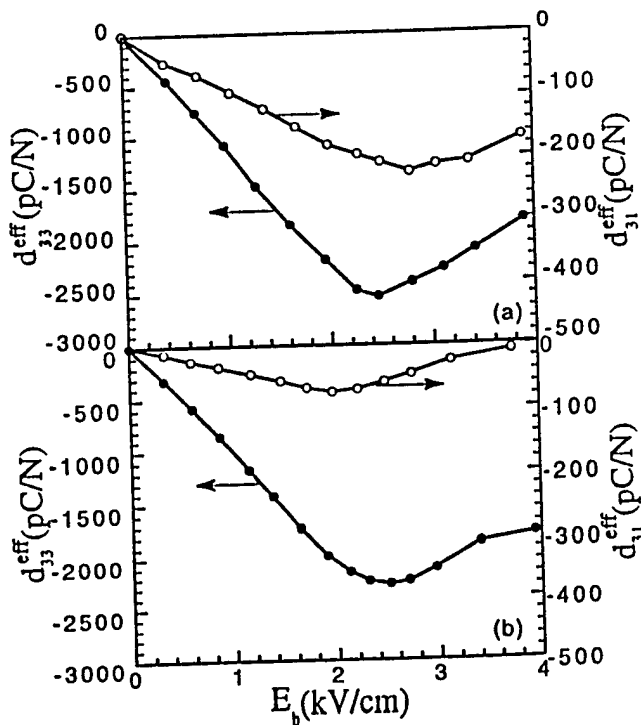


FIGURE 7 DC bias field dependence of the effective d constants of PMN-PT sample #1 (a) and sample #2 (b)

piezoelectric parameters d_{33} and d_{31} and their ratio $|d_{33}/d_{31}|$ are functions of the bias field. The bias field dependence of effective d_{33} and d_{31} constants of PMN-PT ceramic tubes #1 and #2 is illustrated in Fig. 7(a) and 7(b), respectively. Several features can be seen from the results presented in Figs. 6, 7(a) and 7(b). (1) For all samples, the effective longitudinal and transverse d constants have the same sign indicating that in hydrostatic applications, both longitudinal and transverse effects make positive contribution to the total response. (2) The uniaxial piezoelectric response (d_{33}^{eff}) is greatly enhanced. This parameter can be further improved by using samples with a larger ratio of $L/(R_o-r_o)$. Hence, a piezoelectric ceramic tube with appropriate dimensions is a good candidate for uniaxial actuator applications. (3) As indicated by Eq. (3b) the effective d_{31} constant of a tube strongly depends on the ratio r_o/R_o . For the PMN-PT samples, when the ratio r_o/R_o is reduced by 20%, the effective d_{31} constant decreases about 70%. Consequently, strong piezoelectric anisotropy is obtained. (4) Comparing the results of the PMN-PT ceramic, it is found that at the same bias voltage level, radially poled tubular structure can provide much higher d_{33} constant than that of the material parameter. Therefore, the requirements for the power supply equipment are greatly reduced.

Listed in Table 2 is a comparison between experimental results and the calculations by Eqs. (3a) and (3b). It can be seen that for PZT samples the experimental results of the effective d constants are in good agreement with those from the analytical calculations. For PMN-PT samples, the discrepancy between the measured and the calculated values is more obvious (beyond the data scattering). This is because for relaxor ferroelectric materials, induced piezoelectricity strongly depends on the DC bias field as indicated in Figs. 4(a) and 4(b). For the structure of a cylindrical tube, DC bias field is not uniform in the radial direction. Thus, the induced piezoelectric d_{33} and d_{31} coefficients are not constant in the material. The bias field in the calculations and in Figs. 7(a) and 7(b) was taken as the bias voltage divided by the tube wall thickness. For the samples employed in this work the electric field at inner wall surface of the samples is more than double of that at outer wall surface. For example, with a DC bias voltage of 200 V, the actual electric fields are 0.86 kV/cm and 2.15 kV/cm at the outer and inner surfaces of sample #2, respectively. From Fig. 4(a), the corresponding induced d_{33} constants are 390 pC/N and 1070 pC/N, respectively. Apparently, this inhomogeneity of piezoelectric constants in the material is quite significant. Moreover, due to the nonlinear relation between induced piezoelectric constants and the bias field, the induced piezoelectric constants are not monotonically decreasing in the radial direction. Hence, it is not surprising that there is a

PIEZOELECTRIC CYLINDRICAL TUBE

TABLE 2 Effective d coefficients of the ceramic tubes

Sample	d ₃₃ (pC/N)		d ₃₁ (pC/N)	
	Measured	Calculated	Measured	Calculated
PZT-500	-1310	-1308	-51	-46
PMN-PT-1*	-2500	-3558	-210	72
PMN-PT-2*	-2280	-2893	-55	617

* Both measured and calculated d coefficients are at bias field of 2.5 kV/cm.

discrepancy between the predictions of Eqs. (3a) and (3b) and the experimental results for relaxor ferroelectrics. For quantitative predictions of the effective piezoelectric responses of a relaxor ferroelectric ceramic tube, the inhomogeneity of induced piezoelectric coefficients due to the non-uniform bias field needs to be considered.

CONCLUSIONS

Piezoelectric anisotropy can be significantly improved by an appropriate structure design. The experimental results presented above demonstrate that for a radially poled cylindrical tube, practically, a zero transverse d₃₁ coefficient has been obtained for both piezoelectric PZT ceramic and relaxor ferroelectric PMN-PT ceramic, which confirms the predictions from the early analytical calculations. Moreover, the effective uniaxial coefficients have been greatly enhanced compared with the material parameters. Besides the dependence of effective piezoelectric constants on the tube dimensions, the effective transverse coefficient of a relaxor ferroelectric ceramic tube can also be tuned by the material parameters d₃₃ and d₃₁, which are functions of bias field. Due to the non-uniform bias field in the radial direction, the inhomogeneity of induced piezoelectric constants in a tube made of relaxor ferroelectrics needs to be considered in the calculations of the total piezoelectric responses. The structure is promising in applications where large surface displacement and high piezoelectric anisotropy are required.

H. WANG, Q. M. ZHANG, L. E. CROSS and M. C. TROTTIER

ACKNOWLEDGMENT

This work was supported by a SBIR grant from ARPA through Fiber Materials Inc. and by the Office of Naval Research.

REFERENCES

1. D. Damjanovic, T. R. Gururaja, S. J. Jang and L. E. Cross, Ultrason. Symp. Proc., (2), 633 (1986).
2. D. Damjanovic, T. R. Gururaja, S. J. Jang and L. E. Cross, Am. Ceram. Soc. Bull., 66, (4), 699 (1987).
3. T. R. Gururaja, A. Safari, R. E. Newnham and L. E. Cross, in Electronic Ceramics, edited by L. M. Levinson, (Marcel Dekker Inc., New York, 1988) p. 92.
4. Q. M. Zhang, H. Wang and L. E. Cross, Proc. SPIE Smart Struc. Mater., 1916, 244 (1993).
5. R. A. Langevin, J. Acoust. Soc. Amer., 26, 421 (1954).
6. C. P. Germano, J. Acoust. Soc. Amer., 34, 1139-1141 (1962).
7. W. D. Wilder, J. Acoust. Soc. Amer., 62, 769-771 (1977).
8. A. A. Anan'eva, Ceramic Acoustic Detectors, (Consultants Bureau, New York, 1965).
9. J. A. Burt, J. Acoust. Soc. Amer., 64, 1640 (1978).
10. P. H. Rogers, J. Acoust. Soc. Amer., 80, 13 (1986).
11. Trade mark of Piezo Kinetic Inc., Belloefont, PA.

APPENDIX 26

Electric Field Forced Vibration of a Periodic Piezocomposite Plate
with Laminated Structure and
Reflection and Transmission of a Plane Wave at the Fluid-Composite Interface

Q. M. Zhang and Xuecang Geng

Materials Research Laboratory, The Pennsylvania State University
University Park, PA 16802

Abstract:

We address the problems of the vibration of a periodic piezo-composite plate (2-2 composite) under external electric fields and the reflection and transmission of a plane wave incident on the fluid-composite interface based on an analytical method developed recently, which takes into account explicitly the heterogeneous nature of the piezocomposites. It is shown that due to the finite thickness of the composite plate, a series of piezo-active modes at frequencies near and above the stop band edge mode frequency may be excited. It is also shown that as a result of the heterogeneous structure of the composite, the reflection coefficient from the fluid-composite interface is a complex number, which should have important implication on the design of quarter wave matching layer in composite transducers.

I. Introduction.

Piezoceramic polymer composites have been widely used in areas such as ultrasonic medical imaging and non-destructive evaluation and exhibit many attractive features in these applications in comparison with single phase piezoelectric materials.¹ Since as a diphasic material, the effective properties of a composite depend crucially on the properties of the constituents, the quantitative study of their properties is an interesting and important problem in order to optimize composite transducers for different applications. However, due to the fact that for ultrasonic applications, the aspect ratio of the composite unit cell, which is L/d for a composite with 2-2 connectivity as schematically drawn in figure 1, is not large (usually in the range between 2 and 6) and the acoustic wavelength is also comparable to the spatial period d , the usual averaging schemes such as those based on either the Reuss (isostress) model or Voigt (isostrain) model² in treating the elastic and electromechanical properties of a composite become inadequate. While finite element analysis (FEA) can provide some information on how the properties of the constituents affect the ultrasonic performance of a composite transducer under these conditions, it is quite time consuming if a systematic study is intended and to some extent, FEA is a computer experiment and, hence, does not provide a lot of physical insight into the problem investigated. Clearly, analytical models which take into account the heterogeneous structure of a composite and can bridge the gap between the earlier simple models on composite materials and FEA should be developed.

Recently, based on the method of partial wave expansion, a theoretical model was established for composites with a periodic laminate structure and finite aspect ratio L/d .^{3,4} For a periodic laminate composite plate as schematically drawn in figure 1, since the dimension in the x_2 -direction is much larger

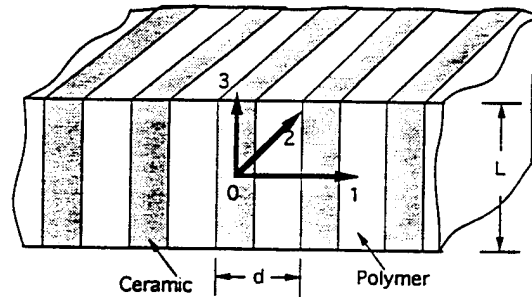


Figure 1. Schematic drawing of a periodic piezoceramic polymer composite plate. The poling direction of the piezoelectric ceramic plates is along the x_3 -direction. The width of ceramic plate is $v d$ and the width of polymer is $(1-v) d$, where v is the ceramic volume content in the composite.

than L and d , the problem can be treated as a two dimensional one. Here, the solution to a bounded composite plate is obtained by summation over the solutions of guided waves in unbounded plates.⁵ Unlike the earlier approach, the solutions to unbounded composite plates are obtained by solving the dynamic elastic equations in the ceramic phase and polymer phase separately and matching the two by the boundary conditions at the ceramic-polymer interface. Hence, the problem of averaging the properties of a composite in the x_1 -direction is avoided.

The guided wave solutions to the dynamic elastic equations in the unbounded ceramic plate are:

$$\begin{aligned} u_3^c &= \sum_{i=1}^3 R_i^c f_i^c \cos(h_i^c x_1) \exp(j \beta x_3) \\ u_1^c &= \sum_{i=1}^3 R_i^c g_i^c \sin(h_i^c x_1) \exp(j \beta x_3) \\ \Phi^c &= \sum_{i=1}^3 R_i^c t_i^c \cos(h_i^c x_1) \exp(j \beta x_3) \end{aligned} \quad (1)$$

where f_i^c , g_i^c , and t_i^c are factors depending on β and h_i , the wave vector components in the x_3 and x_1 directions, and $j = \sqrt{-1}$. Similar equations can be written for the polymer plate.^{3,4}

The superscripts c and p are introduced to denote the ceramic and polymer, respectively. In eq. (1), the symmetry conditions in the x_1 -direction for the piezoelectric active mode in a periodic composite plate are used, and for the sake of

simplicity, the time dependent term ($\exp(j\omega t)$), where ω is the angular frequency and t is time, is omitted. The boundary conditions of the stresses, elastic displacements, and the electric displacement and potential at the ceramic-polymer interface ($x_1 = vd/2$) yield six homogeneous linear equations which relate the six undetermined coefficients R_i^p and R_i^c . The condition for a nontrivial solution of homogeneous linear equations requires that the determinant of the coefficients vanishes, i.e.,

$$K = | \text{coefficients of } R_i | = 0 \quad (2)$$

where the coefficients of R_i are functions of the β , d , the angular frequency ω , the ceramic volume fraction v , and the material parameters of both the polymer and piezoceramic. Equation (3) yields the relationship between β and f , the dispersion curves. For each point on the dispersion curves, the relations among R_i^p and R_i^c can be determined from the homogeneous linear equations. Shown in figures 2(a) and 2(b) are the dispersion curves for composite plates with 15% and 44% ceramic content, respectively. The parameters used in the calculation are those of PZT-5H for the piezoceramic and Spurrs epoxy for the polymer phase, respectively.⁶ In addition, for $\beta=0$, the solutions in the ceramic and polymer plates which satisfy the boundary conditions at $x_1=vd/2$ are:

$$u_1^c = k_1 C \sin(h_{01}^c x_1), u_1^p = k_2 C \sin(h_{01}^p (x_1 - \frac{d}{2})), \quad (3)$$

$$\Phi^c = \Phi^p = C x_3$$

where k_1 and k_2 are constants, $h_{01}^c = \sqrt{\frac{\rho^c}{c_{11}^c}} \omega$, $h_{01}^p = \sqrt{\frac{\rho^p}{c_{11}^p}} \omega$.

In this paper, two situations will be considered explicitly based on the results presented. The first one is a composite plate situated in air and subjected to an AC applied electric field where the electric impedance, resonant mode frequencies, and surface vibration profile will be calculated. The second one is the wave propagation in a fluid-composite system as schematically drawn in figure 3. From the reflection coefficients, the input acoustic impedance at the fluid-composite interface as a function of frequency can be evaluated.^{7,8} Clearly, the quantities evaluated here can be measured experimentally and are of great importance to the understanding of ultrasonic performance and optimum design of a composite transducer.

II. Forced vibration of a finite thickness composite plate.

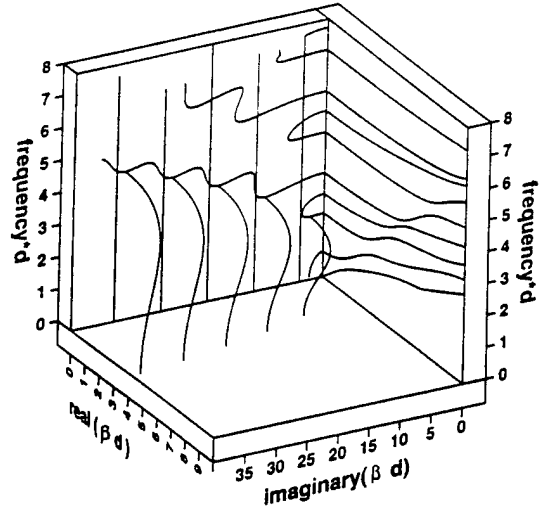
To treat a composite plate situated in air under an AC electric field, u_3 , u_1 , and ϕ are expanded in terms of the eigenfunctions in an unbounded system. For the ceramic plate:

$$u_3^c = \sum_{n=1}^m \sum_{i=1}^3 k_{ni}^c f_{ni}^c \cos(h_{ni}^c x_1) \sin(\beta_n x_3) A_n$$

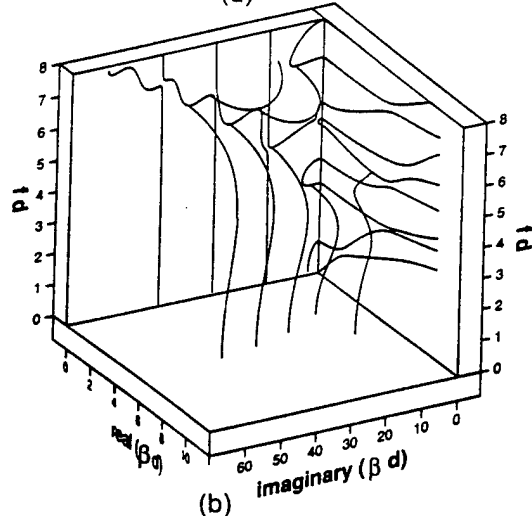
$$u_1^c = \sum_{n=1}^m \sum_{i=1}^3 k_{ni}^c g_{ni}^c \sin(h_{ni}^c x_1) \cos(\beta_n x_3) A_n + C k_1 \sin(h_{01}^c x_1)$$

$$\Phi^c = \sum_{n=1}^m \sum_{i=1}^3 k_{ni}^c t_{ni}^c \cos(h_{ni}^c x_1) \sin(\beta_n x_3) A_n + C x_3 \quad (4)$$

A similar solution can be written for the polymer plate. In eq. (4), k_{ni} , f_{ni} , g_{ni} , and t_{ni} are constants. A_n and C are determined by the boundary conditions which are traction free and $\phi = \pm \phi_0/2$ at $x_3 = \pm L/2$. With a finite number of eigenfunctions in the expansion, the boundary conditions at $x_3 = \pm L/2$ cannot be satisfied at all x_1 . The number of the



(a)



(b)

Figure 2. Dispersion curves for a composite made of PZT-5H ceramic and Spurrs Epoxy with 15% ($v=0.15$) (the top figure) and 44% ceramic volume content ($v=0.44$) (the bottom figure).

eigenfunctions, m , required, hence, is determined by the accuracy needed for the solution. For the problem treated here, we found that it is adequate to use eight eigenmodes in the expansion. In the frequency range studied ($fd < 2$ in figure 2), there are two branches with real β and other branches having either imaginary or complex β , which corresponds the modes confined at the boundary $x_3 = \pm L/2$ (surface modes).

The coefficients A_n and C in eqs. (4) are determined by the variational technique.⁵ Based on u_3 , u_1 , and ϕ thus determined, all the properties related to the vibration problem of a composite plate can be evaluated. Shown in figure 4(a) is the electric impedance spectrum for a composite plate with 44% ceramic content made of PZT-5H piezoceramic and Spurrs epoxy with $L/d = 4.49$. The electric impedance Z_e is calculated from the relation $Z_e = \phi_0/I$ where $I = j \omega \int D_3 dx_1$. The

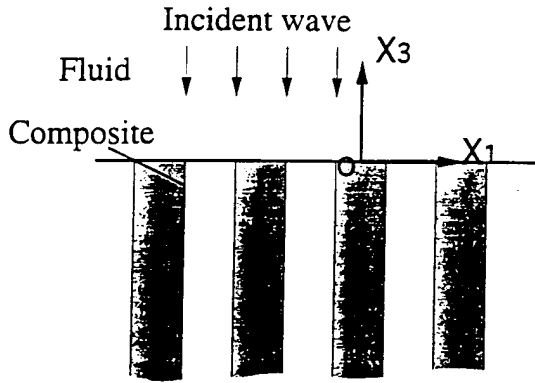


Figure 3. Schematic drawing of a plane wave incident normally at the fluid-2-2 composite interface, where the fluid occupies the upper half space and the piezocomposite the lower half space.

integration is over one unit cell for D_3 at $x_3 = L/2$, where D_3 is the electric displacement vector component along the x_3 -direction ($D_3 = e_{33}u_{3,3} + e_{31}u_{1,1} - \epsilon_{33}^s \phi_{,3}$). For the comparison, the electric impedance measured experimentally from the same composite is shown in figure 4(b) and clearly the theoretical impedance curve reproduces the experimental data quite well. One interesting feature revealed in the figures is that in a composite plate, in addition to the thickness resonance mode, there exist other modes due to the periodic nature of the composite and coupling between the two phases. In figure 5, we display the distributions of u_3 at each mode. Apparently, f_{L1} is the fundamental thickness resonance and f_{t1} is the stop band edge resonance as revealed by the fact that the ceramic and polymer vibrate 180° out of phase at this mode, which has been predicted in the earlier theoretical work.⁹ The frequency position and the distribution of u_3 along the x_3 -axis indicate that f_{L3} is third harmonic of the thickness mode. However, the appearance of f_{t2} is not expected from the earlier theoretical works. By examining the equations of the boundary conditions at $x_3 = \pm L/2$, it can be deduced that a resonance will occur whenever $\beta = (1+2n)\pi/L$, i.e., $\cos(\beta L/2) = 0$. From the dispersion curves of real β , as shown in figure 4(c), it is clear that the fundamental thickness resonance and the stop band edge resonance occur at $\beta = \pi/L$ (f_{L1} and f_{t1}). Similarly, when $\beta = 3\pi/L$, the third harmonic of the thickness mode will occur at f_{L3} . In addition, a mode f_{t2} will also show up at the branch 1 which is at a frequency near and above f_{t1} . By the same argument, it would be expected that f_{t3} , f_{t4} , etc. may also be observed, depending on the electromechanical coupling factors of these modes. It can be shown that the effective coupling factor for these modes decreases rapidly for the higher order modes. These features have been observed experimentally and the results here provide a clear physical picture for the experimental observation.

For a composite plate to work effectively as an electromechanical transduction material, it is required that the ceramic and polymer vibrate in phase with nearly the same amplitude in the x_3 -direction. The evolution of the vibration pattern in the two plates with frequency and the aspect ratio L/d of a composite plate is studied here. Shown in figure 6(a) is the change of the ratio u_{3p}/u_{3c} at $x_3 = L/2$ (at the surface of the composite plate), where u_{3p} and u_{3c} are u_3 at the centers of the

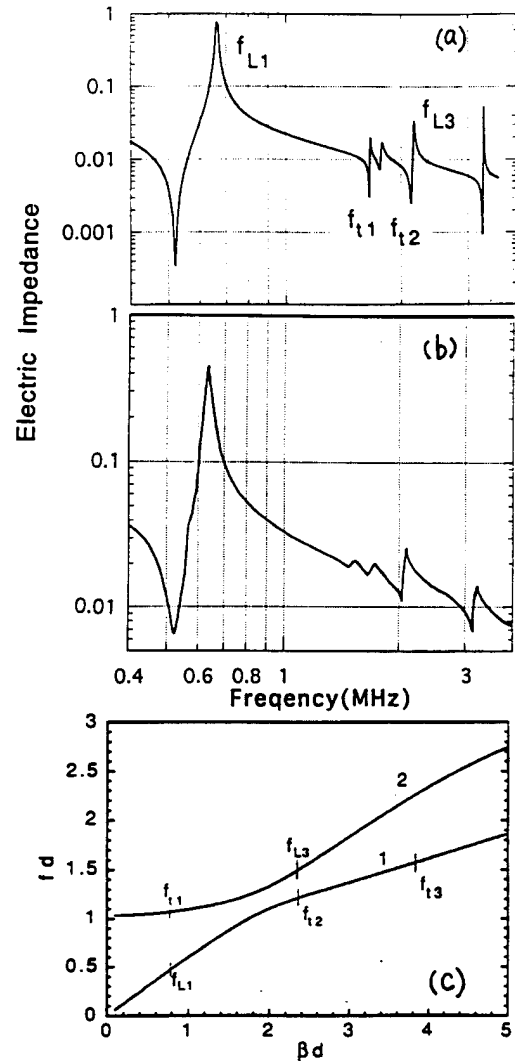


Figure 4. (a) The impedance spectrum for $\nu = 0.44$ composite plate of $L/d = 4.49$. (b) Experimental results for a 2-2 composite with $\nu=0.44$ and $L/d = 4.49$ which can be compared with figure (a), the theoretical result. (c) The dispersion curves for $\nu=0.44$ composite which show the positions of the possible resonant modes in a finite thickness plate. f_{L1} and f_{t1} occur at $\beta = \pi/L$, f_{L3} and f_{t2} occur at $\beta = 3\pi/L$. Hence, f_{t3} will occur at $\beta = 5\pi/L$, etc. Whether these high order modes f_{t2} , f_{t3} , etc. be observed experimentally depends on the electromechanical coupling factors for these modes.

polymer phase ($x_1=d/2$) and the ceramic ($x_1=0$) respectively, with frequency for the composite plate of $L/d = 4$. At frequencies far below any resonance mode, u_{3p}/u_{3c} is always less than one. As L/d increases, this ratio increases and approaches one. These are consistent with the results of the earlier theoretical model developed.¹⁰ As frequency increases towards the thickness resonance, the ratio u_{3p}/u_{3c} also increases towards one. At a frequency f_1 which is near f_s of the thickness mode, where f_s is the series resonant frequency, $u_{3p}/u_{3c} = 1$. This is true as long as $f_{L1} < f_{t1}$. This ratio will

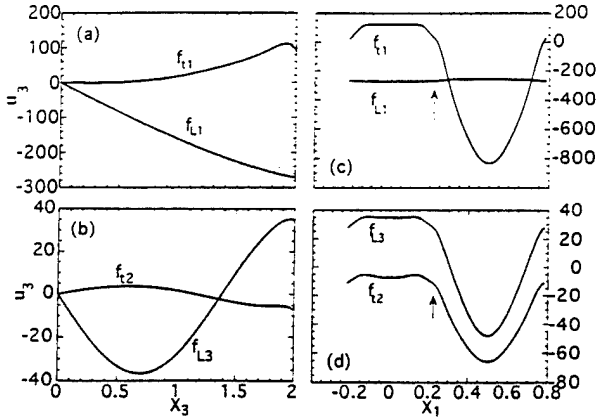


Figure 5. The distributions of u_3 for a composite plate of $\nu=0.44$ and $L=4$ ($d=1$) at f_{L1} , f_{t1} , f_{L3} , and f_{t2} . (a) and (b) u_3 at $x_1=0$ (at the center of ceramic plate) as a function of x_3 where $x_3=0$ is at the center and $x_3=2$ is at the surface of the composite plate. (c) and (d) u_3 at the surface of the composite plate as a function of x_1 . The arrows indicate the position of the interface between the ceramic and polymer. At f_{t1} and f_{L3} , the ceramic and polymer vibrate out of phase with each other, while at f_{L1} and f_{t2} , the two vibrate in phase.

surpass one as the frequency is further increased. In figure 6(b), the change of f_1/f_s vs. the aspect ratio L/d is presented. Clearly, f_1/f_s is near but larger than one except for composite plates with small aspect ratio. Hence, the aspect ratio L/d does not have a significant effect on the ratio of u_{3p}/u_{3c} at frequencies very near f_s of the thickness mode, where u_{3p}/u_{3c} is always near one. However, it will affect the bandwidth in

which u_{3p}/u_{3c} is near one. For example, the bandwidth $\frac{\Delta f}{f_1}$ in which $0.9 < u_{3p}/u_{3c} < 1.1$ increases as the aspect ratio L/d increases, which is shown in figure 6(b). In the practical design of a composite transducer, the aspect ratio L/d required, hence, will be determined by the operation bandwidth needed.

III. Reflection and transmission of a plane wave at fluid-composite interface

We now turn to the problem of the reflection and transmission of a plane wave normally incident at the fluid-composition boundary as depicted in figure 3, where the fluid occupies the upper half space ($z > 0$) and the composite the lower half space ($z < 0$) and a plane wave with wave vector β_0^f incident normally at the boundary. The solutions to the wave equation in the fluid phase ($z > 0$) are plane wave solutions and to satisfy the boundary conditions at the fluid-composite interface, u_1^f and u_3^f are expanded in terms of these plane wave solutions:

$$u_1^f = \sum_{n=1}^J k_{xn} R_n \sin(k_{xn} x_1) \exp(j\beta_n^f x_3)$$

$$u_3^f = \beta_0^f \exp(-j\beta_0^f x_3) - \sum_{n=0}^J \beta_n^f R_n \cos(k_{xn} x_1) \exp(j\beta_n^f x_3) \quad (5)$$

where $k_{xn} = \frac{2n\pi}{d}$ and $\beta_n^f = \sqrt{(\beta_0^f)^2 - (k_{xn})^2}$ are the wave vector components along x_1 and x_3 - directions, respectively. In the frequency range where an ultrasonic piezocomposite transducer is operated, β_n^f is imaginary except $n=0$. The reflection

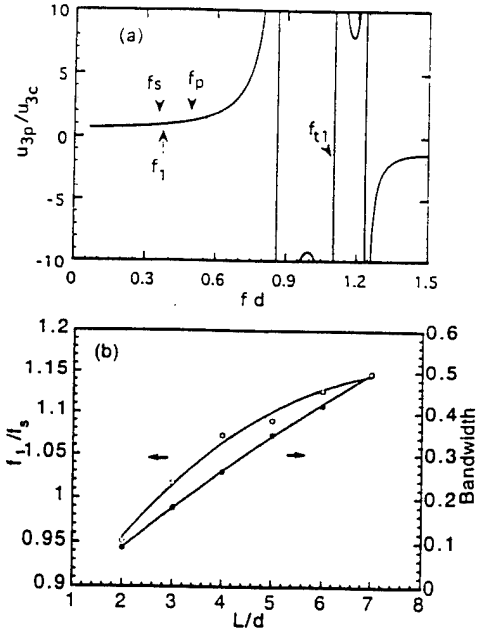


Figure 6. (a) The ratio of u_{3p}/u_{3c} vs. frequency (fd) for the composite plate of $\nu=0.44$ and $L/d=4$. (b) The frequency ratio f_1/f_s and the bandwidth $\Delta f/f_1$, where Δf is defined as the frequency range in which $0.9 < u_{3p}/u_{3c} < 1.1$ as a function of the aspect ratio L/d for a composite plate with $\nu=0.44$.

coefficient, hence, is $-R_0$ which can be measured experimentally.

The solutions in the composite region are:

$$u_1^c = \sum_{n=1}^m \sum_{i=1}^3 jbc_{ni} \sin(h_{ni}^c x_1) \exp(-j\beta_n x_3) A_n$$

$$u_3^c = \sum_{n=1}^m \sum_{i=1}^3 ac_{ni} \cos(h_{ni}^c x_1) \exp(-j\beta_n x_3) A_n \quad (6)$$

$$\Phi^c = \sum_{n=1}^m \sum_{i=1}^3 cc_{ni} \cos(h_{ni}^c x_1) \exp(-j\beta_n x_3) A_n$$

for the ceramic plate and similar equations can be written for the polymer region. In the above equations, bc_{ni} , ac_{ni} and cc_{ni} are proportional constants, A_n and R_n are determined by the boundary conditions at the fluid-composite interface $x_3=0$. The variational technique is used to determine these coefficients. The number of terms in the expansions (J in eqs. (5) and m in eqs. (6)) is determined by the accuracy desired. In the calculation carried out here, $J=5$ and $m=8$ are used.

Shown in figure 7 is the reflection coefficient R for the composites made of PZT-5H piezoceramic and Spurr's epoxy with 15% and 44% ceramic content, respectively, where parameters of water are used for the fluid medium. The large change in the reflection coefficient at fd near 1 for 44% (fd near 0.8 for 15%) is due to the lateral mode in the composites where the ceramic and polymer vibrate out of phase. Evidently, R is not a pure real number but has a imaginary component, reflecting the heterogeneity nature of the composites.⁸ Only at low frequency region, does the imaginary part become zero. This is fundamentally different from single phase materials. From the classical wave propagation in elastic medium problem, the input acoustic impedance of the composite Z_{in} at

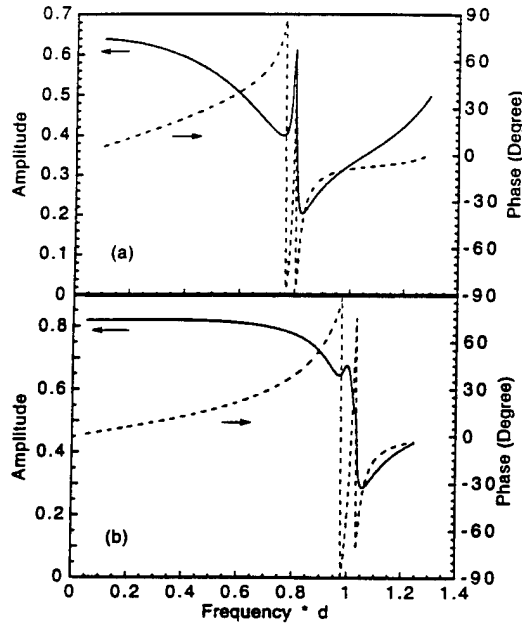


Figure 7. The reflection coefficient R from the water piezocomposite interface for a plane wave normally incident at the interface for (a) the ceramic volume content v in the composite is 15%; (b) the ceramic volume content v in the composite is 44%. The polymer and piezoceramic used in the composites are Spurr's epoxy and PZT-5H. The solid lines are the amplitude and dashed lines are the phase angle of R . The absolute phase angle is that displayed plus 180° . The non-zero phase angle for the reflection coefficient at the fluid-composite interface will affect the choice of the thickness of the matching layer for a composite transducer.

the interface can be calculated from the relation:

$$R = \frac{Z_f - Z_{in}}{Z_f + Z_{in}} \quad (7)$$

where Z_f is the characteristic acoustic impedance of the fluid.^{7,8} Since Z_f is assumed independent of frequency and real for water, Z_{in} exhibits a frequency dependent behavior and has a non-zero phase angle as shown in figure 8. Again, only at low frequencies, Z_{in} is equal to that calculated from the averaged density of the composites times the effective longitudinal velocity.¹¹ The strong frequency dependence of the acoustic impedance for piezocomposites was also observed in an earlier experiment¹² and further experiment will be carried out to verify the analytical results.

Another standard method for calculating the input acoustic impedance of the composite at $x_3=0$ is from the relationship between the stress and the sound velocity at the interface.^{7,8} For a composite considered here, both the stress and velocity are functions of x_1 and to calculate Z_{in} , we assume that the averaged values can be used:

$$Z_{in} = -\frac{\bar{T}_3}{\bar{v}_3} \quad (8)$$

where \bar{T}_3 and \bar{v}_3 are the averaged stress component and averaged velocity (over one unit cell) in the x_3 -direction evaluated at $x_3=0$. The results are also shown in figure 8 (dashed lines). As seen from the figure, the two results agree with each other quite well.

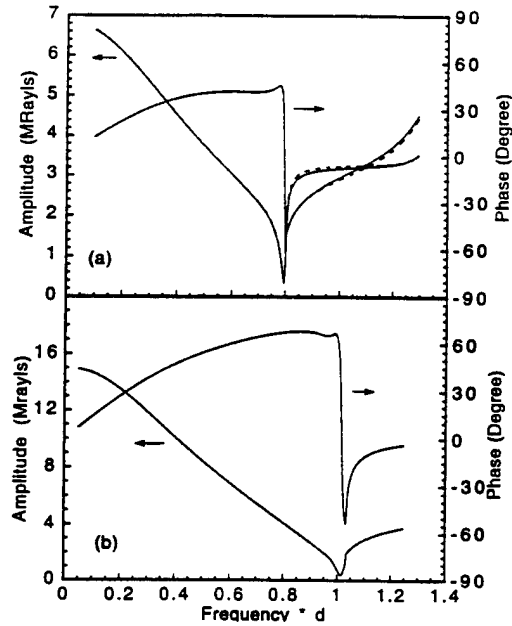


Figure 8. The input acoustic impedance for the composite calculated from the reflection coefficient R (solid lines) and from the stress-sound velocity relationship (dashed lines) for (a) composite with 15% ceramic content and (b) composite with 44% ceramic content. Unlike single phase materials, the input acoustic impedance for a composite is a complex. Only at low frequencies, the acoustic impedance is equal to those calculated from the effective medium theory.

IV. Summary.

Based on the analytical method developed recently, we treated quantitatively the vibration problem of a finite thickness piezoceramic polymer composite under an external AC field and wave propagation and input acoustic impedance at a fluid piezocomposite interface. The results reveal many interesting and important features related to the resonant modes and vibration profiles in a piezocomposite plate, and the characteristics of the reflection and transmission of a plane wave and input acoustic impedance at the fluid composite interface, which should have important implications to the design of the matching layer in a composite transducer. The results are in good agreement with existing experimental data.

V. Acknowledgment.

This work was supported by the Office of Naval Research through the Grant No. N00012-93-1-0304.

References:

1. W. A. Smith, Proc. 1990 IEEE ISAF7, 145 (1990).
2. S. Less and C. L. Davidson, IEEE Trans. on Sonics and Ultrasonics, SU-24, 222 (1977).
3. X. Geng and Q. M. Zhang, Appl. Phys. Lett. 67, (1995).
4. Y. Shui, X. Geng, and Q. M. Zhang, IEEE Trans. UFFC 42, 766 (1995).
5. H. F. Tiersten, "Linear Piezoelectric Plate Vibrations" (Plenum, New York, 1969).
6. PZT-5H is the trade-mark of Morgan Matroc Inc. Spurr's epoxy is the trade-mark of Polysciences, Inc. The parameters used are: PZT-5H: $e_{33} = 23.09 \text{ C/m}^2$, $e_{31} = -6.603$, $e_{15} =$

- 17.0, $c_{11} = 12.72 \times 10^{10} \text{ N/m}^2$, $c_{44} = 2.3 \times 10^{10}$, $c_{33} = 11.74 \times 10^{10}$, $c_{13} = 8.47 \times 10^{10}$, $\epsilon_{11}/\epsilon_0 = 1700$, $\epsilon_{33}/\epsilon_0 = 1470$, $\rho = 7500 \text{ kg/m}^3$. Spurr's epoxy: $c_{11} = 5.4 \times 10^9 \text{ N/m}^2$, $c_{44} = 1.3 \times 10^9$, $\rho = 1100 \text{ kg/m}^3$.
7. B. A. Auld, "Acoustic Fields and Waves in Solid" (John Wiley & Sons, N.Y., 1973).
 8. L. M. Brekhovskikh, "Waves in Layered Media" (Academic Press, N. Y. 1980).
 9. Y. Wang, E. Schmidt, and B. A. Auld, Proc. IEEE Ultrasonic Symp. (1986) p. 685.
 10. Q. M. Zhang, W. Cao, J. Zhao, L. E. Cross, IEEE Trans. UFFC 41, 556 (1994).
 11. W. A. Smith and B. Auld, IEEE Trans. UFFC 38, 40 (1988).
 12. T. R. Gururaja, Ph. D. Thesis, Penn State University (1984).

APPENDIX 27

Dynamic behavior of periodic piezoceramic-polymer composite plates

Xuecang Geng and Q. M. Zhang

Intercollege Materials Research Laboratory, The Pennsylvania State University, University Park, Pennsylvania 16802

(Received 28 June 1995; accepted for publication 5 September 1995)

The dynamic behaviors of periodic piezoceramic-polymer composite plates, especially the effect of the finite thickness on the strain distributions and resonant modes, are studied theoretically. It is found that as long as $f_{L1} < f_{t1}$, where f_{L1} and f_{t1} are the thickness and first piezoelectric active stop band-edge mode frequencies, there exists a frequency f_1 near f_{L1} at which the polymer and ceramic vibrate in phase with equal amplitude in the x_3 direction. The effect of the thickness of a composite plate is to change the bandwidth in which the two vibrate in unison. It is also found that due to the finite thickness effect a series of piezoelectric active modes at frequencies near and above f_{t1} may be excited. © 1995 American Institute of Physics.

For a piezocomposite, it is well known that its properties can be varied over a wide range, therefore, the quantitative study of their properties is an interesting and important problem. Many efforts have been devoted to this study in the past and due to the complexity of the problem, different approaches have been developed to address different aspects of the problem, such as the effective medium model, transmission line theory, and the analysis based on Floquet theory, etc.¹⁻⁵

In this letter, the results of a recent investigation on the dynamic problem of piezocomposite plates as schematically drawn in Fig. 1, especially the effect of the finite thickness (or aspect ratio L/d) on the strain distributions in the two phases and the resonant modes, will be presented. Since the dimension in the x_2 direction is much larger than L and d , the problem is treated as a two-dimensional one. Here, the solution to the vibration of a bounded composite plate is obtained by summation over the solutions of two-dimensional waves in unbounded plates.⁶ Unlike the earlier approach, the solutions to unbounded composite plates are obtained by solving the dynamic elastic equations in the ceramic and polymer phases separately and matching the two by the boundary conditions at the ceramic-polymer interface.

The dynamic elastic equations in the piezoceramic phase are:⁶

$$c_{11}^E u_{1,11} + (c_{13}^E + c_{44}^E) u_{3,13} + c_{44}^E u_{1,33} + e_{31} \phi_{,13} = \rho^c \ddot{u}_1$$

$$c_{44}^E u_{3,11} + (c_{13}^E + c_{44}^E) u_{1,13} + c_{33}^E u_{3,33} + e_{33} \phi_{,33} = \rho^c \ddot{u}_3 \quad (1)$$

$$e_{15} u_{3,11} + (e_{15} + e_{31}) u_{1,13} + e_{33} u_{3,33} - \epsilon_{33}^s \phi_{,33} - \epsilon_{11}^s \theta_{11} = 0,$$

where u_1 and u_3 are the elastic displacements, ϕ is the electric potential, c_{ij}^E is the constant electric field elastic stiffness coefficient, e_{ij} is the piezoelectric coefficient, ϵ_{ij}^s is the dielectric permittivity, and ρ is the density. Similar equations can be written for the polymer phase.

The solutions in the unbounded ceramic plate are:⁶

$$u_3^c = \sum_{i=1}^3 R_i^c f_i^c \cos(h_i^c x_1) \exp(j\beta x_3)$$

$$u_1^c = \sum_{i=1}^3 R_i^c g_i^c \sin(h_i^c x_1) \exp(j\beta x_3) \quad (2)$$

$$\Phi^c = \sum_{i=1}^3 R_i^c t_i^c \cos(h_i^c x_1) \exp(j\beta x_3),$$

where f_i^c , g_i^c , and t_i^c are factors depending on β and h_i , the wave vector components in the x_3 and x_1 directions, and $j = \sqrt{-1}$. Similar equations can be written for the polymer region.

The superscripts c and p are introduced to denote the ceramic and polymer, respectively. In Eq. (2), the symmetry conditions in the x_1 direction for the piezoelectric active mode in a periodic composite plate are used, and for the sake of simplicity, the time dependent term $[\exp(i\omega t)]$ is omitted. The boundary conditions of the stresses, elastic displacements, and the electric displacement and potential at the ceramic-polymer interface ($x_1 = vd/2$) yield six homogeneous linear equations which relate the six undetermined coefficients R_i^c and R_i^p . The condition for a nontrivial solution of homogeneous linear equations requires that the determinant of the coefficients vanishes, i.e.,

$$K = |\text{coefficients of } R_i| = 0, \quad (3)$$

where the coefficients of R_i are functions of the β , d , the angular frequency ω , the ceramic volume fraction v , and the

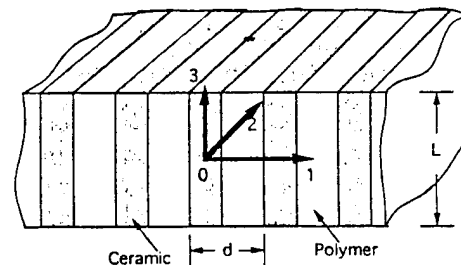


FIG. 1. Schematic drawing of a periodic piezoceramic polymer composite plate. The poling direction of the piezoelectric ceramic plates is along the x_3 direction. The width of ceramic plate is vd and the width of polymer is $(1-v)d$, where v is the ceramic volume content in the composite.

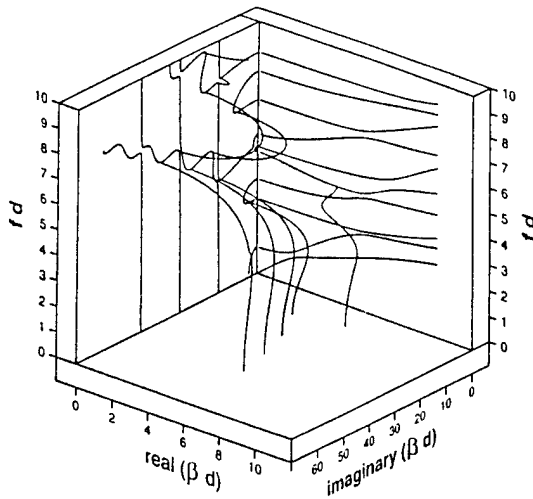


FIG. 2. Dispersion curves for a composite made of PZT-5H ceramic and Spurr's epoxy with 44% ceramic volume content ($v=0.44$).

material parameters of both the polymer and piezoceramic. Equation (3) yields the relationship between β and f , the dispersion curves. For each point on the dispersion curves, the relations among R_i^p and R_i^c can be determined from the homogeneous linear equations. Shown in Fig. 2 are the dispersion curves for a composite plate with 44% ceramic content (in the first quadrant). The parameters used in the calculation are those of PZT-5H for the piezoceramic and Spurr's epoxy for the polymer phase, respectively.⁷ In addition, for $\beta=0$, the solutions in the ceramic and polymer phases which satisfy the boundary conditions at $x_1 = \pm d/2$ are

$$u_1^c = k_1 C \sin(h_{01}^c x_1), \quad u_1^p = k_2 C \sin\left[h_{01}^p \left(x_1 - \frac{d}{2}\right)\right],$$

$$\Phi^c = \Phi^p = C x_3 \quad (4)$$

where k_1 and k_2 are constants, $h_{01}^c = \sqrt{\rho^c / c_{11}^c} \omega$, $h_{01}^p = \sqrt{\rho^p / c_{11}^p} \omega$.

To treat a composite plate under different boundary conditions at $x_3 = \pm L/2$ explicitly, u_3 , u_1 , and ϕ are expanded in terms of the eigenfunctions. For the ceramic region

$$u_3^c = \sum_{n=1}^m \sum_{i=1}^3 k_{ni}^c f_{ni}^c \cos(h_{ni}^c x_1) \sin(\beta_n x_3) A_n$$

$$u_1^c = \sum_{n=1}^m \sum_{i=1}^3 k_{ni}^c g_{ni}^c \sin(h_{ni}^c x_1) \cos(\beta_n x_3) A_n$$

$$+ C k_1 \sin(h_{01}^c x_1) \quad (5)$$

$$\Phi^c = \sum_{n=1}^m \sum_{i=1}^3 k_{ni}^c t_{ni}^c \cos(h_{ni}^c x_1) \sin(\beta_n x_3) A_n + C x_3.$$

A similar solution can be written for the polymer region. In Eq. (5), k_{ni} , f_{ni} , g_{ni} , and t_{ni} are constants. A_n and C are determined by the boundary conditions at $x_3 = \pm L/2$. In this letter, the problem with the boundary conditions of traction free and $\phi = \pm \phi_0/2$ at $x_3 = \pm L/2$ will be treated, which corresponds to a composite plate situated in air and subjected to

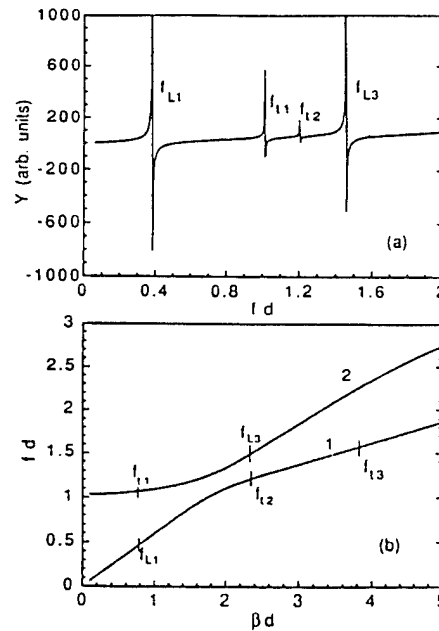


FIG. 3. (a) The admittance spectrum for $v=0.44$ composite plate of $L/d=4$. (b) the dispersion curves for $v=0.44$ composite which show the positions of the possible resonant modes in a finite thickness plate. f_{L1} and f_{t1} occur at $\beta = \pi/L$, f_{L3} and f_{t2} occur at $\beta = 3\pi/L$. Therefore, f_{t3} will occur at $\beta = 5\pi/L$, etc. Whether these high order modes f_{t2} , f_{t3} , etc. be observed experimentally depends on the electromechanical coupling factors for these modes.

an externally applied electric field. With a finite number of eigenfunctions in the expansion, the boundary conditions at $x_3 = \pm L/2$ cannot be satisfied at all x_1 . The number of the eigenfunctions m , required, thereafter is determined by the accuracy needed for the solution. For the problem treated here, we found that it is adequate to use eight eigenmodes in the expansion. In the frequency range studied ($f d < 2$ in Fig. 2), there are two branches with real β and other branches having either imaginary or complex β , which corresponds the modes confined at the boundary $x_3 = \pm L/2$ (surface modes).

The coefficients A_n and C in Eqs. (5) can be determined by either the method of least-squares or selected boundary points method.^{6,8} Here, the latter approach is used due to its simplicity, where several boundary points are selected to determine A_i and C . Based on u_3 , u_1 , and ϕ thus determined, all the properties related to the dynamic behavior of a composite plate can be evaluated. Shown in Fig. 3(a) is the electric admittance spectrum for a composite plate with 44% ceramic content made of PZT-5H piezoceramic and Spurr's epoxy at $L/d=4$. The admittance Y is calculated from the relation $Y = I / \phi_0$ where $I = j \omega \int D_3 dx_1$. The integration is over one unit cell for D_3 at $x_3 = L/2$, where D_3 is the electric displacement vector component along the x_3 -direction ($D_3 = e_{33} u_{3,3} + e_{31} u_{1,1} - \epsilon_{33}^s \phi_{,3}$). One interesting feature revealed in Fig. 3(a) is that in a composite plate, in addition to the thickness resonance mode, there exist other modes due to the periodic nature of the composite and coupling between the two phases. In Fig. 4, we display the distributions of u_3 at each mode. Apparently, f_{L1} is the fundamental thickness resonance and f_{t1} is the stop-band-edge resonance as re-

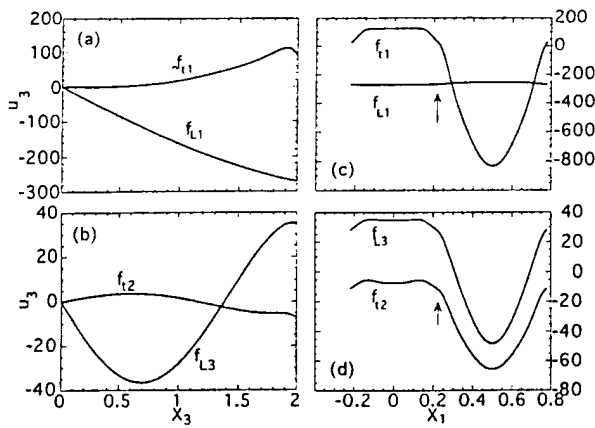


FIG. 4. The distributions of u_3 for a composite plate of $\nu=0.44$ and $L=4(d=1)$ at f_{L1} , f_{11} , f_{L3} , and f_{12} . (a) and (b) u_3 at $x_1=0$ (at the center of ceramic plate) as a function of x_3 where $x_3=0$ is at the center and $x_3=2$ is at the surface of the composite plate. (c) and (d) u_3 at the surface of the composite plate as a function of x_1 . The arrows indicate the position of the interface between the ceramic and polymer. At f_{11} and f_{L3} , the ceramic and polymer vibrate out of phase with each other, while at f_{L1} and f_{12} , the two vibrate in phase.

vealed by the fact that the ceramic and polymer vibrate 180° out of phase at this mode, which has been predicted in the earlier theoretical work.^{4,5} The frequency position and the distribution of u_3 along the x_3 -axis indicate that f_{L3} is the third harmonic of the thickness mode. However, the appearance of f_{12} is not expected from the earlier theoretical works. By examining the equations of the boundary conditions at $x_3 = \pm L/2$, it can be deduced that a resonance will occur whenever $\beta = (1+2n)\pi/L$, i.e., $\cos(\beta L/2) = 0$. From the dispersion curves of real β , as shown in Fig. 3(b), it is clear that the fundamental thickness resonance and the stop-band-edge resonance occur at $\beta = \pi/L$ (f_{L1} and f_{11}). Similarly, when $\beta = 3\pi/L$, the third harmonic of the thickness mode will occur at f_{L3} . In addition, a mode f_{12} will also show up at the branch 1 which is at a frequency near and above f_{11} . By the same argument, it would be expected that f_{13} , f_{14} , etc., may also be observed, depending on the electromechanical coupling factors of these modes. It can be shown that the effective coupling factor for these modes decreases rapidly for the higher order modes. Therefore, the experimental situation, only the modes of f_{12} and sometimes f_{13} are observed. Indeed, these modes have been observed experimentally and the results here provide a clear physical picture.

For a composite plate to work effectively as an electro-mechanical transduction material, it is required that the ceramic and polymer vibrate in phase with nearly the same amplitude in the x_3 -direction. The evolution of the vibration pattern in the two phases with frequency and the aspect ratio L/d of a composite plate is studied here. Shown in Fig. 5(a) is the change of the ratio u_{3p}/u_{3c} at $x_3 = L/2$ (at the surface of the composite plate), where u_{3p} and u_{3c} are u_3 at the centers of the polymer phase ($x_1 = d/2$) and the ceramic ($x_1 = 0$), respectively, with frequency for the composite plate of $L/d=4$. At frequencies far below any resonance mode, u_{3p}/u_{3c} is always less than one. As L/d increases, this ratio increases and approaches one. These are consistent with the

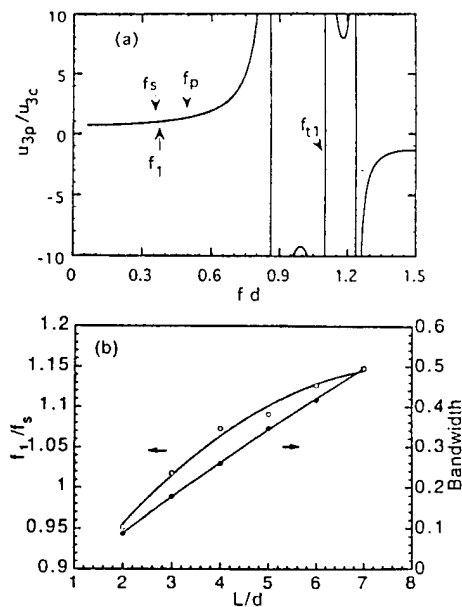


FIG. 5. (a) The ratio of u_{3p}/u_{3c} vs frequency (fd) for the composite plate of $\nu=0.44$ and $L/d=4$. (b) The frequency ratio f_1/f_s and the bandwidth $\Delta f/f_1$, where Δf is defined as the frequency range in which $0.9 < u_{3p}/u_{3c} < 1.1$ as a function of the aspect ratio L/d for a composite plate with $\nu=0.44$.

results of the earlier theoretical model developed.⁹ As frequency increases towards the thickness resonance, the ratio u_{3p}/u_{3c} also increases towards one. At a frequency f_1 which is near f_s of the thickness mode $u_{3p}/u_{3c} = 1$. This is true as long as $f_{L1} < f_{11}$. This ratio will surpass one as the frequency is further increased. In Fig. 5(b), the change of f_1/f_s versus the aspect ratio L/d is presented. Clearly, f_1/f_s is near but larger than one except for composite plates with a very small aspect ratio. Therefore the aspect ratio L/d does not have a significant effect on the ratio of u_{3p}/u_{3c} at frequencies very near f_s of the thickness mode, where u_{3p}/u_{3c} is always near one. However, it will affect the bandwidth in which u_{3p}/u_{3c} is near one. For example, the bandwidth ($\Delta f/f_1$) in which $0.9 < u_{3p}/u_{3c} < 1.1$ increases as the aspect ratio L/d increases, which is shown in Fig. 5(b). In the practical design of a composite transducer, the aspect ratio L/d required, will be determined by the operation bandwidth needed.

The financial support by the Office of Naval Research through Grant. No. N00014-93-1-0304 is greatly appreciated.

¹R. E. Newnham, *Annu. Rev. Mater. Sci.* **16**, 47 (1986).

²W. A. Smith and B. Auld, *IEEE Trans. Ultrason. Ferroelectr. Freq. Control* **38**, 40 (1988).

³A. Alippi, F. Craciun, and E. Molinari, *Appl. Phys. Lett.* **53**, 1806 (1988).

⁴Y. Wang, E. Schmidt, and B. A. Auld, *Proc. IEEE Ultrason. Symp.* (1986), p. 685.

⁵Y. Wang, Ph.D. thesis, Stanford University, 1986.

⁶H. F. Tiersten, *Linear Piezoelectric Plate Vibrations* (Plenum, New York, 1969).

⁷Q. M. Zhang and Xuecang Geng, *J. Appl. Phys.* **76**, 6014 (1994).

⁸T. R. Meeker and A. H. Meitzler, *Phys. Acoust.* **1**, 111 (1964).

⁹Q. M. Zhang, W. Cao, J. Zhao, and L. E. Cross, *IEEE Trans. Ultrason. Ferroelectr. Freq. Control* **41**, 556 (1994).

APPENDIX 28

Transverse Piezoelectric Mode Piezoceramic Polymer Composites with
High Hydrostatic Piezoelectric Responses

Q. M. Zhang

Materials Research Laboratory, The Pennsylvania State University
University Park, Pennsylvania, 16802, U.S.A.

Abstract

In addition to the connectivity of the constituents in a composite, the operation mode also plays an important role in determining the performance of the composite. In this talk, we will present two types of piezoceramic polymer composites developed recently at MRL of Penn State: a 2-2 piezocomposite operated at the transverse piezoelectric (TP) mode and a TP mode honeycomb composite. Both composites exhibit exceptionally high hydrostatic piezoelectric response, high reliability, as demonstrated by the experimental results on these new composites and analytical modeling. Based on analytical models, the optimum design of these composites is also analyzed. One advantage of a TP 2-2 composite, in addition to the high hydrostatic piezoelectric response, is the low fabrication cost. While for a TP mode honeycomb composite, due to the fact that the piezoelectric responses from the three orthogonal directions add together when the transducer is subjected to a hydrostatic pressure, a unique feature of this composite, it has a piezoelectric hydrostatic response considerably higher than those of most other piezoceramic polymer composites.

1. Introduction

Through the efforts in the last two decades, many forms of piezocomposites have been developed. These materials have demonstrated many advantages over conventional single phase ceramic and polymeric materials in the hydrostatic applications. A summary of the performance of these composites can be found in several review articles.^{1,2} One of the common features among these earlier piezocomposites is that they are operated in the longitudinal piezoelectric mode (d_{33} mode). Hence, the hydrostatic piezoelectric coefficient d_h of these composites, such as 1-3 composite and 2-2 composite, is limited to below d_{33} coefficient of the piezoceramic phase in the composite. In addition, the high pressure in deep ocean due to the stress transfer between the polymer and ceramic phases may cause depoling of the piezoceramic.

In piezoceramics, there are three independent piezoelectric coefficients, the longitudinal d_{33} , the transverse d_{31} , and the shear d_{15} coefficients. Hence, it

is interesting to explore piezoceramic polymer composites operated in the piezoelectric d_{31} and d_{15} modes instead of d_{33} mode. Moonie transducer, a recent invention of metal-ceramic composite, is an example which makes use of piezoelectric d_{31} mode and achieves exceptionally high effective linear and hydrostatic piezoelectric responses.³ In this talk, I will present two new piezocomposites operated in the transverse piezoelectric mode (d_{31} or TP mode) and will show that exceptionally high hydrostatic piezoelectric response can be achieved with these TP mode piezocomposites. The transverse mode operation also reduces the high pressure depoling effect.

2. TP mode 2-2 composite

Shown in figure 1 is a schematic drawing of a TP 2-2 composite. Here, two configurations will be evaluated, one without face plates and one with stiff face plates. By employing the model similar to that used in the reference 2, one can derive the following expressions for the effective hydrostatic piezoelectric responses of a TP 2-2 composite:

$$d_h^{cp} = \left\{ 2d_{31}^c \frac{(1-\sigma_p)s_{11}^p + (1-\nu)(s_{12}^p - s_{12}^c)}{(1-\nu)(1-\sigma_c)s_{11}^c + \nu(1-\sigma_p)s_{11}^p} + d_{33}^c \right\} \frac{L\nu}{t} \quad (1)$$

$$d_h^{cpcp} = \left[d_{33}^c + 2d_{31}^c \frac{(1-\sigma_p)s_{11}^p + (1-\nu)(s_{12}^p - s_{12}^c)}{(1-\nu)(1-\sigma_c)s_{11}^c + \nu(1-\sigma_p)s_{11}^p} \right] \frac{2\nu}{\epsilon_{33}^c} \quad (2)$$

where the superscripts p and c refer to polymer and ceramic, respectively. ν is the ceramic volume content and σ is the Poisson's ratio.

Shown in figure 2 are the calculated results from eqs. (1) and (2), where the TP 2-2 composite is made of PZT-5H ceramic embedded in Spurr's epoxy (figure 5(a)) and polyurethane with microballoon (polymer II) (figure 5(b)). The parameters used in the calculation are listed in Table I.

Using stiff uni-directional face plates, which clamp the 2-2 composite in the y-direction while leave the composite free in the x-direction, the hydrostatic piezoelectric response can be improved. It can be shown that in the ideal condition, that is the composite is completely clamped in the y-direction and free in the x-direction, the hydrostatic responses are:

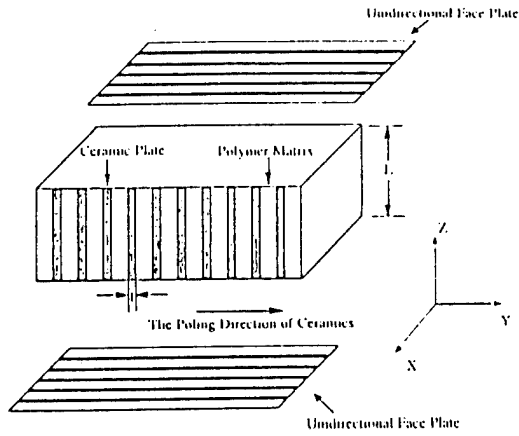


Figure 1. Schematic drawing of a TP 2-2 composite.

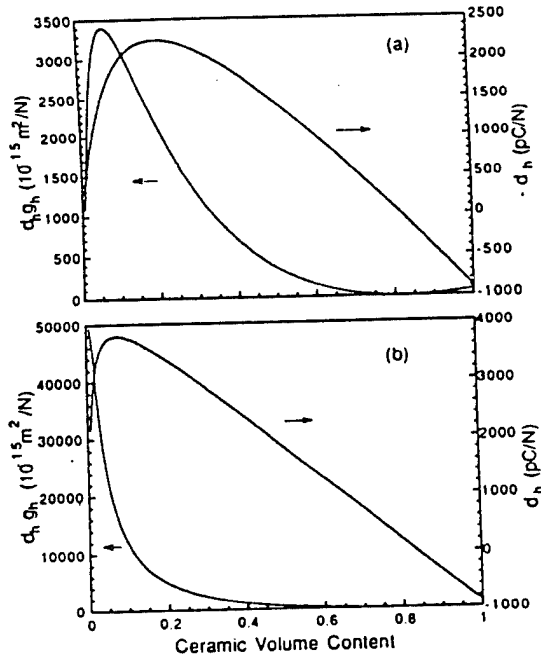


Figure 2. Calculated results of hydrostatic piezoelectric response of TP 2-2 composite. (a) Spurr's epoxy matrix and (b) polyurethane with microballoon matrix.

$$d_h^{CP} = (2d_{31}^c \frac{s_{11}^p (1 - \sigma_p)}{v s_{11}^p (1 - \sigma_p) + (1-v)s_{11}^c (1 - \sigma_c)}) \frac{LV}{t} \quad (3)$$

$$d_h^{CP} g_h^{CP} = (2d_{31}^c \frac{s_{11}^p (1 - \sigma_p)}{v s_{11}^p (1 - \sigma_p) + (1-v)s_{11}^c (1 - \sigma_c)})^2 \frac{v}{\epsilon_{33}^c} \quad (4)$$

Plotted in figure 3 are the results calculated from eqs. (3) and (4) for face plated TP 2-2 composites. Apparently, the hydrostatic responses are improved significantly, as compared with the results in figure 2.

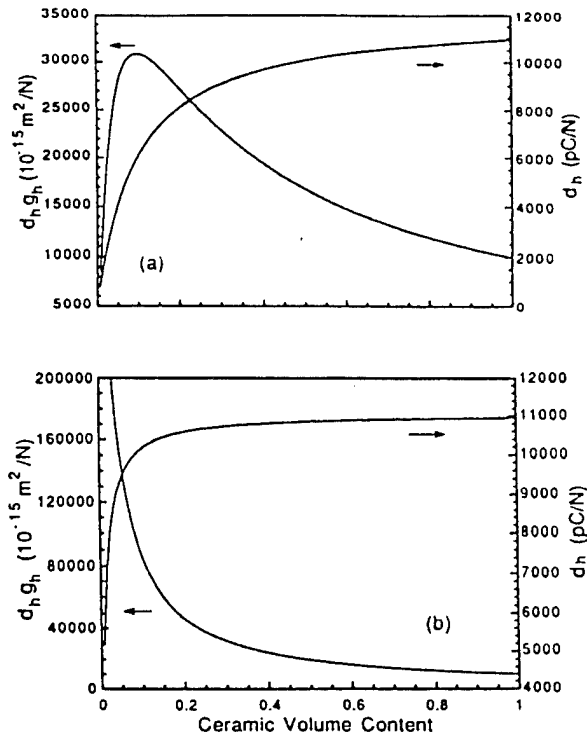


Figure 3. Calculated results of hydrostatic piezoelectric response of TP 2-2 composite with unidirectional face plates. (a) Spurr's epoxy matrix and (b) polyurethane with microballoon matrix.

Table I. The parameters used in the calculation

PZT-5H: $d_{33} = 593$ (pC/N), $d_{31} = -274$, $s_{11} = 0.165$ (10^{-10} m²/N), $s_{33} = 0.207$, $s_{12} = -0.048$, $s_{13} = -0.085$, $\epsilon_{33} = 3400 \epsilon_0$

Polymer I (Spurr's epoxy): $s_{11} = 2.0$ (10^{-10} m²/N), $\sigma = 0.36$

Polymer II $s_{11} = 2.0$ (10^{-9} m²/N), $\sigma = 0.36$

Several TP 2-2 composites were made and evaluated. Listed in Table II are some of the results and the comparison with the theoretical calculation. As seen from the Table, indeed, TP 2-2 composite exhibits exceptionally high hydrostatic piezoelectric response and there is good agreement between the theory and experiment.

3. TP mode Honeycomb composite

The schematical drawing of a TP mode honeycomb structure is shown in figure 4, where the poling and applied electric field directions are across the wall of the honeycomb cell (perpendicular to the z-direction). A hydrostatic transducer can be made by either placing thin layers of polymer on the two end faces to block the opening (air backing) or embedded the whole

Table II. The piezoelectric hydrostatic performance of TP 2-2 composites

	Sample A		Sample B	
	Experiment	Calculated	Experiment	Calculated
d_h (pC/N)	2,020	2,572	6,000	7,700
$d_h g_h$ (10^{-15} m ² /N)	1,468	1,752	30,000	49,900
L (cm)	1.12		1.0	
t (cm)	0.05		0.05	
v (%)	25		15	
Poly. Matrix	Spurrs epoxy		Polyurethane with 50% volume microballoon	
Face plates	No		Unidirectional plates	

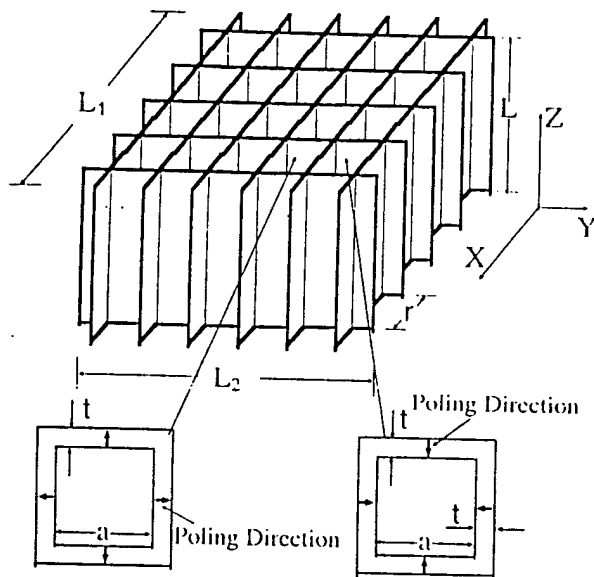


Figure 4. Schematic drawing of a TP honeycomb structure.

honeycomb ceramic into a polymer matrix. If these structures are subjected to hydrostatic pressure, the d_{33} response is eliminated and the hydrostatic piezoelectric response is from the d_{31} component of the piezoelectric. The stress field in the x-, y-, and z-direction will induce three d_{31} responses in the corresponding ceramic plates. For an end capped configuration, it can be shown that the effective hydrostatic response is:

$$d_h^{eff} = \frac{2L a d_{31}}{r^2} \left(\frac{1}{b} + \frac{1}{v} + \frac{s_{13}}{s_{33}(2-b)} \right) \quad (5)$$

$$d_h^{eff} g_h^{eff} = \frac{2 b (1-b) d_{31}^2}{\epsilon_{33}} \left(\frac{1}{b} + \frac{1}{v} + \frac{s_{13}}{s_{33}(2-b)} \right)^2 \quad (6)$$

where $b = t / r$ with $r = t + a$.

Plotted in figure 5 are the results from eqs. (5) and (6) for an end capped TP honeycomb made of PZT-5H with $L = 1$ cm and $a = 0.125$ cm. Clearly, very high hydrostatic response can be achieved with this structure.

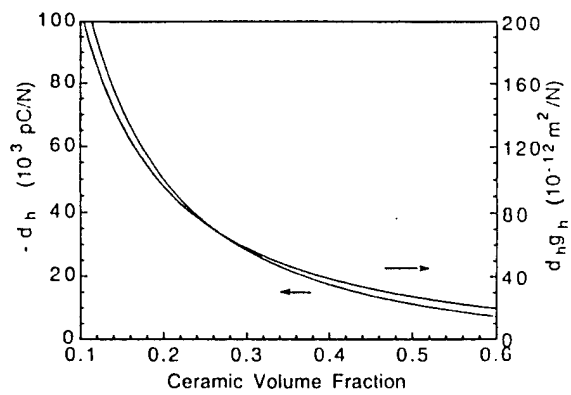


Figure 5. Calculated results of the effective hydrostatic piezoelectric responses from an end capped TP honeycomb transducer made of PZT-5H ceramic.

Figure 6 shows the experimental result of end capped honeycomb transducers. The honeycomb was made of PZT-4 material with $d_{33} = 110$ pC/N and $d_{31} = -40$ pC/N. The comparison between the experimental results and theoretical prediction is made in Table III. There is a good agreement between the theoretical values and experimental results. The discrepancy is mainly caused by the finite size effect where the honeycomb cells at the edges of the samples will have finite d_{33} response.

Table III. Parameters and results of the TP honeycomb samples tested

Configuration	ϵ/ϵ_0	L(cm)	d_h (pC/N) (exp)	d_h (theory)
I End capped	520	1.326	-4,700	-6,200
II End capped	520	1.237	-4,200	-5,784
III Polyurethane with microballoon matrix	570	1.2	-4,666	-5,636

4. Summary

Two new piezocomposites operated at TP mode were developed and evaluated. As a comparison, in figure 7, we summarize the hydrostatic properties of several commonly used transducer materials and the newly developed TP mode composites. It can be seen that these new structures exhibit exceptionally high hydrostatic piezoelectric responses. The author would like to thank the financial support of this work from Office of Naval Research.

References:

- [1] T. R. Gururaja, A. Safari, R. E. Newnham, and L. E. Cross, "Piezoelectric ceramic-polymer composites for transducer applications," in *Electronic Ceramics*, ed. L. M. Levinson, pp. 92-128 (Marcel Dekker, NY, NY 1987).
- [2] W. A. Smith, "The Application of 1-3

Piezocomposites in Acoustic Transducers," Proc. 1990 IEEE ISAF7, pp. 145-152, (Urbana, ILL 1990).
 [3] Q. C. Xu, S. Yoshikawa, J. R. Belsick, and R. E. Newnham, "Piezoelectric Composites with High Sensitivity and High Capacitance for Use at High Pressure," IEEE Trans. UFFC vol. 38, pp. 634-639, 1991.

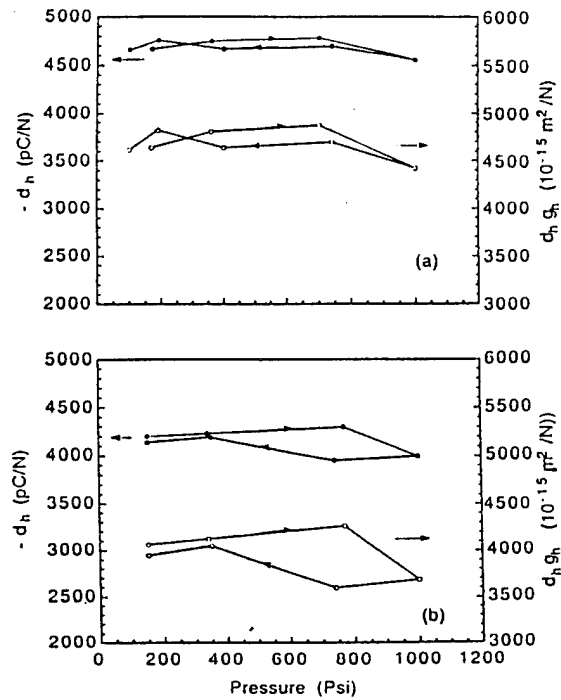


Figure 6. Experimental results of the TP honeycomb (a) sample I and (b) sample II.

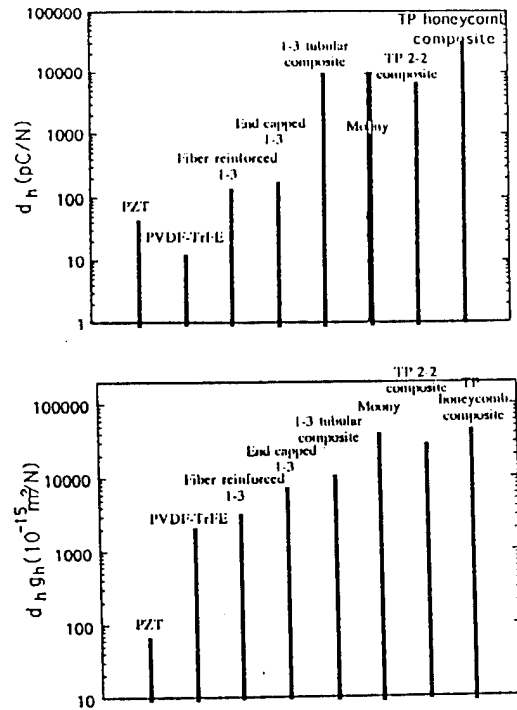


Figure 7.

APPENDIX 29

A High Sensitivity Hydrostatic Piezoelectric Transducer Based on Transverse Piezoelectric Mode Honeycomb Ceramic Composites

Q. M. Zhang, H. Wang, J. Zhao, Joseph T. Fielding, Jr., Robert E. Newnham, *Member, IEEE*, and L. Eric Cross

Abstract—A new piezoelectric composite transducer based on the ceramic honeycomb structure is introduced. The transducer is operated in the transverse piezoelectric (TP) d_{31} mode. The ceramic honeycomb configuration enables one to fabricate a TP honeycomb transducer by either embedding a honeycomb ceramic skeleton into a soft polymer matrix to form a composite or by blocking the openings of the honeycomb cells with thin layers of epoxy to form an end-capped honeycomb structure. With the unique honeycomb configuration and TP operation mode, the piezoelectric d_{33} response of the ceramic is nearly eliminated and the piezoelectric responses from the three orthogonal directions add together when the transducer is subjected to a hydrostatic pressure. As a result, the transducer exhibits exceptionally high hydrostatic piezoelectric response.

1. INTRODUCTION

AS HAS BEEN demonstrated repeatedly, the key to the success of a composite material is to intelligently design the properties and geometric shapes of the constituents. In piezoelectric ceramic-polymer composites, by making use of various connectivity patterns of the ceramic phase and polymer phase, a series of high performance piezoelectric transducers have been realized [1], [2]. However, almost all the existing piezocomposites are operated in the piezoelectric d_{33} mode (longitudinal piezoelectric mode), and in their current forms may have reached the performance limit. To meet the demands and challenges of the ever growing transducer and actuator market, including the so-called smart materials used for vibration control, it is necessary to develop a new generation of piezocomposite materials. The Moonie transducer, a recent innovation, is one example of new composites [3]. Recently, we have demonstrated that by using the transverse piezoelectric mode (d_{31} mode) in 1-3 tubular composites and in 2-2 composites, one can markedly improve the effective piezoelectric hydrostatic response by more than an order of magnitude. This substantial increase in hydrostatic piezoelectric coefficient d_h and figure of merit d_h/g_h compared with those of 1-3 rod composites is on a par with the Moonie transducer [4], [5].

In this paper, we will introduce a new type of hydrostatic transducer made of a honeycomb piezocomposite operated in the transverse piezoelectric mode, which is named in this

Manuscript received February 6, 1995; revised June 16, 1995. This work was supported by the Office of Naval Research.

The authors are with the Intercollege Materials Research Laboratory, Penn State University, University Park, PA 16802 USA.

Publisher Item Identifier S 0885-3010(96)00353-X.

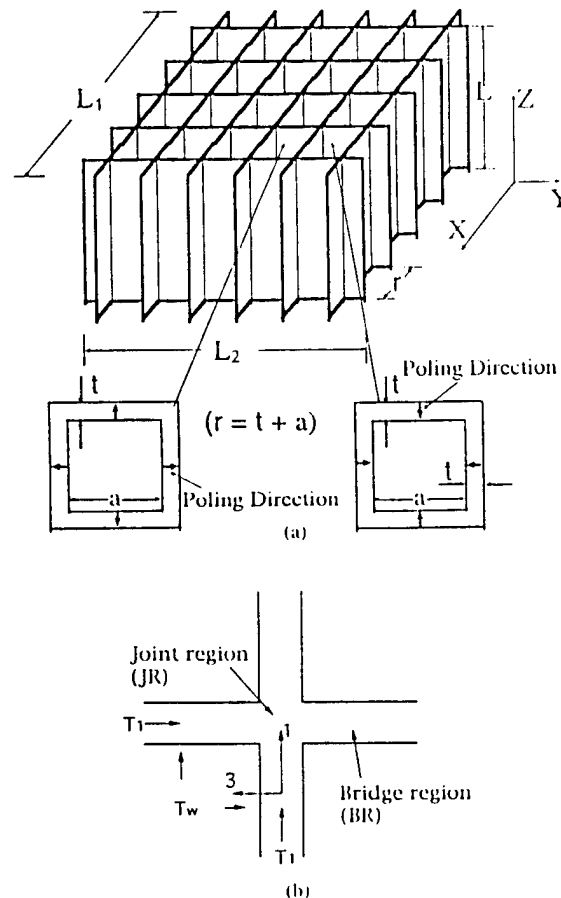


Fig. 1. (a) Schematic drawing of a honeycomb ceramic structure. The ceramic poling direction is indicated in the insert of the figure. Notice the difference in the poling directions between the neighboring cells. In the figure, $r = a + t$. (b) Stress components in the x - y plane of a honeycomb structure subjected to a hydrostatic pressure. The local coordinate system for the ceramic phase is also shown in the figure. The 2-axis of the local coordinate system is perpendicular to the 1- and 3-axes and parallel to the z -axis of the honeycomb structure in (a).

paper as TP mode honeycomb composite transducer. We shall show that with a suitable poling and electrode configuration, the piezoelectric responses in the three orthogonal directions [the x -, y -, and z -directions, as shown in Fig. 1(a)] have the same sign. The 3-D connected ceramic frame in the composite greatly reduces the Poisson's ratio effect of the polymer phase, the most detrimental effect in a regular 1-3 piezocomposite

[6]. As a result, this new composite exhibits a piezoelectric hydrostatic response considerably higher than those of most other piezoceramic polymer composites.

II. PHYSICAL BASIS AND ANALYTICAL MODELING

The basic structure of this new composite is schematically illustrated in Fig. 1, where the ceramic is poled perpendicular to the z -direction as indicated. In this paper, two configurations will be investigated: 1) A honeycomb structure is end-capped with the interior filled with air and the openings of the honeycomb cells blocked by either thin layers of polymer or thin layers of metal, depending on the dimensions of the honeycomb cell. With this configuration, the inside walls of the honeycomb are shielded from the external medium. Hence, as a transducer is subjected to hydrostatic pressure, the stress component perpendicular to the wall, T_w in Fig. 1(b), is zero. 2) A honeycomb ceramic frame is embedded in a polymer matrix to form a composite. The polymer matrix acts as a stress transfer medium as in other piezoceramic polymer composites.

Due to the local variation of the poling directions in the honeycomb structure studied, to facilitate the analysis and discussion, two coordinate systems will be used. One coordinate system is labeled as X - Y - Z and attached to the honeycomb composite, as shown in Fig. 1(a). The other is labeled as 1-2-3 and attached to the ceramic local structure with the 3-direction along the ceramic poling direction as shown in Fig. 1(b).

It should be mentioned that two forms of honeycomb composite transducers were investigated earlier [7], [8]. The difference between the earlier honeycomb composite transducers and the one introduced here is the operation mode. The earlier honeycomb composite transducers are operated in the longitudinal piezoelectric mode. Due to the limitation of this operation mode, the effective hydrostatic piezoelectric response of the earlier honeycomb composite transducers is at least one order of magnitude smaller than that of the TP honeycomb transducers introduced here.

A. Honeycomb Structure with End Caps

When an end-capped honeycomb structure is subjected to hydrostatic pressure, as will be shown later, the piezoelectric response is from the d_{31} component of the piezoceramic. Due to the fact that $T_w = 0$ (because the interior of an end-capped honeycomb is filled with air) and the poling direction of the ceramic is parallel to the thickness direction of the ceramic wall, the d_{33} response is eliminated and the stress field in the x -, y -, and z -directions will induce d_{31} responses in the ceramic plates.

When an end-capped honeycomb structure is subjected to hydrostatic pressure p , the stress component T_1 as shown in Fig. 1(b) will be increased. From the force balance condition, we can obtain the following relation:

$$T_1 = \frac{p}{b} \quad (1)$$

where $b = t/r$ with $r = t + a$ (see Fig. 1). b is smaller than one and (1) indicates that there is a stress amplification in the

x - and y -directions. As a result of this stress amplification in the x - and y -directions as well as the stress amplification in the z -direction (as will be shown later), an exceptionally high piezoelectric response is achieved.

In a honeycomb structure, there are two different ceramic regions, the bridge region (BR) and the joint region (JR). In the current configuration, the piezoelectric response is produced in the bridge region while the joint region is piezoelectrically inactive. In most practical honeycomb structures, the effect of JR is relatively small since the ceramic fraction in a honeycomb structure, which determines the relative weight of JR in the structure, is not very high. For example, even at a ceramic volume fraction of 40%, the ratio between the BR and JR is less than 15%. That is, 85% of the ceramic is piezoelectrically active in this structure. In addition, as the ceramic volume content decreases, the percentage of this inactive region will decrease. In most practical applications, the ceramic volume fraction lies below 40% and the relative weight of the JR will be correspondingly small.

Clearly, the responses of the two regions, i.e., JR and BR, to external stresses are different. In order to determine the stress and strain distributions in these two regions, depending on the manner in which the two regions are connected, either isostrain or isostress approximation is used. That is, in the z -direction the strain in JR is equal to that in BR (isostrain approximation). In the x - and y -directions, the stresses are the same in JR and BR (isostress approximation). The error associated with those approximations is small if L is much larger than r , and a is much larger than t , respectively (see Fig. 1) [9]. For any practical device, L_1 and L_2 are much larger than r . Under these approximations, we can write down the constitutive relations in a TP honeycomb structure. The constitutive relations in the BR are

$$S_{1BR} = s_{11}T_1 + s_{12}T_{2BR} \quad (2a)$$

$$S_2 = s_{12}T_1 + s_{11}T_{2BR} \quad (2b)$$

in JR, the constitutive relations are

$$S_{1JR} = (s_{11} + s_{12})T_1 + s_{12}T_{2JR} \quad (3a)$$

$$S_2 = 2s_{12}T_1 + s_{11}T_{2JR} \quad (3b)$$

where S_{1BR} , S_{1JR} , and S_2 are the strain components in the 1- and 2-directions, respectively, s_{ij} are the elastic compliance, and T_i are the stress components in the ceramic plate. The subscripts BR and JR denote the bridge region and joint region, respectively. The local coordinate system is used in (2) and (3). In writing (2) and (3), the possible clamping effect of the end caps is omitted since the Young's modulus of the end caps used in our experiment is much smaller than that of the ceramic. The force balance condition in the z -direction yields

$$2taT_{2BR} + t^2T_{2JR} = r^2p. \quad (4)$$

T_{2BR} can be found by solving (2), (3), and (4),

$$T_{2BR} = p \left(\frac{1}{\nu} + \frac{s_{12}}{s_{11}(2-b)} \right) \quad (5)$$

where $\nu = b(2-b)$ is the volume content of the ceramic in the honeycomb structure.

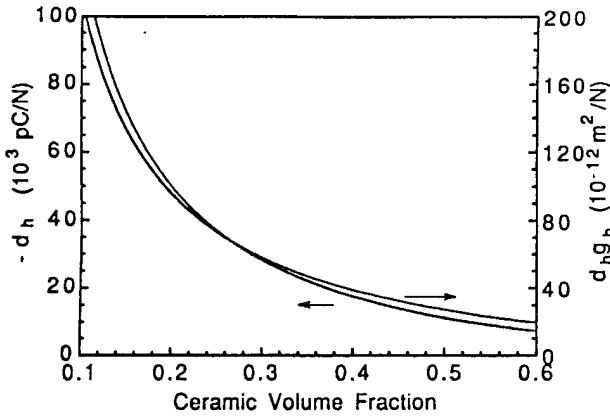


Fig. 2. Model results of the effective d_h and $d_h g_h$ as a function of the ceramic volume content for an end-capped TP honeycomb structure made of PZT-5H ceramic. The dimensions are: $L = 1$ cm and $a = 0.125$ cm.

In this paper, the effective piezoelectric response for this structure is defined as if the honeycomb is a ceramic block which is electroded on the faces perpendicular to the z -direction. The effective hydrostatic piezoelectric coefficient d_h , under this definition, is

$$d_h^{\text{eff}} = \frac{2Lad_{31}}{r^2 p} (T_1 + T_{2BR}) \quad (6)$$

where L is the composite thickness (Fig. 1) and d_{31} is the transverse piezoelectric coefficient of the ceramic material. In (6), $2Lad_{31}(T_1 + T_{3BR})$ is the total charge output from one unit cell under hydrostatic pressure p and r^2 is the unit cell area in the z -direction. Using (1) and (5), (6) can be converted to

$$d_h^{\text{eff}} = \frac{2Lad_{31}}{r^2} \left(\frac{1}{b} + \frac{1}{\nu} + \frac{s_{12}}{s_{11}(2-b)} \right). \quad (7)$$

Similarly, the effective piezoelectric hydrostatic figure of merit $d_h g_h$ can be derived as

$$d_h^{\text{eff}} g_h^{\text{eff}} = \frac{2b(1-b)d_{31}^2}{\epsilon_{33}} \left(\frac{1}{b} + \frac{1}{\nu} + \frac{s_{12}}{s_{11}(2-b)} \right)^2$$

where ϵ_{33} is the dielectric permittivity of the ceramic. In other words, the effective piezoelectric d_h coefficient is defined as the charge output per unit area in the x - y plane ($L_1 L_2$) and the effective g_h coefficient as the ratio of voltage output to the composite thickness L when the composite is subjected to unit hydrostatic pressure.

In Fig. 2, the calculated effective piezoelectric response is shown for a honeycomb structure made of PZT-5H (PZT-5H is the trademark of Morgan Matroc, Inc. for one of its piezoceramics; the parameters are: $d_{33} = 593$ (pC/N), $d_{31} = -274$, $s_{11} = 0.165$ (10^{-10} m²/N), $s_{33} = 0.207$, $s_{12} = -0.048$, $s_{13} = -0.085$, $\epsilon_{33} = 3400\epsilon_0$) ceramic with $L = 1$ cm, $a = 0.125$ cm as a function of ν , the volume content of the ceramic phase [10]. A honeycomb structure with $\nu = 0.3$ can easily be fabricated by extrusion, and as shown in Fig. 2, an effective $|d_h|$ of higher than 30000 pC/N and effective

$d_h g_h$ higher than 50000×10^{-15} m²/N can be obtained for this structure. On the other hand, due to the very high capacitance of this structure, the effective g_h is relatively small. Hence, the structure is an excellent transmitter and actuator, but not an ideal voltage sensor. However, for an electromechanical transducer, the most important factor is the electromechanical coupling factor, and in the hydrostatic application, it is $k_h^2 = d_h g_h / s_h$, where $s_h = (2s_{11} + s_{33}) + (2s_{12} + 4s_{13})$ is the hydrostatic elastic compliance [11]. Clearly, a large $d_h g_h$ is required for a structure to have a large k_h . It should be pointed out that although the physical basis for such a high piezoelectric response of a TP honeycomb structure is quite similar to that of a radially poled and end-capped cylinder [12], the TP honeycomb structure can provide a much higher piezoelectric hydrostatic sensitivity than that produced by the end-capped radially poled cylinders, because in this honeycomb structure the piezoelectric responses from all three-directions, the x -, y -, and z -directions, are utilized while in the end-capped cylinder, most of the response is from the axial direction.

B. Honeycomb Ceramic-Polymer Composite

By embedding a piezoceramic honeycomb structure in a polymer matrix, it is expected that the mechanical integrity, reliability, and shock resistance can be improved, and if a proper polymer is used, the piezoelectric response will not be reduced. To analyze the hydrostatic response of this composite structure, we divide the composite into three regions: the polymer region, the ceramic bridge region, and the ceramic joint region. Because of the presence of the polymer matrix, the stress T_w [see Fig. 1(b)] is no longer zero and its value depends on the elastic properties of the polymer matrix and the dimensions of the honeycomb unit cell, especially the ratio a/L .

The constitutive relations in the bridge region are

$$S_{1BR} = s_{11}T_1 + s_{13}T_w + s_{12}T_{2BR} \quad (8a)$$

$$S_2 = s_{12}T_1 + s_{13}T_w + s_{11}T_{2BR} \quad (8b)$$

$$S_{3BR} = s_{33}T_w + s_{13}T_1 + s_{13}T_{2BR}. \quad (8c)$$

In the joint region, we have

$$S_{1JR} = (s_{11} + s_{12})T_1 + s_{12}T_{2JR} \quad (9a)$$

$$S_2 = s_{11}T_{2JR} + 2s_{12}T_1. \quad (9b)$$

And in the polymer region, we have

$$S_1^p = (S_{11}^p + s_{12}^p)T_w + s_{12}^p T_2^p \quad (10a)$$

$$S_2 = s_{11}^p T_2^p + 2s_{12}^p T_w \quad (10b)$$

where the superscript p refers to the polymer matrix. Other notations are the same as in Section II-A. The local coordinate system is used for the ceramic. For the polymer region, the coordinate system has the 2-axis in parallel to the z -axis of the honeycomb composite, and the 1- and 3-axes in the plane perpendicular to that. In (8), (9), and (10), the isostrain approximation in the z -direction (S_2 is the same in the three

regions) and isostress approximation in the x - and y -directions were used.

The force balance conditions in the x - and z -directions lead to

$$(1-b)T_w + bT_1 = p \quad (11a)$$

$$(1-b)^2T_2^p + 2b(1-b)T_{2BR} + b^2T_{2JR} = p. \quad (11b)$$

Here, the composite is subjected to hydrostatic pressure p . The isostrain condition in the x -direction yields

$$\left(\frac{1}{b} - 1\right)S_{1BR} + S_{1JR} = \left(\frac{1}{b} - 1\right)S_1^p + S_{3BR}. \quad (12)$$

These are the basic equations for the piezoelectric and elastic responses of the composite, which contain 10 unknowns. By eliminating the strain components in the above equations, we get five linear equations for the stress components in the composite where $bb = \frac{1}{b} - 1$, as shown in (13) at the bottom of the page. These stress components are easily evaluated using the matrix method. The effective hydrostatic piezoelectric coefficient, therefore, is

$$d_h^{eff} = \frac{2La}{r^2p}(d_{31}[T_1 + T_{2BR}] + d_{33}T_w) \quad (14)$$

and the hydrostatic figure of merit is

$$d_h^{eff} g_h^{eff} = \frac{2b(1-b)}{\epsilon_{33}p^2}(d_{31}[T_1 + T_{2BR}] + d_{33}T_w)^2. \quad (15)$$

Here again, the definitions of the effective d_h and g_h are the same as those introduced in the previous section.

Shown in Fig. 3 are the results calculated from (14) and (15) for honeycomb composites made of PZT-5H piezoceramic with different polymer matrices. The curve 3 is for a composite with a Spurr's epoxy matrix (Young's modulus $Y = 4.8 \times 10^9$ Pa and Poisson's ratio $\sigma = 0.364$) [10]. The curves 1 and 2 are for composites with a polymer matrix having $Y = 4.8 \times 10^7$ Pa and $Y = 4.8 \times 10^8$ Pa, respectively. All have Poisson's ratio $\sigma = 0.364$. As expected, as Young's modulus of the polymer matrix decreases, the d_h value of a composite approaches that of an end-capped honeycomb which is the upper limit for the composite. In Fig. 4(a), the effect of the polymer compliance on d_h is shown explicitly for a honeycomb composite with 20% ceramic content. In both Figs. 3 and 4, $L = 1$ cm and $a = 0.125$ mm were used in the calculation. Fig. 4(a) shows that as the compliance of the polymer matrix is increased above 10^{-8} m²/N, the effect of the compliance of the polymer matrix becomes negligible. For example, the relative difference in d_h between a composite with $s_{11}^p = 10^{-8}$ m²/N and the end-capped honeycomb structure ($s_{11}^p \rightarrow \infty$) is less than 4%. To

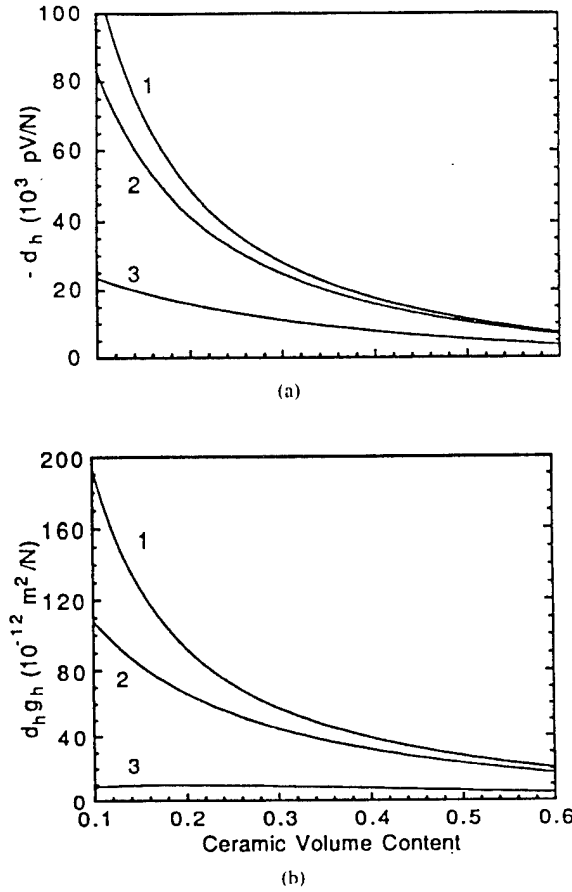


Fig. 3. Model results of the effect of polymer Young's modulus on the effective d_h and $d_h g_h$ of a TP honeycomb composite, where curve 1 is for a composite with a polymer matrix of $Y = 4.8 \times 10^7$ Pa, curve 2 for a polymer matrix of $Y = 4.8 \times 10^8$ Pa, and curve 3 for a polymer matrix of $Y = 4.8 \times 10^9$ Pa (Spurr's epoxy). All have the Poisson's ratio $\sigma = 0.364$. The piezoceramic is PZT-5H.

illustrate this more clearly, in Fig. 4(b), the d_h values from Fig. 4(a) are plotted against the Young's modulus (Y) of the polymer matrix, and the result is a nearly linear relationship between d_h and Y . The d_h value at $Y = 0$ is $-50\,200$ pC/N.

The influence of the Poisson's ratio σ of the polymer matrix on d_h of a honeycomb composite can also be evaluated, and plotted in Fig. 5 are the results from (14) and (15) for a composite of 20% ceramic content and the polymer matrix with the compliance $s_{11} = 10^{-8}$ m²/N. Apparently, σ does not affect d_h very much until it is close to 0.5. This is in strong contrast with 1-3 and 2-2 composites where the Poisson's ratio of the polymer matrix has a strong influence on the hydrostatic performance of the composites. The reason for this difference is that unlike 1-3 and 2-2 composites, the ceramic frame in a

$$\begin{bmatrix} s_{12} & s_{13} - 2s_{12}^p & s_{11} & -s_{11}^p & 0 \\ 2s_{12} & -2s_{12}^p & 0 & -s_{11}^p & s_{11} \\ s_{11}/b + s_{12} - s_{13} & bb(s_{13} - s_{11}^p - s_{12}^p) - s_{33} & bb s_{12} - s_{13} & -bb s_{12}^p & s_{12} \\ b & 1 - b & 0 & 0 & 0 \\ 0 & 0 & 2b(1-b) & (1-b)^2 & b^2 \end{bmatrix} \begin{bmatrix} T_1 \\ T_w \\ T_{2BR} \\ T_2^p \\ R_{2JR} \end{bmatrix} = \begin{bmatrix} 0 \\ 0 \\ 0 \\ p \\ p \end{bmatrix}. \quad (13)$$

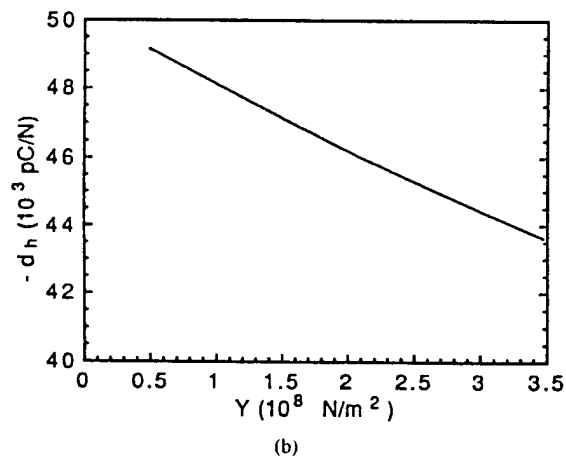
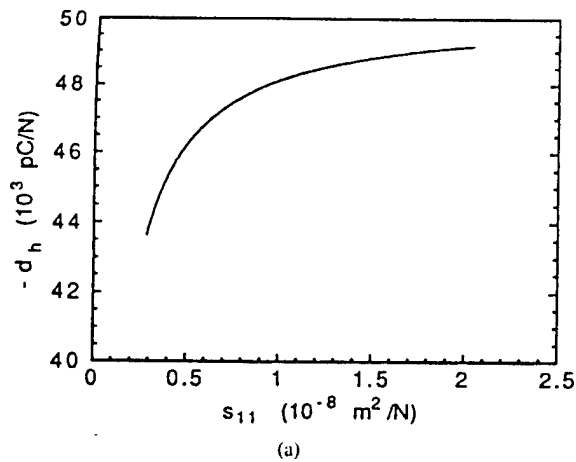


Fig. 4. Model results of the effect of polymer elastic compliance (a) or Young's modulus (b) on the effective d_h of a TP honeycomb composite with 20% ceramic volume fraction. The Poisson's ratio σ of the polymer is fixed at 0.364 and the ceramic is PZT-5H.

honeycomb composite forms a 3-D structure which bears the stresses in all three directions, i.e., the x -, y -, and z -directions, and the polymer phase, due to its low elastic constant, will not affect the stress pattern in the x - and y -directions. Only when the Poisson's ratio of the polymer phase approaches 0.5, which implies the bulk modulus will approach infinity [13], will the polymer phase substantially reduce the effective stress applied on the ceramic and the effective hydrostatic response of the composite.

III. EXPERIMENTAL RESULTS

The honeycomb ceramics used in this study were made by Dr. Lochman of Corning, Inc., using the extrusion technique and specially designed dies. The composition of the material is close to that of PZT-4. The original shape of the honeycomb ceramic is a long cylinder of 1.5 cm diameter. The samples were cut into pieces about 1 cm length with nearly square cross sections, as illustrated in Fig. 6. The dimensions of the square unit cell are: $a = 0.125 \pm 0.004$ cm and $t = 0.22 \pm 0.03$ mm. The ceramic volume content, therefore, is 27.7%. There are small variations in the value of a and t across a sample. The

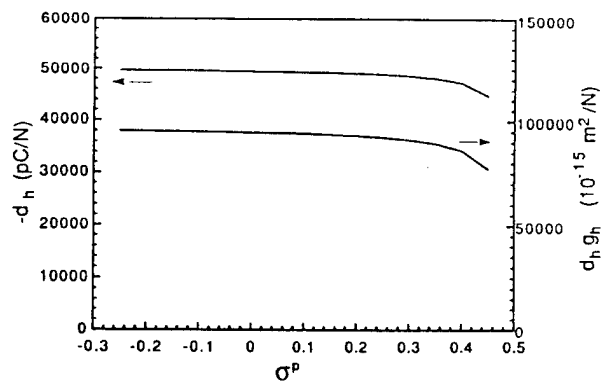
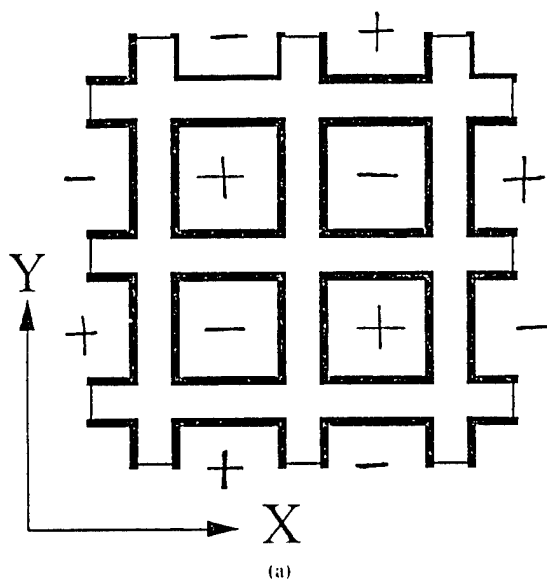


Fig. 5. Model results of the effect of polymer Poisson's ratio on the effective d_h and $d_h g_h$ of a TP honeycomb composite with 20% ceramic volume. The elastic compliance of the polymer matrix is fixed at 10^{-8} m^2/N and the ceramic is PZT-5H.

samples were electroded with electroless nickel. The electric connection was provided by gluing thin copper wires to each cell using conductive epoxy. The samples were then poled with a field of about 40 kV/cm at a temperature of about 60°C for five minutes. Three samples were fabricated and tested. The parameters of the samples are listed in Table I. The piezoelectric d_{33} and d_{31} coefficients of the material were measured using a laser dilatometer on a small ceramic plate cut from a poled honeycomb sample. The average $d_{33} = 110$ pC/N and $d_{31} = -40$ pC/N (the d_{33} coefficient was also measured by a d_{33} meter). Two honeycomb samples were made in the end-capped form by placing thin layers of epoxy (JB KWIK) (JB KWIK is the trademark of JB Welb Co., TX) over the two ends to block all the openings. One sample was made in the composite form with the polymer matrix made of polyurethane (Miles Inc., PA) mixed with 50% volume microballoon.

The effective hydrostatic piezoelectric d_h coefficient of TP honeycomb composites was evaluated by a standard comparison method: A composite and a standard sample with known d_h were placed in a high pressure oil chamber and subjected to a low frequency ac (50 Hz) hydrostatic pressure. The charge outputs of the composite and the standard sample under the ac pressure were measured and were used to calculate d_h of the composite when the areas of the composite and the standard are known. From the measured d_h value and the effective dielectric constant of the composite, g_h as well as $d_h g_h$ were obtained.

Shown in Fig. 7 are the test results of d_h and $d_h g_h$ for these samples where the abscissa is the dc bias hydrostatic pressure. There were no observable changes of d_h as the samples went through pressure cycles, except for data scatter. The comparison between the experimental and theoretical d_h values is made and listed in Table I. The elastic constants for the piezoceramic used in the calculation are those of PZT-4 (PZT-4 is the trademark of Morgan Matroc, Inc., OH: $s_{11} = 0.123$ (10^{-10} m^2/N), $s_{33} = 0.155$, $s_{12} = -0.011$, $s_{13} = -0.053$). The elastic constants for the matrix are: $s_{11} = 5.0$ (10^{-8} m^2/N), $\sigma = 0.364$). Considering the simplicity of the model, the agreement between the experimental results and model calculations is quite good. The discrepancy between



(a)



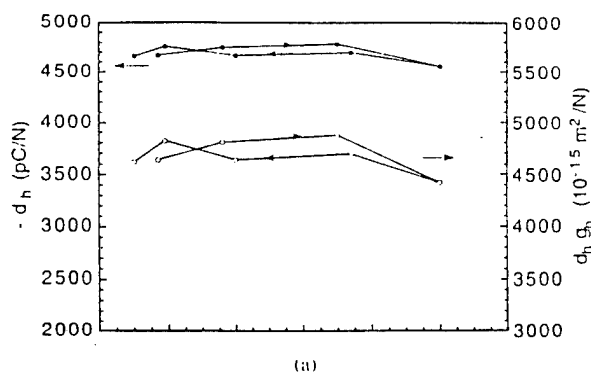
(b)

Fig. 6. (a) The electric connection pattern for the honeycomb structure where all the cells of "+" are connected together and the cells of "-" are connected together. The thick lines on the walls of the cells indicate the electrodes. (b) Photograph showing the honeycomb structure used in the experiment, where the numbers on the meter are in centimeters.

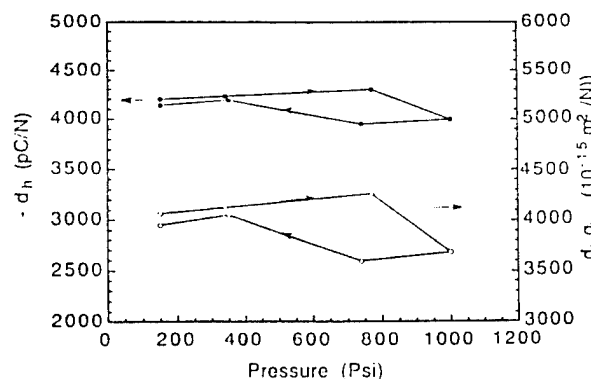
the two is mainly caused by the finite size of a honeycomb structure. That is, in a finite honeycomb structure, there are ceramic walls (bridge regions) in the periphery that are in direct contact with the external pressure source. In these regions, even in the end-capped configuration, T_w is no longer zero and can be close to p . Hence, the effective hydrostatic responses in these cells will be reduced. In the honeycomb samples tested, about 20% of the bridge regions are in the periphery, and hence are subject to the external pressure, which reduces the d_h value since the analytical model does not take these effects into account. The variation of the wall thickness in these samples could result in imperfect poling in the thick wall regions, and consequently a lower material piezoelectric activity, which is another possible reason for the discrepancy between the model predictions and experimental results. Even so, the hydrostatic response from those test samples is quite high considering the fact that the material has $d_{31} = -40$ pC/N and $d_{33} = 110$ pC/N. With improved materials, the effective

TABLE I
PARAMETERS AND RESULTS OF THE TP HONEYCOMB SAMPLES TESTED

Configuration	ϵ/ϵ_0	L_1 (cm)	L_2 (cm)	L (cm)	d_h (pC/N) (exp)	d_h (Theory)
I End-capped	520	1.29	1.44	1.326	-4,700	-6,200
II End-capped	520	1.15	1.27	1.237	-4,200	-5,784
III Polyurethane with microballoon matrix	570	1.1	1.1	1.2	-4,666	-5,636



(a)



(b)

Fig. 7. Experimental results of effective d_h and $d_h q_h$ of the TP honeycomb (a) sample I and (b) sample II. Both samples are in the end-capped configuration (see Table I). The solid and open circles are the experimental results. Solid lines connecting the data points are drawn to guide the eye. Arrows on the solid lines indicate the experimental path (increasing and decreasing pressure).

piezoelectric response of a TP honeycomb transducer can be significantly higher, as predicted in Section II.

For sample III, which has a polymer matrix of polyurethane mixed with 50% volume microballoons, the theoretical predicted d_h value using (13) is the same as that calculated for an end-capped structure since the Young's modulus of the polymer matrix is very low. The experimental d_h value is close to the model value, which demonstrates that a TP honeycomb composite with soft polymer matrix can yield the same level of hydrostatic response as that of an end-capped honeycomb structure.

Hence, the experimental results confirm the prediction of the analytical model and show that a TP honeycomb composite

can provide substantially higher hydrostatic responses than most of the composites developed previously.

IV. CONCLUSION

A new piezoelectric composite transducer based on the ceramic honeycomb structure has been introduced and its hydrostatic piezoelectric performance was modeled analytically. The transducer is operated in the transverse piezoelectric d_{31} mode. The honeycomb configuration enables one to fabricate a TP honeycomb transducer by either embedding a honeycomb ceramic skeleton into a soft polymer matrix to form a composite or blocking the openings of the honeycomb cells with thin layers of epoxy to form an end-capped honeycomb structure. With the unique honeycomb configuration and TP operation mode, the piezoelectric d_{33} response of the ceramic is nearly eliminated and the piezoelectric responses from the three orthogonal directions add together when the transducer is subjected to a hydrostatic pressure. As a result, as predicted by the analytical model and verified by the experimentation, the TP honeycomb transducer exhibits exceptionally high hydrostatic responses such as d_h and $d_h g_h$.

ACKNOWLEDGMENT

The authors wish to thank Dr. B. Wilhelm of Sound Technology, Inc. for making the electro-less nickel electrodes for the honeycomb ceramic structures used in this investigation. They also wish to acknowledge staff members of the Corning Research Laboratories for their assistance in fabricating the honeycomb ceramics.

REFERENCES

- [1] R. E. Newnham, D. P. Skinner, and L. E. Cross, "Connectivity and piezoelectric-pyroelectric composites," *Mater. Res. Bull.*, vol. 13, pp. 525-536, 1978.
- [2] T. R. Gururaja, A. Safari, R. E. Newnham, and L. E. Cross, "Piezoelectric ceramic-polymer composites for transducer applications," in *Electronic Ceramics*, L. M. Levinson, Ed. New York: Marcel Dekker, 1987, pp. 92-128.
- [3] Q. C. Xu, S. Yoshikawa, J. R. Belsick, and R. E. Newnham, "Piezoelectric composites with high sensitivity and high capacitance for use at high pressure," *IEEE Trans. Ultrason., Ferroelect., Freq. Contr.*, vol. 38, pp. 634-639, 1991.
- [4] Q. M. Zhang, H. Wang, and L. E. Cross, "Piezoelectric tubes and 1-3 type tubular composites as tunable actuators and sensors," in *Proc. SPIE-Smart Structures and Materials*, vol. 1916, pp. 244-254, 1993.
- [5] Q. M. Zhang, J. Chen, H. Wang, J. Zhao, L. E. Cross, and M. C. Trottier, "A new transverse piezoelectric mode 2-2 piezocomposite for underwater transducer applications," *IEEE Trans. Ultrason., Ferroelect., Freq. Contr.*, vol. 42, pp. 774-781, 1995.
- [6] W. A. Smith, "The application of 1-3 piezocomposites in acoustic transducers," in *Proc. 1990 IEEE 7th Int. Symp. Appl. Ferroelect.*, Urbana, IL, pp. 145-152.
- [7] T. R. Shrout, L. J. Bowen, and W. A. Schulze, "Extruded PZT-polymer composites for electromechanical transducer applications," *Mater. Res. Bull.*, vol. 15, pp. 1371-1380, 1980.
- [8] A. Safari, A. Halliyal, R. E. Newnham, and I. M. Lachman, "Transverse honeycomb composite transducers," *Mater. Res. Bull.*, vol. 17, pp. 301-309, 1982.
- [9] Q. M. Zhang, W. Cao, J. Zhao, and L. E. Cross, "Piezoelectric performance of piezoceramic-polymer composites with 2-2 connectivity—A combined theoretical and experimental study," *IEEE Trans. Ultrason., Ferroelect., Freq. Contr.*, vol. 41, pp. 556-564, 1994.
- [10] C. G. Oakley, "Analysis and development of piezoelectric composite for medical ultrasound transducer applications," Ph.D. dissertation, Penn State Univ., 1991.
- [11] "Standards on piezoelectric crystals: Determination of the elastic, piezoelectric, and dielectric constants of piezoelectric crystals—The electro-mechanical coupling factors," IEEE Standard 178-1958, R1972.
- [12] R. A. Langevin, "The electro-acoustic sensitivity of cylindrical ceramic tubes," *J. Acoust. Soc. Amer.*, vol. 26, pp. 421-427, 1954.
- [13] L. D. Landau and E. M. Lifshitz, *Theory of Elasticity*. New York: Pergamon, 1986, p. 13.

APPENDIX 30

A New Transverse Piezoelectric Mode 2-2 Piezocomposite for Underwater Transducer Applications

Q. M. Zhang, J. Chen, H. Wang, J. Zhao, L. E. Cross, *Fellow, IEEE*, and M. C. Trottier

Abstract—In this paper, we present a new type of 2-2 piezoelectric ceramic-polymer composite operated at the transverse piezoelectric mode (TP). The new TP mode piezocomposite has exceptionally high hydrostatic piezoelectric response, high reliability, and can be made at low cost. Based on the isostrain approximation, an analytical model is developed to analyze and optimize the effective piezoelectric and the effective elastic properties of the composite. Several composites with the new structure were fabricated and tested. The calculated and experimental results show good agreement. It is shown that a TP 2-2 composite made of PZT plates in a soft polymer matrix with elastically unidirectional face plates yields an effective hydrostatic piezoelectric coefficient d_h of 6,000 (pC/N) and a hydrostatic figure of merit $d_h g_h$ higher than 30,000 (10^{-15} m²/N).

I. INTRODUCTION

THE GROWING market of ferroelectric sensors, actuators, and transducers demands a continuous improvement on the performance of the underlying materials. With single phase piezoelectric materials, however, it becomes increasingly difficult to considerably improve the material properties, such as, piezoelectric coefficients, acoustic impedance and material density. On the other hand, many composite materials, which incorporate several constituent phases with complementary properties, are offering many unique and attractive features. For example, in hydrostatic and medical imaging applications, piezoceramic polymer composites with the 1-3 connectivity pattern exhibit low density, high hydrostatic piezoelectric response, high electromechanical coupling factor, and better acoustic impedance matching, etc. [1], [2]. However, for many emerging applications, such as, large area acoustic projectors and adaptive materials for fluid borne noise control, in order to generate high radiation power at a wide frequency band a transducer is required to generate a large surface displacement while operated with a moderate driving voltage. And apparently, a conventional 1-3 composite cannot meet these requirements. In spite of the fact that the material has a relatively high hydrostatic piezoelectric figure of merit $d_h g_h$, its piezoelectric d_h coefficient is limited by the longitudinal piezoelectric strain coefficient d_{33} of the ceramic phase. While

increasing the composite thickness will increase the surface displacement, the escalated electric impedance with thickness and limited improvement accomplished by this method clearly disfavor this approach. In addition, for deep water applications, the loading pressure is against the poling direction of piezoceramic rods in a 1-3 composite. Due to the stress amplification in a piezocomposite [3], this pressure induced depolarization effect can become severe in a composite with low piezoceramic content, which is often a preferred choice in order to yield a high hydrostatic piezoelectric figure of merit. Consequently, the performance of a composite degrades, causing reliability problem in the transducer.

To overcome these problems, recently we have designed and developed a 1-3 tubular composite operated in the transverse piezoelectric d_{31} mode [4], [5]. The 1-3 tubular composite has exhibited an exceptionally high effective piezoelectric coefficient d_h , the hydrostatic figure of merit $d_h g_h$ and has little problem of the depoling from the high loading pressure. The one possible drawback of this composite is that with the current technology the manufacture cost is relatively high. Following the similar line of operation of 1-3 tubular composites, in this paper, we shall present a new composite—a transverse piezoelectric d_{31} mode 2-2 piezocomposite, which possesses most of the advantages of a 1-3 tubular composite. Moreover, it can be made with lower manufacture cost and simpler fabrication process.

As had been introduced earlier by Newnham *et al.*, piezocomposites can be classified into different categories based on the connectivity pattern of the constituents, which determines the effective material properties of a composite [6]. However, even within the same connectivity pattern, piezocomposites can be operated in different piezoelectric modes, i.e., longitudinal piezoelectric mode (LP), transverse piezoelectric mode (TP), and shear piezoelectric mode (SP) or even in mixed modes. Apparently, the response behavior of a piezocomposite is quite different when operated in different piezoelectric modes. To distinguish this difference, it is necessary to specify the operation mode besides the connectivity for a composite. With this spirit, the new 2-2 piezocomposite is named as a TP 2-2 composite. For the sake of simplicity, in this paper, the piezocomposites operated in LP mode will just be referred to their connectivity pattern without specifying their operation mode.

In this paper, we shall present the theoretical analysis of the response behavior of this new composite and the key

Manuscript received November 7, 1994; revised February 15, 1995. This work was supported by the Office of Naval Research and by a Grant of SBIR.

Q. M. Zhang, J. Chen, H. Wang, J. Zhao, and L. E. Cross are with the Intercollege Materials Research Laboratory, The Pennsylvania State University, University Park, PA 16802 USA.

M. C. Trottier is with the Fiber Materials Inc., Biddeford, ME 04005 USA. IEEE Log Number 9411940.

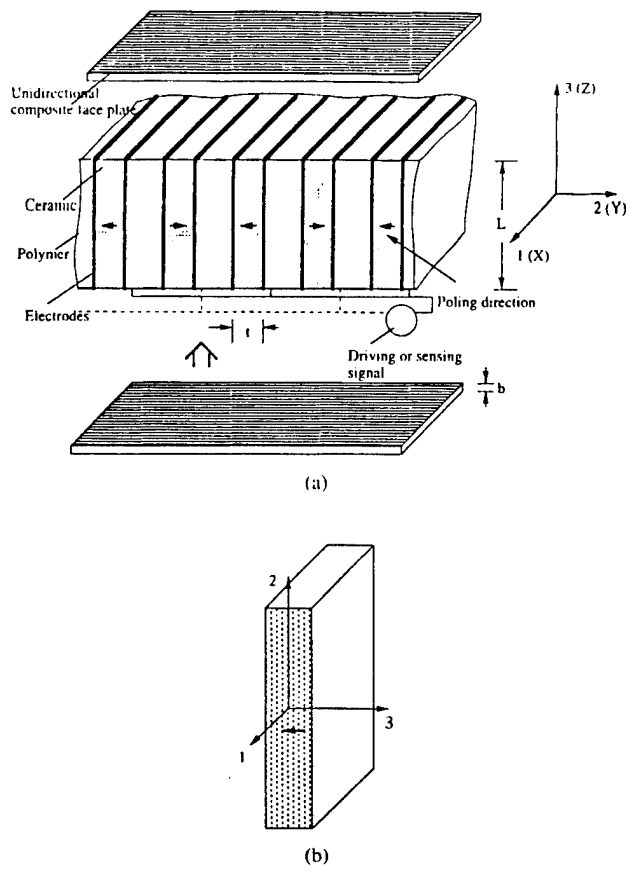


Fig. 1. (a) Schematic drawing of a TP 2-2 piezocomposite. (b) The local coordinate system for piezoceramic plate, it is different from that for the composite in (a).

parameters in the design process, elucidate the differences between a TP 2-2 composite and 1-3, 2-2 piezocomposites, and demonstrate its superior performance.

II. DESIGN DETAILS

A schematical drawing of a TP 2-2 piezocomposite is shown in Fig. 1, where the piezoceramic thin plates form a parallel array and are embedded in a soft polymer matrix. The ceramic plates are electroded over the side faces with the polarization direction parallel to the acoustic radiation plane, as shown in the figure. Therefore, the action of the composite is through the transverse piezoelectric d_{31} mode of the ceramic plates. Although the magnitude of d_{31} of a piezoceramic is smaller than that of the longitudinal coefficient d_{33} , as will be shown later, the large ratio of L/t in a composite introduces an amplification factor and as a result, the effective d_{33} coefficient of a TP 2-2 composite can be much higher than d_{33} coefficient of the piezoceramic. Consequently, the new piezocomposite can generate much higher acoustic power than the 1-3 rod composite.

The theoretical analysis developed in this paper is based on the so-called isostrain approximation. Hence, the results derived represent the upper limit of the piezoelectric response of a composite. However, for a 2-2 composite properly designed, the stress transfer between the ceramic plates and polymer

matrix is close to that predicted by the isostrain model [7]. Furthermore, in most practical cases, the unidirectional face plates will be used for TP 2-2 composites, which will improve the stress transfer between the ceramic plates and polymer matrix to the level of the isostrain model.

Due to the special arrangement of the piezoceramic plates in a TP 2-2 composite, two coordinate systems will be employed in the analysis: one is attached to the composite structure as shown in Fig. 1(a) where the Y -axis is along the ceramic poling direction, and the subscripts for all the effective coefficients of a composite are based on this coordinate system; the other, shown in Fig. 1(b), is attached to the ceramic plate (the local coordinate system) and to conform with the convention, the z -axis is along the ceramic poling direction. The parameters of the piezoceramic plates are labeled with respect to this local coordinate system and they will be specified by the superscript c . All the other parameters used in the analysis will be labeled with the composite coordinate system. The superscripts p and cp are used for the parameters of the polymer phase and the effective parameters of the composite, respectively.

Analysis of the Responses of TP 2-2 Piezocomposite

The constitutive relations in the piezoceramic plate can be expressed as:

$$S_1^c = s_{11}^c T_1^c + s_{12}^c T_2^c + s_{13}^c T_3^c + d_{31}^c E_3^c \quad (1a)$$

$$S_3^c = s_{13}^c T_1^c + s_{13}^c T_2^c + s_{33}^c T_3^c + d_{33}^c E_3^c \quad (1b)$$

$$D_3^c = d_{31}^c T_1^c + d_{31}^c T_2^c + d_{33}^c T_3^c + \epsilon_{33}^c E_3^c \quad (1c)$$

where S_i and T_i are the strain and stress components in the ceramic plate, s_{ij} are the elastic compliance, $E_3^c = V/t$ is the electric field along the ceramic poling direction generated by the total applied voltage V over the thickness t of the ceramic plate, ϵ_{33} is the dielectric permittivity, and d_{ij} are the piezoelectric coefficients, all are for the ceramic plate (see Fig. 1(b)). For a polarized ceramic, which point group symmetry is ∞om , the equation for S_2^c is similar to that of S_1^c .

The constitutive equations for the polymer matrix are similar to those of the ceramic except that all the parameters in (1) are replaced by those of the polymer phase.

For a composite material, at the long wavelength limit, the effective parameters can be introduced to describe the responses when it is subjected to an external electric field and/or stress field. By utilizing these effective parameters, the constitutive equations for a composite can be expressed as:

$$S_2^p = s_{12}^p T_1 + s_{22}^p T_2 + s_{12}^p T_3 + d_{32}^p E_3 \quad (2a)$$

$$S_3^p = s_{13}^p T_1 + s_{12}^p T_2 + s_{33}^p T_3 + d_{33}^p E_3 \quad (2b)$$

$$D_3^p = d_{31}^p T_1 + d_{32}^p T_2 + d_{33}^p T_3 + \epsilon_{33}^p E_3 \quad (2c)$$

where T_i are the external stresses applied on the composite, which can be quite different from those in either the ceramic or polymer phase (T_i^c and T_i^p), $E_3 = V/L$ is different from E_3^c in (1), where L is the thickness of the composite. The s_{ij}^p , d_{ij}^p , and ϵ_{33}^p are the effective coefficients of the composite.

Due to the symmetry of the composite, the equation for S_1^{cp} is similar to that of S_3^{cp} . In writing down (2), a TP 2-2 composite is regarded as an effective piezoelectric medium with the electrode areas in perpendicular to the z -axis (Fig. 1(a)).

To evaluate the effective material parameters for a composite, the following approximations will be employed:

- 1) The strains in the polymer phase and ceramic phase are equal in the x -direction and in the z -direction, that is, $S_3^{cp} = S_2^c = S_3^p$ and $S_1^c = S_1^p = S_1^p$, this is the isostrain approximation.
- 2) The stresses in the y -direction in the polymer phase and ceramic phase are equal, which is derived from the static force balance condition.
- 3) The stresses in the z - and x -directions are related through $T_3 = vT_2^c + (1-v)T_3^p$ and $T_1 = vT_1^c + (1-v)T_1^p$, where v is the volume content of the ceramic phase in the composite. For the quantities in the ceramic phase, local coordinate system is used.

Except otherwise specified, the x -, y -, and z -directions in the derivations and discussions through out the paper are referred to those of the composite (Fig. 1(a)).

With the constitutive equations and the above conditions, the effective coefficients for a TP 2-2 composite can be derived. For example, the effective piezoelectric coefficients are:

$$d_{33}^{cp} = \left\{ d_{31}^c \frac{(1-\sigma_p)s_{11}^p}{(1-v)(1-\sigma_c)s_{11}^c + v(1-\sigma_p)s_{11}^p} \right\} \frac{Lv}{t} \quad (3a)$$

$$d_{32}^{cp} = \left\{ 2d_{31}^c \frac{(1-v)(s_{12}^p - s_{12}^c)}{(1-v)(1-\sigma_c)s_{11}^c + v(1-\sigma_p)s_{11}^p} + d_{33}^c \right\} \cdot \frac{Lv}{t} \quad (3b)$$

$$d_{31}^{cp} = d_{33}^{cp} \quad (3c)$$

where σ_p and σ_c are the Poisson's ratio of the polymer and ceramic phases, respectively. If $s_{11}^p \gg s_{11}^c$, (3a) can be reduced to

$$d_{33}^{cp} = d_{31}^c \frac{L}{t} \quad (4)$$

Equation (4) indicates that in a TP 2-2 composite with a large ratio of L/t , d_{33}^{cp} can be significantly larger than d_{33}^c . The amplification factor L/t is similar to that in the TP 1-3 tubular composite [4], [5], which is one of the advantages of this type of composite structure.

The effective elastic compliances of a TP 2-2 composite, thus derived, are

$$\begin{aligned} s_{33}^{cp} &= \frac{(s_{11}^c s_{12}^p + s_{11}^p s_{12}^c) A_{12} - s_{11}^c s_{11}^p A_{22} - s_{12}^c s_{12}^p A_{11}}{A_{12}^2 - A_{11} A_{22}} \\ s_{13}^{cp} &= \frac{(s_{12}^c s_{12}^p + s_{11}^p s_{22}^c) A_{12} - s_{12}^c s_{11}^p A_{22} - s_{22}^c s_{12}^p A_{11}}{A_{13}^2 - A_{11} A_{22}} \\ s_{11}^{cp} &= s_{33}^{cp} \\ s_{22}^{cp} &= (1-v)s_{22}^p + vs_{33}^c - \frac{2v(1-v)[(s_{13}^c)^2 - (s_{12}^p)^2]}{A_{11} + A_{13}} \\ s_{12}^{cp} &= s_{13}^c - \frac{(1-v)(s_{11}^c + s_{13}^c)(s_{13}^c - s_{12}^p)}{A_{11} + A_{13}} \end{aligned} \quad (5)$$

where

$$A_{ij} = (1-v)s_{ij}^c + vs_{ij}^p; \quad i, j = 1, 2, 3.$$

From the definition $d_h = d_{33} + d_{31} + d_{32}$, the effective hydrostatic piezoelectric coefficient of a TP 2-2 composite can be obtained

$$d_h^{cp} = \left\{ 2d_{31}^c \frac{(1-\sigma_p)s_{11}^p + (1-v)(s_{12}^p - s_{12}^c)}{(1-v)(1-\sigma_c)s_{11}^c + v(1-\sigma_p)s_{11}^p} + d_{33}^c \right\} \cdot \frac{Lv}{t} \quad (6)$$

By taking a TP 2-2 composite as a parallel plate capacitor with the electrodes perpendicular to the z -axis, the effective dielectric constant of the composite is obtained,

$$\epsilon_{33}^{cp} = \frac{\epsilon_{33}^c v L^2}{t^2}. \quad (7)$$

The effective hydrostatic figure of merit $d_h g_h$ is

$$d_h^{cp} g_h^{cp} = \left[d_{33}^c + 2d_{31}^c \frac{(1-\sigma_p)s_{11}^p + (1-v)(s_{12}^p - s_{12}^c)}{(1-v)(1-\sigma_c)s_{11}^c + v(1-\sigma_p)s_{11}^p} \right]^2 \cdot \frac{v}{\epsilon_{33}^c}. \quad (8)$$

Equations (6) and (8) reveal that under the isostrain approximation, d_h^{cp} depends linearly on the ratio of L/t while the figure of merit $d_h^{cp} g_h^{cp}$ is independent of L/t . This is caused by the effective dielectric constant of a TP 2-2 composite, which is proportional to L^2/t^2 as seen in (7) and cancels the L/t dependence in $d_h^{cp} g_h^{cp}$.

Shown in Fig. 2 are the hydrostatic piezoelectric responses of a TP 2-2 composite as a function of the ceramic volume content in a composite, calculated using (6) and (8). The parameters for the piezoelectric phase are those of PZT-5H. To compare the effect of the Young's modulus of the polymer matrix on the response behavior, two sets of parameters are used for the polymer matrix, which are listed in Table I. In the calculation, $L/t = 20$ is used since it is a typical value for piezoelectric plates commercially available and suitable for the composite, which, in general, corresponds to a ceramic plate with $L = 1$ cm and $t = 0.5$ mm. The results indicate that a TP 2-2 composite has the potential to yield very high hydrostatic piezoelectric response and apparently, increasing the ratio of L/t can significantly increase the hydrostatic d_h coefficient. Fig. 2 also reveals that at high ceramic volume contents, the effective d_h for a TP 2-2 composite goes through zero. This is the result of increased influence of piezoceramic d_{33} on the hydrostatic response of a TP 2-2 composite as the ceramic volume content increases. It is clear from (6) that as the ceramic volume content v approaches 100%, the effective d_h for a TP 2-2 composite will approach $d_h^c L/t$, where d_h^c is the hydrostatic piezoelectric coefficient of the ceramic and is positive. Therefore, to achieve high hydrostatic piezoelectric responses, a low ceramic volume content is preferred for a TP 2-2 composite.

One major concern in design a piezoceramic polymer composite for hydrostatic applications is the Poisson's ratio effect

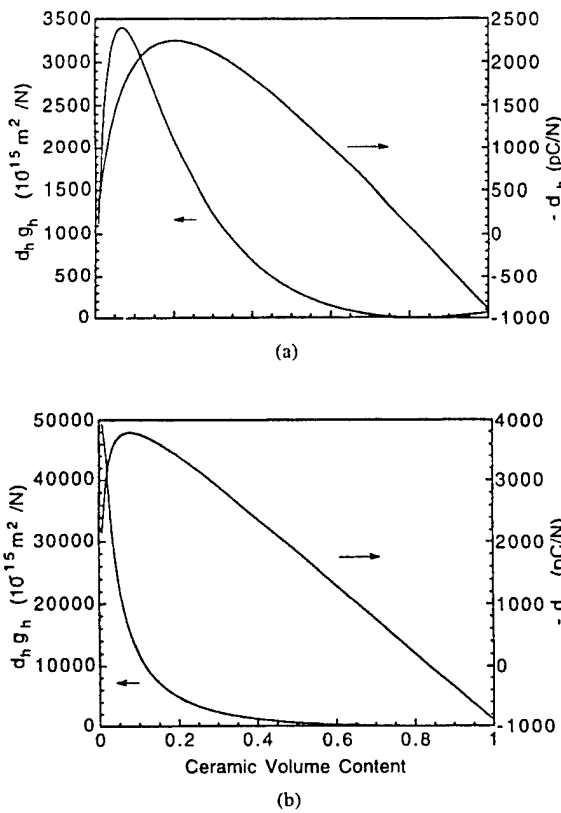


Fig. 2. The piezoelectric hydrostatic responses of TP 2-2 composites as a function of the volume content of the ceramic phase. $L/t = 20$ is used in the calculation. To illustrate the effect of the polymer elastic properties on the composite performance, two polymers with different compliances are evaluated: (a) PZT-5H and Spurr's epoxy matrix and (b) PZT-5H and polymer II as the polymer matrix (see Table I).

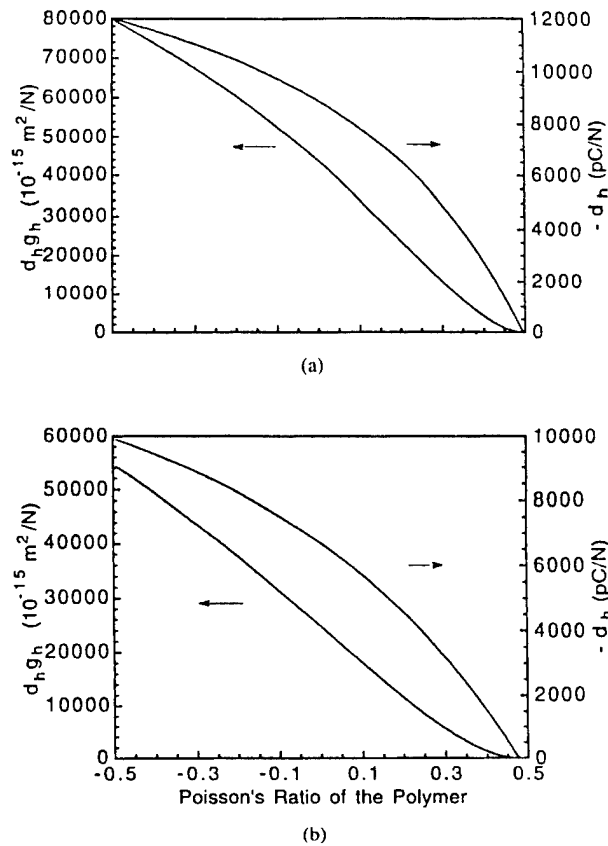


Fig. 3. The effect of Poisson's ratio on the hydrostatic responses of TP 2-2 composites. $L/t = 20$ is used in the calculation and the ceramic volume content is 15%. (a) PZT-5H and a polymer matrix with $s_{11} = 2.08 (10^{-9} \text{ m}^2/\text{N})$ and (b) PZT-5H and a polymer matrix with $s_{11} = 2.08 (10^{-10} \text{ m}^2/\text{N})$.

TABLE I

THE PARAMETERS USED IN THE THEORETICAL CALCULATION

PZT-5H:	$d_{33} = 593 \text{ (pC/N)}$, $d_{31} = 274$, $s_{11} = 0.165 (10^{-10} \text{ m}^2/\text{N})$, $s_{33} = 0.207$, $s_{12} = -0.048$, $s_{13} = -0.085$, $\epsilon_{33} = 3400 \epsilon_0$
Polymer I (Spurr's epoxy):	$s_{11} = 2.0 (10^{-10} \text{ m}^2/\text{N})$, $\sigma = 0.36$
Polymer II	$s_{11} = 2.0 (10^{-9} \text{ m}^2/\text{N})$, $\sigma = 0.36$

* ϵ_0 is the vacuum permittivity; PZT-5H is the trademark of Morgan Matric Inc. Vemtron Div. (Bedford, OH); Spurr's epoxy is the trademark of Polysciences, Inc. (Warrington, PA).

of the polymer matrix [2], [3], [8]. For example, even though a TP 1-3 tubular composite can yield very high hydrostatic piezoelectric response, its performance is very sensitive to the Poisson's ratio of the polymer matrix. For 1-3 rod composites, the Poisson's ratio of the polymer matrix also plays a very important role. Since the key factor determining the performance of a piezocomposite is the effective stress transfer between the polymer matrix and the ceramic phase, in composites with 1-3 connectivity pattern, the Poisson's ratio effect of the polymer matrix cuts down the effective transferable stress between the two phases by a factor of $(1 - 2\sigma)$ where σ is the Poisson's ratio of the polymer matrix and results in a poor performance of a composite if σ is large. On the other hand, for a TP 2-2 composite, the ceramic plates can be viewed as equivalent to the laterally reinforcing fiber glass employed in the earlier works of 1-3 composites to reduced the Poisson's ratio effect

of the polymer matrix [8]. Due to this difference, it is expected that the Poisson's ratio of the polymer phase will have a less effect here than that in 1-3 composites. Shown in Fig. 3 are the dependence of the hydrostatic piezoelectric response of TP 2-2 composites on the Poisson's ratio of the polymer matrix as calculated from (6) and (8). In comparison with 1-3 composites, the effect of the polymer Poisson's ratio is less severe albeit it is still significant. In general, for a TP 2-2 composite, the larger the volume content of the ceramic phase is, the less the polymer Poisson's ratio effect will be. The Poisson's ratio effect can also be reduced if a polymer matrix with a larger Young's modulus is used.

The dependence of the hydrostatic piezoelectric responses on the Young's modulus of the polymer matrix is also examined and the analytical results are presented in Fig. 4. Generally speaking, in order to raise the hydrostatic piezoelectric response of a composite, a polymer matrix with a smaller Young's modulus is preferred. On the other hand, as shown in Fig. 4, the piezoelectric responses of a composite increase with the compliance (reciprocal of the Young's modulus) of the polymer matrix only in a certain range. Further increasing the compliance does not affect the sensitivity of a composite significantly. In addition, the mechanical integrity of a composite will be reduced if the Young's modulus of the polymer is too small. In practical design of a TP 2-2 composite, these factors have to be considered and balanced.

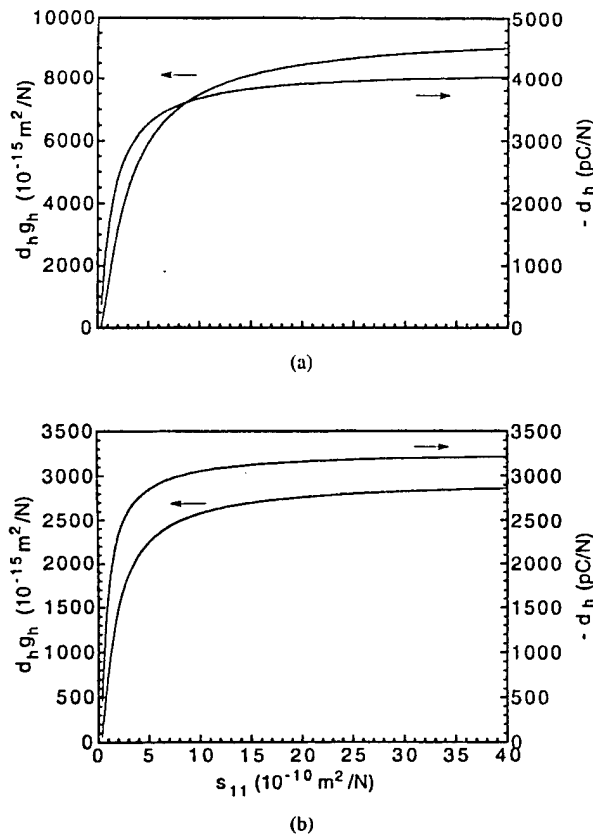


Fig. 4. The effect of the compliance of polymer matrix on the hydrostatic responses of TP 2-2 composites. $L/t = 20$ was used in the calculation. The Poisson's ratio of the polymer is fixed at 0.364. (a) 15% volume content of PZT-5H and (b) 30% volume content of PZT-5H1. Notice that for each configuration, there is a threshold of s_{11} , beyond which further increasing s_{11} will not improve the hydrostatic responses of the composite.

Effects of Face Plate

The results derived above show that a TP 2-2 composite exhibits much better hydrostatic performance over that of a 1-3 composite [9]. However, the Poisson's ratio of the polymer phase still has a considerable effect on the piezoelectric response of the composite. Since in most cases, the Poisson's ratio of a soft polymer is around 0.4, by reducing or eliminating this Poisson's ratio effect of the polymer matrix, the hydrostatic response of a TP 2-2 composite can be improved remarkably, as shown in Fig. 3. An effective means to achieve this is to incorporate stiff face plates into a composite structure, a practice which has been used previously in 1-3 composites. As has been demonstrated by several experimental studies, stiff face plates can improve the stress transfer between the two constituents and raise the hydrostatic piezoelectric response of the composite structure considerably [10].

The function of the stiff face plate on a TP 2-2 composite structure are mainly two folds: one is to improve the stress transfer between the two constituents, and the other is to clamp the composite in the lateral dimensions [10]. The result of the later effect is to reduce or eliminates the Poisson's ratio effect of the polymer matrix and the piezoelectric d_{33} response of the ceramic plates (6) and (8). For TP 2-2 composites subjected to hydrostatic pressure, due to the arrangement of the

piezoceramic plates, the piezoelectric responses in both the x - and z -directions are utilized. Hence, to the advantage of high hydrostatic response of the composite, a face plate should be specially designed so that the composite will only be clamped in the y -direction while the x -direction is still free. In other words, an ideal face plate used in a TP 2-2 composite should be elastically unidirectional such that the Young's modulus Y of the face plate in the y -direction is much larger than that of the composite, while in the x -direction, it is much smaller than that of the TP 2-2 composite, or more precisely,

$$\frac{L}{2b} Y_{11}^{cp} > Y_{11}^f \quad \text{and} \quad Y_{22}^f > \frac{L}{2b} Y_{22}^{cp} \quad (9)$$

where L and b are the thicknesses of the composite and the face plate, respectively. A factor of 2 is included in (9) to account for the fact that there are two face plates for each composite as shown in Fig. 1.

In Fig. 5, the compliances (reciprocal of the Young's modulus) of a TP 2-2 composite in both the x - and y -directions calculated from (5) are presented. It can be seen that the TP 2-2 configuration automatically makes Y_{11}^{cp} larger than Y_{22}^{cp} . Therefore, (9) can be satisfied even for a face plate with isotropic elastic properties. However, in most practical situations, to make the face plate effective, the quantities on left hand sides of the inequalities in (9) should be several times of those on the right hand sides. If the difference between Y_{11}^{cp} and Y_{22}^{cp} is not very large, an elastically anisotropic face plate will be necessary.

The effective piezoelectric response of a TP 2-2 composite with face plates can be analyzed using the similar procedure as that outlined in the preceding section. In order to simplify the analysis, we assume that in a face plated TP 2-2 composite, the 2-2 composite can be treated as an effective medium with the effective parameters derived in the preceding section. The validity of this approximation has been demonstrated in an earlier investigation [10]. In combination with the isostrain approximation, the effective piezoelectric responses and other material properties of a TP 2-2 composite with face plates, then, can be analyzed. Due to the scope of this paper, we will discuss only the situation when the composite is subjected to a hydrostatic pressure p .

With the constraints of the face plates, the effective stress a TP 2-2 composite experiences becomes

$$\begin{aligned} T_1^{cp} &= \frac{(D_{12}B_2 - D_{22}B_1)}{D_{12}^2 - D_{11}D_{22}} p \\ T_2^{cp} &= \frac{(D_{12}B_1 - D_{11}B_2)}{D_{12}^2 - D_{11}D_{22}} p \\ T_3^{cp} &= p \end{aligned} \quad (10)$$

where T_i^{cp} , $i = 1, 2, 3$, are the stress tensor in a TP 2-2 composite under the constrain of face plates and p is the hydrostatic pressure. The parameters D_{ij} , B_i are

$$\begin{aligned} D_{ij} &= (1 - \gamma)s_{ij}^{cp} + \gamma s_{ij}^f; \quad i, j = 1, 2 \\ B_i &= (s_{ii}^f + s_{12}^f) + (1 - \gamma)(s_{i3}^f - s_{i3}^{cp}); \quad i = 1, 2 \end{aligned}$$

where s_{ij}^f is the elastic compliance of the face plate, and $\gamma = L/(L + 2b)$, b is the thickness of the face plate. The effective

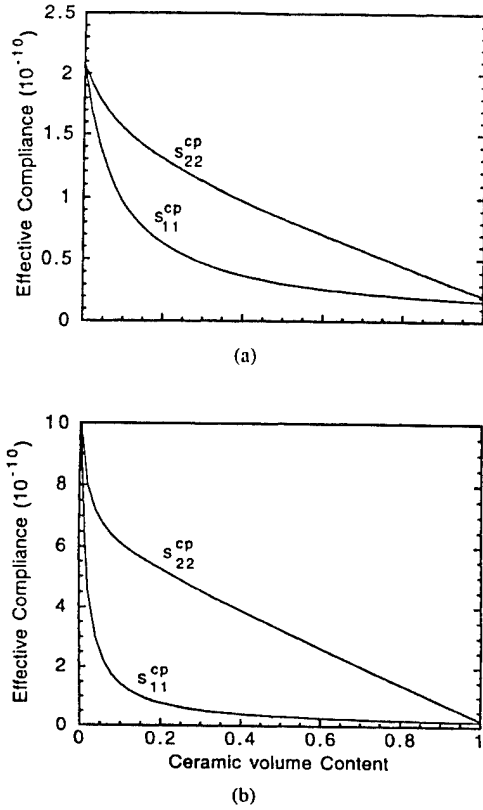


Fig. 5. The effective compliance s_{11} and s_{22} of a TP 2-2 composite as a function of the ceramic volume content. (a) a TP 2-2 composite made of PZT-5H in Spurr's epoxy matrix and (b) a TP 2-2 composite made of PZT-5H and a polymer matrix with the Young's modulus = $0.96 (10^9 \text{ N/m}^2)$ and Poisson's ratio = 0.364 . Notice that in a TP 2-2 composite, s_{11} is always less than s_{22} . The effective Young's modulus of a composite is the reciprocal of the effective compliance.

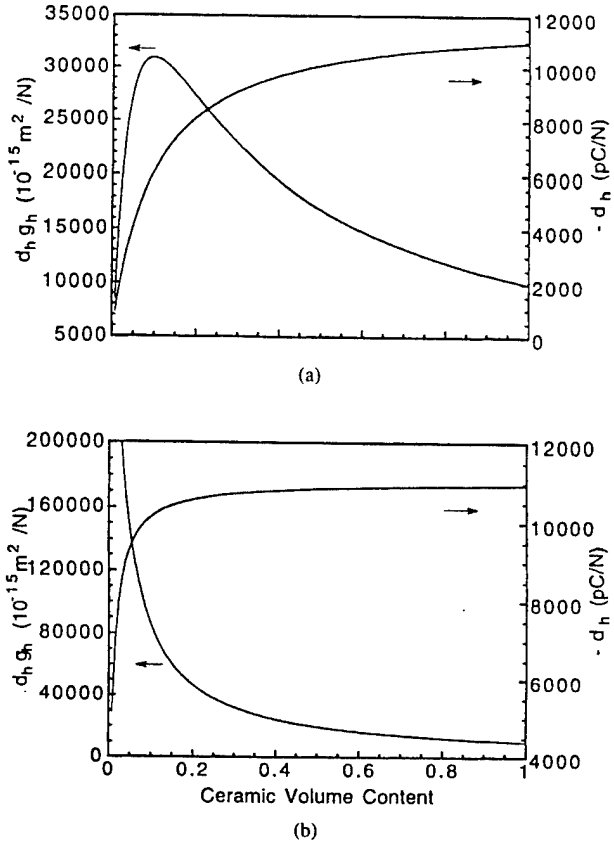


Fig. 6. The effective piezoelectric hydrostatic responses of a TP 2-2 composite with unidirectional face plates. (a) a TP 2-2 composite made of PZT-5H and Spurr's epoxy; (b) a TP 2-2 composite made of PZT-5H and the polymer II (see Table I). To simplify the calculation, the elastic properties of the face plate are assumed that in the inequality (9), the quantities in the left hand sides are much larger than those in the right hand sides so that $T_1^{cp} = p$ and $T_2^{cp} = 0$.

hydrostatic piezoelectric coefficient d_h can be obtained from

$$d_h^{cp} = \frac{d_{33}^{cp} T_3^{cp} + d_{31}^{cp} T_1^{cp} + d_{32}^{cp} T_2^{cp}}{p} \quad (11)$$

where d_{ij}^{cp} are those defined in (3). From (11), the hydrostatic figure of merit $d_h g_h$ for a face plated TP 2-2 composite can also be evaluated.

In an ideal situation where the pressure in the y -direction is totally born by the face plates so that $T_2^{cp} = 0$ while in the x -direction the face plates do not affect the stress in the composite, that is, $T_1^{cp} = p$, the hydrostatic responses of a TP 2-2 composite reaches their maximum values,

$$d_h^{cp} = \left(2d_{31}^c \frac{s_{11}^p (1 - \sigma_p)}{v s_{11}^p (1 - \sigma_p) + (1 - v) s_{11}^c (1 - \sigma_c)} \right) \frac{Lv}{t} \quad (12a)$$

$$d_h^{cp} g_h^{cp} = \left(2d_{31}^c \frac{s_{11}^p (1 - \sigma_p)}{v s_{11}^p (1 - \sigma_p) + (1 - v) s_{11}^c (1 - \sigma_c)} \right)^2 \frac{v}{\epsilon_{33}^c} \quad (12b)$$

In inequalities (9), this situation corresponds to that the quantities on the left hand sides are much greater than those of the right hand sides.

In Fig. 6, the hydrostatic responses calculated using (12) for an ideal face plated TP 2-2 composite are presented. Appar-

ently, the unidirectional face plates considerably improve the hydrostatic performance of a TP 2-2 composite in comparison with that without face plates. A detailed investigation of the effect of face plates on the hydrostatic performance of a TP 2-2 composite and other practical design issues will be presented in another publication.

III. EXPERIMENTAL RESULTS

Aimed at verifying the concept of the new composite material and demonstrating the potential of a TP 2-2 composite as a high sensitivity hydrostatic transducer material, several TP 2-2 composites were fabricated with the ceramic volume content ranging from 15–30%. The piezoceramic plates used were PZT-500. The piezoelectric coefficients d_{33} and d_{31} of the ceramic plates were measured using a laser dilatometer and d_{33} ranges from 410–440 pm/V and d_{31} from -188 to -200 pm/V. The dielectric constant is about 2,250.

The hydrostatic piezoelectric d_h coefficient of TP 2-2 composites was evaluated by a standard comparison method: a composite and a standard sample with known d_h were placed in a high pressure oil chamber and subjected to a low frequency AC (50 Hz) hydrostatic pressure. The charge outputs of the composite and the standard sample under the AC

TABLE II
THE PIEZOELECTRIC HYDROSTATIC PERFORMANCE OF TP 2-2 COMPOSITES

	Sample A		Sample B		Sample C	
	Experiment	Calculated	Experiment	Calculated	Experiment	calculated
d_h (pC/N)	750	1,100	3,250	3,870	6,000	7,700
$d_h g_h$ (10^{-15} m ² /N)	1,100	2,366	10,000	14,200	30,000	49,900
L (cm)	1.0		1.0		1.0	
t (cm)	0.1		0.1		0.05	
v (%)	25		25		15	
Poly. Matrix	Spurs epoxy		Polyurethane with 50% volume microballon		same as Sample B	
Face plates	No		Unidirectional plates b = 0.15 cm		same as Sample B	

pressure were measured and were used to calculate d_h of the composite when the areas of the composite and the standard are known. From the measured d_h value and the effective dielectric constant of the composite, g_h as well as $d_h g_h$ were obtained.

In Table II, the experimental results are presented along with the theoretical values calculated using the equations derived in the preceding sections. The information on each sample is also listed in the table. The results here clearly demonstrated that even with PZT-500 ceramic of which the piezoelectric coefficients are about two thirds of those of PZT-5H, a TP 2-2 composite can still yield very high hydrostatic piezoelectric response in comparison with that of TP 1-3 tubular composites [4]. It is expected that the piezoelectric hydrostatic response of a TP 2-2 composite with PZT-5H piezoceramic plates will be considerably higher than those in Table II. A detailed experimental study on TP 2-2 composites will be carried out in the future.

The unidirectional face plates used in the sample B and C were made from strips of glass reinforced polymer (GRP) plates embedded in polyurethane. Since the elastic properties of the face plates are not well characterized, in the calculation of d_h , (12a) is used instead of the more general form of (11). From Table II, it can be seen that for samples B and C, although the theoretical values of d_h are higher than the experimental ones, the difference is not significant considering the simplicity of the model used in deriving (12). However, for sample A, the theoretical d_h value is much higher than the experimental one which indicates that for a nonface plated composite, the isostrain model may overestimate the effective piezoelectric response of a composite as one would expect. Nevertheless, the analytical analysis based on the isostrain model still provides a valuable guideline in preliminary design of a composite. The theoretical g_h value listed in Table II is obtained by dividing the theoretical d_h by the experimentally measured effective dielectric permittivity of the composite. Other parameters used in the calculation are listed in Table III.

IV. SUMMARY

By employing a unique design of a 2-2 piezocomposite, a new type of composite transducer material operated in

TABLE III
SOME OF THE PARAMETERS USED IN THE THEORETICAL CALCULATION OF TABLE II

PZT-500: $d_{33} = 425$ (pC/N), $d_{31} = 194$, $s_{11} = 0.154$ (10^{-10} m²/N), $s_{33} = 0.184$,
 $s_{12} = -0.054$, $s_{13} = -0.07$

Polyurethane with 50% volume microballon: $s_{11} = 5.0$ (10^{-8} m²/N), $\sigma = 0.36$

* PZT-500 is the trademark of Piezo Kinetics Inc. (Bellefonte, PA).

TABLE IV
COMPARISON OF HYDROSTATIC PIEZOELECTRIC
RESPONSE AMONG SEVERAL COMPOSITES

	Vol %	d_h (pC/N)	$d_h g_h$ (10^{-15} m ² /N)	Ref.
1-3 rod composite, end capped	25	265	20,000	1
1-3 tubular composite	25.6	-9,862	10,195	4
2-2 composite	20	50	830	7
TP 2-2 composite, end capped	15	-6,000	30,000	

transverse piezoelectric mode is introduced. Based on the isostrain model, the design parameters of this composite are analyzed. Both experimental and theoretical results show that this new composite can yield exceptionally high hydrostatic piezoelectric response. In Table IV, a comparison is made among 1-3 rod composite, 1-3 tubular composite, 2-2 composite, and TP 2-2 composite. Apparently, TP 2-2 composites possess exceptionally high d_h and $d_h g_h$. In addition, the simple 2-2 structure makes the composite easy to be fabricated with relatively low manufacture cost. The TP operation also allows the composite to be used at high hydrostatic pressure with little depoling effect.

REFERENCES

- [1] T. R. Gururaja, A. Safari, R. E. Newnham, and L. E. Cross, "Piezoelectric ceramic-polymer composites for transducer applications," in *Electronic Ceramics*, L. M. Levinson, Ed. New York: Marcel Dekker, 1987, pp. 92-128.
- [2] W. A. Smith, "The application of 1-3 piezocomposites in acoustic transducers," in *Proc. 1990 IEEE ISAF7*, 1990, pp. 145-152.
- [3] Q. M. Zhang, Wenwu Cao, H. Wang, and L. E. Cross, "Characterization of the performance of 1-3 type piezocomposites for low frequency applications," *J. Appl. Phys.*, vol. 73, pp. 1403-1410, 1993.
- [4] Q. M. Zhang, H. Wang, and L. E. Cross, "Piezoelectric tubes and tubular composites for actuator and sensor applications," *J. Mater. Sci.*, vol. 28, p. 3962, 1993.
- [5] J. Chen, Q. M. Zhang, L. E. Cross, and M. Trotters, "Modeling and design of 1-3 tubular composite for smart transducer applications," in *Proc. Second Int. Symp. Intell. Mater.*, 1994, pp. 316-326.
- [6] R. E. Newnham, D. P. Skinner, and L. E. Cross, "Connectivity and piezoelectric-pyroelectric composites," *Mater. Res. Bull.*, vol. 13, pp. 525-536, 1978.
- [7] Q. M. Zhang, Wenwu Cao, J. Zhao, and L. E. Cross, "Piezoelectric performance of piezoceramic-polymer composites with 2-2 connectivity—A combined theoretical and experimental studies," *IEEE Trans. Ultrason. Ferroelect. Freq. Cont.*, vol. 41, pp. 556-563, 1994.
- [8] M. J. Haun, P. Moses, T. R. Gururaja, W. A. Schulze, and R. E. Newnham, "Transversely reinforced 1-3 and 1-3-0 piezoelectric composites," *Ferroelect.*, vol. 49, pp. 259-264, 1983.
- [9] W. A. Smith, "Modeling of 1-3 composite piezoelectrics: Hydrostatic response," *IEEE Trans. Ultrason. Ferroelect. Freq. Cont.*, vol. 40, pp. 41-49, 1993.
- [10] J. Zhao, Q. M. Zhang, and Wenwu Cao, "Effects of face plates and edge strips on hydrostatic piezoelectric response of 1-3 composites," submitted to *J. Mat. Sci.*

APPENDIX 31

Effects of Face Plates on Surface Displacement Profile in 2-2 Piezoelectric Composites

Wenwu Cao, Q. M. Zhang, J. Z. Zhao, and L. E. Cross, *Fellow, IEEE*

Abstract—A simple model is developed to describe the inhomogeneous surface deformation profile of face plated 2-2 type piezocomposites. The contribution of face plate to the equilibrium condition is approximated as from simple elastic bending of the plate. Analytical solutions were obtained for the inhomogeneous surface displacement profile. From these solutions one can predict the variation of the nonuniform surface displacement in a 2-2 composite with respect to material and geometry parameters. It is shown that the surface displacement uniformity depends on several factors: the ceramic aspect ratio, the spacing between ceramic plates, the thickness of face plate, the Young's modulus of the polymer and of the face plate. The calculated results indicate that stiffer face plates, softer polymer resin, and closer ceramic spacing could make the piezocomposite transducers to have more uniform surface displacement.

I. INTRODUCTION

ONE of the key features of piezoelectric composites is the stress transfer capability between the hard ceramic and the soft polymer, which gives the composite a high level of piezoelectric capability and at the same time, lowers the effective acoustic impedance of the composite to make it more suitable for underwater and medical applications [1]–[4]. The polymer phase can also reduce the Q-value of the transducer to suppress ringing. However, as reported in our early works [5]–[7], the difference in elastic stiffness between the two constituents in the composite causes surface displacement to be nonuniform under external (electric or elastic) fields. This nonuniformity reduces the efficiency of stress transfer between the two constituents, hence degrading the piezoelectric performance of the transducers, and causing the physical properties of piezocomposites to depend on the aspect ratio of the ceramic and their spacing. In some actuator applications, such as short wavelength plane wave generators, uniform surface displacement is preferred. According to our previous analyses [5], more uniform surface displacement requires the polymer to have large shear modulus but small Young's modulus, which is difficult to achieve since the Poisson's ratio for most of the known materials is between 0.3–0.4. A common practice to overcome this problem is to add stiff face plates to the composites. The question is how to

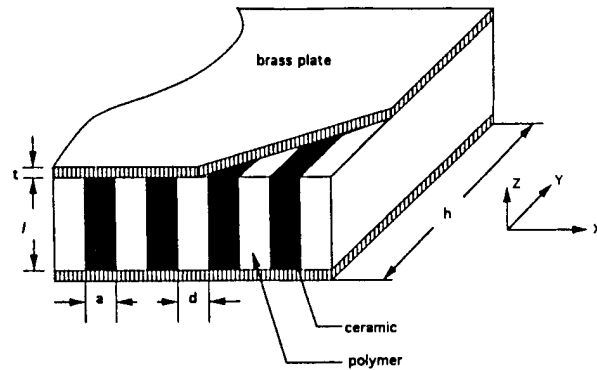


Fig. 1. Schematic of a face plated 2-2 piezocomposite and the coordinate system used in the calculations.

determine the proper thickness of the face plates and how to choose the face plate material, considering the fact that face plates are not piezoelectric, which effectively increases the inactive volume of the composite. In addition, other properties, such as the acoustic impedance, mechanical loss and structural stability will all be affected by the addition of face plates. It is therefore important to understand and evaluate the face plate effects and try to optimize the selection of face plate material and geometry for practical applications. In this paper we extend the model of [5] by including the contribution of the face plates in constructing the equilibrium condition at the composite surface. Brass was used as the face plate material in our calculations, but the procedure can be easily generalized for face plates made of other materials. A comparison with stainless steel and GRP (glass reinforced polymer) face plates is briefly made.

II. THE MODEL

The 2-2 lamellar composite and the coordinate system used in the calculations are given in Fig. 1, where z is the poling direction, a and d are the width of the ceramic and polymer, respectively. We choose the system with $h \gg l$, so that the properties of the system may be considered to be independent of y . The origin of the x -coordinate is set at the center of one of the polymer plate. In a previous paper [5], a linear model for the 2-2 composite without face plates was reported. In that model we have assumed the strain component along the z -direction to be constant for any given x . Our recent analysis using series expansion for the displacement field [8] and results from finite element analyses show that the strain

Manuscript received November 3, 1993; revised February 22, 1994 and May 23, 1994; accepted May 24, 1994. This work was supported by the Office of Naval Research.

The authors are with the Materials Research Laboratory, The Pennsylvania State University, University Park, PA 16802 USA.

IEEE Log Number 9406697.

is quite uniform along z -direction except near the surface region.

The addition of face plate not only reduces the surface displacement nonuniformity, but also forces the strain to be more uniform inside the composite, making the constant z -strain a better assumption. Based on this consideration, as a first attempt to model the face plated composite, we extend our previous work [5]. The equilibrium condition at the surface of a 2-2 composite was given there; all we need to do here is to add the contribution of the face plates. This is accomplished by treating the face plate deformation as simple elastic bending of a thin plate. The force density generated from the face plate is Du_{xxxx} [7], where u is the surface displacement in the z -direction, the subscript x represents derivative with respect to the coordinate x , and D is the flexural rigidity of the face plate,

$$D = \frac{Y^f t^3}{12(1 - \sigma^2)} \quad (1)$$

In (1) Y^f and σ are, respectively, the Young's modulus and the Poisson's ratio of the face plate, and t is the thickness of the face plate.

The equilibrium condition at the composite surface $z = l/2$ is simply the addition of the Du_{xxxx} term to the equilibrium condition (7) of [5],

$$\begin{aligned} Du_{xxxx}(x, l/2) + \frac{l}{4}\mu^p u_{xx}(x, l/2) \\ - \frac{2}{l}Y^p u(x, l/2) = 0, \\ -\frac{d}{2} < x < \frac{d}{2} \end{aligned} \quad (2)$$

$$\begin{aligned} Du_{xxxx}(x, l/2) + \frac{l}{4}\mu^c u_{xx}(x, l/2) - \frac{2}{l}Y_{33}^c u(x, l/2) \\ + Y_{33}^c d_{33} E = 0, \\ \frac{d}{2} < x < \frac{d}{2} + a \end{aligned} \quad (3)$$

where μ^p and Y^p are the shear modulus and Young's modulus of the polymer, $\mu^c (= c_{44})$ and $Y_{33}^c (= 1/s_{33})$ are the shear modulus and Young's modulus of the ceramic, respectively. d_{33} is the piezoelectric constant of the ceramic, E is the electric field along the poling direction, i.e., z -direction.

Equations (2) and (3) are the static equilibrium condition at the surface of the composite, which can be solved analytically to give the hyperbolic cosine solutions:

$$u(x, l/2) = A \cosh(\beta^p x), \quad -d/2 < x < d/2 \quad (4)$$

$$\begin{aligned} u(x, l/2) = B \cosh \left[\beta^c \left(x - \frac{a+d}{2} \right) \right] + \frac{l}{2} d_{33} E, \\ \frac{d}{2} < x < \frac{d}{2} + a \end{aligned} \quad (5)$$

$$u(x + n[a + d], l/2) = u(x, l/2), \quad n = 1, 2, 3 \dots \quad (6)$$

where

$$\beta^p = \sqrt{\frac{-l\mu^p + \sqrt{l^2\mu^{p2} + 128DY^p/l}}{8D}} \quad (7)$$

$$\beta^c = \sqrt{\frac{-l\mu^c + \sqrt{l^2\mu^{c2} + 128DY_{33}^c/l}}{8D}} \quad (8)$$

Equation (6) represents the periodic boundary condition of the system. Here we have selected the solution so that it recovers the solution of [5] in the limit of $l \rightarrow 0$. The coefficients A and B can be determined from the nonslip interface boundary condition and the force balance condition at $x = d/2$ [5]:

$$A = \frac{\frac{l}{2} d_{33} E}{\frac{\beta^c Y^p}{\beta^p Y_{33}^c} \sinh\left(\beta^p \frac{d}{2}\right) \coth\left(\beta^c \frac{a}{2}\right) + \cosh\left(\beta^p \frac{d}{2}\right)} \quad (9)$$

$$B = \frac{-\frac{l}{2} d_{33} E}{\frac{\beta^p Y_{33}^c}{\beta^c Y^p} \sinh\left(\beta^c \frac{a}{2}\right) \coth\left(\beta^p \frac{d}{2}\right) + \cosh\left(\beta^c \frac{a}{2}\right)} \quad (10)$$

Based on the inhomogeneous solutions (4) and (5) for the surface displacement we can derive the physical properties of the composite from the properties of the three constituents, i.e., ceramic, polymer and face plates. As shown in our earlier works [5]–[7], without face plates, the physical properties of composites depend strongly on the aspect ratio of the ceramic and their spacing. This aspect ratio dependence is a direct consequence of the displacement inhomogeneity in the polymer and the ceramic, which is in turn produced by the active and passive nature of the two constituents. It is expected that the addition of face plates to a composite will enforce deformation uniformity. In contrast to the stress transfer in a nonface plated composite for which the transferred stress is pure shear stress, the additional stress transferred between the ceramic and the polymer via the face plate is primarily a normal stress in the z -direction. The degree of uniformity in a face-plated composite depends on several factors: the thickness of the plate, the Young's modulus of the polymer, the Young's modulus of the face plate, the ceramic content as well as the ceramic aspect ratio and element spacing. All of these factors are now included in the solutions (4) and (5), which makes it very convenient to evaluate the influence of each material parameter. As an example, we have calculated the inhomogeneous surface displacement profiles for a PZT5H-Spurs epoxy composite with brass face plates under an electric field E . Parameters were varied to show the general trend for the optimization of the composite configuration. The material constants used in the calculations are given in Table I.

Fig. 2 shows the calculated inhomogeneous surface displacement variations as a function of the increase of face plate thickness l . The dimensions of the composite used in the calculations are: $l = 5$ mm, $a = 1$ mm, and $d = 2$ mm. A voltage of $\sqrt{2}$ volts is applied to the sample along the z

TABLE I
ELASTIC, PIEZOELECTRIC AND DIELECTRIC PROPERTIES OF PZT 5H, BRASS PLATE AND SPURRS EPOXY USED IN OUR CALCULATIONS.

	γ 10^{10} N/m^2	μ 10^{10} N/m^2	d_{33} 10^{-12} C/m	d_{31} 10^{-12} C/m	σ
PZT5H	11.74	2.3	593	-274	.364
SpurrsEpoxy	.48	.18			
Brass	9.0				.31

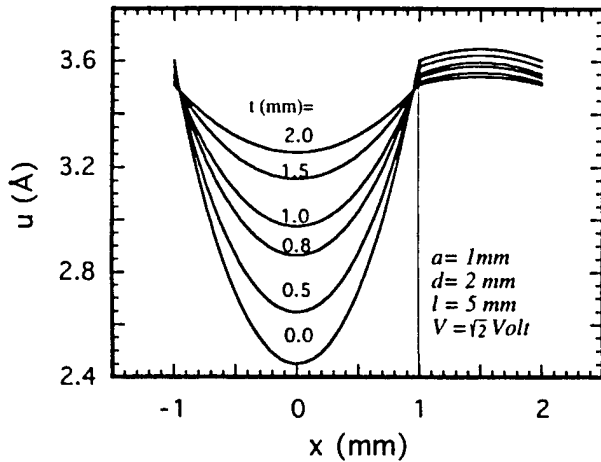


Fig. 2. Calculated surface displacement profiles for a PZT5H-Spurrs epoxy 2-2 composite with different face plate thickness. The volume fraction of the ceramic is 1/3.

-direction (poling direction). For $t = 0$ (i.e., no face plates), the displacement at the center of the polymer surface differs substantially from the displacement at the center of the ceramic surface. When $t > 0$, the polymer surface displacement increases rapidly with the increase of the face plate thickness, and at the same time, the displacement of the ceramic is somewhat reduced. Because the effect of the face plate is to make the polymer move more and the ceramic move less, the overall composite surface displacement becomes more uniform as shown in Fig. 2. One notices that the surface displacement changes caused by the addition of face plates appear mainly in the polymer, which is due to the large difference in elastic stiffness between the polymer and the ceramic. The improvement on the surface displacement uniformity becomes less as the isostrain condition is approached. We believe for a brass face plate thickness greater than 2 mm in this configuration, the physical properties can be well accounted for by the isostrain approximation [4].

Without a face plates, composites made of soft polymer will have more severe displacement nonuniformity than composites made of hard polymer because soft polymers have a smaller shear modulus which cannot effectively transfer stress between the polymer and the ceramic. After adding face plates to the composite, the situation is reversed. Composites made of softer polymer will have more uniform displacement than composites made of harder polymer. This is due to the fact that the additional stress transferred by the face plate from the ceramic to the polymer is in the form of a normal stress. Both the ceramic and the polymer interact directly with the face plates.

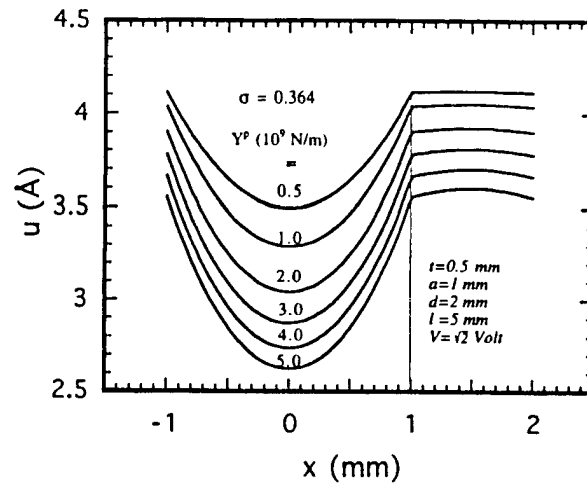


Fig. 3. Calculated surface displacement profiles for different Young's modulus of the polymer. The Poisson's ratio for the polymer is kept at $\sigma^p = 0.364$. Ceramic volume fraction is 1/3 and the face plate thickness is $t = 0.5$ mm.

Since the polymer phase is nonpiezoelectric, it adds to the loading on the ceramic phase, the level of this loading is proportional to the stiffness of the polymer. In other words, a softer polymer has less resistance to elastic deformation, therefore, will be easier to be driven toward more uniform displacement with the ceramic phase with the help of face plates. This situation is illustrated in Fig. 3 where the surface displacement is plotted for different elastic stiffnesses of the polymer. The face plate thickness was kept constant for these calculations at $t = 0.5$ mm and the Poisson's ratio for the polymer is fixed at 0.364. Since the elastic stiffness of different types of polymers can easily differ by one order of magnitude, it is relatively easy to control this parameter. One can see from Fig. 3 that the surface displacement uniformity is improved substantially by reducing the Young's modulus of the polymer, and more importantly, the total effective displacement of the composite is also increased due to the reduction of the self loading produced by the polymer. For air kerf (infinitely soft resin) face plated composite the displacement would be uniform. When the polymer is stiff, the ceramic surface shows noticeable curvature, but for very soft polymer composites, only the polymer phase shows nonuniform surface displacement while the ceramic surface is practically flat as shown in Fig. 3.

Another important issue is the selection of the face plate material. From (4) and (5) one can draw the conclusion that stiffer materials are preferred for the purpose of achieving more uniform surface displacement. For comparison, we have calculated the surface displacement profile for three different face plate materials: steel, brass and GRP, and the results are shown in Fig. 4. We found that stiffer face plate does improve the uniformity of the surface displacement, however, the effect of using a stiffer face plate is much less than reducing the Young's modulus of the polymer.

Under the application of an electric field E , the maximum surface displacement difference, Δu , between the center of the polymer and the center of the ceramic can be derived using (4) and (5),

$$\Delta u = \frac{l}{2} d_{33} E + B - A. \quad (11)$$

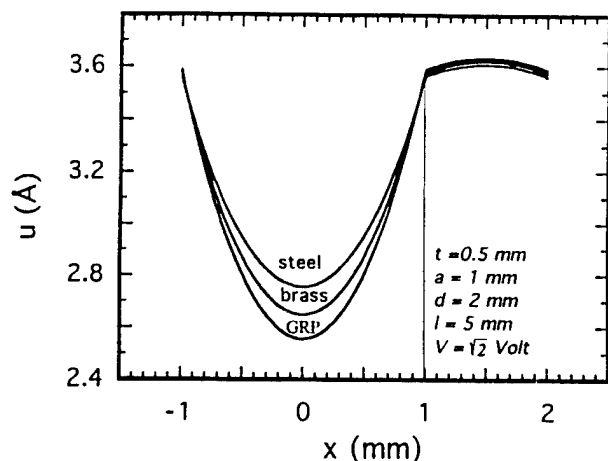


Fig. 4. The surface displacement variation caused by the change of face plate material. The face plate thickness is chosen as $t = 0.5$ mm.

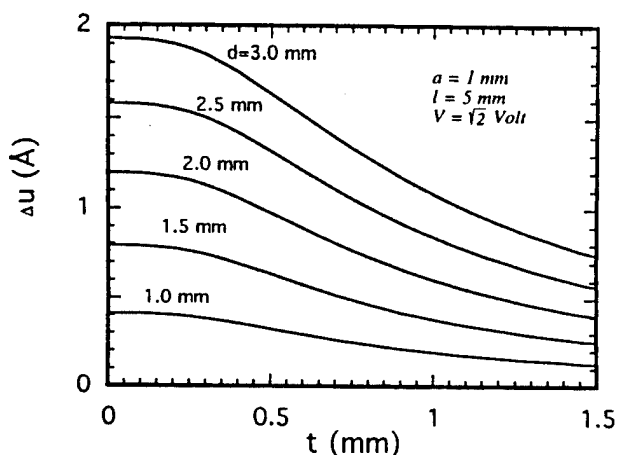


Fig. 5. The calculated maximum displacement difference Δu for different face plate thickness t in a 2-2 composite with ceramic spacing d as a parameter. The ceramic plate thickness is $a = 1$ mm.

This quantity can be used as a measure of the uniformity in surface displacement. Fig. 5 shows Δu versus face plate thickness for a 2-2 composite calculated at five different volume contents. The ceramic plate thickness is fixed at 1 mm in the calculations. The results show that the improvement on the surface displacement uniformity becomes less effective after the brass face plate thickness is beyond certain limit. The effects of face plate is more pronounced for composites made of large spaced ceramics, or large d -value. One of the important conclusions should be mentioned is that the ceramic spacing plays more important role than the face plates in terms of making the surface displacement more uniform. This is clearly seen in Fig. 5 for composites without face plates ($t = 0$).

III. SUMMARY AND CONCLUSIONS

A theoretical model is proposed to calculate the surface displacement profile in face plated 2-2 piezoelectric ceramic-polymer composites. Predictions on the influence of geometry and material properties of each constituents to the surface displacement uniformity are given. It is concluded that the

nonuniform displacement in face plated composites can be improved by several methods: (a) increase face plate thickness; (b) increase the Young's modulus of the face plate; (c) reduce the Young's modulus of the polymer; (d) increase the ratio of l/a ; and (e) increase the ceramic volume ratio. Both (d) and (e) can reduce the spacing between the ceramics.

The addition of face plates to the composite structure makes it possible to use softer polymer resin, which can reduce the polymer loading and improve the effective electromechanical conversion property of the composite. Face plates allows normal stress transfer along z -axis between the ceramic and the polymer, which makes the overall surface displacement of the composite more uniform and the interior deformation more close to isostrain condition.

REFERENCES

- [1] D. P. Skinner, R. E. Newnham, and L. E. Cross, "Flexible composite transducers," *Materials Res. Bull.*, vol. 13, pp. 599-607, 1978.
- [2] W. A. Smith, "The application of 1-3 piezocomposites in acoustic transducers," in *Proc. 1990 IEEE 7th Int. Symp. on Applicat. of Ferroelect. (ISAF90)*, 1990, pp. 145-152.
- [3] W. A. Smith, "Composite piezoelectrics: Basic research to a practical device," *Ferroelect.*, vol. 87, pp. 309-320, 1988.
- [4] W. A. Smith, A. Shaulov, and B. A. Auld, "Tailoring the properties of composite piezoelectric materials for medical ultrasonic transducers," in *Proc. 1985 IEEE Ultrason. Symp.*, 1985, pp. 642-647.
- [5] W. Cao, Q. Zhang, and L. E. Cross, "Theoretical study on the static performance of piezoelectric ceramic-polymer composites with 2-2 connectivity," *IEEE Trans. Ultrason., Ferroelect., Freq. Cont.*, vol. 40, pp. 103-109, 1993.
- [6] W. Cao, Q. Zhang, and L. E. Cross, "Theoretical study on the static performance of piezoelectric ceramic-polymer composites with 1-3 connectivity," *J. Appl. Phys.*, vol. 72, pp. 5814-5821, 1992.
- [7] Q. M. Zhang, W. Cao, H. Wang, and L. E. Cross, "Characterization of the performance of 1-3 type piezocomposites for low frequency applications," *J. Appl. Phys.*, vol. 73, pp. 1403-1410, 1993.
- [8] Q. M. Zhang, W. Cao, J. Zhao, and L. E. Cross, "Piezoelectric performance of piezoceramic-polymer composites with 2-2 connectivity—A combined theoretical and experimental study," *IEEE Trans. Ultrason., Ferroelect. Freq. Cont.*, in press.
- [9] Landau and E. M. Lifshitz, *Theory of Elasticity*. Oxford: Pergamon Press, 1986.



Wenwu Cao received the B.S. degree in physics from Jilin University, Changchun China in 1982 and the Ph.D. degree in condensed matter physics in 1987 from the Pennsylvania State University, University Park, PA.

He was a Research Associate in the Materials Research Laboratory of the Pennsylvania State University from 1987 to 1988, a postdoctoral associate at the Laboratory of Atomic and Solid State Physics, Cornell University from 1989 to 1990. He is currently a Senior Research Associate and Associate Professor of Materials at the Materials Research Laboratory, the Pennsylvania State University. He has conducted both theoretical and experimental research in the area of condensed matter physics, including theories on proper- and improper- ferroelastic phase transitions, static and dynamic properties of domains and domain walls in ferroelectric and ferroelastic materials. In addition, he has performed measurements on second- and third-order elastic constants, linear and nonlinear dielectric constants and piezoelectric constants in ferroic single crystals and ceramics. His current interests are the formation of domain structures and their contributions to the dielectric, elastic and piezoelectric properties in ferroelectric materials, the static and dynamics behavior of piezoelectric ceramic-polymer composites as well as computer modeling on the design of piezoelectric sensors and actuators for underwater acoustics and medical ultrasonic imaging using finite element method.

Dr. Cao is a Member of the American Physical Society, and the American Ceramic Society.

Q. M. Zhang received the B.S. in physics from Nanjing University, China in 1981 and Ph.D. in physics from the Penn State University in 1986.

He is currently an Assistant Professor of materials at the Materials Research Laboratory of the Pennsylvania State University. His research interests involve: piezoceramic and polymeric materials for sensor, actuator, and transducer applications; piezo-composites characterization and modeling; intelligent materials, structures, novel materials with large electromechanical effect, and nano-composites; electro-optic properties and their applications; optical instrumentations; effects of defect structures on the dielectric, piezoelectric, and elastic properties of piezo-materials; structural investigation of interface and defects in ferroelectrics. From 1986 to 1988, he was a Research Associate at Materials Research Laboratory of the Pennsylvania State University. From 1988 to 1991, he was at Brookhaven National Laboratory as a Research Scientist, conducting research on interface, surface, and thin films as well as their phase transformation behavior with neutron and synchrotron X-ray scattering.

Dr. Zhang is a Member of American Ceramic Society, American Physical Society, and the Neutron Scattering Society of America.

L. Eric Cross (SM'79-F'84) received the B.Sc. degree (honors) in physics in 1948 from Leeds University, Leeds, United Kingdom, and the Ph.D. degree in physics in 1953 from Leeds University, Leeds, United Kingdom. He is an Evan Pugh Professor of Electrical Engineering in the Materials Research Laboratory at the Pennsylvania State University, University Park, PA. He was a University Scholar, an Assistant Professor, and an ICI fellow in the University of Leeds. After a short period at the Electrical Research Association in Leatherhead, Surrey, he moved to the U.S. to take up a position in the developing Materials Research Laboratory (MRL) at Pennsylvania State University, where he was the Laboratory Director from 1985 to 1989. His interests are in dielectric and ferroelectric crystals, piezoelectrics and electrostrictive ceramics and composites for sensor, actuator, and transducer applications, and as components in "smart" materials and structures. He has coauthored more than 300 technical and sections of six books.

Dr. Cross is a Member of the National Academy of Engineering, and a Fellow of the American Institute of Physics, the American Ceramic Society, the IEEE, and the American Optical Society, and a Member of the Japanese Physical Society. He is Chairman of the IEEE Committee on Ferroelectrics, U.S. Representative for ferroelectrics on IUPAP, and a Member of the Defense Sciences Research Council of DARPA.



J. Zhao received the B.S. in physics from Henan Normal University, China in 1981 and the M.S. in solid state physics from Jilin University in 1988.

He is currently a Research Assistant at the Materials Research Laboratory of the Pennsylvania State University. His research interests are piezoceramics and ceramic-polymer composites for sensor, actuator, and transducer applications. From 1988 to 1991, he was a researcher at ZhengZhou Institute of Technology, China conducting research on diamond growth.

APPENDIX 32

Plane wave propagation in finite 2-2 composites

Wenwu Cao^{a)} and Wenkang Qi

Materials Research Laboratory, The Pennsylvania State University, University Park, Pennsylvania 16802

(Received 4 November 1994; accepted for publication 19 June 1995)

A common practice in the study of wave propagation in stratified structures is to use the Floquet (or Bloch) condition to derive the dispersion relation, leading to the passband and stopband structures. However, the Floquet condition is valid only for an infinite system while a real system always has finite dimensions. We report a study on wave propagation in a finite 2-2 composite by using the transfer (T) matrix technique. Through introducing a new definition for the dispersion relation using the T matrix, the passbands and stopbands are calculated for a finite system without the Floquet condition. The formation of stopbands and passbands with the increase of composite size can now be clearly seen. The spatial profile of the vibration pattern inside a finite composite can also be calculated using this technique, which reveals strong edge effects. The effects of randomization on the wave localization in a 2-2 composite are also studied. © 1995 American Institute of Physics.

I. INTRODUCTION

The dynamic behavior of piezoelectric composites has attracted the attention of many researchers after it has been successfully applied to under water acoustics and medical ultrasound imaging.¹⁻¹⁹ Conceptual understanding was achieved in many aspects for composite structures, and some guidelines for composite transducer design were also developed. However, there are still many unanswered questions regarding the composite structure. Some of the most fundamental and interesting topics include wave propagation inside the composite structure, mode coupling, and band structures for a finite system.

Several methods were introduced in the study of wave propagation in periodic composites, such as the T -matrix method,^{10,14,16,20} the effective medium method,^{13,14} and the finite element method.¹⁵⁻¹⁷ Each method has certain merits but also limitations. Among these methods, the finite element method is the most powerful method which can deal with complex geometry. However, it is limited by the power of the computer, and the results from the finite element analysis often do not lead to a clear conceptual understanding of the physical origin of the observed phenomena. Another accurate method is the transfer matrix (T -matrix) method, which is especially suitable to study wave propagation in one-dimensional layered structures, such as 2-2 composites. The T -matrix method has been used to study the dilational Lamb wave in a 2-2 composite in conjunction with the Floquet theory.^{10,14,16,20} Many interesting results, including the band structures, were obtained, which have provided conceptual understanding of some wave propagation characteristics in composites.

Wave propagation in stratified structures, such as a 2-2 composite illustrated in Fig. 1, have been studied extensively using transfer matrix.²¹⁻²⁵ In the past, band structures were calculated by using a combination of T matrix and the Floquet theory, because the traditional T -matrix method alone does not provide enough information to determine the band structures. The problem of Floquet theory is that it is valid only for an infinite system. Therefore, the band structures

obtained in all the previous studies do not accurately describe the wave propagation characteristics in finite systems. It is predictable that the Floquet condition will be strongly violated when a composite contains only a few cells. Focusing on this problem, we introduce an extension to the T -matrix technique which enables the T -matrix technique to calculate the band structures for a finite stratified structures, such as 2-2 composites, without using Floquet condition.

As an example, we will consider the transverse wave propagation in a 2-2 composite; one can easily calculate the longitudinal wave analogously.

II. T MATRIX AND THE NEW DISPERSION RELATION

As mentioned above, the main objective of this study is to derive a substitute for the Floquet condition to calculate the band structures for a finite stratified structure. We begin with a brief review on the T -matrix technique and then introduce some new definitions.

Assuming a shear acoustic plane wave $\psi(x,t)$ enters a ceramic-polymer composite system shown in Fig. 1 from the left at $x=0$, we can write the wave function at the n th cell in the following form:

$$\psi_n = A_n e^{i(\omega t - k_p x)} + B_n e^{i(\omega t + k_p x)},$$
$$(n-1)d < x < nd - a \quad (\text{in polymer}); \quad (1)$$

$$\psi_n = C_n e^{i(\omega t - k_c x)} + D_n e^{i(\omega t + k_c x)},$$
$$nd - a < x < nd \quad (\text{in ceramic}), \quad (2)$$

where

$$k_m = \omega \sqrt{\rho_m / c_{55}^m} \quad (m = p, c) \quad (3)$$

is the wave number, a and b are the thickness of the ceramic layer and polymer layer, respectively, $a + b = d$ is the period of the cell (see Fig. 1), ω is the angular frequency, ρ_m and c_{55}^m are the density and the shear elastic stiffness of the m constituent. The subscripts/superscripts p and c indicate that the physical quantities are for the polymer and the ceramic, respectively. The requirements of the wave function ψ and the shear stress T_5 to be continuous at the ceramic-polymer interface lead to the following relations among the coefficients, A_n , B_n , C_n , and D_n , in the n th cell:

^{a)}Electronic mail: wcao@sun01.mrl.psu.edu

$$\begin{pmatrix} A_n \\ B_n \end{pmatrix} = \frac{1}{2Z_p} \begin{pmatrix} (Z_p + Z_c)e^{i(k_p - k_c)(nd - a)} & (Z_p - Z_c)e^{i(k_p + k_c)(nd - a)} \\ (Z_p - Z_c)e^{-i(k_p + k_c)(nd - a)} & (Z_p + Z_c)e^{i(k_p + k_c)(nd - a)} \end{pmatrix} \begin{pmatrix} C_n \\ D_n \end{pmatrix} = [T_{nd-a}] \begin{pmatrix} C_n \\ D_n \end{pmatrix}. \quad (4a)$$

Similarly, we can derive the relations among the coefficients C_n , D_n and A_{n+1} , B_{n+1} between adjacent cells,

$$\begin{pmatrix} C_n \\ D_n \end{pmatrix} = \frac{1}{2Z_c} \begin{pmatrix} (Z_p + Z_c)e^{i(k_c - k_p)nd} & (Z_c - Z_p)e^{i(k_c + k_p)nd} \\ (Z_c - Z_p)e^{-i(k_c + k_p)nd} & (Z_p + Z_c)e^{i(k_c + k_p)nd} \end{pmatrix} \begin{pmatrix} A_{n+1} \\ B_{n+1} \end{pmatrix} = [T_{nd}] \begin{pmatrix} A_{n+1} \\ B_{n+1} \end{pmatrix}, \quad (4b)$$

where

$$Z_m = \rho_m v_m = \sqrt{\rho_m c_{55}^m} \quad (m = p, c) \quad (5)$$

is the acoustic impedance and v_m is the acoustic velocity for material m . From Eqs. (4a) and (4b) we can derive the recurrence relation for the coefficients A_n and B_n ,

$$\begin{pmatrix} A_n \\ B_n \end{pmatrix} = [T_{nd-a}][T_{nd}] \begin{pmatrix} A_{n+1} \\ B_{n+1} \end{pmatrix}. \quad (6)$$

Considering a system of N cells, we can derive the following relation, according to the above recurrence relation:

$$\begin{pmatrix} A_1 \\ B_1 \end{pmatrix} = [T] \begin{pmatrix} A_{N+1} \\ B_{N+1} \end{pmatrix}, \quad (7)$$

where the T matrix in Eq. (7) is a second rank tensor given by

$$[T] = [T_{d-a}][T_d] \dots [T_{nd-a}][T_{nd}] \dots [T_{Nd-a}][T_{Nd}]. \quad (8)$$

For convenience, we assume that the composite is made of N cells and is immersed in a polymer medium. Since the incident wave enters the composite from the left, $B_{N+1} = 0$, in other words, only a transmitted wave exists in the medium on the right side of the composite.

Now, let us define a transmission function $H(\omega)$,

$$H(\omega) = \frac{A_{N+1} e^{-ik_p Nd}}{A_1} = \frac{1}{T_{11}} e^{-ik_p Nd}, \quad (9)$$

which describes both the amplitude and phase relationships between the incident wave at $x=0$ and the transmitted wave at $x=Nd$. Similarly, we can define a reflection function $G(\omega)$,

$$G(\omega) = \frac{B_1}{A_1} = \frac{T_{21}}{T_{11}}, \quad (10)$$

which describes the amplitude and phase relationships between the incident wave and the reflected wave at $x=0$.

Clearly, the transmission and reflection coefficients are (see the Appendix)

$$t = H(\omega) \cdot H^*(\omega) \quad (11)$$

and

$$r = G(\omega) \cdot G^*(\omega). \quad (12)$$

It is easy to verify that (see the Appendix)

$$t + r = 1. \quad (13)$$

In order to calculate the dispersion relation without using Floquet theory, an effective real wave vector k' needs to be defined for the composite, which should give the same phase change as $H(\omega)$ over a distance Nd . In this spirit, we introduce the following definition:

$$k' = \frac{\text{Ang}[H(\omega)]}{Nd} = \text{arctg} \left(\frac{\text{Im}[H(\omega)]}{\text{Re}[H(\omega)]} \right), \quad (14)$$

where $\text{Ang}[H(\omega)]$ represents the phase angle of $H(\omega)$.

Before we extract the stopband information from this new definition, let us examine the characteristics of the dispersion relation shown in Fig. 2, which is derived from the Floquet condition for an infinite system. The piecewise dispersion curve represents the passbands while the gaps are the stopbands. In each of the passbands, the phase velocity $v_{ph} = \omega/k$ is a monotonically decreasing function of frequency. v_{ph} is always a minimum at the upper passband edge frequency ω_n^U , and a maximum at the lower passband edge frequency ω_n^L .

The derivation of the band structures was based on the nonexistence of real k , and the band edges are those frequencies corresponding to the discontinuities of the dispersion relation.²² For a finite system, these discontinuities are expected to be smoothed out and solutions for the finite system should approach the discontinuity limit as the number of cells in the system becomes very large. We found that this goal can be precisely achieved using the new definition Eq. (14). One important point is that the newly defined k' will always have a finite value, although it may become extremely small in certain frequency regions when the system becomes very large. We will see later that the dispersion relation obtained from Eq. (14) approaches the Lee and Yang solution (Ref. 22) for very large systems.

Next, we need to define the bands using the new definition. In reference to the characteristics of the phase velocity in the band structure of Fig. 2, one may define the band structures of a finite system by using the maxima and the minima of the phase velocity $v_{ph} = \omega/k'$. These extrema can be easily calculated, and serve as the boundary mark between different frequency bands. For a finite system, the band structures will not be fully developed, they are pseudopassbands and pseudostopbands which have many similar characteristics as the true bands. A pronounced difference from the solution of Lee and Yang is that the phase velocity also can be defined inside the pseudostopbands.

Lee and Yang²² have shown that the wave number is purely imaginary inside a stopband for an infinite system. For a finite system, the real part of the wave number always exists even inside the pseudostopbands; therefore the wave number will be a complex number in general, i.e., $k = k' - ik''$. The imaginary part k'' may be calculated according to the following equation:

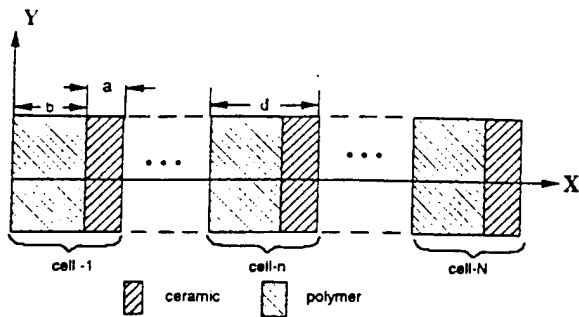


FIG. 1. Schematic plot of a N -cell 2-2 ceramic-polymer composite with $1/3$ of ceramic volume content. The y dimension is assumed to be infinite so that the system can be treated as one dimensional.

$$k'' = -\frac{\ln|H(\omega)|}{Nd}, \quad (15)$$

which can be nonzero inside the passbands for a finite system.

III. WAVE PROPAGATION IN A FINITE PERIODIC SYSTEM WITHOUT DAMPING

Using Eqs. (3), (4), (8), and (9), the transmission function $H(\omega)$ is calculated as a function of N for a system shown in Fig. 1. The volume content of the ceramic is fixed at $1/3$, i.e., $a/d = 1/3$, and the material parameters used in the calculations are given in Table I.

Figures 3(a)–3(e) show the change of the magnitude of $H(\omega)$ as a function of frequency for composites of $N=1, 2, 10, 50$, and 100 . The frequency is normalized with respect to ω_0 , where ω_0 is defined as

$$\omega_0 = \frac{\pi v_c v_p}{b v_c + a v_p}, \quad (16)$$

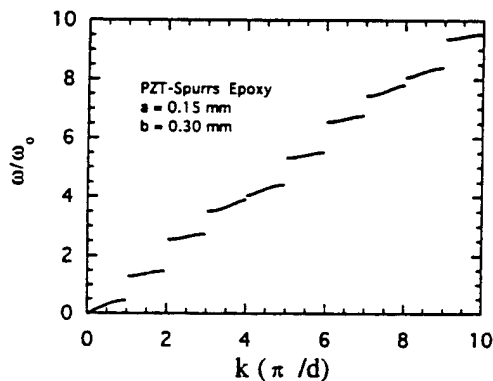


FIG. 2. Dispersion relation for an infinite system obtained from Floquet theory. The frequency unit $\omega_0 = \pi v_c v_p / (b v_c + a v_p) = 9491601/s$, v_c and v_p are the acoustic velocities of the ceramic and the polymer, respectively. The width of each stopband is different, which depends on both the degree of acoustic impedance mismatch and the volume content of ceramic.

TABLE I. Material properties for the ceramic and polymer constituents of the 2-2 composite.

Ceramic	$c_{55}^c = 2.4 (10^{10} \text{ N/m}^2)$	$\rho_c = 7800$
Polymer	$c_{55}^p = 1.59 (10^9 \text{ N/m}^2)$	$\rho_p = 1160$

v_c and v_p are the shear acoustic velocities of the ceramic and the polymer, respectively. The development of the band structures with the increase of cell number N can be seen clearly from Figs. 3(a) to 3(e).

It is interesting to note that some band structure characteristics start to show even for a single layer ceramic inclusion. Complete transmission, i.e., $|H(\omega)| = 1$, can be achieved at isolated frequencies due to structural resonance. As the number of cells N increases, complete transmission occurs at more and more frequencies. Eventually, as N goes to infinity, true passbands are formed. The stopbands correspond to total reflection, i.e., $|H(\omega)| = 0$. For a finite system such condition cannot be achieved; however, the value of $|H(\omega)|$ can become negligible inside the pseudostopbands.

When $N=10$, pseudostopbands are clearly visible but the passbands are not well defined. In general, it appears that the number of frequencies which allow the wave to pass

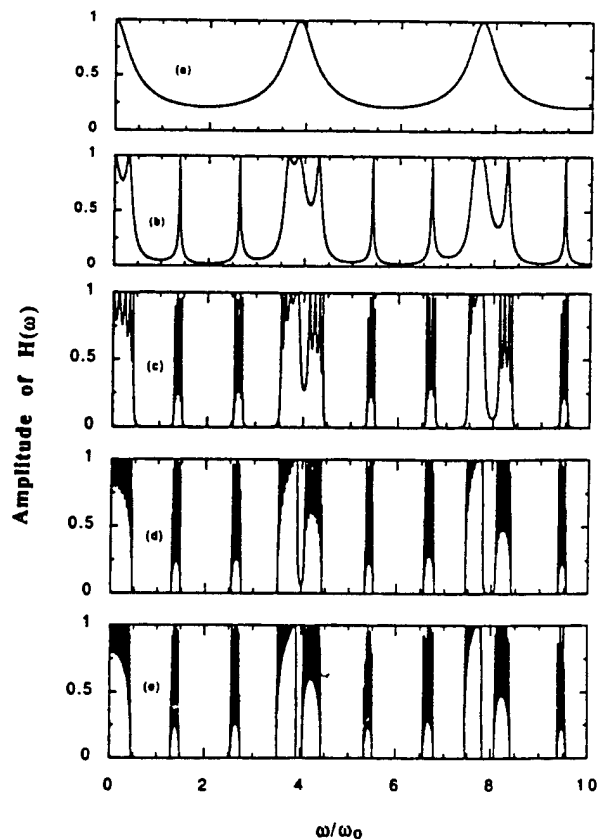


FIG. 3. The magnitude of transmission function vs frequency for different size composites. The development of band structure with the increase of number of cells N is calculated for the following cases: (a) 1 cell, (b) 2 cells, (c) 5 cells, (d) 10 cells, and (e) 50 cells.

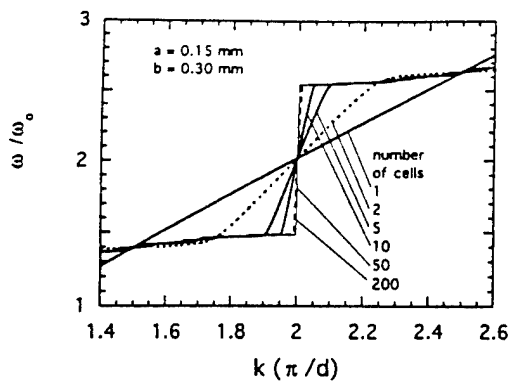


FIG. 4. The development of the second stopband with the increase of N . The deviation is quite large for systems containing less than 10 cells, but when N is greater than 200, the Floquet treatment can give reasonable description.

through the structure without reflection is equal to $N-1$. Therefore, it is conceivable that complete passbands will form only when $N \rightarrow \infty$.

This fact is seen more clearly in the dispersion relations depicted in Fig. 4. Using Floquet's condition, Lee and Yang²² have derived the dispersion relation for an infinite periodic system (see Fig. 2), sharp discontinuities occur at $k = n\pi/d$. While for a finite system, some degree of round off occur at these discontinuities. The edges of the passbands become sharper as the number of cells N increases (Fig. 4). When $N=200$, the dispersion relation almost coincides with that of an infinite system derived by Lee and Yang²² (see Fig. 4).

For an infinite system, one can derive the evanescent wave solutions for frequencies inside the stopbands using Floquet theory. The magnitude of these evanescent waves decays exponentially in space, but the phase angle, which is determined by the real part of the wave number, is independent of frequency ($k' = 0$). For a finite system, on the other hand, the real part of the wave number is always nonzero, hence, the phase angle will be frequency dependent inside the pseudostopbands. The decay of the magnitude is slower inside a pseudostopband than inside a true stopband. It is apparent that the band edges are not well defined when N is small, and gradually become sharper as N increases.

Figure 5 shows the vibration pattern at a given frequency inside a passband for composites with different numbers of cells. We can see the resonance nature of the patterns, with the polymer vibrating at much larger amplitude than the ceramic.

Figure 6 shows the comparison of the vibration patterns occurred in a ten-cell composite at three distinct frequencies. These three frequencies are selected as follows: $1.36364 f_0$ is in the first passband with a maximum value of $|H(\omega)|$, $1.55 f_0$ is at the upper edge of the first passband, and $2.009 f_0$ is at the center of the second stopband with a minimum value of $|H(\omega)|$. Different from the infinite system, there is no sharp edge between the passband and the stopband. As a result, a gradual transition can be seen from the passing resonant wave pattern to the localized evanescent wave pattern. The evanescent wave is practically localized within 2-3

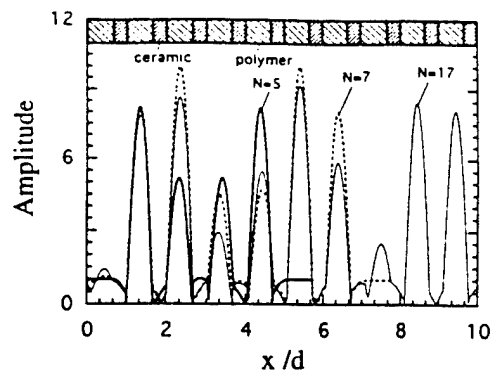


FIG. 5. Typical spatial vibration pattern for a completely transmitted wave with frequency in the first passband. The pattern changes for different N , the internal vibrational magnitude can be much larger than that of the incident wave and is also much larger in the polymer phase than in the ceramic phase.

cells. According to symmetry analysis on the vibration patterns shown in Fig. 7, the upper edge of the second stopband resonance is piezoelectrically active for the 1/3 ceramic volume percent composite, i.e., all the ceramic elements are vibrating in phase. Therefore, this mode will couple strongly to the thickness mode affecting the performance of a composite transducer.²⁶

It is a common practice to reduce the size of the composite cells in designing high-frequency composite transducers. The rule of thumb is that the upper edge of the second stopband resonance should be twice as high as the transducer operating frequency. This will place the thickness mode inside the first stopband of the transverse wave to minimize the coupling.⁴ In reality, there are technical limitations for making fine scale ceramic inclusions. An alternative to reduce the shear wave resonance effects is to introduce randomness into the composite structures, since randomness can destroy many shear resonance modes.²⁶⁻²⁹

IV. WAVE PROPAGATION IN APERIODIC FINITE SYSTEM

Theoretically speaking, true randomness can only be achieved in an infinite system. In reality, we seek wave localization which can be achieved with limited number of cells. The questions of interest are

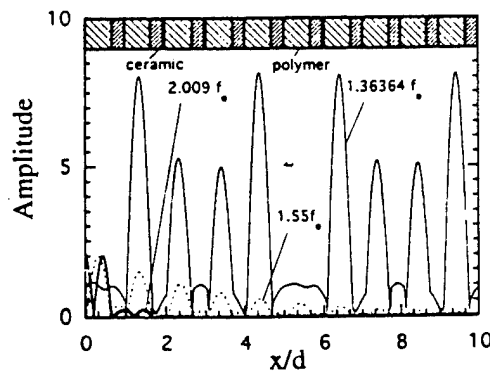


FIG. 6. Vibration pattern of a 10 cell composite. (—) A frequency in the passband. (—) A frequency in the pseudostopband. (---) A frequency near the edge of the pseudostopband.

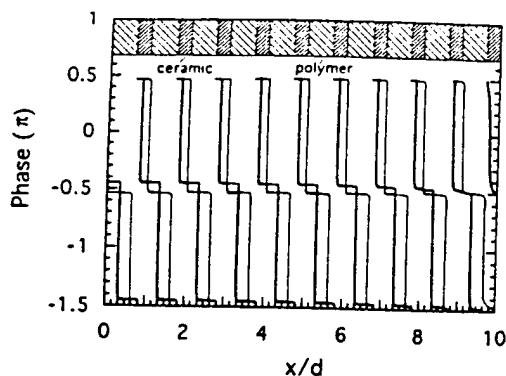


FIG. 7. Phase profiles for the upper and lower band edge frequencies of the second pseudostopband. (—) upper band edge frequency; (---) lower band edge frequency. The lower band edge frequency vibration is piezoelectric active since all the ceramics are in phase. Slight phase lagging occurred due to finite size, which can be seen by comparing the phase angle of the first layer and of the last layer.

- (1) How much randomness is sufficient?
- (2) What is the size dependence of the random effect?

With the 2-2 composite structure discussed above, these questions can be conveniently studied using the T -matrix technique plus the new definition of Eqs. (14) and (15). Both vibration profile and band structures can be calculated for an aperiodic 2-2 composite.

There are several ways to introduce randomness into a 2-2 composite. The simplest way is either randomizing the spacing between ceramic plates (randomizing b), or changing the ceramic plate thickness while leaving their spacing constant (randomizing a). Since the effects of randomization of b or a are similar due to the symmetry of the structure, we only give the results for randomizing b to illustrate the physical characteristics. When a or b is randomized, the number of passing frequencies will be greatly reduced and all the pseudostopbands become wider. The random effects are greatly enhanced when both a and b are randomized at the same time, with new characteristics produced as discussed below.

Figure 8 shows the comparison between the magnitudes of transmission function $H(\omega)$ for randomizing b and for randomizing both a and b . The composite has 20 cells and the ceramic volume percent is kept at 1/3 on the average in order to compare with the results of the periodic composite calculated in Sec. III. An interesting fact in the case of randomizing b is that the transmission is not completely destroyed for all frequencies, there still exist some frequencies which allow the waves to completely pass through [$|H(\omega)| = 1$] as shown in Fig. 8. The reason is that a resonance length scale, i.e., the ceramic thickness a , still remains in the composite. Conversely, when randomness is introduced in both the ceramic thickness a and their spacing b , all but the first passband are eliminated. There appears to be a cut-off frequency for wave propagation in the random composite. Intuitively, the first passband should represent the propagation of waves with wavelengths comparable to and larger than the size of the composite system. The bandwidth is also expected to become narrower as the number of cells increases. How-

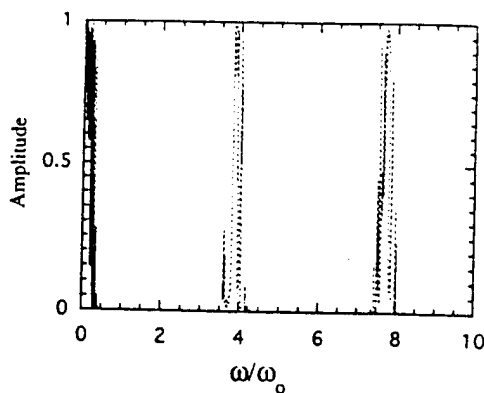


FIG. 8. The band structures for a randomly spaced ceramic plate composite (randomizing b , dashed curve) and a completely random composite (randomizing both a and b , solid curve), respectively. For the randomly spaced composite, the stopband width becomes much wider compared with the periodic structure, but there are still passing waves at higher frequencies. While for the completely random structure, no passing wave after a cut-off frequency.

ever, direct correlation between the dimension of the composite and the cut-off frequency was not found in our calculations.

An important point here is that the characteristics of localized waves in the random structure are quite different from those of the stopband waves. Although the magnitude of the waves shows exponential decay in space for both cases, the phase of the stopband waves is independent of frequency, while the phase of the localized waves shows strong frequency dependence. There are many stopbands in a periodic composite, each of the bands has a bandwidth characterized by the band edges. While in a random composite, the band structure consists of only one passband, no waves can go through the structure at frequencies above the cut-off frequency.

Considering the efficiency of cross-talking elimination, the stopband waves decay faster than the random localized waves, as illustrated in Fig. 9. The decay rate is the highest for the frequency at the center of each stopband; typically the wave vanishes in 2-3 cells. The decay rate becomes slower

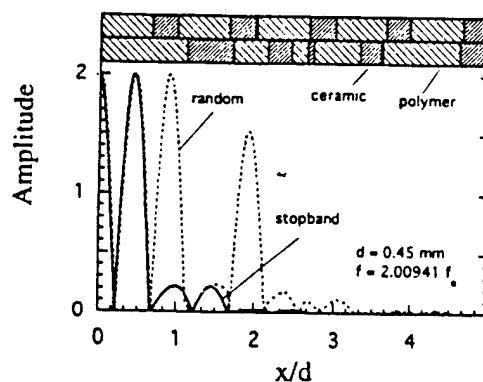


FIG. 9. Comparison of the transmission function for a periodic structure at a pseudostopband frequency and for a completely random structure at the same frequency.

as the frequency moves away from the center frequency of the stopband. On the other hand, localized waves are not so sensitive to frequency as long as the frequency is above the cut-off frequency. The localized waves have much broader bandwidth, although the decay rate for the localized waves is relatively slower than for the stopband waves. A typical localized wave can be confined within 6–7 cells. These quantitative evaluations can be used as general guidelines for the design of random composites.

V. SUMMARY AND CONCLUSIONS

We have studied shear wave propagation in a 2-2 composite structure using the T -matrix technique. A new definition is introduced for the effective wave number k [Eqs. (14) and (15)]. Using the new definition, the dispersion relation for a finite composite system is calculated without using the Floquet theory, which is valid only for an infinite system.

The formation of the band structures with the increase of composite cells can be seen clearly from the calculated results (Fig. 4). Our results show that the boundaries between stopbands and passbands become unclear for a finite system. Pseudostopbands can develop quickly with the increase in the number of cells in the composite. Stopband-like frequency regions are already formed in a composite of 10 cells as shown in Fig. 3. For a system with more than 200 cells, the dispersion relation calculated using the new definition is nearly identical with that obtained from Floquet theory (see Fig. 4).

Wave patterns inside the composites can be quite complicated and the magnitude of vibration could be much larger than the incident wave due to resonance. It is demonstrated that the polymers vibrate at much larger amplitude than the ceramics. These shear resonance modes are undesirable for thickness mode transducers because they not only reduce the efficiency of the transducer, but also prolong the ringdown in the pulse mode, producing poor resolution.

There are two ways to solve this problem: one is to reduce the cell dimensions, which can push the shear resonance to higher frequencies and place the operating frequency inside the first stopband to reduce the coupling,¹⁵ and the other is to introduce randomness into the structure, which can effectively destroy the shear resonance in a much broader band, and also can overcome the technical limitations encountered in fabricating fine scale composites. It is shown that the waves can be confined within 6–7 cells if both a and b are randomized. Therefore, this technique could be very useful and cost effective in producing high-frequency composite transducers of small size.

ACKNOWLEDGMENT

Financial support for this work is provided by the Office of Naval Research under Grant No. N00014-92-J-1501.

APPENDIX

From Eqs. (3) and (4) we have

$$|T_{nd-a}||T_{nd}| = 1, \quad (\text{A1})$$

so that

$$|T| = |T_{d-a}||T_d| \dots |T_{nd-a}||T_{nd}| \dots |T_{Nd-a}||T_{Nd}| = 1, \quad (\text{A2})$$

$$\begin{aligned} |T| &= T_{11}T_{22} - T_{12}T_{21} \\ &= T_{11}T_{11}^* \left(1 - \frac{T_{12}T_{12}^*}{T_{11}T_{11}^*} \right) = \frac{1}{t} (1-r) = 1, \end{aligned} \quad (\text{A3})$$

$$t+r=1.$$

Note $[T_n]$ is in the form of $\begin{bmatrix} T_{11} & T_{12} \\ T_{12}^* & T_{11}^* \end{bmatrix}$; therefore, the total matrix $[T]$ which is a product of each individual matrix also has the relation

$$T_{22} = T_{11}^*, \quad (\text{A4})$$

$$T_{21} = T_{12}^*, \quad (\text{A5})$$

$$\begin{aligned} \begin{pmatrix} a & b \\ b^* & a^* \end{pmatrix} \begin{pmatrix} c & d \\ d^* & c^* \end{pmatrix} &= \begin{pmatrix} ac+bd^* & ad+bc^* \\ b^*c+a^*d^* & b^*d+a^*c^* \end{pmatrix} \\ &= \begin{pmatrix} e & f \\ f^* & e^* \end{pmatrix}. \end{aligned} \quad (\text{A6})$$

¹A. Alippi, F. Cracium, and E. Molanari, *J. Appl. Phys.* **64**, 2238 (1988).

²A. Alippi, F. Cracium, and E. Molanari, 1988 IEEE Ultrasonics Symposium Proceedings, 1988, p. 623.

³A. Alippi, F. Cracium, and E. Molanari, *Appl. Phys. Lett.* **53**, 1806 (1988).

⁴W. A. Smith, A. A. Shaulov, and B. A. Auld, *Ferroelectrics* **91**, 155 (1989).

⁵W. A. Smith and B. A. Auld, *IEEE Trans. Ultrasonic, Ferroelectrics, and Frequency Control* **38**, 40 (1990).

⁶W. A. Smith, Proceedings of 1990 IEEE 7th International Symposium on Applications of Ferroelectrics (ISAF90) 1990, Vol. 145.

⁷G. Hayward and J. A. Hossack, *J. Acoust. Soc. Am.* **88**, 599 (1990).

⁸J. A. Hossack, B. A. Auld, and H. D. Batha, Proceedings of IEEE 1991 Ultrasonic Symposium, 1991, p. 651.

⁹C. G. Oakley, Ph.D. thesis, The Pennsylvania State University, 1991.

¹⁰Y. Wang, E. Schmidt, and B. A. Auld, Proceedings of IEEE 1986 Ultrasonic Symposium, 1986, p. 685.

¹¹K. Y. Hashimoto and M. Yamaguchi, Proceedings of IEEE 1986 Ultrasonic Symposium, 1986, p. 697.

¹²B. A. Auld, H. A. Kunkel, Y. A. Shui, and Y. Wang, Proceedings of IEEE 1983 Ultrasonic Symposium, 1983, p. 554.

¹³C. Potel and J. F. Belleval, *J. Acoust. Am.* **93**, 2669 (1993).

¹⁴Y. Wang and B. A. Auld, Proceedings of IEEE 1985 Ultrasonic Symposium, 1985, p. 637.

¹⁵B. A. Auld, Y. A. Shui, and Y. Wang, *J. Phys. (Paris)* **45**, 159 (1984).

¹⁶Y. Wang, Ph.D. thesis, Stanford University, 1986.

¹⁷J. A. Hossack and G. Hayward, *IEEE Trans. Ultrasonic, Ferroelectrics, and Frequency Control* **38**, 618 (1991).

¹⁸W. Friedrich, R. Lerch, K. Prestele, and R. Soldner, *IEEE Trans. Ultrasonic, Ferroelectrics, and Frequency Control* **37**, 248 (1990).

¹⁹H. L. W. Chan and J. Unsworth, *IEEE Trans. Ultrasonic, Ferroelectrics, and Frequency Control* **36**, 434 (1990).

²⁰C. G. Oakley, Ph.D. thesis, The Pennsylvania State University, 1991.

²¹W. T. Thomson, *J. Appl. Phys.* **21**, 89 (1949).

²²E. H. Lee and W. H. Yang, *SIAM J. Appl. Math.* **25**, 492 (1973).

²³V. K. Kinra and Eric L. Ker, *Int. J. Solid Struct.* **19**, 393 (1983).

²⁴A. M. B. Braga and G. Hermann, *J. Acoust. Soc. Am.* **91**, 1211 (1991).

²⁵R. Esquivel-Sirvent and G. H. Coccoletzi, *J. Acoust. Soc. Am.* **95**, 86 (1994).

²⁶B. A. Auld and J. A. Hossack, *Electron. Lett.* **27**, 1284 (1991).

²⁷P. Sheng and Z. Zhang, *Phys. Rev. Lett.* **57**, 1879 (1986).

²⁸T. R. Kirkpatrick, *Phys. Rev. B* **31**, 5746 (1985).

²⁹R. Esquivel-Sirvent and G. H. Coccoletzi, *J. Acoust. Soc. Am.* **95**, 86 (1994).

APPENDIX 33

FINITE ELEMENT ANALYSIS AND EXPERIMENTAL STUDIES ON THE THICKNESS RESONANCE OF PIEZOCOMPOSITE TRANSDUCERS

Wenkang Qi¹ and Wenwu Cao^{1,2}

1. Intercollege Materials Research Laboratory
 2. Department of Mathematics
- The Pennsylvania State University
University Park, PA 16802

Finite element method (FEA) has been used to calculate the thickness resonance frequency and electromechanical coupling coefficient k_t for 2-2 piezocomposite transducers. The results are compared with that of the effective medium theory and also verified by experiments. It is shown that the predicted resonance frequencies from the effective medium theory and the unit cell modeling using FEA deviate from the experimental observations for composite systems with a ceramic aspect ratio (width/length) more than 0.4. For such systems, full size FEA modeling is required, which can provide accurate predictions of the resonance frequency and thickness coupling constant k_t .

Key words: Aspect ratio; composite transducers; effective medium theory; finite element analysis; piezocomposites.

1. INTRODUCTION

A transducer is usually characterized by two major properties: sensitivity and resolution. The sensitivity is related to the electromechanical coupling coefficient, while the resolution is related to the center frequency and bandwidth. At the beginning of the ultrasonic imaging industry, two types of piezoelectric materials were used as transducer materials: lead zirconate titanate (PZT) and polyvinylidene fluoride (PVDF). PZT has high acoustic impedance, making it very difficult to send ultrasonic energy into the human tissue, which has very low acoustic impedance. In addition, the Q value of PZT is very high so that the bandwidth is narrow resulting in poor resolution due to ringing effects. On the other hand, PVDF has a very good acoustic impedance match with human tissue, but its electromechanical coupling coefficient is very low, resulting in low sensitivity. In addition, the low dielectric constant of PVDF also creates the problem of electric impedance mismatch, which limits the application of PVDF in array transducers.

The advent of piezoelectric composites greatly improved this situation [1,2]. Piezocomposites have large coupling coefficients as well as low acoustic impedance, making them ideal transducer materials. Nowadays, piezoelectric composites are widely used in making underwater acoustic and medical ultrasonic transducers [2-4]. However, due to the biphasic nature and the large difference in the elastic stiffness between the polymer and the ceramic, the surface displacement is often nonuniform [5-8]. It is therefore difficult to accurately predict the resonance frequency of the composite transducers using simplified models.

The most commonly-used method for designing composite transducers is the effective medium model[4]. Experience reveals that the actual resonance frequency of the designed composite transducer is often lower than the theoretical estimates from the effective medium theory. Motivated by this discrepancy, we have conducted a combined experimental and finite element analysis to give a detailed assessment of the effective medium model and to derive the conditions for the application of such theoretical estimates. We also intended to evaluate the validity of the commonly used unit cell FEA modeling [9-11]. For simplicity, we only analyze a 2-2 composite transducer, but the conclusions are also valid for 1-3 type composite transducers.

2. EFFECTIVE MEDIUM MODEL FOR 2-2 PIEZOCOMPOSITES

A typical 2-2 composite is shown in figure 1. It is a layered structure of alternating polymer and piezoceramic constituents.

The constitutive relations for the polymer phase can be written as the following,

$$T_1 = C_{11}S_1 + C_{12}S_2 + C_{12}S_3 \quad (1a)$$

$$T_2 = C_{12}S_1 + C_{11}S_2 + C_{12}S_3 \quad (1b)$$

$$T_3 = C_{12}S_1 + C_{12}S_2 + C_{11}S_3 \quad (1c)$$

$$T_4 = C_{44}S_4 \quad (1d)$$

$$T_5 = C_{44}S_5 \quad (1e)$$

$$T_6 = C_{44}S_6 \quad (1f)$$

$$D_1 = \epsilon_{11}E_1 \quad (1g)$$

$$D_2 = \epsilon_{11}E_2 \quad (1h)$$

$$D_3 = \epsilon_{11}E_3 \quad (1i)$$

Here, T_l and S_l ($l = 1, 2, \dots, 6$) are the stress and strain components, respectively, in Voigt notation, E_i and D_i ($i = 1, 2, 3$) are the electric field and electric displacement respectively, C_{ij} are the elastic stiffness constants and ϵ_{ij} are the dielectric constants.

Similarly, if we take the x_3 -direction as the poling direction, the constitutive relations in the ceramic phase can be written as:

$$T_1 = C_{11}^E S_1 + C_{12}^E S_2 + C_{13}^E S_3 - e_{31} E_3 \quad (2a)$$

$$T_2 = C_{12}^E S_1 + C_{11}^E S_2 + C_{13}^E S_3 - e_{31} E_3 \quad (2b)$$

$$T_3 = C_{13}^E S_1 + C_{13}^E S_2 + C_{33}^E S_3 - e_{33} E_3 \quad (2c)$$

$$T_4 = C_{44}^E S_4 - e_{15} E_2 \quad (2d)$$

$$T_5 = C_{44}^E S_5 - e_{15} E_1 \quad (2e)$$

$$T_6 = C_{66}^E S_6 \quad (2f)$$

$$D_1 = e_{15} S_5 + \epsilon_{11}^S E_1 \quad (2g)$$

$$D_2 = e_{15} S_4 + \epsilon_{11}^S E_2 \quad (2h)$$

$$D_3 = e_{31} S_1 + e_{31} S_2 + e_{33} S_3 + \epsilon_{33}^S E_3 \quad (2i)$$

where e_{ij} are the piezoelectric constants, and the superscripts, E and S, refer to quantities at constant electric field and strain, respectively.

We can follow the same procedure as in [4] and use all the assumptions proposed there to derive the effective properties (denoted with an overbar) of a 2-2 composite,

$$\overline{C_{33}^E} = V \left[C_{33}^E - V' \frac{(C_{12}^E - C_{13}^E)^2}{V' C_{11}^E + V C_{11}} \right] + V' C_{11} \quad (3a)$$

$$\overline{e_{33}} = V \left[e_{33} - V' e_{31} \frac{(C_{13}^E - C_{12}^E)}{V' C_{11}^E + V C_{11}} \right] \quad (3b)$$

$$\overline{\epsilon_{33}^S} = V \left[\epsilon_{33}^E + \frac{e_{31}^2 V'}{V' e_{11}^E + V C_{11}} \right] \quad (3c)$$

$$\overline{C_{33}^D} = \overline{C_{33}^E} + \frac{(\overline{e_{33}})^2}{\overline{\epsilon_{33}^S}} \quad (3d)$$

$$\overline{h_{33}} = \frac{\overline{e_{33}}}{\overline{\epsilon_{33}^S}} \quad (3e)$$

$$\overline{\beta_{33}^S} = \frac{1}{\overline{\epsilon_{33}^S}} \quad (3f)$$

$$\bar{\rho} = V \rho^C + V' \rho^P \quad (3g)$$

In the above expressions, V and V' are the volume percentages of ceramic and polymer, respectively, $V' = 1-V$, and ρ^P and ρ^C are the densities of the ceramic and polymer. Using the conventional definition, one can derive all the relevant effective quantities for the thickness mode operation,

$$\bar{k}_t = \frac{\bar{h}_{33}}{\sqrt{C_{33}^D \beta_{33}^S}} = \frac{\bar{e}_{33}}{C_{33}^D \epsilon_{33}^S} \quad (4)$$

$$\bar{Z} = \sqrt{C_{33}^D \bar{\rho}} \quad (5)$$

$$\bar{v}_l = \sqrt{\frac{C_{33}^D}{\bar{\rho}}} \quad (6)$$

$$f_r = \frac{\bar{v}_l}{2L} \quad (7)$$

\bar{v}_l and L are the longitudinal wave speed and the thickness of the composite in the poling (x_3) direction and f_r is the resonance frequency given by the effective medium theory.

Using the above equations, we have calculated the effective thickness resonance frequency for a 2-2 composite of 1 mm thick. Compared with a 1-3 composite transducer of the same thickness, the resonance frequency of a 2-2 composite is higher than that of a 1-3 composite of the same ceramic volume content as shown in Figure 2. The same is true also for the thickness coupling constant \bar{k}_t , as plotted in figure 3.

Although the effective medium theory is relatively simple and sometimes gives reasonable estimate for the resonance frequency, it fails to account for the aspect ratio effect, which can be substantial if the a/L (width/length) ratio is not sufficiently small [6,7]. For systems with large a/L ratio and low ceramic content, the isostrain assumption is not valid.

In addition, since a real transducer always contains a finite number of cells, one would not expect a very good match with experimental results from a unit cell model that automatically assuming periodic boundary conditions. For this reason, we have performed FEA on 2-2 composite transducers using both the unit cell and full dimension models.

3. FINITE ELEMENT ANALYSIS

The nonuniform displacement at the surface of composite transducers has been observed experimentally[5,8]. This inhomogeneity can greatly affect the overall performance of a

transducer. For low frequencies, the situation may be treated by using elasticity theory and describing the two constituents separately. Some approximations can be used in solving the low frequency problem since there are no countable phase difference in the structure[6-8]. However, when the operating frequency is high and close to the thickness resonance, we must use FEA for an accurate theoretical prediction.

A commercial package ANSYS® is used in our study and two models were analyzed:

- (1) A unit cell model, which was also analyzed by several other researchers[9-11];
- (2) A finite real dimensional system.

These FEA results are checked against our experiment results.

After some test runs, we found that the results from a 2-D model are almost the same as those from a 3-D model for the geometry we have chosen. Therefore, for computational efficiency, we performed only 2-D modeling. The models and the coordinate system are shown in figure 4.

One of our objectives is to study the change of the thickness resonance frequency and the electromechanical coupling coefficient k_t with respect to the change of ceramic aspect ratio. Both the thickness resonance and the anti-resonance frequencies were calculated. The resonance frequency is calculated under short circuit condition (constant E) while the anti-resonance frequency is calculate in open circuit condition (constant D)[12]. From these two resonance frequencies, the electromechanical coupling coefficient k_t can be calculated using the formula,

$$k_t^2 = \frac{\pi f_r}{2f_a} \tan\left(\frac{\pi(f_a - f_r)}{2f_a}\right) \quad (8)$$

where f_r and f_a are the resonance and anti-resonance frequencies, respectively.

First, we performed analysis on the unit cell model. Only a quarter of the unit cell is needed due to symmetry [Fig. 4(a)]. A composite of real dimensions was then analyzed. Again, only a quarter of the piece was analyzed due to symmetry [Fig. 4(b)]. The results are plotted in figure 5 together with the experimental results.

4. RESULTS AND DISCUSSIONS

In order to verify the theoretical results, we made a series of 2-2 composite transducers using PZT-5H and Spurr's epoxy. The dimension along the x_2 -axis (into the paper) is made large enough so that the system can be treated as two dimensional. We start by making a thick 2-2 piezocomposite in the x_3 -dimension, and later gradually increased the a/L ratio by shortening L , i.e., shortening the x_3 -dimension without changing the other dimensions. After each cutting, the sample is re-electroded and the resonance frequency measured using a HP 4194A impedance analyzer. From the impedance curves, the resonance and anti-resonance frequencies can be obtained, and the electromechanical coupling coefficient k_t can be determined using Eq.(8).

Another experiment was also performed to check the dimensional effect in the x_1 -direction. In other words, reducing the number of cells in the composite structure to see if it affects the resonance frequency in the x_3 -dimension. Impedance measurements were also used as the means to characterize this effect.

Figure 5 shows the comparison of the resonance frequencies calculated by the effective medium theory, unit cell FEA and real dimensional model FEA together with the experimental results. When the ceramic ratio a/L is less than 0.4, all theoretical models agree quite well with the experimental observations. But for a/L greater than 0.4, the effective medium theory prediction is too high while the prediction from the unit cell FEA model is too low. Only the real dimensional model provide accurate prediction for the resonance frequency.

The coupling constant k_t calculated from effective medium theory is independent of the aspect ratio, as shown in figure 3. However, experimental results demonstrate a fluctuation of k_t with change of aspect ratio, as shown in figure 6. This fluctuation is mainly caused by the coupling between the thickness mode and other lateral modes or their higher harmonics.

When the thickness, L , is reduced, the resonance frequency is shifted to higher frequencies. Whenever the resonance frequency approaches one of the lateral modes or their higher harmonics, energy will be lost to the lateral modes and the coupling constant k_t is reduced. Further increase of the thickness resonance frequency may recover some of the lost energy through mode decoupling until reaching the next lateral mode, which causes another reduction of the coupling constant. Therefore, we expect the k_t value to go up and down with the decrease in L . As shown in figure 6, this mode coupling effect is well accounted for by the FEA. Both the unit cell model and the real dimensional model show this fluctuating feature and the real dimensional model provides better agreement with the experimental observations.

The difference between unit cell and real dimensional model indicate that the resonance frequency in the x_3 -dimension will also depend on the composite size in the x_1 -dimension (number of cells). However, this effect is weak when the a/L ratio is small.

5. SUMMARY AND CONCLUSIONS

We have performed both experimental and FEA investigations on the resonance frequency of a 2-2 piezoelectric composite transducer and compared with the effective medium theory estimation. It is found that the effective medium theory gives good estimates when the a/L ratio is less than 0.4, but the calculation of the coupling constant is incorrect whenever the thickness mode gets close to one of the lateral modes. When the a/L ratio is larger than 0.4, the effective medium theory prediction will be higher than the actual resonance frequency of the composite transducer. The FEA results depend strongly on the details of the model. Unit cell modeling seems to underestimate the resonance frequency for composites with large a/L ratio but the fluctuation of k_t can be reasonably predicted. The most accurate modeling is the real dimensional FEA, which gave good predictions for both resonance frequency and coupling constant for all aspect ratios investigated.

This work was supported by The Office of Naval Research under Grant No. N00014-93-1-0340 and The Whitaker Foundation under Special Opportunity Award.

REFERENCES

- [1] Newnham, R.E, Bowen, L.J., Klicker, K.A., and Cross, L.E., Composite piezoelectric transducer, *Materials in Engineering* 2, 93-106 (1980).
- [2] Smith, W.A., The Role of Piezocomposites in Ultrasonic Transducers, in 1989 IEEE Ultrasonic Symposium Proceedings, pp. 755-766.
- [3] Hayward, G. and Hossack, J.A., Unidimensional Modeling of 1-3 Composite Transducer, in 1989 Ultrasonic International Conference Proceedings, pp 531-536.
- [4] Smith, W.A., Modeling 1-3 composite piezoelectric: thickness-mode oscillations, *IEEE Trans. Ultrason. Ferroelec. Freq. Contr.* 38, 40-47 (1991).
- [5] Auld, B. A., Kunkel, H.A., Shui, Y.A., and Wang, Y., Dynamic Behavior of Periodic Piezoelectric Composites, in 1983 IEEE Ultrasonics Symposium, pp 554-558.
- [6] Cao, W., Zhang, Q., and Cross, L.E., Theoretical study on the static performance of piezoelectric ceramic-polymer composites with 2-2 connectivity, *IEEE Trans. Ultrason. Ferroelec. Freq. Contr.* 40, 103-109 (1993).
- [7] Cao, W., Zhang, Q., and Cross, L.E., Theoretical study on the static performance of piezoelectric ceramic-polymer composites with 1-3 connectivity, *J. Appl. Phys.* 72, 5814-5821 (1992).
- [8] Zhang, Q. M., Cao, W., Zhao, J., and Cross, L.E., Piezoelectric performance of piezoceramic-polymer composites with 2-2 connectivity --a combined theoretical and experimental study, *IEEE Trans. Ultrason. Ferroelec. Freq. Contr.* 41, 556-564 (1994).
- [9] Hossack, J. A., and Hayward, G., Finite-element analysis of 1-3 composite transducers, *IEEE Trans. Ultrason. Ferroelec. Freq. Contr.* 38, 618-629 (1991).
- [10] Hladky-Hennion, A., and Decarpigny, J., Finite element modeling of active periodic structures: application to 1-3 piezocomposites, *J. Acoust. Soc. Am.* 94, 621-635 (1993).
- [11] Hossack, J. A., Auld, B.A., and Batha, H.D., Techniques for Suppressing Spurious Resonant Modes in 1:3 Composite Transducers, in 1991 IEEE Ultrasonics Symposium, pp 651-655.
- [12] Lerch, R., Simulation of piezoelectric devices by two- and three-dimensional finite elements, *IEEE Trans. Ultrason. Ferroelec. Freq. Contr.* 37, 233-246 (1990).

Table I. Material properties of PZT and epoxy.

Elastic compliance ($10^{-12} \text{ m}^2/\text{N}$)										
	s_{11}^E	s_{33}^E	s_{12}^E	s_{13}^E	s_{44}^E	s_{66}^E				
PZT	16.5	20.7	-4.78	-8.45	43.5	42.6				
Epoxy	286.7	286.7	-97.9	-97.9	769	769				
Piezoelectric constants, d_{ij} , (10^{-12} C/N) Dielectrics constants, k_{ij} , (ϵ_0) Coupling constants, $k_{i\lambda}$ and k_t , and Density ρ (kg/m^3)										
	d_{15}	d_{31}	d_{33}	$\epsilon_{11}^s/\epsilon_0$	$\epsilon_{33}^s/\epsilon_0$	k_{15}	k_{31}	k_{33}	k_t	ρ
PZT	741	-274	593	1700	1470	0.675	0.39	0.75	0.50	7800
Epoxy				4.0	4.0					1097

FIGURE CAPTIONS:

- Fig. 1 Configuration of 2-2 composite investigated in this study.
- Fig. 2 Resonance frequencies for 2-2 and 1-3 composites calculated using the effective medium theory for different ceramic volume content.
- Fig. 3 Coupling constant k_t calculated for 2-2 and 1-3 composites of different ceramic volume content.
- Fig. 4 2-D models used in the finite element analysis. (a) unit cell model; (b) full dimension model.
- Fig. 5 Comparison of observed resonance frequencies and theoretical predictions from the effective medium theory, unit cell and full dimension finite element models at different ceramic aspect ratios. The widths of the ceramic and polymer are $a = 0.273$ mm and $b = 0.362$ mm, respectively.
- Fig. 6 Comparison of observed coupling constant k_t and theoretical calculations from the effective medium theory, unit cell and full dimension finite element models at different ceramic aspect ratios. The widths of the ceramic and polymer are $a = 0.273$ mm and $b = 0.362$ mm, respectively.

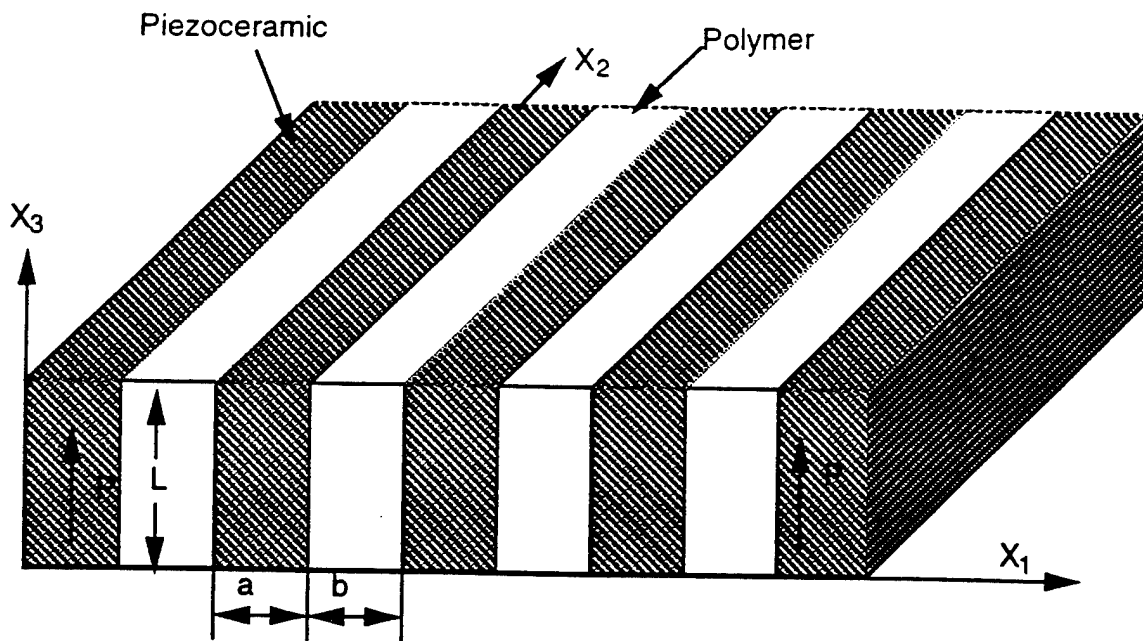


Fig. 1

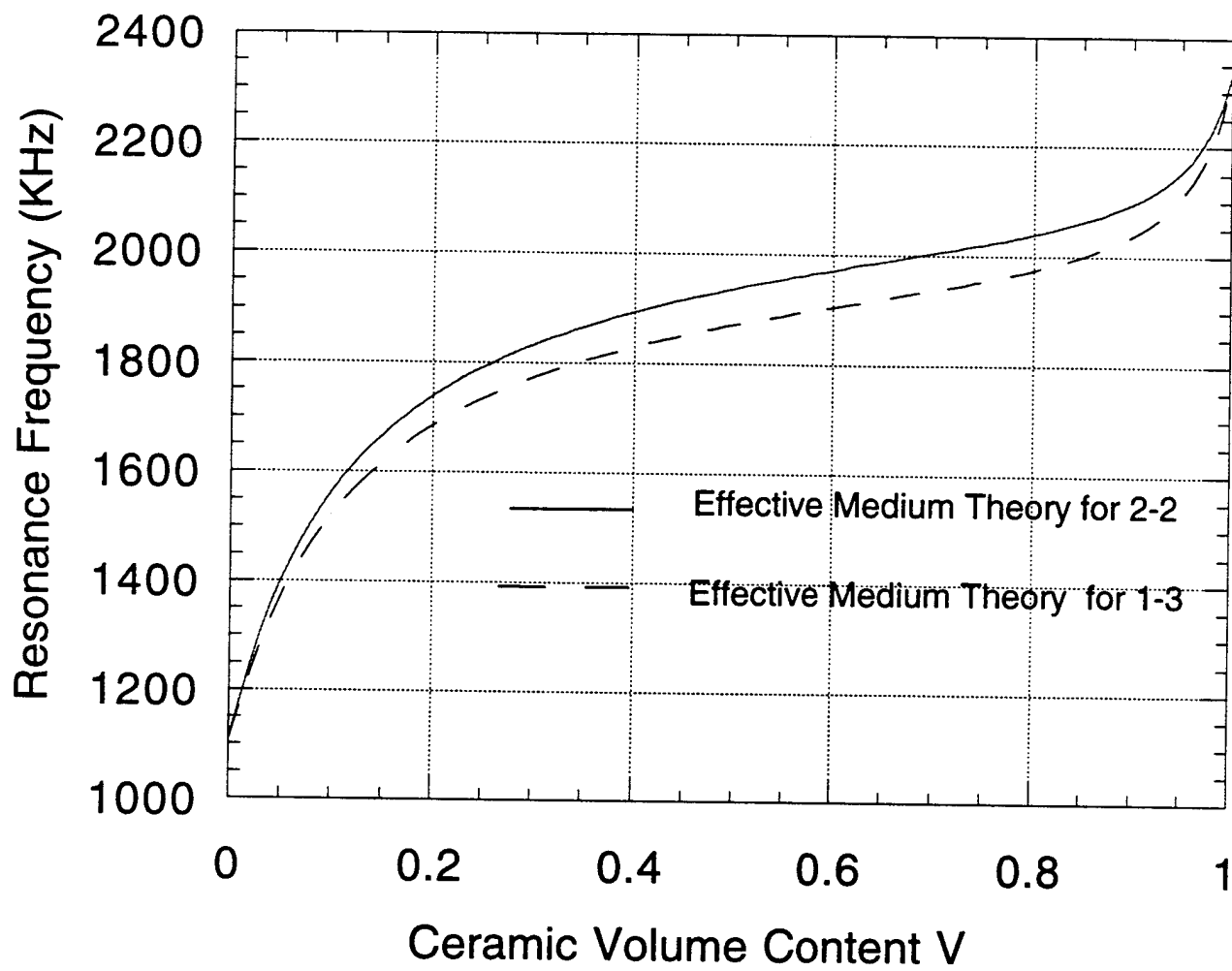


Fig. 2

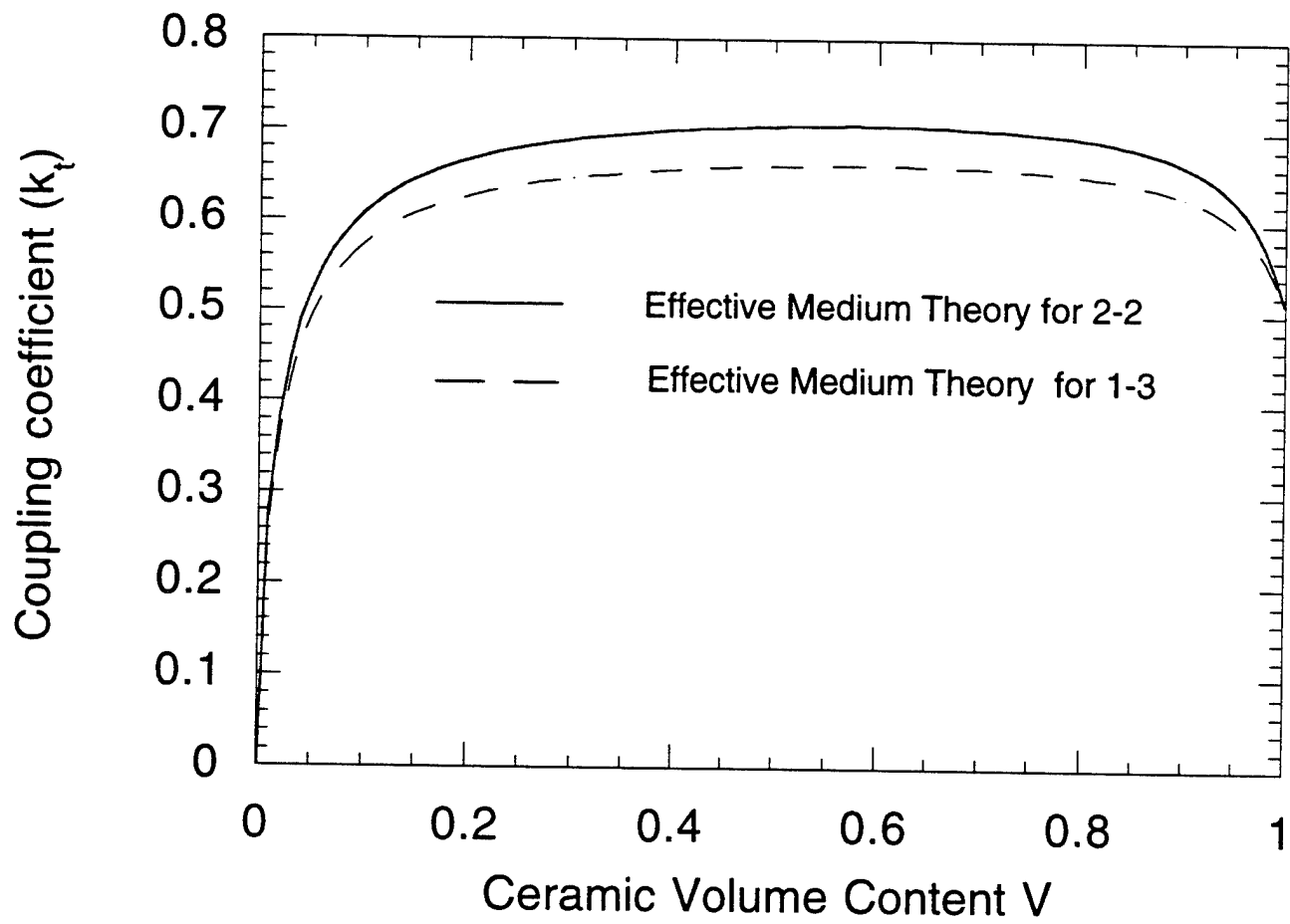
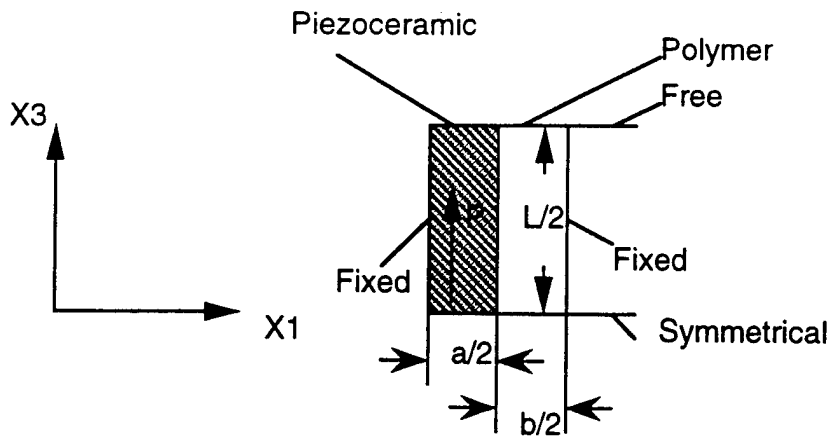
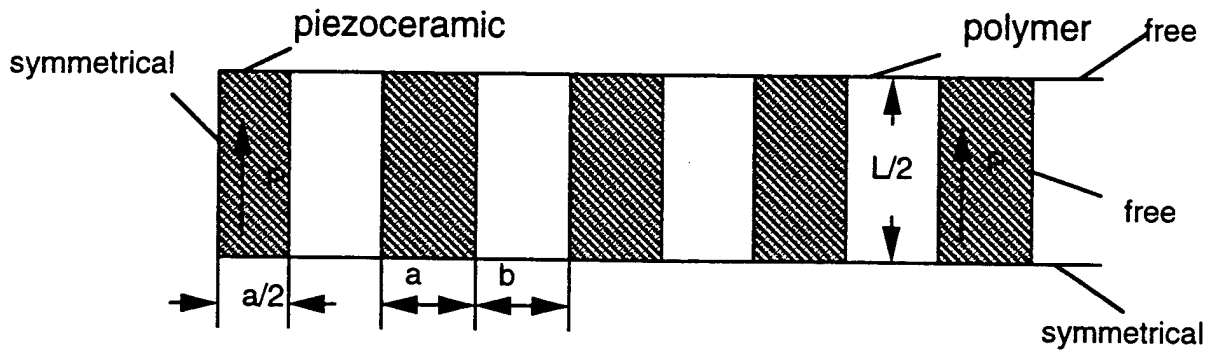


Fig. 3



(a)



(b)

Fig. 4

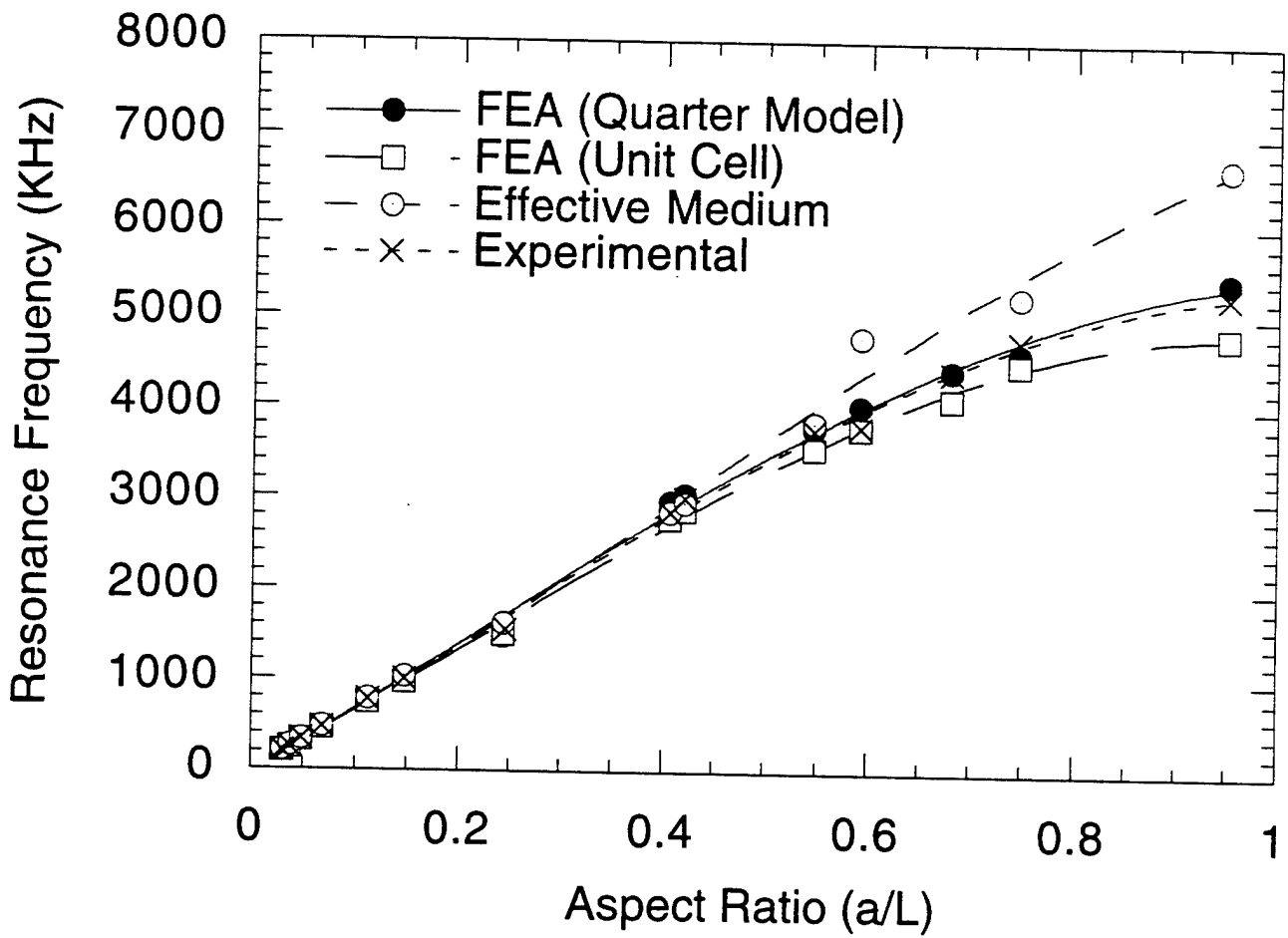


Fig. 5

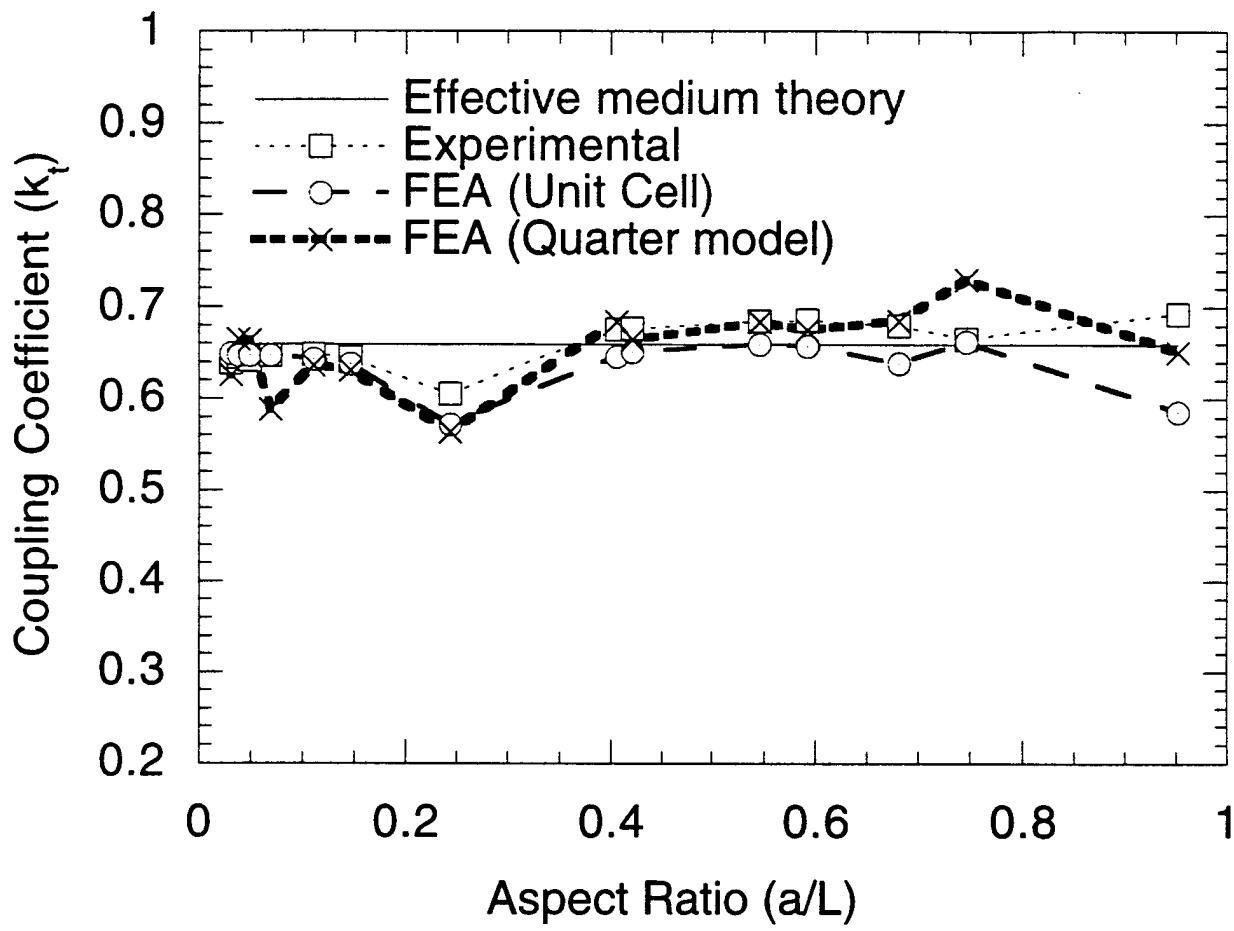


Fig. 6

APPENDIX 34

Multisource excitations in a stratified biphase structure

Wenwu Cao^{a)} and Wenkang Qi

Materials Research Laboratory, The Pennsylvania State University, University Park, Pennsylvania 16802

(Received 6 March 1995; accepted for publication 22 June 1995)

A stratified biphase structure can have many mechanical resonance modes due to the existence of several length scales in the system. The resonance effect is greatly enhanced if there are periodic synchronized multiple driving sources in the structure. For example, a single beam or a linear array composite transducers used in medical ultrasonic imaging. Such resonance behavior can be studied using an extended transfer matrix technique which we name: multisource T-matrix technique. Using this technique we have studied the effects of randomization in a 2-2 composite. It is found that for dispersing the pitch resonance the randomization of ceramic spacing is more effective for low ceramic content, while randomization of ceramic width is more effective for high ceramic content. © 1995 American Institute of Physics.

I. INTRODUCTION

Transfer matrix (T matrix) is one of the tools used in the study of wave propagation characteristics in stratified structures.¹⁻⁹ In all the previous studies using T matrix, the Floquet relation must be used to derive the dispersion relation. However, the Floquet relation is valid only for an infinite system, it is not appropriate to use it for a finite system. On the other hand, the transfer matrix technique can be used for systems of any size so long as the wave propagation has one-dimensional nature. With this consideration recently we have introduced a definition of a complex wave number \tilde{k} using the T matrix alone so that the dispersion relation can be derived for a finite system without the Floquet condition.¹⁰ Using this new definition the development of band structures with the increase of the number of cells in the composite can be calculated directly.

In a 2-2 composite transducer, the active components are often driven simultaneously. In other words, there are more than one wave sources in the structure. For such systems, the band structure study, which only deals with single-wave propagation, would not be as useful since new resonance feature will be produced by the interference of multiwave sources. There will be interference between the incident and reflected waves, and also among waves of different sources.

Although of practical importance, theoretical studies on such multisource driven system have not been reported in the literature. It is the intention of this paper to extend the transfer matrix technique to address this problem.

A typical single beam 2-2 composite transducer is shown in Fig. 1, where the piezoelectric ceramics are the active components of the transducer and the polymers are the passive components. When an electric potential is applied to the transducer through the top and bottom electrodes, the ceramic components will either contract or expand to generate acoustic signals through piezoelectric coupling, whereas the polymer components will play the passive role of damping and acoustic coupling agent to a low acoustic impedance medium.

In reality, the resonance behavior of the system shown in Fig. 1 depends on both the position of the driving source and the number of the driving sources. For simplicity, we assume the system to be linear, so that the principle of superposition can be used.

Following the spirit of the single-source transfer matrix technique, we introduce here an algorithm of multisource transfer matrix for the study of stratified structures. Quantitative calculations have been carried out for a 2-2 ceramic-polymer composite as shown in Fig. 1 with both periodic and random arrangements. We choose the shear wave as an example for this study, other waves can be studied in a similar fashion.

II. TRANSFER MATRIX FOR MULTISOURCE DRIVEN 2-2 COMPOSITES

As shown in Fig. 1, when all the ceramic elements are being driven in the z direction with an alternating field, shear waves are being generated at all the ceramic-polymer interfaces. It can be shown (Appendix) that for a linear system the wave functions in the n th cell can be written in the following from:

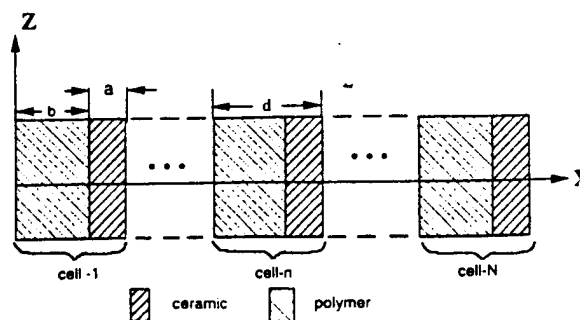


FIG. 1. Structure of a 2-2 ceramic-polymer composite, where a and b are the ceramic width and polymer width, respectively, $d = a + b$ is the pitch.

^{a)}Electronic mail: wcao@sun01.mrl.psu.edu

$$\psi_{np} = A_n e^{i(\omega t - k_p x)} + B_n e^{i(\omega t + k_p x)} \quad (\text{in polymer}), \quad (1a)$$

$$\psi_{nc} = C_n e^{i(\omega t - k_c x)} + D_n e^{i(\omega t + k_c x)} + E e^{i\omega t} \quad (\text{in ceramic}), \quad (1b)$$

where k_p and k_c are the wave numbers of the polymer and ceramic, respectively.

Basically, inside the polymer there is a forward wave and a backward wave with their amplitudes given by complex numbers (Appendix). While inside the ceramic, an additional position-independent vibration has to be included to specify the external drive. Among all the coefficients in Eqs. (1a) and (1b), E is a real number, A_n , B_n , C_n , and D_n are all complex numbers.

Similar to the case of single-wave propagation in composite, there are two boundary conditions at each interface, i.e., continuity and force equilibrium. Using Eqs. (1a) and (1b), these two conditions can be explicitly written at the n th P-C (from polymer to ceramic) interface, i.e., at $x = x_n^{\text{PC}}$,

$$A_n e^{-ik_p x_n^{\text{PC}}} + B_n e^{ik_p x_n^{\text{PC}}} = C_n e^{-ik_c x_n^{\text{PC}}} + D_n e^{ik_c x_n^{\text{PC}}} + E, \quad (2a)$$

$$\begin{aligned} Z_p(-A_n e^{-ik_p x_n^{\text{PC}}} + B_n e^{ik_p x_n^{\text{PC}}}) \\ = Z_c(-C_n e^{-ik_c x_n^{\text{PC}}} + D_n e^{ik_c x_n^{\text{PC}}}), \end{aligned} \quad (2b)$$

or

$$\begin{aligned} \begin{pmatrix} C_n \\ D_n \end{pmatrix} &= \frac{1}{2Z_c} \begin{pmatrix} (Z_c + Z_p)e^{-i(k_p - k_c)x_n^{\text{PC}}} & (Z_c - Z_p)e^{i(k_p + k_c)x_n^{\text{PC}}} \\ (Z_c - Z_p)e^{-i(k_p + k_c)x_n^{\text{PC}}} & (Z_c + Z_p)e^{i(k_p - k_c)x_n^{\text{PC}}} \end{pmatrix} \begin{pmatrix} A_n \\ B_n \end{pmatrix} - \frac{E}{2} \begin{pmatrix} e^{ik_c x_n^{\text{PC}}} \\ e^{-ik_c x_n^{\text{PC}}} \end{pmatrix} \\ &= [T(x_n^{\text{PC}})] \begin{pmatrix} A_n \\ B_n \end{pmatrix} - \frac{E}{2} \begin{pmatrix} e^{ik_c x_n^{\text{PC}}} \\ e^{-ik_c x_n^{\text{PC}}} \end{pmatrix}, \end{aligned} \quad (3a)$$

where Z_p and Z_c are the acoustic impedance of the polymer and ceramic, respectively.

Similarly, we can obtain another relationship at $x = x_n^{\text{CP}}$, the n th C-P (from ceramic to polymer) interface,

$$\begin{aligned} \begin{pmatrix} A_{n+1} \\ B_{n+1} \end{pmatrix} &= \frac{1}{2Z_p} \begin{pmatrix} (Z_p + Z_c)e^{i(k_p - k_c)x_n^{\text{CP}}} & (Z_p - Z_c)e^{i(k_p + k_c)x_n^{\text{CP}}} \\ (Z_p - Z_c)e^{-i(k_p + k_c)x_n^{\text{CP}}} & (Z_p + Z_c)e^{-i(k_p - k_c)x_n^{\text{CP}}} \end{pmatrix} \begin{pmatrix} C_n \\ D_n \end{pmatrix} + \frac{E}{2} \begin{pmatrix} e^{ik_p x_n^{\text{CP}}} \\ e^{-ik_p x_n^{\text{CP}}} \end{pmatrix} \\ &= [T(x_n^{\text{CP}})] \begin{pmatrix} C_n \\ D_n \end{pmatrix} + \frac{E}{2} \begin{pmatrix} e^{ik_p x_n^{\text{CP}}} \\ e^{-ik_p x_n^{\text{CP}}} \end{pmatrix}. \end{aligned} \quad (3b)$$

Therefore, the recurrence relation between the vibration amplitudes of the forward and backward waves in the n th and $(n+1)$ th polymer elements is given by

$$\begin{aligned} \begin{pmatrix} A_{n+1} \\ B_{n+1} \end{pmatrix} &= [T(x_n^{\text{CP}})][T(x_n^{\text{PC}})] \begin{pmatrix} A_n \\ B_n \end{pmatrix} - \frac{E}{2} [T(x_n^{\text{CP}})] \\ &\quad \times \begin{pmatrix} e^{ik_c x_n^{\text{PC}}} \\ e^{-ik_c x_n^{\text{PC}}} \end{pmatrix} + \frac{E}{2} \begin{pmatrix} e^{ik_p x_n^{\text{CP}}} \\ e^{-ik_p x_n^{\text{CP}}} \end{pmatrix}. \end{aligned} \quad (4)$$

It is interesting to see from Eq. (4) that the recurrence relation has similar features as the one for a single-source situation, in fact, the first term on the rhs of Eq. (4) is just the single-source transfer matrix. There are two additional terms proportional to the driving magnitude E , which will vanish upon the elimination of these internal vibration sources.

Once the vibration in the first cell is known, the amplitude in the n th cell can be calculated repeatedly using Eq. (4):

$$\begin{aligned} \begin{pmatrix} A_{n+1} \\ B_{n+1} \end{pmatrix} &= [T(x_n^{\text{CP}})][T(x_n^{\text{PC}})] [T(x_{n-1}^{\text{CP}})][T(x_{n-1}^{\text{PC}})] \dots [T(x_1^{\text{CP}})][T(x_1^{\text{PC}})] \begin{pmatrix} A_1 \\ B_1 \end{pmatrix} \\ &\quad \underbrace{\hspace{10em}}_{2n \text{ matrix}} \\ &\quad - [T(x_n^{\text{CP}})][T(x_n^{\text{PC}})] [T(x_{n-1}^{\text{CP}})][T(x_{n-1}^{\text{PC}})] \dots [T(x_1^{\text{CP}})] \\ &\quad \underbrace{\hspace{10em}}_{(2n-1) \text{ matrix}} \begin{pmatrix} \frac{E}{2} e^{ik_c x_1^{\text{PC}}} \\ \frac{E}{2} e^{-ik_c x_1^{\text{PC}}} \end{pmatrix} \end{aligned}$$

$$\begin{aligned}
& + [T(x_n^{\text{CP}})][T(x_n^{\text{PC}})][T(x_{n-1}^{\text{CP}})][T(x_{n-1}^{\text{PC}})] \dots [T(x_2^{\text{CP}})][T(x_2^{\text{PC}})] \begin{pmatrix} \frac{E}{2} e^{ik_p x_2^{\text{CP}}} \\ \frac{E}{2} e^{-ik_p x_2^{\text{CP}}} \end{pmatrix} + \dots \\
& \quad \quad \quad (2n-2) \text{ matrix} \\
& + (-)^{2n-m} [T(x_n^{\text{CP}})][T(x_n^{\text{PC}})][T(x_{n-1}^{\text{CP}})][T(x_{n-1}^{\text{PC}})] \dots [T(x_{2n-m}^{\text{CP}})] \begin{pmatrix} V_1(x_{2n-m}) \\ V_2(x_{2n-m}) \end{pmatrix} \\
& \quad \quad \quad (2n-m) \text{ matrix} \\
& - [T(x_n^{\text{CP}})] \begin{pmatrix} \frac{E}{2} e^{ik_c x_n^{\text{PC}}} \\ \frac{E}{2} e^{-ik_c x_n^{\text{PC}}} \end{pmatrix} + \begin{pmatrix} \frac{E}{2} e^{ik_p x_n^{\text{CP}}} \\ \frac{E}{2} e^{-ik_p x_n^{\text{CP}}} \end{pmatrix}, \tag{5}
\end{aligned}$$

where

$$\begin{pmatrix} V_1(x_{2n-m}) \\ V_2(x_{2n-m}) \end{pmatrix} = \begin{cases} \begin{pmatrix} \frac{E}{2} e^{ik_c x_{2n-m}^{\text{PC}}} \\ \frac{E}{2} e^{-ik_c x_{2n-m}^{\text{PC}}} \end{pmatrix} & \text{if } 2n-m \text{ is odd} \\ \begin{pmatrix} \frac{E}{2} e^{ik_p x_{2n-m}^{\text{CP}}} \\ \frac{E}{2} e^{-ik_p x_{2n-m}^{\text{CP}}} \end{pmatrix} & \text{if } 2n-m \text{ is even.} \end{cases} \tag{6}$$

The vibration pattern for the ceramic elements can be calculated using Eq. (3a).

III. GLOBAL COORDINATES VERSUS LOCAL COORDINATES

Equation (5) could be simplified by using local coordinates if the structure is periodic. The idea is based on the fact that each wave function $\psi_{np}(x)$ is valid only in a spatial interval of $(n-1)d < x < nd - a$, where a is the width of ceramic and $d = a + b$ is the period with b being the width of the polymer.

Let us introduce a local coordinate

$$y = x - (n-1)d \tag{7a}$$

for the forwarding wave and

$$y' = x - (nd - a) \tag{7b}$$

for the backward wave so that each wave function is considered to be generated at the nearest interface of the position of interest x , then the transfer matrix Eq. (5) can be greatly simplified.

Using these local coordinates, we can rewrite the wave functions Eqs. (1a) and (1b) in the following form:

$$\begin{aligned}
\psi_{np} &= \hat{A}_n e^{i(\omega t - k_p [x - (n-1)d])} \\
&+ \hat{B}_n e^{i(\omega t + k_p [x - (nd - a)])} \quad (\text{in polymer}), \tag{8a}
\end{aligned}$$

$$\begin{aligned}
\psi_{nc} &= \hat{C}_n e^{i(\omega t - k_c [x - (nd - a)])} + \hat{D}_n e^{i(\omega t + k_c [x - nd])} \\
&+ E e^{i\omega t} \quad (\text{in ceramic}), \tag{8b}
\end{aligned}$$

where

$$\hat{A}_n = A_n e^{-ik_p(n-1)d}, \tag{9a}$$

$$\hat{B}_n = B_n e^{ik_p(nd-a)}, \tag{9b}$$

$$\hat{C}_n = C_n e^{-ik_c(nd-a)}, \tag{9c}$$

$$\hat{D}_n = D_n e^{ik_c nd}, \tag{9d}$$

compared with Eqs. (1a) and (1b).

The physical meaning of Eqs. (8a) and (8b) is very clear. Each polymer-ceramic interface now becomes the origin of the acoustic source whose strength is the superposition of all the waves propagating inside the structure. Again, we must note that the coefficients are all complex numbers except E . It can be shown that the recurrence relation becomes much simpler using the local coordinate representation:

$$\begin{pmatrix} A_{n+1} \\ B_{n+1} \end{pmatrix} = [T] \begin{pmatrix} A_n \\ B_n \end{pmatrix} + [V], \tag{10}$$

where

$$[T] = \frac{1}{4Z_c Z_p} \begin{pmatrix} e^{-k_p b} [4Z_c Z_p \cos(k_c a) - 2i(Z_c^2 + Z_p^2) \sin(k_c a)] & -2i(Z_c^2 - Z_p^2) \sin(k_c a) \\ 2i(Z_c^2 - Z_p^2) \sin(k_c a) & e^{ik_p b} [2i(Z_c^2 + Z_p^2) \sin(k_c a) + 4Z_c Z_p \cos(k_c a)] \end{pmatrix}, \quad (11)$$

$$[V] = \frac{E}{2} \begin{pmatrix} 1 - \cos(k_c a) + i \frac{Z_c}{Z_p} \sin(k_c a) \\ e^{ik_p b} \left[1 - \cos(k_c a) - i \frac{Z_c}{Z_p} \sin(k_c a) \right] \end{pmatrix}. \quad (12)$$

Note that both $[T]$ and $[V]$ are independent of n . One now needs to perform the T-matrix calculation once. The vibration in the n th cell can be easily derived if vibration in the first cell is known. For instance, the polymer vibration recurrence relation now becomes

$$\begin{pmatrix} A_{n+1} \\ B_{n+1} \end{pmatrix} = [T]^n \begin{pmatrix} A_1 \\ B_1 \end{pmatrix} + [[T]^{n-1} + [T]^{n-2} + \dots + [T] + [I]][V] = [T]^n \begin{pmatrix} A_1 \\ B_1 \end{pmatrix} + [[I] - [T]^n][[I] - [T]]^{-1}[V], \quad (13)$$

where $[I]$ is the unit matrix and the exponent -1 represents the matrix inversion. The above recurrence relation can be further simplified to become

$$\begin{pmatrix} A_{n+1} - V'_1 \\ B_{n+1} - V'_2 \end{pmatrix} = [T]^n \begin{pmatrix} A_1 - V'_1 \\ B_1 - V'_2 \end{pmatrix} \quad (14)$$

with

$$\begin{pmatrix} V'_1 \\ V'_2 \end{pmatrix} = [[I] - [T]]^{-1} \begin{pmatrix} V_1 \\ V_2 \end{pmatrix}. \quad (15)$$

Equation (14) is much simpler for numerical calculations compared to Eq. (5) which involves explicitly the coordinates of all the cells.

IV. DAMPING EFFECTS

In a ceramic-polymer composite transducer, high damping in the polymer is desirable for reducing the ringing down to increase the resolution and the bandwidth of the transducer. We can study this situation by introducing complex wave numbers and acoustic impedance when the multisource T-matrix technique described in Secs. II and III is used.

Let α_p and α_c represent the damping constants of the polymer and ceramic, respectively, the damped waves may be written in the following form:

$$\begin{aligned} \psi_{np} &= A_n e^{-\alpha_p x} e^{i(\omega t - k_p x)} \\ &+ B_n e^{\alpha_p x} e^{i(\omega t + k_p x)} \quad (\text{in polymer}), \end{aligned} \quad (16)$$

$$\begin{aligned} \psi_{nc} &= C_n e^{-\alpha_c x} e^{i(\omega t - k_c x)} + D_n e^{\alpha_c x} e^{i(\omega t + k_c x)} \\ &+ E e^{i\omega t} \quad (\text{in ceramic}). \end{aligned} \quad (17)$$

If we introduce two complex wave numbers

$$\tilde{k}_p = k_p - i\alpha_p, \quad (18)$$

$$\tilde{k}_c = k_c - i\alpha_c, \quad (19)$$

Eqs. (15) and (16) will have the same format as that of Eqs. (1a) and (1b). In addition, we can generalize the definition of the acoustic impedance to include an imaginary part,

$$\tilde{Z}_p = \frac{\tilde{k}_p \nu^p}{\omega} = Z_p - i \frac{\alpha_p \nu^p}{\omega}, \quad (20)$$

$$\tilde{Z}_c = \frac{\tilde{k}_c \nu^c}{\omega} = Z_c - i \frac{\alpha_c \nu^c}{\omega}. \quad (21)$$

All the derivations in Secs. II and III can be duplicated for the damped system with these complex wave numbers, \tilde{k}_p and \tilde{k}_c , and the complex impedance, \tilde{Z}_p and \tilde{Z}_c . The results are the same except replacing the real, k_p , k_c , Z_p , and Z_c by their complex counterpart. The resonance magnitude will be greatly reduced as we will see from the calculations below.

V. RESULTS AND DISCUSSIONS

In a composite transducer, the polymer phase can be chosen to be lossy in order to reduce the level of spurious resonance from the shear waves, while the damping in ceramic is relatively small and have little flexibility for adjustment. For simplicity damping is introduced only in the polymer ($\alpha_c = 0$) in the calculations. The damping factor in our calculation is assumed to be a linear function of frequency

$$\alpha_p = \alpha_0 (5.41 \times 10^{-5} f - 20.49) / m, \quad (22)$$

where f is the frequency in Hertz and α_0 is an adjustable factor. The coefficients were so chosen that when $\alpha_0 = 5$, the rhs of Eq. (22) divided by the conversion factor $\ln 10 = 2.3$ will give the α_p value in dB.

Most of the composite transducers operate in the thickness mode, i.e., resonance in the z direction shown in Fig. 1. Because the pitch scale (the period) d is usually made very small in conventional transducer design in order to make the pitch resonance will be at a much higher frequency than the thickness mode. The transducer will not function well when the spurious transverse modes occur.

In order to study the relevant shear modes in a multisource system, we define an average amplitude of the ceramic components M as a measure to characterize those relevant shear modes,

$$M = \frac{1}{N} \sum_{n=1}^N \int_{\text{ceramic}} |\psi_c| dx, \quad (23)$$

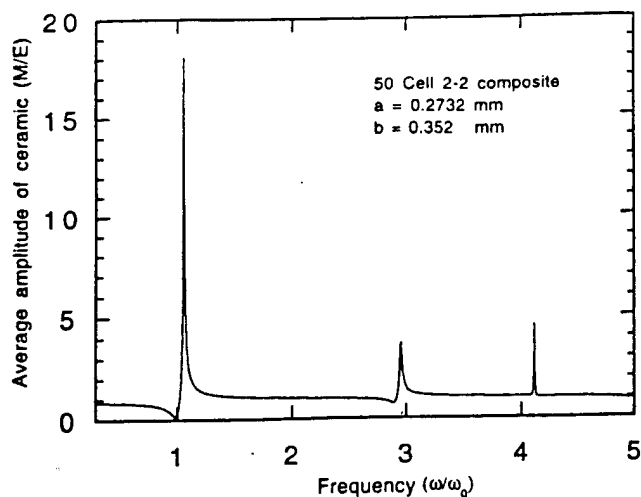


FIG. 2. Frequency dependence of the average ceramic vibration amplitude for shear wave propagation in a multisource driven system. Polymer damping is chosen at $\alpha_0=2$.

where the integration is on the ceramic element only to account for the piezoelectric effect. N is the total number of the cells in the composite.

To be more general, M is normalized by the magnitude of the applied drive $|E|$, and the frequency is normalized by the half wavelength shear wave resonance frequency of the polymer element,

$$\omega_0 = \frac{\pi \nu_p}{b}, \quad (24)$$

where ν_p is the shear acoustic velocity of the polymer.

Figure 2 shows the frequency dependence of M for a 50 cell 2-2 composite with the polymer width $b=0.352$ mm and the ceramic width $a=0.2732$ mm (44% ceramic by volume). The physical properties of ceramic and polymer used for the calculations are given in Table I. Figure 2 shows three peaks of M , corresponding to the pitch resonance, its third harmonic, and a higher shear resonance. Other peaks at much lower frequencies related to the overall size of the composite structure have much smaller magnitude and therefore ignored here.

The most pronounced low-frequency peak is the one near ω_0 , or $\omega/\omega_0 \sim 1$, corresponding to the pitch resonance, we call it the main peak. In transducer design, this main peak is the most interesting one which determines the frequency limit for the composite transducer. In what follows we will devote most of the effort to study this main peak.

In order to see the physical meaning of those peaks in Fig. 2, we have calculated the space profile and phase variation inside the composite at these corresponding peak fre-

TABLE I. Material properties for the ceramic and polymer constituents of the 2-2 composite.

Ceramic:	$c_{55}^c = 2.4 (10^{10} \text{ N/m}^2)$,	$\rho_c = 7800$.
Polymer:	$c_{55}^p = 1.59 (10^9 \text{ N/m}^2)$,	$\rho_p = 1160$.

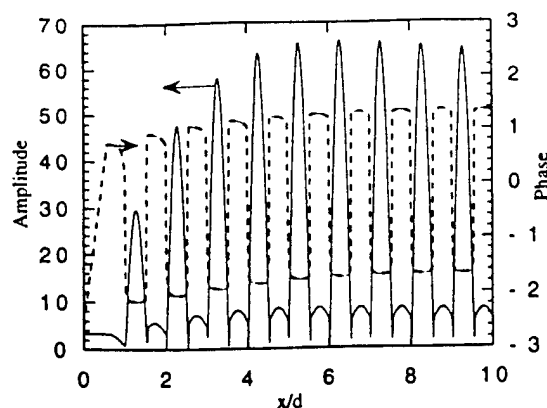


FIG. 3. Space profile of the vibration amplitude and phase for a 50 cell composite at the main peak frequency of $\omega=1.056\omega_0$.

quencies. Figure 3 is the space profile of a 50-cell composite at the main peak frequency of $1.056\omega_0$. We can see clearly that the pattern corresponds to the full wavelength pitch resonance with the ceramic and polymer elements vibrating 180° out of phase. It is important to note that this is the first excited mode in this structure due to the symmetry of the driving force applied to the composite, whereas in the single drive analysis, other nonpiezoelectric active modes will also appear.¹⁰ The second important point that should be noted in Fig. 3 is the strong edge effects, which are unavoidable in a finite system. The edge effects can be seen more clearly in Fig. 4 which displays the space profile and the phase variation of several composites made of 6, 10, and 50 cells. Both the magnitude and the phase are affected by the composite size. As a consequence, the main peak of the average magnitude also shows some degree of size dependence, both the magnitude and the peak frequency are smaller for composites with lesser cells, but these values saturate after $N>100$.¹¹

The amplitude of the main peak is affected strongly by the damping in the polymer phase as shown in Fig. 5. The peak value M_{\max} changes drastically with the increase of the damping coefficient α_0 defined in Eq. (22). This suggests that lossy polymer can play an important role in reducing the effects of the pitch resonance.

VI. EFFECTS OF RANDOMIZATION

Considering the fact that the main peak is from the pitch resonance due to the periodic nature, it should be reduced or eliminated if the periodicity is destroyed.¹²⁻¹⁵ There are two kinds of fabrication processes in making a composite, one is placing ceramic elements of the same size with certain spacing in between and then filling in the gaps with polymer resin; the other is to dice a solid ceramic to create the kerfs and then filling in those kerfs with polymer. The former has a fixed ceramic dimension, or constant a , while the latter has a constant polymer width b (saw blade thickness). Therefore, randomizing a would be easier for the latter fabrication process and randomizing b would be easier for the former fabrication process. Using the multisource T-matrix techniques

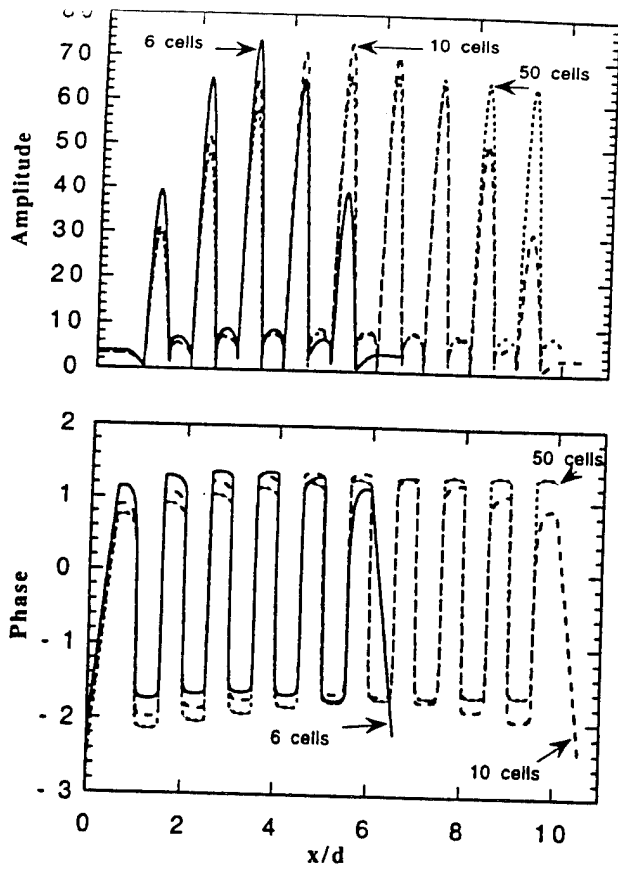


FIG. 4. Comparison of the vibration amplitude and phase for composites consisting 6, 10, and 50 cells. Only the first 10 cells were plotted for the 50 cell composite.

described in Sec. II, we have studied the effects of randomization for the multisource driven system in both cases of a random and b random.

Figure 6 shows the effects of randomizing ceramic spacing b . It is expected that the randomization of b will have a strong effect because the main resonance peak shown in Fig. 2 appears to be close to the polymer half-wavelength resonance frequency.

The randomized ceramic spacing b_i is chosen according to the following formula:

$$b_i = (1 - \chi)b_0 + \chi C_r r_i, \quad C_r = \frac{N b_0}{\sum_{i=1}^N r_i}, \quad (25)$$

where b_0 is the arithmetic mean of the ceramic spacing (or polymer width), N is the total number of cells, r_i ($i = 1, \dots, N$) is a set of random numbers between 0 and 1, and χ is the percentage of randomization which is defined to be the variable percentage of b_i . We have studied the cases of $\chi = 5\%$, 10% , 20% , and 50% .

As shown in Fig. 6, the resonance nature changes dramatically with the introduction of randomness. The magnitude of the main resonance peak is reduced by 40% with only 5% randomness. At the same time, there are more small bumps created in the vicinity of the original main peak. Theoretically speaking, more randomness in the structure is

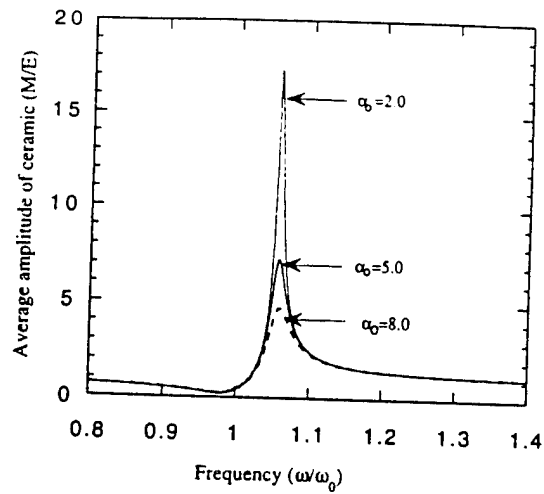


FIG. 5. Effect of damping on the main resonance peak. α_0 are chosen to be 2, 5, and 8, respectively.

better in terms of dispersing the main resonance peak, but the effect is the strongest within the first 20% randomness.

We also found that the influence of randomizing b on the main peak becomes much weaker for high ceramic volume percent composites for which the major contribution to the main low-frequency resonance will come from the ceramic. On the other hand, randomizing a has different effects as shown in Fig. 7, where the results were calculated for a composite with 45% ceramic. When the ceramic percentage is less than 60% ceramic volume content, the main low-frequency peak is reduced but still relatively strong even for 50% randomness of a . Interestingly, the shape of the peak remains practically the same. However, when the ceramic percent is more than 70%, the shape of the main peak will be destroyed through randomizing a . Figure 8 shows the calcu-

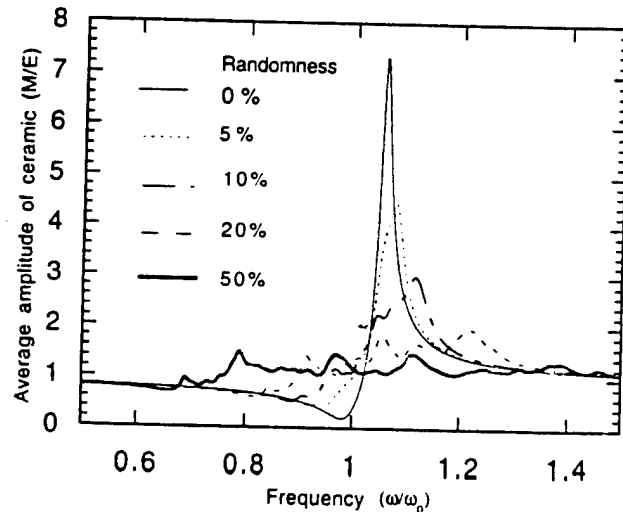


FIG. 6. Effects of randomizing b for a composite with 45% ceramic volume content. The percentages of randomness are 5%, 10%, 20%, and 50%, respectively. The effectiveness decreases with the increase of ceramic content.

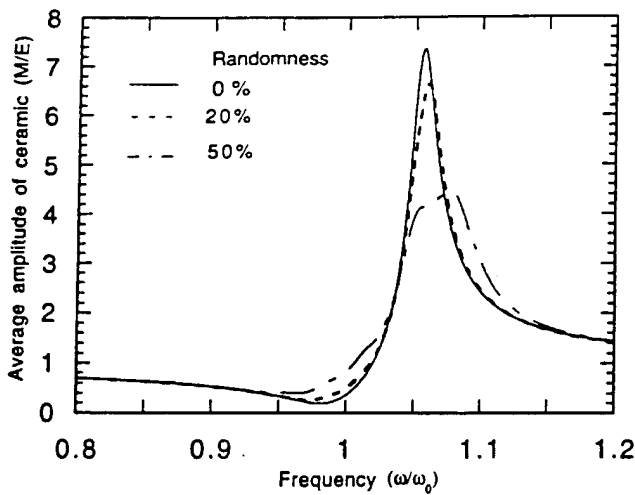


FIG. 7. Effects of randomizing a for a 45% ceramic composite. The percentages of randomness are 5%, 10%, 20%, and 50%, respectively. The influence on the low-frequency main peak is much smaller compared with randomizing b as shown in Fig. 6.

lated results for a composite contains 80% ceramic. We can see that the effect of randomizing a is much larger compared with the results shown in Fig. 7.

VII. SUMMARY AND CONCLUSIONS

We have derived the recurrence relation for the vibration amplitude among different cells in a multisource driven stratified structure using an extended multisource T-matrix technique. Ceramic-polymer composites with 2-2 connectivity is a perfect example of such situation. The new criteria Eq. (23) introduced here can directly identify the relevant shear modes that affect the thickness mode operation. Analyses show that the lowest shear mode, corresponding to the

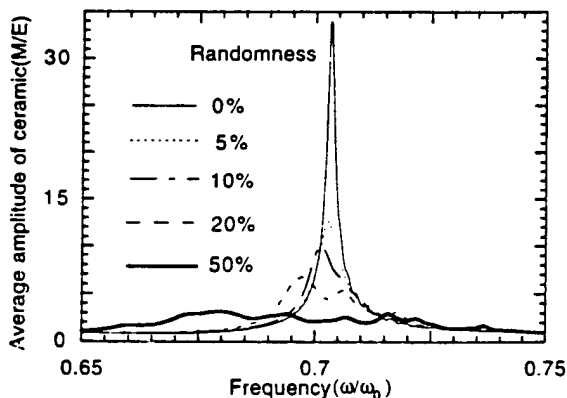


FIG. 8. Effects of randomizing a for a composite with 80% ceramic volume content. The percentages of randomness are 5%, 10%, 20%, and 50%, respectively. Note this peak does not appear for a low ceramic content composite, for which the lowest peak is near ω_0 as shown in Fig. 6.

pitch resonance, is the most important mode which couples strongly to the thickness resonance in a periodic composite transducer.

The pitch resonance can be destroyed by randomization. For moderate ceramic volume content (60% or less), the main peak is primarily linked to the spacing between the ceramics. In this case, we found that randomizing the spacing between ceramics, i.e., b is much more effective than randomizing a , the ceramic width. On the other hand, for very high percentage ceramic content (70% or more), the effect of randomizing a becomes more effective than randomizing b since the main low-frequency peak is tied more to the ceramic dimension. These results can provide useful guidelines for making random composite transducers.

ACKNOWLEDGMENT

This research is supported by the Office of Naval Research under Grant No. N00014-92-J-1501.

APPENDIX

Assuming there are m acoustic sources located at $-a_1, -a_2, \dots, -a_m$ sending waves to forward direction, then the wave form at position x is the linear superposition of these waves:

$$\begin{aligned} \psi(x) = & A_1 e^{i[\omega t - k(x+a_1)]} + A_2 e^{i[\omega t - k(x+a_2)]} + \dots \\ & + A_m e^{i[\omega t - k(x+a_m)]} = [A_1 e^{-ika_1} + A_2 e^{-ika_2} + \dots \\ & + A_m e^{-ika_m}] e^{i(\omega t - kx)}, \end{aligned} \quad (A1)$$

where

$$A = A_1 e^{-ika_1} + A_2 e^{-ika_2} + \dots + A_m e^{-ika_m}$$

is a complex number. Therefore, both the forward and backward waves can be written as a simple wave form even for the multisource system except the amplitude is now a complex number.

For the ceramic elements the wave function also should include the uniform driving of the external field.

- ¹W. T. Thomson, *J. Appl. Phys.* **21**, 89 (1949).
- ²E. H. Lee and W. H. Yang, *SIAM J. Appl. Math.* **25**, 492 (1973).
- ³C. G. Oakley, Ph.D. thesis, The Pennsylvania State University, 1991.
- ⁴Y. Wang, E. Schmidt, and B. A. Auld, *Proceedings of IEEE 1986 Ultrasonic Symposium*, 1986, p. 685.
- ⁵B. A. Auld, H. A. Kunkel, Y. A. Shui, and Y. Wang, *Proceedings of IEEE 1983 Ultrasonic Symposium*, 1983, p. 554.
- ⁶C. Potel and J. F. Belleval, *J. Acoust. Am. Soc.* **93**, 2669 (1993).
- ⁷Y. Wang and B. A. Auld, *Proceedings of IEEE 1985 Ultrasonic Symposium*, 1985, p. 637.
- ⁸Y. Wang, Ph.D. thesis, Stanford University, 1986.
- ⁹A. M. B. Braga and G. Hermann, *J. Acoust. Soc. Am.* **91**, 1211 (1991).
- ¹⁰W. Cao and W. Qi, *J. Appl. Phys.* **78**, 4627 (1995).
- ¹¹W. Cao and W. Qi (unpublished).
- ¹²J. A. Hossack, B. A. Auld, and H. D. Batha, *Proc. IEEE 1991 Ultrasonic Symposium*, 1991, p. 651.
- ¹³B. A. Auld and J. A. Hossack, *Electron. Lett.* **27**, 1284 (1991).
- ¹⁴P. Sheng and Z. Zhang, *Phys. Rev. Lett.* **57**, 1879 (1986).
- ¹⁵T. R. Kirkpatrick, *Phys. Rev. B* **31**, 5746 (1985).